Proceedings of the
NASA Laboratory Astrophysics Workshop

NASA Ames Research Center
Moffett Field California
May 1–3, 2002

Edited by:

Farid Salama
NASA Ames Research Center
Moffett Field, California

The NASA STI Program Office ... in Profile

Since its founding, NASA has been dedicated to the advancement of aeronautics and space science. The NASA Scientific and Technical Information (STI) Program Office plays a key part in helping NASA maintain this important role.

The NASA STI Program Office is operated by Langley Research Center, the lead center for NASA's scientific and technical information. The NASA STI Program Office provides access to the NASA STI Database, the largest collection of aeronautical and space science STI in the world. The Program Office is also NASA's institutional mechanism for disseminating the results of its research and development activities. These results are published by NASA in the NASA STI Report Series, which includes the following report types:

- TECHNICAL PUBLICATION. Reports of completed research or a major significant phase of research that present the results of NASA programs and include extensive data or theoretical analysis. Includes compilations of significant scientific and technical data and information deemed to be of continuing reference value. NASA counterpart of peer-reviewed formal professional papers, but having less stringent limitations on manuscript length and extent of graphic presentations.

- TECHNICAL MEMORANDUM. Scientific and technical findings that are preliminary or of specialized interest, e.g., quick release reports, working papers, and bibliographies that contain minimal annotation. Does not contain extensive analysis.

- CONTRACTOR REPORT. Scientific and technical findings by NASA-sponsored contractors and grantees.

- CONFERENCE PUBLICATION. Collected papers from scientific and technical conferences, symposia, seminars, or other meetings sponsored or co-sponsored by NASA.

- SPECIAL PUBLICATION. Scientific, technical, or historical information from NASA programs, projects, and missions, often concerned with subjects having substantial public interest.

- TECHNICAL TRANSLATION. English-language translations of foreign scientific and technical material pertinent to NASA's mission.

Specialized services that complement the STI Program Office's diverse offerings include creating custom thesauri, building customized databases, organizing and publishing research results ... even providing videos.

For more information about the NASA STI Program Office, see the following:

- Access the NASA STI Program Home Page at *http://www.sti.nasa.gov*

- E-mail your question via the Internet to help@sti.nasa.gov

- Fax your question to the NASA STI Help Desk at (301) 621-0134

- Telephone the NASA STI Help Desk at (301) 621-0390

- Write to:
NASA STI Help Desk
NASA Center for AeroSpace Information
7121 Standard Drive
Hanover, MD 21076-1320

Acknowledgements

This report is available from:

NASA Center for AeroSpace Information
7121 Standard Drive
Hanover, MD 21076-1320
301-621-0390

National Technical Information Service
5285 Port Royal Road
Springfield, VA 22161
703-605-6000

Complete information on the Workshop and all related documents can also be found at http://www.astrochemistry.org/nasalaw.html. The papers presented at the Workshop will also be published by the NASA Astrophysics Data System (ADS) at http://adsabs.harvard.edu/.

PREFACE

The NASA Laboratory Astrophysics Workshop, sponsored by the NASA Office of Space Science (OSS), was hosted by NASA's Ames Research Center, May 1–3, 2002. The purpose of this Workshop was to discuss the current state of knowledge in this interdisciplinary field and to assess the scope of its contributions to NASA's space missions.

This report comprises a record of the complete proceedings of the Workshop including a White Paper that describes the science priorities ("needs") identified during break-out group discussions. The Laboratory Astrophysics White Paper, which has been provided to OSS for incorporation into its strategic planning efforts, can be found in these proceedings beginning on page 3.

Farid Salama
November 2002

TABLE OF CONTENTS

INTRODUCTION

The NASA Laboratory Astrophysics Workshop (LAW) was convened at NASA Ames Research Center, Moffett Field, California, May 1-3, 2002. This programmatic Workshop is held periodically by NASA's Office of Space Science (OSS) to discuss the current state of knowledge in the interdisciplinary field of laboratory astrophysics and to assess how well the current programs are supporting NASA's space missions. The objective of the Workshop is to identify science priorities ('needs') in support of NASA's space missions and to provide input to the OSS in the form of a White Paper for incorporation into it's strategic planning. The Laboratory Astrophysics White Paper can be found in these proceedings beginning on page 3 while the purpose and the goals of the Workshop are detailed in the Workshop Charter in Appendix B.

The Workshop was organized along the four Science Themes defined by OSS for its strategic planning efforts: Origins, Structure and Evolution of the Universe, Solar System, and Sun-Earth Connection. In addition to these four themes, the Workshop also included connections to Astrobiology, the study of life in the Universe.

The Workshop attracted more than 130 participants[1] with interests and expertise in astrophysics, astronomy, physics, chemistry, and planetary sciences. Laboratory astrophysicists and astrochemists, theoreticians and modelers, observers, instrument developers, space mission scientists were joined by OSS program managers to discuss the latest developments in the field of Laboratory Astrophysics as well as the state of the program.

The first two days of the Workshop were devoted to over 100 oral and poster presentations that sampled the exceptionally rich spectrum of research programs in this multidisciplinary field. Topics ranged from high-energy astrophysics to the study of interstellar dust and solar system objects. Each science topic session was introduced by an invited overview presentation describing the needs in the field followed by a series of contributed oral and poster presentations sampling the research programs supported by NASA's OSS.

The third day was devoted to discussions within science focus groups[2] that examined the current status of the NASA-supported Laboratory Astrophysics research programs and whether these programs meet NASA's needs for future space missions. The White Paper resulting from this forum and based on the needs identified by these focus groups has been reported to OSS for incorporation into its strategic planning efforts.

The NASA Laboratory Astrophysics Workshop was a great success thanks to the enthusiastic response and participation of the community of scientists and OSS program managers, and to the high level of dedication of the Workshop Science Organizing Committee and Local Organizing Committee.

---

1. The Participant's Roster, showing the complete contact information for each participant, is in Appendix D.
2. All participants were invited to join one focus group corresponding to their own interests (see Appendix C).

Science Organizing Committee (SOC) Members [3]

David Leckrone (NASA Goddard Space Flight Center)
John Mathis (Univ. of Wisconsin)
Melissa McGrath (Space Telescope Science Institute)
Richard Miller (Georgia State Univ.)
Thomas Phillips (Caltech)
Farid Salama (NASA Ames Research Center)
Wilton Sanders (Univ. of Wisconsin)
Peter Smith (Harvard-Smithsonian Center for Astrophysics)
Theodore Snow (Univ. of Colorado)
Alexander Tielens (Kapteyn Astronomical Inst.)

Ex-officio SOC Members – NASA Discipline Scientists

Philippe Crane (Ultraviolet, Visible & Gravitational Astrophysics)
Hashima Hasan (Ultraviolet, Visible & Gravitational Astrophysics)
John Hillman (Planetary Astronomy and Atmospheres)
Louis Kaluzienski (High Energy Astrophysics)
Donald Kniffen (High Energy Astrophysics)
Eric Smith (IR, submm Astrophysics)
Jay Frogel (IR, submm Astrophysics)

NASA Astronomy and Physics Working Group (APWG), Laboratory Astrophysics

James Lawler (Univ. of Wisconsin)
Guy Stringfellow (Univ. of Colorado)

Workshop Local Organizing Committee (LOC)

Farid Salama (NASA Ames Research Center), Chairperson
Sara E. Acevedo (SETI Institute), Workshop Organizer
Jason Dworkin (SETI Institute), Web Master
Ludovic Biennier (NRC, NASA Ames Research Center)
Lou Allamandola (NASA Ames Research Center)
Andrew Mattioda (NRC, NASA Ames Research Center)
Robert Walker (NASA Ames Research Center)

---

3. Complete contact information for all SOC Members is in Appendix E; information for each LOC Member can be found in the Participants Roster (Appendix D).

LABORATORY ASTROPHYSICS WHITE PAPER

SUMMARY OF LABORATORY ASTROPHYSICS NEEDS
(DRAFT June 12, 2002)

BASED ON DISCUSSIONS HELD AT THE
NASA 2002 LABORATORY ASTROPHYSICS WORKSHOP
(NASA Ames Research Center, May 1-3, 2002)

Report prepared by the Scientific Organizing Committee:

    Farid Salama, Committee Chair
    David Leckrone
    John Mathis
    Melissa McGrath
    Richard Miller
    Thomas Phillips
    Wilton Sanders
    Peter Smith
    Theodore Snow, Report Editor
    Alexander Tielens

The NASA Laboratory Astrophysics Workshop (NASA LAW) met at NASA Ames Research Center from 1-3 May 2002 to assess the role that laboratory astrophysics plays in the optimization of NASA missions, both at the science conception level and at the science return level. Space missions provide understanding of fundamental questions regarding the origin and evolution of galaxies, stars, and planetary systems. In all of these areas the interpretation of results from NASA's space missions relies crucially upon data obtained from the laboratory.

We stress that Laboratory Astrophysics is important not only in the interpretation of data, but also in the design and planning of future missions. We recognize a symbiosis between missions to explore the universe and the underlying basic data needed to interpret the data from those missions.

In the following we provide a summary of the consensus results from our Workshop, starting with general programmatic findings and followed by a list of more specific scientific areas that need attention. We stress that this is a "living document" and that these lists are subject to change as new missions or new areas of research rise to the fore.

I. General findings:

- The number and scope of NASA missions requiring supporting laboratory data (especially spectroscopy) has risen dramatically, but the funding for Laboratory Astrophysics has remained flat. The current funding profile cannot meet the needs of existing missions or prepare for future missions.

- Critical compilation of databases was identified as a high priority need. For example, NIST has been maintaining the highest quality atomic database in the world, a resource relied upon for basic data in several communities, but for which NIST does not provide internal support. The over-strained NASA budget has not been able to provide the level of support required to maintain this database, and resources from other agencies have also diminished. We are concerned that such databases may not survive.

- Laboratory facilities are aging and major funding is required to replace them with modern, state-of-the-art equipment. Unless new facilities can be built it will become increasingly difficult for laboratory astrophysics to keep up with the demand for atomic and molecular data to support space-based and ground-based observatories.

- The training of new scientists in Laboratory Astrophysics is crucial for the future of the field, but the low level of funding is making it increasingly more difficult to attract students and train the scientists of tomorrow to provide the required laboratory data. Retention of existing groups is also a concern as it is dependent on continuing sources of grant funds.

- Within the next decade four major infrared and/or submillimeter astronomical observatories will be launched, whose success will depend largely on accurate and comprehensive laboratory data on atomic and molecular transitions in these spectral regions, which are to date largely unexplored in the lab. Lab data in these spectral regimes are crucial to the success of these missions.

- Major needs exist for laboratory data to help in the interpretation of spectra from current and planned UV and X-ray missions. This need extends also to upcoming IR an submillimeter missions, which will observe highly-redshifted UV features.

- Spectroscopy is of the essence. Until the 1990s, sensitivities in most spectral ranges were too low to permit high resolution spectroscopy, and missions like IRAS and ROSAT concentrated on broad-band mapping and photometry. The situation is drastically different today as recent, current, and planned future missions provide high-resolution spectra to look at detailed chemical and physical processes on solar system, stellar, galactic, and extragalactic scales over a wide range of photon energies.

- The demands on laboratory astrophysics for high signal-to-noise and high spectral resolution are unprecedented. Many of NASA's planned missions have spectroscopic capabilities with exquisite sensitivity, and most will have extremely high spectral resolving power. A host of new spectral features numbering in the millions will need to be identified and interpreted.

To meet the objectives of these planned missions and to make their findings accessible to the community in clear, understandable terms, we will need the support of a coherent and vigorous Laboratory Astrophysics program that integrates theory, modeling, and experiment.

II. Needs for laboratory data supporting specific missions and spectral bands.

We now consider the more specific scientific connections between laboratory astrophysics and various current and planned NASA missions. These needs for laboratory data differ significantly among wavelength ranges. Hence the various spectral regions are considered here in order of increasing wavelength. Within each wavelength interval we specify the current or planned missions whose data interpretation depends on the results of Laboratory Astophysics studies.

The X-Ray Spectral Region

Missions: Chandra, XMM-Newton, Astro-E2, and Constellation-X

X-ray observations can be used to address a number of fundamental questions in astrophysics. Relativistically broadened metal lines in AGN and quasars can be used to study black holes. High resolution spectra of AGN, quasars, XRBs, and CVs help us learn about accretion in the vicinity of compact objects. X-ray emission from infrared bright galaxies tell us about the relationship between the AGN and starburst components of galaxies. Stellar winds, supernova remnants, and the ISM can be used to study nucleosynthesis and the evolution of our Galaxy and the universe. Observations of galaxy clusters and the IGM provide information on the formation of large scale structure in the universe, the formation of galaxies, and provide constraints on the dark matter component of the universe. Stellar coronal observations can be used to study the connection between the stellar photosphere and corona and the physical processes involved in heating and mass supply to stellar coronae.

X-rays provide a quantitative understanding of highly ionized plasmas, both electron-ionized and photoionized. Electron-ionized plasmas are formed in stellar coronae, supernova remnants, the ISM, galaxies, and clusters of galaxies. Photoionized plasmas are found in planetary nebulae, H II regions, the IGM, AGN, XRBs, and CVs. Interpreting X-ray spectra from all these sources depends critically upon input from laboratory astrophysics. Priorities for measurements include atomic rate coefficients for low and high temperature dielectronic recombination, state-specific and total charge transfer for multiply charged ions on H and H_2, collisional excitation, inner shell photoabsorption, and photoexcitation and photoionization cross sections as well as fluorescence and Auger yields. Measurements of fundamental spectroscopic quantities are also needed, including M- and L-shell emission and satellite line identifications and wavelengths (accurate to one part in 10^5) for Ne, Mg, Si, S, Ar, Ca, Fe, and Ni.

While most atomic data used to interpret X-ray plasmas are compiled from theoretical calculations, laboratory measurements are needed to determine the accuracy of rates for critical diagnostics. As an example, the strong set of Fe XVII X-ray emission lines provides information on temperatures, densities, and opacities, but, despite recent laboratory studies, their astrophysical interpretations remain unclear. Laboratory surveys of the X-ray spectral content are also needed to provide critical tests of the completeness of spectral models. For moderate resolution X-ray data, complete models are required for global spectral fitting; at higher resolution, completeness studies are necessary in order to assess blending around diagnostic lines.

The atomic data for collisionally ionized plasmas, relevant to stellar coronae, galaxies, and clusters of galaxies, have received the best critical evaluations and laboratory tests. Non-equilibrium effects of X-ray spectra, such as those expected in supernova remnants, require further studies, as the atomic rate coefficients are often less accurate away from equilibrium temperatures. Priorities for future work need to include critical tests of the atomic data used for X-ray photoionized plasmas, such as found in accretion disks and black hole environments. Since spectral models for photoionized sources need to make assumptions about the astrophysics (e.g., energy balance and geometry) to incorporate atomic physics, it is critical that laboratory studies benchmark the essential atomic data, therefore studies of low temperature dielectronic recombination should receive high priority.

New results from Chandra and XMM-Newton suggest additional areas in need of laboratory astrophysics. Recent astrophysical observations have tentatively identified X-ray absorption by molecules, a new area for laboratory measurements of edge physics, which can lead to differentiation between gas and dust in diffuse media. Closer to home, objects in the solar system, such as comets, the Jovian aurora, the Io plasma torus, and the Jovian Galilean satellites (Io, Europa, Ganymede), emit X-rays. Cometary X-ray emission is tentatively attributed to charge transfer between the solar wind ions and the comet. If charge transfer is the correct mechanism, these observations provide a sample of the comet coma material as well as information on the solar wind velocity and elemental charge states. Accurate cross sections for charge transfer are needed, to compute both state-specific partial rates and total rates, for multiply charged ions on H and H_2. Laboratory measurements of charge exchange cross sections will help to validate the models for solar system X-ray emission, and may be of importance in X-ray photoionized plasmas as well.

Summary of needs for lab data to support X-ray astrophysics:

- Atomic rate coefficients for:
  + low and high temperature dielectronic recombination;
  + state-specific and total charge transfer for multiply charged ions on H and H_2;
  + collisional excitation and ionization;
  + inner shell photoabsorption;
  + photoexcitation and photoionization cross sections;
  + fluorescence and Auger yields.

- Measurements of fundamental spectroscopic quantities:
  + M- and L-shell emission and satellite line identifications and wavelengths (accurate to one part in 10^5) for Ne, Mg, Si, S, Ar, Ca, Fe, and Ni.

- Measurements of X-ray absorption spectra due to molecules.

The UV Spectral Region

Missions: HST(STIS), HST(COS), and FUSE, for low redshift; SOFIA, Herschel, and NGST for higher redshifts

This spectral region will provide ages and metallicities of old galaxies, the sequence of galaxy formation, tests of cosmological models, and an understanding of the relative importance of r- versus s-process nucleosynthesis of neutron capture elements as a function of time since the Big Bang. The UV region also provides insights on chemically/isotopically peculiar stars, on segregation of elements in stellar photospheres, and on mass transfer in binary systems. These problems need comprehensive classified spectral line lists in the UV, including wavelengths accurate to 1 part in 10^7, transition probabilities accurate to 5 to 10%, and hyperfine/isotopic parameters for high abundance Fe group elements in the first three stages of ionization, and similar spectral line lists in the UV for strong lines of lower abundance elements including the neutron capture elements.

We draw special attention to the far-UV spectral region where FUSE operates. Here special coatings and detectors are needed, with the result that lab data are lagging far behind the astronomical data. The lack of experimental data in this spectral region has hampered progress in theoretical studies as well as the interpretation of astronomical data.

The UV region is key to interpreting visible and UV spectra of important interstellar molecules, such as large organic species that carry the ubiquitous IR emission bands (UIBs) and diffuse interstellar bands (DIBs) and that may be related to the origin of life. Studies of the UV characteristics of such molecules and their dependence on molecular structure and charge state is of key importance for our understanding of this ubiquitous molecular component of the ISM. Identification of UV spectra of large aromatics, and in particular of PAHs, is especially important to address these issues and represents one of the key science goals of the HST(COS). UV spectra are uniquely capable of identifying specific molecules, in contrast with the less specific transitions observed in the IR. Lab studies provide spectroscopy of large organic molecules (such as PAHs) and their ions in the solid and in the gas phases, measurements of chemical reaction rate coefficients, and recombination cross sections. This work must be complemented by quantum theory calculations so that the lab data are properly interpreted.

The molecule CO is a key component of dense interstellar clouds and a probe of local interstellar conditions. Measurements are needed of oscillator strengths for UV intersystem bands for CO and its isotopomers, improved wavelength measurements in the UV, and photodissociation cross sections including their J-dependence at appropriate interstellar temperatures.

Astronomers also require an improved understanding of the energetics of interstellar dust in a variety of environments (photon-pumping mechanisms, etc.). Such insight arises from spectroscopic signatures that provide direct information on the composition and evolution of dust. Previous studies in the UV have focused on the only identified spectral feature (at 2200 Å), but all materials should show UV spectral signatures. Laboratory measurements of the optical properties of bulk materials such as carbonaceous solids, metallic carbides, sulfides, oxides, as well as weak features of other common materials, are needed, as well as studies of the properties of very small (nano-sized) particles of the same substances, which differ from the bulk properties.

7

The UV wavelength region, often used in conjunction with other wavelengths, provides an understanding of the fundamental processes (and especially the energy balance) associated with emissions from planetary atmospheres and magnetospheres, including planetary aurora and dayglow emissions (relevant for all planets and satellites with atmospheres and magnetospheres), as well as comets. Laboratory studies must provide reaction rates and electron impact excitation rate coefficients.

Light reflected from atmospheres of planets, in which absorption from the planetary atmosphere is superposed upon the solar spectrum, leads to a determination of the composition and structure of planetary atmospheres and interiors. Different wavelengths probe various depths in the atmosphere. Laboratory studies must provide line lists for the parent species (primarily those arising from methane, water, and carbon monoxide), extensive sets of rate coefficients for all classes of reactions used in the photochemical models, and an understanding of the radiative transfer and temperature effects on line shapes. Low temperature rate constants are needed in many cases. It is not known how the products of many photodissociation rates are distributed in energy states. Equations of state, solubility, and molecular diffusion in H_2/He mixtures at low temperature and high density are needed for studies of giant planets that can also be used as a basis for understanding brown dwarfs.

Lack of reflectance spectra (UV-visible-NIR) of low temperature frosts/volatile ices has inhibited interpretation of the Galileo data. Unless something is done in the near future, the situation will be similar for Saturn Cassini data. Water is reasonably well covered, and the mid- and far-IR has been done for astrophysical ices, although not at the 50-150K temperatures relevant for solar system objects. Optical constants/properties of organic solids (important for most "red" solid bodies in the outer solar system) and of solid sulfur are needed.

Summary of needs for lab data to support UV astrophysics:

- Comprehensive line lists and f-values for atoms and ions in all stages, for: rare elements seen in stars (e.g., neutron-capture elements);
    + ionization stages not previously studied;
    + the far-UV spectral region.
- Molecular spectra of small molecules, including:
    + CO (and CO isotopomer) intersystem bands;
    + large organics such as PAHs and heterocycles;
    + molecules expected to be abundant in planetary atmospheres;
    + other species possibly detectable at high S/N in astronomical spectra.
- Spectra and ionization analyses of large organic molecules such as PAHs and derivatives.
- Photodissociation cross sections of important interstellar molecules such as CO and H_2O.
- UV pumping rates leading to IR emission by molecules.
- Optical, physical , and chemical and properties of dust analogues, including:
    + optical properties of bulk materials such as carbonaceous solids, metallic carbides, sulfides, oxides;
    + weak spectral features of other common materials;

+ comparative physical, chemical, and spectroscopic properties of interstellar and interplanetary particles

+ formation processes and rates for molecule formation (especially molecular hydrogen) on grain surfaces;

+ studies of nano-sized particles.

- Spectra and excitation cross-sections of molecules important in planetary atmospheres, particularly for species arising from methane, water, and carbon monoxide; and sulfur-bearing species.

- Reflectance spectra (UV-visible-NIR) of low temperature frosts/volatile ices relevant for studies of satellites of the outer planets.

- UV-visible optical constants/properties of organic solids (important for most "red" solid bodies in the outer solar system) and of solid sulfur.

The Infrared and Sub-millimeter Spectral Region

Missions: HST(NICMOS), SIRTF, SOFIA, Herschel, and NGST

The infrared and submillimeter wavelength region is of paramount importance for studies of the cold, molecular and dusty universe. The formation of stars and planetary systems takes place deep inside cold gas and dust clouds, often obscured by hundreds of visual magnitudes of extinction. At high redshifts, the assembly of galaxies through the merging of smaller units is accompanied by large amounts of obscuring dust. In order to penetrate these dusty regions and probe the processes occuring deep within, observations at infrared and submillimeter wavelengths are essential. Moreover, these wavelengths provide sensitive probes of the physical conditions in and dynamics of such regions through the pure rotation and ro-vibrational transitions of small molecules as well as the detailed profiles of transitions in larger molecules and those associated with dust. NASA will launch and participate in a number of missions centered on this wavelength region (SIRTF, SOFIA, Herschel, NGST) which will chart the star formation history of the universe, star and planet formation in the Milky Way, the galactic life cycle of the elements, and the molecular universe, in general. Together these span most of the key questions in modern astronomy.

The ensemble of current and planned IR/sub-mm missions will bring in enormous quantities of data in spectral regions where little is known. Laboratory studies are essential in order to support the analyses of these data. Accurate frequency measurements and band analyses are needed for atomic and molecular species having transitions between 500 GHz and 2 THz, a largely unexplored spectral region important for many kinds of astrophysical studies, including low- and high-density interstellar gases and plasmas, circumstellar clouds and disks, cool star atmospheres, and star- and planet-forming regions. Studies of interstellar dust will also be especially important.

Mid-IR spectra of individual objects such HII regions, reflection nebulae, and planetary nebulae as well as the general interstellar medium of galaxies as a whole are dominated by a set of mid-IR emission features due to large PAH molecules. Studies of the IR characteristics of such molecules and their dependence on molecular structure and charge state is of key importance for our understanding of this ubiquitous molecular component of the ISM.

At long wavelengths, the continuum dust opacity is uncertain by an order of magnitude. IR/sub-mm transitions of interstellar dust grains must be used to determine their specific mineral composition, hence their opacities, which determine inferred grain temperatures and the masses of dusty objects, including the interstellar medium of entire galaxies. Emission bands from warm astronomical environments such as circumstellar regions, planetary nebulae, and star-forming clouds lead to the determination of the composition and physical conditions in regions where stars and planets form. The compositions of cool stars provide the nucleosynthetic history of our galaxy and of others.

The laboratory data essential for investigations of dust include measurements of emission and absorption spectra (opacities at various wavelengths, especially in the FIR) of candidate grain materials (both carbonaceous and silicaceous). Metallic carbides, sulfides, oxides, as well as weak features of common materials, are important. For abundant materials (e.g., forms of carbon such as PAHs), the measurements should range from molecules to nano- particles to bulk materials.

Also vital are measurements of molecular wavelengths and transition probabilities in the near-IR, where cool stars emit most of their flux. There are many as-yet unexploited transitions of important species.

Summary of needs for lab data to support IR and sub-mm astrophysics:

- Frequency measurements and band analyses for molecular species whose transitions lie between 500 GHz and 2 THz.

- Accurate wavelengths and transition probabilities of far-IR/sub-mm atomic fine structure transitions that are key diagnostics of conditions in low-density environments.

- Spectra and transition probabilities for small molecules such as light hydrides and metal hydrides which are important indicators of composition and which also dominate the cooling in low-density environments.

- Spectra and ionization analyses of large organic molecules such as PAHs.

- IR/sub-mm spectra of solid-state transitions in candidate grain materials:
    + for metallic carbides, sulfides, oxides, as well as weak features of common materials;
    + specific mineral compositions;
    + dust opacities;
    + optical properties for sizes ranging from molecules to nano- particles to bulk materials.

- Near-IR spectra and line strengths for atomic species and isotopes needed for abundance analyses in cool stars, for common and rare elements and isotopes.

- Reflectance spectra (UV-visible-NIR) of low temperature frosts/volatile ices relevant for studies of satellites of the outer planets.

Non-Wavelength-Specific needs involve fundamental physical and chemical processes that affect the scientific output of all NASA missions

Understanding of celestial objects requires knowledge of the rates of relevant physical and chemical processes. Only laboratory data can provide reaction rates, sticking coefficients, and desorption rates for processes in the gas phase, on the surfaces of small (nano-sized) and larger (micro-sized) grains, within interstellar ices, and on solar system objects such as icy satellites and Kuiper Belt objects. For instance, a quantitative understanding of the formation of the most important interstellar molecule, H_2, is very important and still incomplete. The quantitative understanding of the energy balance of the ISM (from the diffuse component to dense clouds) and the resulting phase structure requires studies of photoelectric yield and recombination cross sections of astrophysically relevant molecules and dust materials. Energetic processing of molecules, ices and dust materials by particle bombardment, and FUV and X-ray irradiation can substantially modify the composition and structure of these materials.

Low velocity collisions of icy dirt balls and mechanical properties of cryogenic porous ice/rock aggregates have direct relevance to the Kuiper Belt. The limitations on the available lab data will also hamper interpretations of thermal IR spectra to be obtained from the surface in 2004 by the Mars Exploration Rovers. The situation is similar in the visible to NIR, which will be studied extensively at the tens-of-meters scale by a NIR spectrometer on the 2005 Mars Reconnaissance Orbiter mission.

Web-accessible, critically evaluated databases should become available. The efficiency gains obtained by eliminating the need for individual scientists to search original literature for data are significant. Critical evaluation and the establishment of reliable error bars on the data are important. Reliable error bars add much confidence to scientific conclusions based on the interpretation of astrophysical observations with the data and modeling with the data.

Summary of needs for lab measurements of physical and chemical processes:

- Atomic rates and cross sections, especially for processes relevant to X ray properties of plasmas (see above).

- Quantitative studies of processes relevant to the formation of molecular hydrogen and other molecules on grains.

- Chemical reaction rates for large and small molecules of interest for all astrophysical environments.

- Charge balance measurements (ionization and electron recombination cross sections), especially for large organic molecules such as PAHs.

- Photoelectric yield and recombination cross sections of astrophysically relevant dust materials.

- Processing of molecules, ices, and dust materials by particle bombardment and FUV and X-ray irradiation.

- Low velocity collisions of icy dirt balls and mechanical properties of cryogenic porous ice/rock aggregates.

- Development and maintenance of web-accessible, critically evaluated data bases.

NASA's Laboratory Astrophysics Workshop: Opening Remarks

Hashima Hasan

Office of Space Science, NASA Headquarters, Washington DC

1. Introduction

The Astronomy and Physics Division at NASA Headquarters has an active and vibrant program in Laboratory Astrophysics. The objective of the program is to provide the spectroscopic data required by observers to analyze data from NASA space astronomy missions. The program also supports theoretical investigations to provide those spectroscopic parameters that cannot be obtained in the laboratory; simulate space environment to understand formation of certain molecules, dust grains and ices; and production of critically compiled databases of spectroscopic parameters.

NASA annually solicits proposals, and utilizes the peer review process to select meritorious investigations for funding. As the mission of NASA evolves, new missions are launched, and old ones are terminated, the Laboratory Astrophysics program needs to evolve accordingly. Consequently, it is advantageous for NASA and the astronomical community to periodically conduct a dialog to assess the status of the program. This Workshop provides a forum for producers and users of laboratory data to get together and understand each others needs and limitations. A multi-wavelength approach enables a cross fertilization of ideas across wavelength bands.

2. NASA's Office of Space Science Strategic Planning Process

The Workshop is timely, because the Office of Space Science (OSS) is currently in the process of preparing its new strategic plan. The process can be summarized as follows:

1) The National Academy of Science identifies the scientific priorities for astronomy and astrophysics every ten years.

2) OSS prepares strategic plan every three years as input to congressionally mandated NASA strategic plan.
   a) Space Science Advisory Committee (SScAC) is responsible for OSS strategic plan.
   b) Each subcommittee of the SScAC receives community input (e.g., workshops, working group reports, professional society meetings, etc.) to prepare roadmap for its science theme within context of National Academy recommendations.
   c) Roadmaps are submitted to SScAC for incorporation into OSS Strategic Plan.

3) OSS Performance Plan and metrics are prepared annually based on Presidents budget.

4) OSS Performance Report is prepared based on evaluation by SScAC and NASA Advisory Council.

3. OSS Advisory Structure
(governed by Federal Advisory Committee Act)

Community advice to OSS is provided through its advisory committees. The top level committee, the Space Science Advisory Committee advises the Associate Administrator for Space Science. The SScAC has four subcommittees, each of which represents the four science themes within OSS. Each subcommittee provides advice to the OSS Science Director responsible for the theme, The two subcommittees relevant to Astronomy and Physics are the Origins Subcommittee, and the Structure and Evolution of the Universe Subcommittee.

4. Workshop Outcome

The Scientific Organizing Committee (SOC) will distil the ideas discussed and debated in this Workshop into a concise White Paper. The objective of the exercise will be to clearly enunciate NASAs Laboratory Astrophysics needs for past and current missions, and to identify those for future missions. Broad areas of research required in the laboratory, theoretical computations and modeling should be identified as should the needs for maintaining critically compiled databases. The White Paper should be a valuable resource to scientists proposing to the Laboratory Astrophysics program, as well as to funding agencies in their budget planning process.

~ ~ **INVITED** ~ ~

Laboratory Astrophysics –
Without it there is no Astronomical Science

Martin Harwit

Astronomy Department, Cornell University, Ithaca, NY

Abstract

I review the historically earliest achievements of laboratory astrophysics and identify some urgent needs in support of major space missions in the decade ahead.

1. Origins of Laboratory Astrophysics

In 1815 Joseph Fraunhofer, an expert optical instrument maker, was able to improve the dispersion of light from the Sun, to more clearly discern a series of dark features that William Hyde Wollaston had first noticed in 1802. He had no idea what these were, but identified them sequentially, with alphabetic labels, A, B, C ... starting at the longest wavelength, 7594 Å and going to shorter. The lines at 3968 and 3934 Å were designated, respectively, H and K. Had a laboratory spectroscopist been around at the time, we would now not be referring to a star's H and K lines, but would, instead, be speaking of its ionized calcium features.

Laboratory spectroscopy, however, did not come into its own until 1859, 45 years after Fraunhofer's death. That year, the physicist Gustav Robert Kirchhoff and the chemist Robert Wilhelm Bunsen after whom the Bunsen burner is named were able to show that a minute trace of an individual element introduced into a flame could be identified by its unique signature of spectral emission lines. In their paper, published in the Philosophical Magazine in 1860, the two authors described how they were able to quantitatively estimate the tiny amount of strontium needed to produce clearly identifiable lines:

"We quickly heated an aqueous solution of chloride of strontium, of a known degree of concentration, in a platinum dish over a large flame until the water was evaporated and the basin became red-hot. The salt then began to decrepitate, and was thrown in microscopic particles out of the dish in the form of a white cloud carried up into the air. On weighing the residual quantity of salt, it was found that in this way 0.077 grm. of chloride of strontium had been mixed in the form of a fine dust with the air of the room, weighing 77000 grms. As soon as the air in the room was perfectly mixed, by rapidly moving an open umbrella, the characteristic lines of the strontium-spectrum were beautifully seen."

Kirchhoff and Bunsen also noted that the bright lines they found in the laboratory corresponded in wavelength to some of the dark lines that Fraunhofer had identified in the Sun. The two men were in no doubt about these coincidences and the momentous importance of their laboratory work. They wrote (Kirchhoff & Bunsen, 1860):

"... the method of spectrum-analysis ... opens out the investigation of an entirely untrodden field, stretching far beyond the limits of the earth, or even of our solar system. For, in order to examine the composition of luminous gas, we require, according to this method, only to see it; and it is evident that [this] mode of analysis must be applicable to the atmospheres of the sun and the brighter fixed stars."

Within a few years, William Huggins and H. Allen Miller, in England, had devised a spectrometer that could be mounted on a telescope. Huggins started by looking at a number of bright stars; but then, one evening, he pointed his telescope at a nebula in Draco, now known as the planetary nebula NGC 6543. In contrast to the stellar spectra he had observed, he found no continuum. He wrote (Huggins & Allen, 1846):

"On August 29, 1864, I directed the telescope armed with the spectrum apparatus to this nebula. At first I suspected some derangement of the instrument had taken place; for no spectrum was seen, but only a short line of light perpendicular to the direction of dispersion. I then found that the light of this nebula, unlike any other ex-terrestrial light which had yet been subjected by me to prismatic analysis, was not composed of light of different refrangibilities, and therefore could not form a spectrum. A great part of the light from this nebula is monochromatic ..."

Huggins detected three spectral lines. Thanks to laboratory results available to him, he could identify one of these as due to hydrogen; it is now known as the Hβ line. The other two were not identified until six decades later, when Ira Bowen (1927) showed them to be forbidden lines of doubly ionized oxygen atoms, [O III].

2. The Situation Today

Today, we are in somewhat the same situation that faced Huggins when he found unidentified spectral lines. An unpublished spectrum of the highly luminous semi-regular variable star VY Canis Major found in the archives of the Infrared Space Observatory (ISO) exhibits many hundreds of lines between 2.5 and 45 μm, most of which are unidentified. Until we obtain greater insight into molecular spectra, we are unlikely to make significant progress on understanding the photospheres of cool and evolved stars.

Within the next five years, four major infrared astronomical observatories are to be launched – the Space Infrared Telescope Facility, SIRTF, the Stratospheric Observatory for Infrared Astronomy, SOFIA, the Herschel Space Observatory, and ASTRO-F. In addition, large ground based telescopes will continue to probe the infrared through available atmospheric windows; the Next Generation Space Telescope, NGST, will carry out observations in the near- and mid-infrared; and the Atacama Large Millimeter Array, ALMA, is expected to begin operations at submillimeter wavelengths within a decade. All these facilities will have spectroscopic capabilities, all with exquisite sensitivity and most with extremely high spectral resolving powers. A whole host of new spectral features will be discovered and will require identification. Much of the present workshop is devoted to laboratory studies in support of the new data that these facilities will provide on infrared and submillimeter spectra of gases. The question, however, is whether the level of effort currently pursued, world-wide, is sufficiently high?

The Herschel Space Observatory, expected to fly in 2007, is likely to gather spectral information on perhaps thousands of spectral features of interstellar material at extremely low temperatures. The overwhelming majority of these will not have been identified unless urgently needed laboratory spectral work can be funded. If reasoned follow-up observations are to be undertaken to study newly unveiled spectral features, during the limited lifetime of this cryogenically cooled mission, we will need to obtain laboratory data in advance, rather than long after it has flown. We are unlikely soon to get another chance to fly a similarly costly observatory to carry out a separate set of follow-on observations. Our operations will need to be far more streamlined, incorporating laboratory studies into a mission plan sufficiently far in advance so that data needed to interpret likely findings are in hand by the time the mission is launched.

The situation is similar in the high-energy domain. Spectra obtained with the Chandra and XMM-Newton observatories show many weak X-ray lines, most of which remain unidentified. They are critical to understanding processes taking place at temperatures ranging in the many millions of degrees Kelvin, in accretion disks around neutron stars and black holes, in highly energetic jets emanating from Active Galactic Nuclei (AGNs), and in massive clusters of galaxies. A great deal of work remains to be done if the nature of these features is to be understood before Chandra and XMM-Newton are decommissioned.

3. A New Era

Today's astrophysical space projects are qualitatively different from those conducted a decade ago. Until the mid-1990s, sensitivities were too low, in most spectral ranges, for anything but imaging, photometry, and spectrophotometry. Most of the information gathered dealt with the mapping of sources and with their spectral energy distributions. IRAS, launched in 1983 was typical of such efforts, as was ROSAT, launched in 1990. With ISO, launched in 1995, and with Chandra and XMM, both launched in 1999, the emphasis of astrophysics has dramatically changed. With the advent of higher-resolution spectroscopy in virtually every spectral region observed by powerful new space missions, we are entering an era where we will be looking not merely at structure, temperature, and densities of sources, but at the chemical reactions and physical processes on solar system, stellar, galactic and intergalactic scales. Gamma-ray observations have not yet reached this more advanced stage, but undoubtedly soon will.

Dynamical processes can no longer be understood in isolation. A close coupling exists between the dynamics of a source and the chemical processes and magnetic configuration changes taking place – we speak now of chemodynamics, combustion fronts, conflagration fronts and Alfvén numbers of magnetohydrodynamic shocks. On all of these topics, experiments and theory need to complement each other to provide us the physical and chemical insights needed to fully interpret observational data.

4. Archiving the Information in Online Catalogs

The laboratory investigations emphasized at this workshop are of immense importance in themselves, but are given great added value if they can be made readily accessible. The literature on laboratory results and attendant theoretical calculations is enormous but largely inaccessible – lost in a motley array of publications and archives serving the most diverse disciplines ranging from combustion engineering to astrophysics and from aerodynamics to nuclear chemistry.

A full-scale incorporation of laboratory investigations into more accessible archives needs to be accompanied by a system that permits researchers to quickly find the data they need in machine-readable form, while also providing some sense of the quality of each data set. Such efforts are not easy. They require judgment and insight. Unfortunately, the importance of such efforts to our science have been generally underestimated and they remain badly underfunded. Unless cataloging efforts receive considerably greater support, we will not have reliable access to laboratory astrophysical data already in hand to properly interpret data from space missions to be launched in the decade ahead.

5. Concluding Thoughts

Laboratory astrophysics, despite best efforts, has not kept up with the increasingly sophisticated missions we launch into space. Not comprehending the significance of key findings in time, we are unable to design the logical follow-on observations we should be carrying out while a mission is still in progress. Returning many years later to pursue a puzzle not understood in time will prove costly.

While we cannot unerringly foresee all the supporting laboratory data that currently planned missions will require, we do know that our efforts need to be greatly expanded. We must do our best to convince our funding agencies that supporting laboratory astrophysics – experimental efforts coupled to theoretical underpinnings – is now the right investment at the right time. These efforts are basic to advance our understanding of the structure and evolution of the Universe and the origins of the vibrant world around us.

Without laboratory astrophysics there can be no astronomical science!

REFERENCES

Bowen, I. 1927, *PASP* **39**, 295
Huggins, W. & Miller, W. A. 1864, *Philosophical Transactions Royal Society of London*, **154**, 139
Kirchhoff, G. & Bunsen, R. 1860, *Philosophical Magazine* 4th series, **20**, 89

~ ~ *INVITED* ~ ~

X-ray Spectroscopy and Atomic Data

Ehud Behar and Steven M. Kahn

Columbia Astrophysics Laboratory, Columbia University, New York, NY

Abstract

The Laboratory Astrophysics program employing the Lawrence Livermore National Laboratory (LLNL) Electron Beam Ion Trap (EBIT) has been providing useful atomic data in support of the X-ray missions *Chandra* and *XMM-Newton*. Major achievements have been made for Fe-L ions in hot, collisional plasmas, relevant to stellar coronae, supernova remnants, elliptical galaxies, and galaxy clusters. Measurements for L-shell ions of other cosmically important elements are also required, some of which are in the LLNL EBIT pipeline. On the other hand, data for inner-shell excited lines relevant to photoionized plasmas near accretion sources are largely lacking. Even the wavelengths of these lines are only poorly known, which severely limits their use for diagnostics, despite the great potential.

1.   Introduction

With the advent of the high-resolution grating spectrometers on board the *Chandra* and *XMM-Newton* X-ray observatories, spectroscopy has taken central stage in the rejuvenated field of X-ray Astronomy. The increasing role of spectroscopy as a tool for astrophysical measurements has naturally drawn attention to the relevant atomic physics and atomic data, as those are directly linked with the ability to draw meaningful conclusions from observed spectra. The X-ray wavelength band between 1 and 100 Å, which is covered complementally by the *Chandra* and *XMM-Newton* spectrometers, contains a rich forest of spectral lines emitted by highly charged ions that form at electron temperatures of kT_e = 0.1 - 3 keV. At these high temperatures, most of the cosmically abundant elements from C to Ni are stripped down to their K shell (i.e., $n = 1$, n being the principal quantum number) and emit relatively few spectral lines. Additionally, many strong lines of L-shell ($n = 2$) ions of Si to Ni fall in this wavelength range. The eight ionization stages in the L shell can provide more precise information on the temperature structure of the source, independent of elemental abundances, than the two K-shell ionization stages are capable of.

2.   The Central Role of Fe-L

The most prominent L-shell X-ray lines in astrophysical spectra are those of iron. Fe-L line emission has been used recently to probe the hot temperature structure in stellar coronal sources (Brinkman *et al.* 2001), supernova remnants (van der Heyden *et al.* 2002) and galaxy clusters (Peterson *et al.* 2001). In general, transitions for both K- and L- shell ions can be calculated with available atomic codes. Nevertheless, historically, the Fe L-shell lines have been considered highly uncertain, presumably because of the increasing complexity of multi-electron atoms.

To address these issues, an X-ray spectroscopy laboratory-astrophysics program was initiated 11 years ago and is still active today (PI's Kahn and Beiersdorfer). The program is built around the unique capabilities of the LLNL EBIT to measure electron ion interactions. Driven by the astrophysical motivation, these efforts have, so far, focused primarily on the Fe L-shell complex. In particular, high-precision measurements for wavelengths and collisional excitation cross-sections (relative and absolute) have been published. Also, peculiar line ratios of Fe^{16+} that have been puzzling astronomers for years have been investigated and much of the atomic uncertainty has been disentangled from the real astrophysical issues. For more details see the contribution of Brown *et al.* in these proceedings.

As the first astrophysical grating spectra became available, our team has made a systematic attempt to test the ability of existing models to reproduce the observed emission line intensities. It was found (Behar, Cottam, & Kahn 2001a; Brinkman *et al.* 2001) that, generally, the observed line intensities could be fairly well reproduced by state-of-the-art distorted wave calculations. For instance, the HULLAC code (Bar-Shalom, Klapisch, & Oreg 2001) was used in those works. In particular, the Fe-L line intensities in the model including all of the high-n lines were found to fare quite well, implying that the calculated excitation rates and ensuing radiative cascades are fairly adequate. Conversely, accurate wavelengths still needed to be incorporated from laboratory measurements. A more detailed confrontation of the atomic calculations with Fe-L spectra of stellar coronae can be found in Behar *et al.* (2001b), where a comparison of calculations with the spectra of bright stellar coronal sources such as Capella and HR 1099 confirms that, just like the K-shell atomic data, the Fe L-shell data, when calculated correctly, are highly reliable and therefore very useful. The latest versions of the widely used databases MEKAL (Mewe, Kaastra, & Liedahl 1995) and APEC (Smith *et al.* 2001) now incorporate similar HULLAC data calculated by D. Liedahl with an earlier version of the code.

3. Remaining Atomic Data Issues

Although in general state-of-the-art models are doing well, several discrete, but nonetheless important, discrepancies still remain. In particular, the ratios of the 3s - 2p line intensities relative to those of the 3d - 2p transitions of the same charge state were found to be anomalously high for both Fe^{16+} and Fe^{17+}. Similar effects have also been found in other late-type stars, and even in elliptical galaxies (Xu *et al.* 2002), which suggests that they are not associated with the astrophysical conditions. The origin of this discrepancy has been recently studied in many theoretical and experimental works (Laming *et al.* 2001; Doron & Behar 2002; Beiersdorfer *et al.* 2002), not all in agreement with each other. Additionally, the L-shells of other cosmically abundant elements remain largely unexplored. Major efforts in this direction are being conducted by Lepson *et al.* (see these proceedings).

This is the place to note that the atomic processes associated with the X-ray emission depend on the type of plasma at the source. So far, we have focused on hot, collisional plasmas that are governed by electron impact ionization and excitation. This type of plasma is relevant to X-ray observations of stellar coronae, supernova remnants, the hot ISM in old galaxies, the intergalactic haloes of galaxy clusters, and to the overwhelming majority of laboratory plasmas.

On the other hand, X-ray sources that are ionized and excited by an external radiation field, e.g., active galactic nuclei (AGN) and X-ray binaries, require atomic data for photon impact processes. Modeling line emission from photoionized sources involves radiative recombination and photoexcitation rates (i.e., oscillator strengths). In a recent paper on the X-ray spectrum of the type II AGN NGC 1068 (Kikhabwala *et al.* 2002), we have shown that the available data for the K-shell ions are very good for reproducing the X-ray spectra from photoionized sources. Work is in progress to test the status of the Fe-L data for photoionized sources. Similar data are routinely used to model absorption spectra. In absorption, however, one also observes inner-shell transitions, for which until recently there was an enormous lack of atomic data.

4.   The Urgent Need for Inner-shell Absorption Measurements

The grating spectrometers on board *Chandra* and *XMM-Newton* enable us for the first time to detect X-ray absorption lines due to inner-shell photoexcitation. Since gas under almost any conditions absorbs X-rays, these lines are ubiquitous to X-ray absorption observations. Detections of inner-shell absorption lines have been reported mostly in the ionized outflows of AGN, but also for absorption by neutral ISM. Inner-shell absorption can probe the entire range of ionization states from neutral up to highly-ionized Li-like species. Consequently, these lines impose unprecedented, strict, constraints on the ionization structure in the absorbing medium. Since there were extremely few relevant atomic data for these features in the literature, in order to analyze the spectra, we had to embark on a tedious endeavor of calculating numerous lines (Behar, Sako, & Kahn 2001c; Behar & Netzer 2002). Calculations by the Ohio State team have also contributed to this effort (Pradhan 2000; Nahar, Pradhan, & Zhang 2001; Pradhan *et al.* 2002). None of these calculations have been benchmarked in the laboratory.

One case where X-ray absorption lines (including inner-shell excited) are particularly useful is for measuring velocities in AGN outflows (e.g., Kaspi *et al.* 2001). For these measurements, the rest frame wavelengths of the lines need to be known to very high accuracies. The case of inner-shell $K\alpha$ absorption by oxygen is particularly interesting because it could potentially relate the traditional X-ray absorber (O^{6+} and O^{7+}) with absorbers of other wavebands (e.g., O^{5+} in the UV). Whether these absorbers represent the same kinematic systems or not has been debated in the AGN community for some time now. The correct diagnostics of the inner-shell absorption lines could potentially provide a conclusive answer to this interesting astrophysical question. In order to demonstrate the large uncertainties of the currently available atomic data, in Table 1 we present three different calculations for the wavelengths of the strongest $K\alpha$ inner-shell absorption lines of O^{1+} through O^{5+} and also compare them with the deduced wavelengths from the *Chandra*/LETGS obs ervation of NGC 5548, courtesy of J. Kaastra. The wavelengths from NGC 5548 were obtained assuming that the outflow velocities of all ions are similar to that of the well-calibrated O^{6+} velocity. This assumption may not be valid, but with the lack of laboratory measurements, it provides a rough idea of where to expect these lines.

Although one might have expected the R-matrix method to be the most rigorous, it is clear from the table that at the current state of the atomic data, it is virtually impossible to determine what are the correct rest frame positions of these lines. The discrepancies among

the various methods reach 50 mÅ, which corresponds here to uncertainties in the measured velocities of 700 km/s. This uncertainty is of the same order as typical outflow velocities in nearby active galaxies, implying that these lines are practically useless for this purpose, despite their great potential. Laboratory measurements are desperately needed.

5. Suggested Z Pinch Measurements

Currently, the best available facility for producing inner-shell absorption lines and measuring their wavelengths and optical depths is the z pinch at Sandia National Laboratory. The powerful z pinch experiments (X-ray fluxes reaching 10^{19} erg s^{-1} cm^{-2}) produce long-lived (6 ns), steady- state, photoionized gas (Bailey et al. 2001), which can be studied with high resolution spectrometers, in both emission and absorption simultaneously. The ionizing spectrum can be characterized quite accurately by a blackbody spectrum. The control over the position and density of the targets in these experiments provides a sensitive handle on the ionization state and column density in the absorbing medium. These capabilities were demonstrated by Bailey et al. (2001), where absorption by photoionized Ne has been measured. The spectrum obtained with a crystal spectrometer in that experiment shows many nicely resolved individual lines, which allows for accurate wavelength and equivalent- width measurements.

Table 1. Wavelengths in Å for the strongest 1s - 2p inner- shell absorption lines in O ions.

Ion	R-matrix [a]	Cowan's Code [b]	HULLAC [c]	NGC 5548 [d]
O^{1+}	23.27	23.31	23.30	$\cdots$
O^{2+}	23.08	23.10	23.11	23.17 ± 0.01
	23.02	23.08	23.05	23.00 ± 0.02
	22.93	23.01	22.98	$\cdots$
O^{3+}	22.73	22.77	22.73	22.74 ± 0.02
	22.67	22.76	22.78	$\cdots$
	22.67	22.76	22.73	$\cdots$
O^{4+}	22.35	22.38	22.33	22.38 ± 0.01
O^{5+}	22.05	22.05	22.00	22.01 ± 0.01
	21.87	21.85	21.79	$\cdots$

[a] From Pradhan et al. (2002)

[b] Raassen & Kaastra, private communication

[c] Present work

[d] Kaastra, private communication

6. Summary and Prospects

Many atomic data needs for hot, collisional plasmas relevant to X-ray spectroscopic observations, now regularly obtained with the gratings on board *Chandra* and *XMM-Newton*, have been provided by the ongoing LLNL EBIT programs of Kahn and Beiersdorfer. Particularly, these programs have provided the most important data for Fe-L emission by hot gas and work is in progress to measure many more high-quality data for other L-shell systems. Now that we actually have high-resolution cosmic spectra, we can determine better than before which atomic data are the most crucial. Thus, the most urgent needs of the X-ray astronomy community for collisional plasmas will continue to be addressed with the EBIT Laboratory Astrophysics Program. Photoionized gases have received less attention as they are more rare in nature and very few laboratory experiments have sufficient X-ray flux to produce them. Particularly missing are measurements for inner-shell absorption lines. The current uncertainties in the positions of these lines considerably limit our ability to use them for diagnostics. In the future, we intend to try to use z pinch experiments to remedy this deficiency.

REFERENCES

Bailey, J., *et al.* 2001, *J. Quant. Spectr. Radiat. Transfer*, **71**, 157.

Bar-Shalom, A., Klapisch, M., & Oreg, J. 2001, *J. Quant. Spectr. Radiat. Transfer*, **71**, 169.

Behar, E., Cottam, J., & Kahn, S.M. 2001a, *ApJ*, **548**, 966.

Behar, E., *et al.*, 2001b in *X-ray Astronomy 2000* ASP Conference Series Vol. 234, ed. R. Giacconi, S. Serio, & L. Stella (ASP, San Francisco), page 85.

Behar, E., Sako, M., & Kahn, S.M. 2001c, *ApJ*, **563**, 497.

Behar, E. & Netzer, H. 2002, *ApJ*, **570**, 165.

Beiersdorfer, P., *et al.* 2002, *ApJ Letters*, **submitted**.

Brinkman, A.C., *et al.* 2001, *A&A*, **365**, L324.

Brown, G.V., *et al.*, 1998, *ApJ*, **502**, 1015 (erratum 532, 1245 [2000]).

Brown, G.V., Beiersdorfer, P., Chen, H., Chen, M.H., & Reed, K.J. 2001, *ApJ*, **557**, L75.

Doron, R., & Behar, E. 2002, *ApJ*, **574**, July 20 issue.

Kaspi, S., *et al.* 2001, *ApJ*, **554**, 216.

Kinkhabwala, A., *et al.* 2002, *ApJ*, in press (astro-ph/0203290).

Laming, J.M., *et al.* 2000, *ApJ*, **545**, L161.

Mewe, R., Kaastra, J.S., & Liedahl, D.A. 1995, *Legacy*, 6, 16.

Nahar, S.N., Pradhan, A.K., & Zhang, H.L. 2001 *Phys. Rev. A* **63**, 060701(R).

Peterson, J.R., *et al.* 2001, *A&A*, **365**, L104.

Pradhan, A.K. 2000 *ApJ*, **545**, L165.

Pradhan, A.K., *et al.* 2002, *ApJ*, (astro-ph/0204116).

Smith, R.K., Brickhouse, N.S., Liedahl, D.A., & Raymond, J.C. 2001, *ApJ*, **556**, 69.

van der Heyden, *et al.*, *A&A*, in press (astro-ph/0203160).

Xu, H., *et al.* 2002, *ApJ*, submitted (astro-ph/0110013).

~ ~ *INVITED* ~ ~

Atomic Data and Stellar Chemical Compositions

Christopher Sneden

Department of Astronomy & McDonald Observatory, University of Texas at Austin

James E. Lawler

Department of Physics, University of Wisconsin at Madison

John J. Cowan

Department of Physics and Astronomy, University of Oklahoma

Harriet L. Dinerstein

Department of Astronomy & McDonald Observatory, University of Texas at Austin

Abstract

New high resolution spectrographs for 8-meter telescopes, and NASA missions such as HST, FUSE, and SOFIA, provide spectra of unprecedented quality for stars and nebulae over a large metallicity range. Analyses of these spectra should yield a reconstruction of the origin and evolution with time of all major element groups in the Periodic Table. Rapid progress has been made in our understanding of the trends with metallicity and scatter at a given metallicity for some elements, but large abundance uncertainties remain for many others, due to lack of accurate atomic data for many transitions that are accessible in stellar spectra. We review some recent successes in campaigns to upgrade the atomic data for the first three ionization stages of many rare-earth elements, and show the application of these new data to solar and stellar abundances. Examples are given of abundances extracted from complex UV stellar spectra for elements important for nucleosynthesis studies, discoveries of previously unidentified features of heavy elements in planetary nebulae, and one of the many new frontiers in abundance work: investigations of the IR spectra of globular cluster stars. These examples demonstrate the need for further development of comprehensive sets of accurate atomic parameters for many species present in stars and nebulae.

1. Introduction

Fifty years ago there were only a few coudé spectrographs operating on 2m to 3m telescopes, and their available detectors were limited to low quantum efficiency photographic plates. High resolution spectroscopy in those times meant the study of relatively bright stars in the "optical" wavelength domain (about 3500–8500 Å), and the typical spectra that were obtained had S/N values less than about 50. Today large ground-based telescopes have 10m apertures, high-throughput echelle spectrographs, and low-noise CCD detectors that are nearly photon-counting devices; thus high resolution, high S/N optical spectra can be obtained for much fainter stars that live in far reaches of the Galaxy. New large-aperture infrared-optimized telescopes such as Gemini and Subaru will provide dramatic advances in IR spectroscopy of faint sources. Wavelength domains inaccessible to ground-based high resolution spectroscopy have been opened by NASA missions, such as HST, FUSE, and (in the near future) SOFIA. Trustworthy abundance analyses from these spectra depend not only on the observed data but

Trustworthy abundance analyses from these spectra depend not only on the observed data but on the quality of modeling efforts, including realistic descriptions of the physical states of the objects being studied and reliable atomic (and molecular) data. When spectroscopic data were poor there was little pressure on the quality of atomic data (transition probabilities, collisional cross-sections, hyperfine and isotopic splitting constants). But current stellar and nebular spectra clearly reveal features that have only rudimentary lab data. Here we point to a few recent successes that marry high quality astronomical spectra with excellent lab data, and suggest a few other areas in need of more work.

2.   Success: Neutron-Capture Elements in Very Metal-Poor Stars

Neutron-capture elements ($Z > 30$) are those whose major isotopes are formed through slow or rapid neutron bombardment reactions (the s- and r-processes, respectively) in very late stages of stellar evolution. The Sun's abundance mix reflects major contributions by both synthesis extremes. But some very metal-poor stars born at the early stages of our Galaxy exhibit large relative enhancements of these elements with respect to iron, and the abundance pattern of those elements with $Z > 55$ is very well matched by pure r-process synthesis. This assertion is fortified by derivation of reliable abundances for a large number of n-capture elements (including nearly every one of the lanthanide rare earths, $57 \leq Z \leq 71$) in a few well-studied stars (e.g., Sneden *et al.* 2002, Hill *et al.* 2002, Cowan *et al.* 2002). Those papers show that abundances derived from multiple lines of a given species are often in excellent agreement. This would not be possible without the recent publication of high quality lab data for these elements, mainly by groups in the United States (e.g., Lawler *et al.* 2001), Belgium (e.g., Palmeri *et al.* 2000) and Sweden (e.g., Nilsson *et al.* 2002). Such improvements in lab data, which result in small internal uncertainties, help in three ways: (a) in stellar spectra with large numbers of detected lines of individual species, separation of clean features from blended transitions that are not useful for abundance determinations; (b) in stars with more limited spectral information, confident employment of only a small number of lines; and (c) potential discovery of other abundance limitations, such as poorly determined atomic partition functions or flaws in the physical modeling of the stellar atmospheres. This work must continue, for many species easily detectable in stellar spectra lack published modern lab analysis (e.g. Nd II, He II).

3.   UV Spectra of Very Light Elements: Contamination Problems

Be and B are light elements destroyed in stellar interiors and probably manufactured in cosmic ray spallation reactions. Understanding the abundance trends of these elements with metallicity is an important component of Galactic chemical evolution studies, but observationally there are difficulties because the only strong transitions of these elements lie below 3200 Å. Here we just consider the case of Be. The Be II resonance lines lie near 3130 Å, just barely accessible to ground-based spectroscopy. Boesgaard and collaborators have investigated these lines in a series of papers, and Boesgaard *et al.* (1999) summarize their studies of Be in metal-poor stars. Figure 1 of that paper illustrates the obvious source of abundance uncertainty: the Be II transition probabilities are very well determined, but the lines are extremely blended with

other atomic and molecular species that mostly are without accurate lab gf's. For metal-rich stars it is difficult to derive trustworthy Be abundances in spite of the excellent efforts of the Boesgaard group and other teams. Further progress in atomic data might be more helpful than additional stellar spectra for this problem.

4. Heavy Elements in Planetary Nebulae: A New Frontier

Planetary nebulae exhibit strong emission lines of multiply ionized species of abundant light elements, but recent work suggests that heavier elements with smaller abundances may be detectable as well. Péquignot & Baluteau (1994) proposed that many neutron-capture elements including Kr, Xe, and Ba are present in NGC 7027. New examination of high quality spectra of this and another planetary nebula at both IR and optical wavelengths (Dinerstein 2001) provides strong evidence that Kr and Se are indeed present in such objects. A noteworthy feature of Dinerstein's analysis is the effort expended in solidifying the proposed identifications of some observed emission lines as [Kr III] and [Se IV] features. These identifications depend on the most basic of atomic data: accurately known energy levels. Also necessary for abundance determinations are collisional cross-sections and transition probabilities. These are beginning to become available (e.g. Schöning 1997; Schöning & Butler 1998) but much more work is needed. The Kr and Se detections represent the tip of a large iceberg. Many unidentified weak emission lines exist in the spectra of planetary nebulae and wavelength regions which require NASA missions have barely been touched. New lab studies of species likely to be present in nebular conditions are highly desirable.

5. Help Wanted: Atomic Lines in IR Spectra

Some atmospheric windows permit acquisition of high resolution spectra in some IR windows, and the SOFIA mission will include a high resolution mid IR spectrograph (Richter *et al.* 1998). These instruments will reveal atomic spectral features that often are identified but lack any other lab data. As one example, Pilachowski & Sneden (2002) gathered high resolution 2μm spectra of stars in the globular cluster M3, in an effort to determine carbon isotopic ratios from the CO bands. The spectra also contain regions of unblended atomic lines; for example in 2.22μm to 2.26μm range there are nearly ten detectable lines of the neutral species of Mg, Si, Ti, and Fe. Frustratingly, the NIST group has only one of these lines even listed in its atomic spectra database, and that line has no transition probability. One is stuck with the option of either using predicted values from R. L. Kurucz's compendium of semi-empirical gf's, or doing a differential analysis with respect to the Sun or other star. Further lab work is needed here, or the time, effort, and money that went into the telescopes, instruments, and observations will be only partially usable.

Acknowledgments

REFERENCES

Boesgaard, A. M., et al. 1999, *AJ*, **117**, 1549.

Cowan, J. J., et al. 2002, *ApJ*, **572**, 861.

Dinerstein, H. L. 2001, *ApJ*, **550**, L223.

Hill, V., et al. 2002, *A&A*, **387**, 560.

Lawler, J. E., Wickliffe, M. E., Cowley, C. R., & Sneden, C. 2001, *ApJS*, **137**, 341.

Nilsson, H., et al. 2002, *A&A*, **382**, 368.

Palmeri, P., Quinet, P., Wyart, J.-F., & Biémont, E., 2000, *Phys. Scr.*, **61**, 323.

Péquignot, D., & Baluteau, J. P. 1994, *A&A*, **283**, 593.

Pilachowski, C. A., & Sneden, C. 2002, *BAAS*, **33**, 1513.

Richter, M. J. et al. 1998, *Proc. SPIE*, **3354**, 962.

Schöning, T. 1997, *A&AS*, **122**, 277.

Schöning, T., & Butler, K. 1998, *A&AS*, **128**, 581.

Sneden, C., et al. 2000, *ApJ*, **533**, L139.

Theoretical Studies of Pressure Broadened
Alkali-Metal Atom Resonance Lines

J. F. Babb and K. Kirby

Harvard-Smithsonian Center for Astrophysics, Cambridge, MA

H.-K. Chung

Lawrence Livermore National Laboratory, Livermore, CA

Abstract

We discuss our recent calculations of pressure broadening of alkali-metal atomic resonance lines by perturbing gases and their applications to studies of brown dwarf and extrasolar giant planet atmospheres.

1. Introduction

A new frontier has been opened with the discovery of numerous brown dwarfs and extrasolar giant planets (EGPs) (Burrows *et al.* 2001). Brown dwarfs and EGPs have many similarities and there is a substantial overlap of their parameter space of temperature, mass, atmospheric composition and chemistry. Theoretical calculations of the spectra of brown dwarfs (Schweitzer *et al.* 1996; Marley *et al.* 1996; Allard *et al.* 1996; Martin *et al.* 1999; Kirkpatrick *et al.* 1999, 2000; Schweitzer *et al.* 2001) and irradiated planets (Seager & Sasselov 1998, 2000; Seager *et al.* 2000; Sudarsky *et al.* 2000; Barman *et al.* 2001; Hubbard *et al.* 2001; Brown 2001) have established the importance of the alkali-metal resonance lines and their role as diagnostic probes of the environment in which they are produced.

In November 2001, NASA announced the first detection of the atmosphere of an extrasolar giant planet, using the STIS spectrograph on board the Hubble Space Telescope (HST). The planet was detected during its transit of the star HD 209458 in the sodium resonance line doublet around 589 nm. This work (Charbonneau *et al.* 2002) has demonstrated that it is possible to obtain information on extra-solar planetary atmospheres using HST instruments, and the observations have already generated considerable interest among modelers, e.g. Barman *et al.* (2002). Thus, it is a NASA priority to provide the fundamental research and *analysis* necessary to detect and *characterize* other planetary systems. In addition, vital spectroscopic information which informs the planning of possible future space missions that would perform spectroscopy of extra-solar planets is a high priority.

The resonance lines of sodium and potassium are so profoundly pressure-broadened in L-dwarfs and T-dwarfs that their wings extend several hundred nanometers from the line center, cf. (Tinney *et al.* 1998; Martin *et al.* 1997). The absorption lines appear to be the broadest ever observed in an astronomical object (Pavlenko 2001; Burrows *et al.* 2001; Allard *et al.* 2001). Collisions with H_2 and He account for most of the broadening, but other molecules present in the atmospheres of these objects will also contribute. This strong pressure-broadening "stretches the current theories of line broadening beyond their limit of validity," as pointed out by Marley *et al.* (2002).

Reliable calculations of pressure broadening in the far spectral wings require accurate potential energy curves or surfaces describing the interaction of the ground and excited states of the absorber atom with the perturber atom or molecule. In addition, transition dipole moments for the resonance line absorption, as a function of the geometry of the absorber-perturber system, are necessary.

In our previous work on Na-Na (Chung et al. 2001b), we utilized combinations of published experimental data, ab initio calculations and molecular interaction potentials from ultra-cold atom studies. Quantum-mechanical calculations of the absorption spectra were carried out for four different temperatures from 1470 K to 1070 K demonstrating the strong temperature sensitivity of the line wings and excellent agreement with experiment (Schlejen et al. 1987) was obtained. Moreover, it is apparent that the use of van der Waals broadening to describe the line wings would be exceptionally poor.

In further studies (Chung et al. 2001a, 2002), theoretical calculations of the line profile of Na perturbed by He were performed using potentials of Theodorakopoulos & Petsalakis (1993). Our preliminary results for a range temperatures are shown in Fig. 1 and agreement with experimental measurements (Chung et al. 2002) carried out at about 900 K is satisfactory.

The methods used herein can be applied to determine the spectra of other alkali-metal atoms such as K under the influence of He or other perturbing gases such as H_2. These calculations are in progress and they will be benchmarked against measurements in our group of Na resonance lines broadened by H_2, N_2, and CH_4 (Shurgalin et al. 2002).
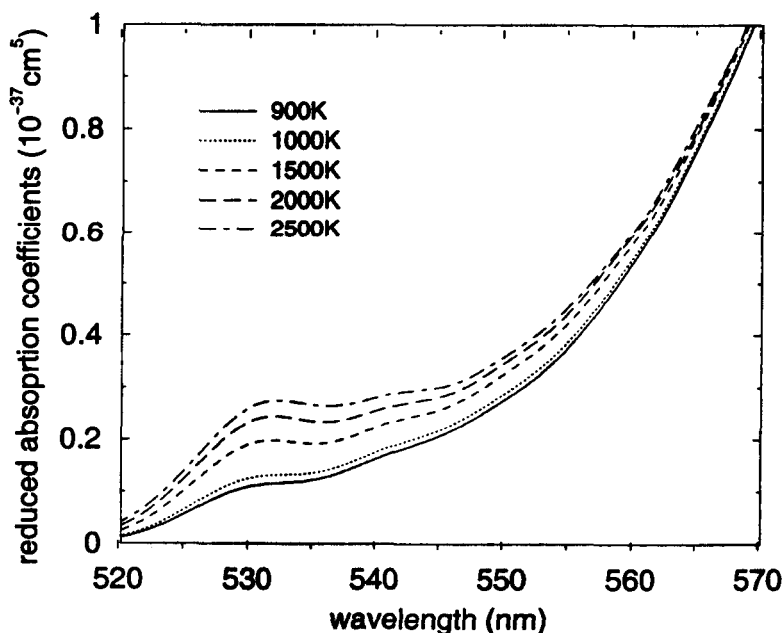
Fig. 1.— Calculations of the reduced absorption coefficients in the blue wing of the Na D line perturbed by He at temperatures of 900 K, 1000 K, 1500 K, 2000 K and 2500 K.

Acknowledgments

REFERENCES

Allard, F., Hauschildt, P. H., Alexander, D. R., Tamanai, A., & Schweitzer, A. 2001, *ApJ*, **556**, 357.

Allard, F., Hauschildt, P. H., Baraffe, I., & Chabrier, G. 1996, *ApJ*, **465**, L123.

Barman, T. S., Hauschildt, P. H., & Allard, F. 2001, *ApJ*, **556**, 885.

Barman, T. S., Hauschildt, P. H., Schweitzer, A., Stancil, P. C., Baron, E., & Allard, F. 2002, *ApJ*, **569**, L51.

Brown, T. M. 2001, *ApJ*, **553**, 1006.

Burrows, A., Hubbard, W. B., Lunine, J. I., & Liebert, J. 2001, *Rev. Mod. Phys.*, **73**, 719.

Charbonneau, D., Brown, T. M., Noyes, R. W., & Gilliland, R. L. 2002, *ApJ*, **568**, 377.

Chung, H.-K., Kirby, K., & Babb, J. F. 2001a, *Bull. Am. Phys. Soc.*, **46**, 36.

—. 2001b, *Phys. Rev. A*, **63**, 032516.

Chung, H.-K., Shurgalin, M., Yoshino, K., Parkinson, W. H., Kirby, K., & Babb, J. F. 2002, in preparation.

Hubbard, W. B., Fortney, J. J., Lunine, J. I., Burrows, A., Sudarsky, D., & Pinto, P. 2001, *ApJ*, **560**, 413.

Kirkpatrick, J. D., Reid, I. N., Liebert, J., Cutri, R. M., Nelson, B., Beichman, C. A., Dahn, C. C., Monet, D. G., Gizis, J. E., & Skrutskie, M. F. 1999, *ApJ*, **519**, 802.

Kirkpatrick, J. D., Reid, I. N., Liebert, J., Gizis, J. E., Burgasser, A. J., Monet, D. G., Dahn, C. C., Nelson, B., & Williams, R. J. 2000, *AJ*, **120**, 447.

Marley, M. S., Saumon, D., Guillot, T., Freedman, R. S., Hubbard, W. B., Burrows, A., & Lunine, J. I. 1996, *Science*, **272**, 1919.

Marley, M. S., Seager, S., Saumon, D., Lodders, K., Ackerman, A. S., Freedman, R. S., & Fan, X. 2002, *ApJ*, **568**, 335.

Martín, E. L., Delfosse, X., Basri, G., Goldman, B., Forveille, T., & Zapatero Osorio, M. R. 1999, *AJ*, **118**, 2466.

Martín, E. L., Basri, G., Delfosse, X., & Forveille, T. 1997, *A&A*, **327**, L29.

Pavlenko, Y. V. 2001, *Astronomy Reports*, **45**, 144.

Schlejen, J., Jalink, C. J., Korving, J., Woerdman, J. P., & Müller, W. 1987, *J. Phys. B*, **20**, 2691.

Schweitzer, A., Gizis, J. E., Hauschildt, P. H., Allard, F., & Reid, I. N. 2001, *ApJ*, **555**, 368.

Schweitzer, A., Hauschildt, P. H., Allard, F., & Basri, G. 1996, *MNRAS*, **283**, 821.

Seager, S. & Sasselov, D. D. 1998, *ApJ*, **502**, L157.

—. 2000, *ApJ*, **537**, 916.

Seager, S., Whitney, B. A., & Sasselov, D. D. 2000, *ApJ*, **540**, 504.

Shurgalin, M., Chung, H.-K., Yoshino, K., Parkinson, W. H., Kirby, K., & Babb, J. F. 2002, in preparation.

Sudarsky, D., Burrows, A., & Pinto, P. 2000, *ApJ*, **538**, 885.

Theodorakopoulos, G. & Petsalakis, I. D. 1993, *J. Phys. B*, **26**, 4367.

Tinney, C. G., Delfosse, X., Forveille, T., & Allard, F. 1998, *A&A*, **338**, 1066.

Laboratory Study of the Diagnostic Utility
of the 3C/3D Line Ratio in Fe XVII

G. V. Brown

NASA Goddard Space Flight Center, Greenbelt, MD

P. Beiersdorfer, H. Chen, M. H. Chen, and K. J. Reed

Physics and Advanced Technology, Lawrence Livermore National Laboratory, Livermore, CA

Abstract

Fe XVII X-ray emission is present in a multitude of sources, such as the corona of the Sun, Capella, and Procyon. Two of the strongest lines observed in these spectra are the resonance and intercombination lines located at 15.01 and 15.26 Å, respectively. As part of the laboratory astrophysics program at the electron beam ion traps EBIT-I & EBIT-II located at the Lawrence Livermore National Laboratory we have measured this line ratio for the case where the relative abundance of Fe XVI to Fe XVII is ~ 1. Our results show that an Fe XVI innershell satellite line coincides with the intercombination line and can significantly reduce the relative intensity, R, of the resonance to intercombination line. The fact that the apparent relative intensity of the resonance and intercombination line in Fe XVII is sensitive to the strength of an Fe XVI innershell satellite, and therefore, the relative abundance of Fe XVI to Fe XVII, makes the line ratio a diagnostic of temperature, and explains the anomalously low ratios observed in the solar and stellar coronae.

1. Introduction

The L-shell line emission of Fe XVII is present over a large temperature range and is observed in the corona of the Sun and in extra-solar sources. Two of the most distinct lines observed from Fe XVII are the $1s^2 2s^2 2p^5_{1/2} 3d_{3/2}$ $^1P_1 \rightarrow 1s^2 2s^2 2p^6$ $^1S_0$ resonance and $1s^2 2s^2 2p^5_{3/2} 3d_{5/2}$ $^3D_1 \rightarrow 1s^2 2s^2 2p^6$ $^1S_0$ intercombination lines at 15.01 and 15.26 Å known as 3C and 3D, respectively.

Values of the relative intensity, R, of these two lines between 1.6 and 2.8 have been measured in non-flaring active regions of the solar corona. Values in the range of 2.6 to 2.8 have been measured from Capella, and recently, Raassen *et al.* (2002) have reported a value of 1.8 from Procyon. By contrast, measurements on the LLNL electron beam ion trap EBIT-II gave an average value of 3.04 ± 0.12 for electron impact excitation (Brown *et al.* 1998). The EBIT-II value agrees with only some of the higher values measured in the Sun and is marginally in agreement with the Capella ratio. A second experiment conducted at EBIT-II (Brown *et al.* 2001) has shown that an Fe XVI innershell satellite line coincides with the Fe XVII intercombination line 3D. Figure 1 shows the results of measuring the X-ray emission between 14.9 and 15.7 Å from Fe XVI and XVII with different amounts of Fe XVI present (Brown *et al.* 2001). When the relative abundance of ~ 1 (figure 1a) the relative line intensity is below 2. When no Fe XVI is present, as in figure 1c, the ratio is 3. Because R is sensitive to the relative abundance of Fe XVI and Fe XVII, it is a measure of the charge balance and thus of the electron temperature.
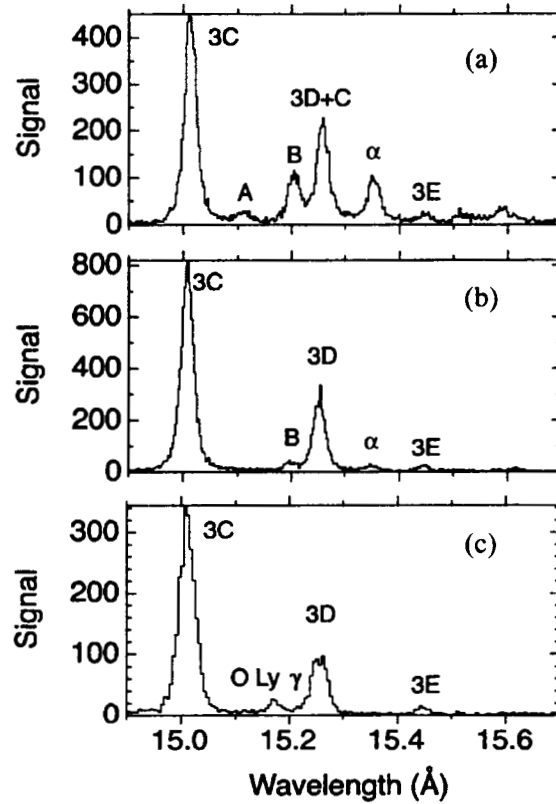
Fig. 1. Fe L-shell spectra measured for different ionization balances: (a) very low ionization balance; (b) low ionization balance (c) standard (equilibrium) ionization balance (typical for EBIT II) obtained by injection with the MeVVA. Lines 3C, 3D, and 3E are from Fe XVII. Lines A, B, and C are innershell satellites from Fe XVI, and line α is an Fe XV innershell satellite. Although oxygen is a typical background gas in EBITs, O Lyman γ is not present in (a) and (b) because iron is continuously supplied to the trap as $Fe(CO)_5$ and so it displaces the oxygen from the trap. However, when using a MeVVA, oxygen can accumulate because iron is only injected about once per second as in (c).
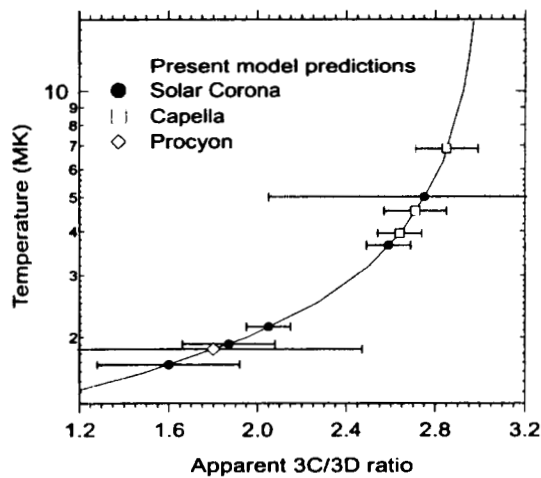
Fig. 2.— Correlation of the apparent 3C-to-3D ratio with the electron temperature. The solar points corresponding to cooler temperatures are from non-flaring active regions while the hotter solar points are from flaring active regions. The Capella data is from observations with both the LETG and the HETG on the *Chandra X-Ray Observatory*. The Procyon data is from the RGS1 on board *XMM-Newton*.

2. Discussion

The fact that an Fe XVI innershell satellite line coincides with line 3D explains the relatively low ratios measured in Capella, Procyon, and non-flaring active regions of the Sun, and can be used to predict their temperature. Figure 2 shows a plot of temperature versus R. Included are the ratios measured in the corona of the Sun, Capella, and Procyon and their predicted temperatures. We note that we do not include the value of 2.89 ± 1.8 measured by RGS2 on XMM-$Newton$ (Raassen et al. 2002), because of the large error bars. However, using the value of 1.8 ± 0.7 measured by RGS1, we predict a temperature range of 1-3 MK, consistent with the values of the peak of the emission measure given by the XMM data.

In addition to explaining the results observed in non-terrestrial sources, the line coincidence also explains the low ratios observed in other laboratory devices. Beiersdorfer et al. (2001) measured an average value of 2.48 ± 0.40 using a flat crystal Bragg spectrometer on the Princeton Large Torus tokamak. The only process available to explain the low ratio in this device is the Fe XVI line coincidence. The presence of Fe XVI is expected because the tokamak data is integrated over different temperature regions of the plasma. The ratio of 2.50 ± 0.13, measured by Laming et al. (2000) in the NIST electron beam ion trap, can also be explained by the Fe XVI line coincidence. When using an electron beam ion trap to measure X-ray emission from iron charges states greater than or equal to Fe XVII, Fe XVI is present during the ionization phase of the injection cycle, i.e, the time immediately after the injection of iron. This contamination can be avoided if only the equilibrium portion of the trapping cycle is used, i.e, the ionization phase is gated out. This is the case for the spectrum in figure 1c measured at the LLNL EBIT-II where the Fe XVI contamination is not present.

3. Summary

In summary, we have taken advantage of the fact that an innershell satellite line from Na-like Fe XVI coincides with the intercombination line 3D in Fe XVII to predict the temperature of solar and stellar coronae. This temperature diagnostic is only one of the many line diagnostics that have become available to the astrophysical community as a result of the synergy between laboratory astrophysics programs and the high-resolution spectral data provided by the *Chandra X-ray Observatory* and *XMM-Newton*. Also, this line coincidence explains the low ratios measured in other laboratory experiments where an influential amount of Fe XVI exists.

Acknowledgments

REFERENCES

Beiersdorfer, P., et al. 2001, *Phys. Rev. A*, **64**, 032705.
Brown, G. V., et al. 1998, *Astrophys. J.*, **502**, 1015.
Brown, G. V., et al. 2001, *Astrophys. J. Lett.*, **557**, L75.
Laming, M., et al. 2000, *Astrophys. J. Lett.*, **545**, L161.
Raassen, A. J., et al. 2002, *Astron.& Astrophys.*, in press.

Laboratory Astrophysics at the LLNL Electron Beam Ion Traps
EBIT-I & EBIT-II

G. V. Brown, K. R. Boyce, R. L. Kelley, F. S. Porter, C. K. Stahle,
A.E. Szymkowiak, and W. Tillotson

NASA Goddard Space Flight Center, Greenbelt, MD

P. Beiersdorfer, H. Chen, M. J. May, D. Thorn

Physics and Advanced Technology, Lawrence Livermore National Laboratory, Livermore, CA

E. Behar, M. F. Gu, S. M. Kahn

Columbia Astrophysics Laboratory, Columbia University, New York, NY

Abstract

In order to provide a complete, accurate set of atomic data for interpreting spectra provided by missions such as *XMM-Newton*, the *Chandra X-Ray Observatory*, and *Astro-E2*, we have harnessed the Lawrence Livermore National Laboratory's electron beam ion traps EBIT-I, EBIT-II, and Super-EBIT for laboratory astrophysics. In support of this work we have developed a number of unique techniques, including the ability to experimentally simulate a Maxwellian distribution of electron energies and measuring low-energy charge exchange cross sections using the "magnetic trapping mode". We have also built and operated a full suite of spectrometers spanning the 1–7000 Å wavelength band, the most recent being a spectrometer based on a spare Astro-E 6 X 6 microcalorimeter array. Results of our efforts include a complete list of wavelengths of the Fe L-shell transitions, measurements of absolute and relative cross sections for direct impact, dielectronic, and resonance excitation, and measurements of low energy charge transfer reactions. A brief overview of the LLNL ebit facility, its capabilities, and some results will be discussed.

1. Introduction

Invented at the Lawrence Livermore National Laboratory (LLNL), the electron beam ion trap; EBIT (Levine *et al.* 1988) has proven to be a useful tool for laboratory astrophysics. The success of the LLNL EBIT, EBIT-I, lead to the second EBIT, EBIT-II, completed at LLNL in 1990. EBIT-I was then modified to operate at higher electron beam energies and was renamed Super-EBIT. Later, several other EBITs were built (Silver *et al.* 1994; Gillaspy 1997; Biedermann *et al.* 1997; Curell *et al.* 1996; López-Urrutia *et al.* 2001). All of these EBITs are based on the Livermore EBIT-I design, but none is an exact replica, making the operating parameters and capabilities of each device distinct.

Over the last decade the LLNL EBITs have been harnessed as tools for laboratory astrophysics in support of the *Chandra*, *XMM-Newton*, and *Astro-E2* X-ray observatories. During this time several collaborations have been developed with astrophysical science programs, such as the Columbia Astrophysics Laboratory and the NASA/Goddard Space Flight Center. Our program has included the development of a plethora of instruments and methods for investigating astrophysically relevant problems.

2. Operating Parameters and Results

EBIT-I is the current electron beam ion trap operating at LLNL. A detailed description can be found in (Beiersdorfer *et al.* 2000). EBIT-I operates at an electron density of $\sim 5 \times 10^{11}$ cm^{-3} and has a mono-energetic electron beam energy that can be adjusted from ~ 100 eV to 100,000 eV for a given experiment. It has five ports that observe the trap directly. For these ports we choose from over 20 spectrometers covering a range of 1–7000 Å. Typically, an experiment consists of a set of vacuum crystal spectrometers (occupying two ports) covering the 10–18 Å region continuously with 1 eV resolution; a flat-field grating spectrometer that covers the 10–50 Å region; a curved-crystal spectrometer for K-shell measurements, for example, of Fe XXV; and, the NASA/GSFC spare Astro-E spectrometer, the XRS. The XRS is a 6 X 6 square microcalorimeter array consisting of 32 active channels with an area of ~ 13 mm^2 (Porter *et al.* 2001). Because of the high gain stability of all 32 active channels, we are able to accumulate data continuously without significant gain drift for over 12 hours.

In order to address problems encountered in the analysis of astrophysical spectra, we have developed several advanced operating techniques for EBIT- I. For example, to measure contributions from processes such as dielectronic recombination and resonance excitation, the e$^-$ beam is swept linearly from below excitation threshold to above threshold while the spectrum is recorded as a function of beam energy. An example of one of these experiments is given in figure 1. With the addition of the NASA/GSFC XRS, we can provide absolute excitation cross sections by normalizing to radiative recombination (Chen *et al.* 2002) (figure 2). Other results and measuring techniques include the development of a Maxwellian temperature simulator making it possible to measure spectra in thermal plasmas at different temperatures; we measured the wavelengths and identified all the Fe L-shell X-ray emission from Fe XVII–XXIV (Brown *et al.* 2002, 1998); we resolved a long standing problem with relative line intensities (Brown *et al.* 2001). Using the magnetic trapping mode (Beiersdorfer *et al.* 1994), where the electron beam is off and the ions are trapped by the magnetic field of EBIT-I, we are able to measure charge exchange recombination cross sections (see Beiersdorfer *et al.* these proceedings). The complete list of results is too numerous to list here[1].

In support of present and future X-ray missions we will continue to study astrophysically relevant radiation processes and to develop new methods and instrumentation. This includes building and installing a new dedicated EBIT Calorimeter Spectrometer (ECS). The cryogenic and refrigerator lifetime of the ECS will see a dramatic improvement, increasing the data acquisition - cryogenic Dewar refill cycle. The ECS, in addition to the regular upgrades to our spectroscopic equipment, will improve our ability to address astrophysically relevant problems.

---

[1] Visit http://www-phys.llnl.gov/Research/EBIT/ and http://homepage.mac.com/ebit for a more complete list of measurements conducted at the LLNL EBIT facility
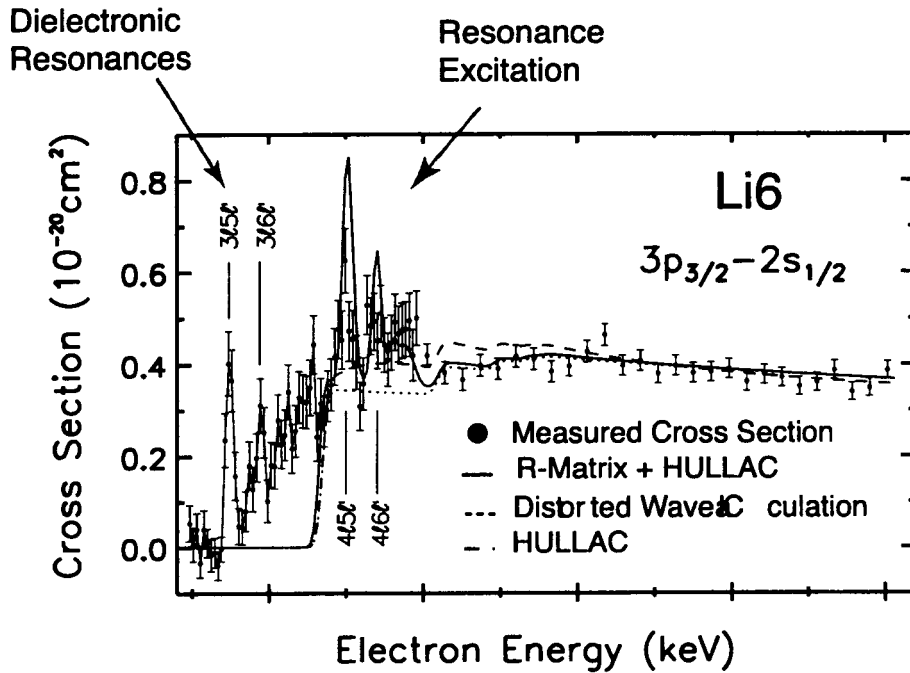
Fig. 1.— Measured cross section as a function of electron impact energy for the $3p_{3/2} \rightarrow 2s_{1/2}$ Fe XXIV line at 10.6 Å (Gu et al. 1999) labeled Li6. Notice the contribution below threshold from dielectronic recombination and the enhancement near threshold from resonance excitation.
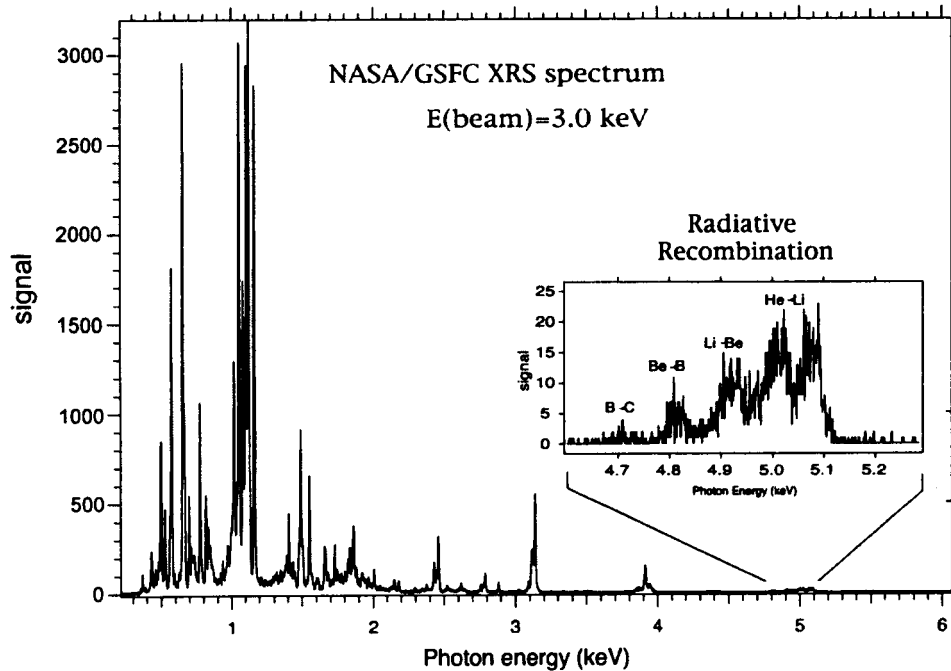
Fig. 2.— A spectrum recorded by the NASA/GSFC microcalorimeter array. This spectrum includes the weak emission from radiative recombination (RR). The measurement or the RR emission, even with a 32 pixel array, requires long integration times.

Acknowledgments

REFERENCES

Biedermann, C., *et al.* 1997, Phys. Rev. A, 56, R2522

Beiersdorfer, P., *et al.* 2000, in Atomic Data Needs for X-ray Astronomy, ed. M. A. Bautista, T. R. Kallman, & A. K. Pradhan, NASA Goddard Space Flight Center, 103–116

Beiersdorfer, P., *et al.* 1994, *Rapid Communications in Mass Spectrometry*, **8**, 141

Brown, G. V., *et al.* 2002, *Astrophys. J. Supp.*, **140(2)**, 589.

Brown, G. V., *et al.* 1998, *Astrophys. J.*, **502**, 1015.

Brown, G. V., *et al.* 2001, *Astrophys. J. Lett.*, **557**, L75–L78.

Chen, H., *et al.* 2002, *Astrophys. J. Lett.*, **567**, L169.

Curell, F. J., *et al.* 1996, *J. Phys. Soc. Japan*, **65**, 3186.

Gillaspy, J. 1997, *Phys. Scr.*, **T71**, 99.

Gu, M. F., *et al.* 1999, *Astrophys. J.*, **518**, 1002.

Levine, M., *et al.* 1988, *Phys. Scr.*, **T22**, 157.

López- Urrutia, J. C., *et al.* 2001, **T92**, 110112.

Porter, F. S., *et al.* 2000, *Proc. SPIE*, **4140**, 407.

Silver, *et al.* 1994, *Rev. Sci. Instrum.*, **65**, 1072.

High Energy Lab Astrophysics Using Particle & Photon Beams

Pisin Chen

Stanford Linear Accelerator Center, Stanford University, Stanford, CA

Abstract

Current frontier astrophysical phenomena typically involve one or more of the following conditions: (1) Very high intensity, high temperature processes; (2) Extremely high energy events; (3) Super strong field environments. Laboratory experiments can explore the most complex aspects of the problem as well as verify the validity of simulations designed for environments far from accessible in terrestrial conditions. Several outstanding astrophysical issues are reviewed, showing examples of possible lab experiments to help elucidate them.

1. Introduction

Current frontier astrophysical phenomena typically involve the following conditions:

- Very high intensity, high temperature processes, such as gamma ray bursts (GRBs);
- Extremely high energy events, e.g., ultra high energy cosmic rays (UHECRs) and blazars;
- Super strong field environments, such as around black holes (BH) and neutron stars (NS).

Insights into the underlying fundamental physical mechanisms and processes that generate these phenomena require controlled laboratory experiments. Furthermore, the complexity of such systems renders the eventual understanding far beyond the reach of any fully theoretical treatment. Progress can only be made with a joint effort of carefully designed experiments coupled with sophisticated astrophysical simulations. Laboratory experiments can explore the most complex aspects of the problem as well as verify the validity of simulations designed for environments far from accessible in terrestrial conditions. Current technologies can produce high energy particle beams and laser beams with intensities at or above 10^{22} Watt/cm at sufficiently high repetition rates. Such high intensity of EM energy can couple efficiently with high density plasma or solid material. Electron and positron beams can also be converged to form a relativistic plasma. In addition, high energy, high intensity electron beams can be efficiently converted to high fluence photon beams (tunable from x-ray to gamma-ray) by either colliding with laser pulses or channeling through an undulator or a crystal. A facility that combines this variety of beams can provide a unique tool for investigations of critical astrophysical issues.

2. Universe as a Laboratory

Our Universe is a vast laboratory which produces physical phenomena in their most extreme conditions far beyond the reach of terrestrial settings. Here we give a few examples.

Ultra High Intensity Processes. GRBs are by far the most violent release of energy in the universe, second only to the big bang itself. Within seconds (for short bursts) about $\epsilon_{GRB} \sim 10^{52}$erg of energy is released through gamma rays with a spectrum that peaks around several hundred keV. Existing models for GRB, such as the relativistic fireball model (18), typically assume either neutron-star-neutron-star (NS-NS) coalescence or super-massive star collapse as the progenitor. The latter has been identified as the origin for the long burst GRBs

(with time duration $\sim 10 - 100$ sec.) by recent observations (17, 11). The origin of the short burst GRBs, however, is still uncertain, and NS-NS coallescence remains a viable candidate. Even if the progenitors are identified, many critical issues remain to be addressed. What is its underlying dynamics?

Extremely High Energy Events. UHECR events exceeding the Greisen-Zatsepin-Kuzmin (GZK) cutoff (12, 22) ($\sim 5 \times 10^{19}$eV for protons originated from a distance larger than ~ 50 Mps), have been found in recent years (4, 19, 1, 15). Observations also indicate a change of the power-law index in the UHECR spectrum (events/energy/area/time), $f(\epsilon) \propto \epsilon^{-\alpha}$, from $\alpha \sim 3$ to a smaller value at energy around $10^{18} - 10^{19}$eV. So far theories that attempt to explain the UHECR can be largely categorized into "top-down" and "bottom-up" scenarios. In addition to relying on exotic particle physics beyond the standard model, the main challenges of the top-down scenarios are their difficulty in compliance with the observed event rate and the energy spectrum (16), and the fine-tuning of particle lifetimes. The main challenges of the bottom-up scenarios, on the other hand, are the GZK cutoff, as well as the lack of an efficient acceleration mechanism (16). To circumvent the GZK limit, several authors propose the "Z-burst" scenario (21, 10) where neutrinos, instead of protons, are the actual messenger across the cosmos. Even if the GZK-limit can be circumvented through the Z-burst scenario, the challenge for a viable acceleration mechanism remains acute. The existing paradigm for cosmic acceleration, namely the Fermi mechanism (9) (including diffusive shock acceleration (2, 14, 3, 5)), is not effective in reaching ultra high energies. These acceleration mechanisms rely on the random collisions of the high energy particle against magnetic field domains or the shock media, which necessarily induce increasingly more severe energy losses at higher particle energies. Are there alternatives, and how can we verify them?

Super Strong Field Environments. In the vicinity of compact objects such as neutron star and black hole, the electromagnetic as well as gravitational fields are believed to be extremely intense. For example the magnetic fields around a neutron star is approaching the Schwinger critical field strength, i.e., $\sim 4 \times 10^{13}$G, while the gravitational collapse of a super massive star to a charged black hole may generate an electric field that is comparably intense. In addition, gravity near the event horizon of a black hole is so strong that general relativity has to be invoked in order to properly describe its dynamics. Furthermore, under such super-strong fields quantum effects play essential roles. For example under the Schwinger critical field condition the QED vacuum becomes unstable and e^+e^- pairs can be copiously created spontaneously. Black holes, on the other hand, can provide a fertile test bed for the eventual understanding of quantum gravity, for example, via Hawking radiation (13). Can any of these be tested in the laboratory setting?

3. Laboratory Studies of the Universe

Many aspects of the above mentioned extreme astrophysical phenomena, though not reproducible in the earth-bound laboratory, can be investigated by using the very high intensity photon and particle beams with the state-of-the-art technologies. The information so obtained can either be extrapolated to the actual astrophysical problems, or help to reveal their underlying physical mechanisms. Laboratory experiments can also help to characterize or calibrate

astrophysical observations. Furthermore, the very complex astrophysical environments mentioned above often renders fully theoretical treatment impossible, and large scale computer simulations are indispensable. Yet limited by the CPUs and other constraints, even computer simulations require approximations and assumptions. Laboratory experiments can help to bench-mark the simulation codes and provide their validation. The utilities of laser and the particle beam are well complementary to each other. Laser photons, whose energy is typically at the eV range, can couple more effectively with solid material, and is most suitable in the study of supernova explosion dynamics as well as the equation of state in *high density* processes. Particle beams, whose energy can be tens of GeV per particle, tend to be more penetrating and thus more suitable for the studies of *high energy* astrophysical processes. It is thus desirable that any facility for high energy laboratory astrophysics will employ both particle and photon beams. The merger of an electron beam and a positron beam can provide a relativistic "plasma" in the lab frame. A tunable photon beam (from x-ray to γ-ray) can in principle be prepared by colliding a laser beam against a particle beam. Good quality x-ray can also be produced by sending the particle beam through an undulator. Many critical issues discussed above can be investigated using high intensity beams.

4. Possible Experiments

Extensive Air Shower Experiment. There currently exist two different experimental techniques in the detection of UHECR. These are the air fluorescence technique, employed by the HiRes experiment (1), and the ground array detection employed by the AGASA experiment (19). Both HiRes and AGASA have observed ultra high energy events above the GZK-cutoff. These two experiments, however, disagree in absolute flux of UHECR as well as in the shape of the UHECR energy spectrum. The HiRes UHECR flux measurement is systematically smaller than the AGASA measurement. The kink in the HiRes spectrum around 30 EeV may indicates a pile-up due to the GZK effect, or the appearance of a new extra-galactic component. This kink is not observed at this energy by AGASA. This existing discrepancy between HiRes and AGASA still lacks a resolution. For ground-based as well as the future space-based observations, energy estimation of an extensive air shower depends on an accurate knowledge of atmospheric fluorescence efficiency. Air fluorescence is a useful tool for cosmic ray measurements because its emission spectrum is in the near-ultraviolet (300–400 nm) where the atmosphere exhibits almost no absorption and a relatively long scattering length (10–20 km) and because the yield (in photons per meter per electron) is virtually independent of altitude up to about 15 km. High energy electron beams are ideal for such a study for the following reasons:

A. An extensive air shower produced by a hadron at relevant cosmic-ray energies is a superposition of electromagnetic sub-showers. Most of the shower energy at shower maximum is carried by electrons near the critical energy of air (100 MeV). The atmospheric fluorescence energy measurement is dominated by the luminosity of the shower at its maximum development.
B. Important N_2 fluorescence transitions (upper levels of the Nitrogen 2P system) are not accessible by proton excitation. Electron beams are required to study all relevant transitions.
C. The energy distribution of electrons in the resulting shower as it exits the target into a controlled atmosphere is calculable and similar to what is expected in a UHE shower near shower

maximum. Incidentally, a 10 GeV electron beam with 10^{10} particles carries a total energy $\sim 10^{20}$ eV, the same order of magnitude as UHECR.

The superposition of showers produced by a high energy beam can be modeled by softwares and the fluorescence yield can be measured at various stages of the shower development, allowing detailed comparison with Monte Carlo simulations. If carried out, such an experiment should help to partially resolve the discrepancy between HiRes and AGASA, and would provide reliable and much needed shower data for future fluorescence-based UHECR experiments.

Cosmic Acceleration Experiments. In addition to the first order (diffusive shock) and second order Fermi accelerations, there exist other interesting proposals, such as the idea of "Zevatron" (6). Another cosmic acceleration mechanism was recently introduced (8), which is based on the wakefields excited by the Alfven shocks in a relativistically flowing plasma. In the cosmic plasma wakefield acceleration model, there exists a threshold condition for transparency below which the accelerating particle is collision-free and suffers little energy loss in the plasma medium. The stochastic encounters of the random accelerating-decelerating phases results in a power-law UHECR energy spectrum: $f(\epsilon) \propto 1/\epsilon^2$. By invoking GRB atmosphere as the site for such an acceleration, protons with energies much beyond the GZK-limit can be produced. When the Z-burst scenario is further invoked, the estimated event rate in this model agrees with that from UHECR observations. To test this mechanism, one can envision a setup where a c^+ beam and a c^- beam converge into a relativistic "plasma." Alfven shocks can be excited by sending this "plasma" through the superposition of a solenoid field and an undulator field. Plasma wakefields so excited will randomly accelerate or decelerate beam particles, resulting in a power-law energy spectrum. The acceleration gradient observed can then be extrapolated to and confronted against the astrophysical conditions. The diffusive shock acceleration can in principle also be investigated using such a relativistic plasma.

Event Horizon Experiment. The celebrated Hawking effect (13) suggests that BH is not entirely black, but emits a blackbody radiation with temperature $kT_H = \hbar g/2\pi c$, where g is the gravitational acceleration at the BH event horizon. Unfortunately the Hawking radiation for a typical astrophysical BH is too faint for observation. Through the Equivalence Principle there exists a similar effect, the Unruh effect (20), for a particle "detector" undergoing uniform acceleration. The accelerating detector would find itself surrounded by a heat bath with temperature $kT_U = \hbar a/2\pi c$, where a is the proper acceleration of the particle. The very fundamental Hawking-Unruh effect can in principle be investigated via extremely violent acceleration provided by a standing-wave of ultra-intense lasers (7).

We argue that high intensity lasers and particle beams are powerful tools in laboratory investigations of high energy astrophysics. An experimental complex that can provide a combination of different beams can be instrumental in addressing many frontier astrophysical problems.

REFERENCES

(1) Abu-Zayyad, T. *et al.* 1999, *Proc. ICRC*, **3**, 264.

(2) Axford, W. I., E. Leer, and G. Skadron 1977, in *Proc. 15th ICRC (Plovdic)*, **11**, 132.

(3) Bell, A. R. 1978, *Mon. Not. R. Ast. Soc.*, **182**, 147.

(4) Bird, D. J. *et al.* 1993, *Phys. Rev. Lett.*, **71**, 3401.

(5) Blandford, R. D. and Ostriker, J. F. 1978, *ApJ Lett.*, **221**, L29.

(6) Blandford, R. D. 1999, astro-ph/9906026.

(7) Chen, P. and Tajima, T. 1999, *Phys. Rev. Lett.*, **83**, 256.

(8) Chen, P. *et al.* 2002, astro-ph/0205287.

(9) Fermi, E. 1949 *Phys. Rev.* **75**, 1169; 1954, *ApJ*, **119**, 1.

(10) Fargion, D., Mele, B., and Salis, A. 1999, *ApJ*, **517**, 725.

(11) Garnavich, P. M. *et al.* 2002, astro-ph/0204234.

(12) Greisen, K. 1966, *Phys. Rev. Lett.*, **16**, 748.

(13) Hawking, S. W. 1974, *Nature*, **248**, 30.

(14) Krymsky, G. F. 1977, *Dokl. Acad. Nauk. SSR*, **234**, 1306.

(15) Lawrence, M. A., Reid, R. J., and Watson, A. A. 1991, *J. Phys. G: Nucl. Part. Phys.*, **17**, 773.

(16) Olinto, A. V. 2000, *Phys. Rep.*, **333- 334**, 329.

(17) Price, A. P. *et al.* 2002, astro- ph/0203467.

(18) Rees, M. J. and Meszaros, P. 1992, *Mon. Not. R. Ast. Soc.*, **158**, 41.

(19) Takeda, M. *et al.* 1998, *Phys. Rev. Lett.*, **81**, 1163.

(20) Unruh, W. 1976, *Phys. Rev. D*, **14**, 870.

(21) Weiler, T. 1999, *Astropart. Phys.*, **11**, 303.

(22) Zatsepin, G. T. and Kuzmin, V. A. 1966, *JETP Lett.*, **4**, 78.

Measurement of Absolute Excitation Cross Sections
in Highly-Charged Ions
Using Electron Energy Loss and Merged Beams

A. Chutjian, Steven J. Smith, and J. Lozano

Jet Propulsion Laboratory, California Institute of Technology, Pasadena, CA

There is increasing emphasis during this decade on understanding energy balance and phenomena observed in high electron temperature plasmas. The UV spectral return from FUSE, the X-ray spectral return from the HETG on Chandra and the LETGS on XMM-Newton are just beginning. Line emissions are almost entirely from highly-charged ions (HCIs) of C, N, O, Ne, Mg, S, Si, Ca, and Fe. The Constellation-X mission will provide X-ray spectroscopy up to photon energies of 0.12 nm (10 keV) where primary line emitters will be HCIs. A variety of atomic parameters are required to model the stellar and solar plasma. These include cross sections for excitation, ionization, charge-exchange, X-ray emission, direct and indirect recombination, lifetimes and branching ratios, and dependences on l, m mixing by external E and B fields[1]. In almost all cases the atomic quantities are *calculated*, and few comparisons to experiment have been carried out.

Collision strengths and Einstein A-values are required to convert the observed spectral intensities to electron temperatures and densities in the stellar plasma. The JPL electron energy-loss and merged-beams approach [2] has been used to measure absolute collision strengths in a number of ions, with critical comparison made to the best available theories. Experimental comparisons to R- Matrix and Breit-Pauli theoretical results have been presented for C^{3+} [3], O^{2+} [4], O^{5+}[5], S^{2+}[6] and Fe^{9+} [7]. Work is planned in the targets Mg^{7+} and in the higher charge states $Fe^{(10-15)+}$. A schematic diagram of the JPL Highly-Charged Ion Facility (HCIF) is shown in Fig. 1. Details are given in Refs. [1,2]. The three available beam lines are for measurements of metastable lifetimes in HCIs [8], HCI-neutral X-ray emission and charge-exchange cross sections [9], and absolute excitation cross sections [4,7].

We give two representative examples, in O^{2+} and Fe^{9+}, of the absolute excitation work at the HCIF. Transitions in O^{2+} are detected in diffuse nebulae-HIII regions, planetary nebulae, in our own Sun, and in the Io torus. Show in Fig 2 are absolute excitation cross sections for the $2s^22p^2\ ^3P_{0,1,2} \rightarrow 2s^22p^2\ ^1D_2$ transition. Relevant points are: (a) the experiments extend through the theshold region; (b) the cross sections are absolute; (c) one can measure cross sections to about 2.5 times the threshold energy. Also, these above-threshold cross sections are "nearly absolute" in that a small correction must be applied to account for high-angle, elastically-scattered electrons whose velocities can alias those of low-angle inelastically- scattered electrons. (d) One detects rich resonance structure throughout this energy range. Upon comparison with an accurate R-matrix calculation [10] experiment confirms the presence of the resonances near 2.7 and 4.2 eV, but does not detect the resonance near 3.1 eV, perhaps because this resonance is weaker and narrower than is calculated.
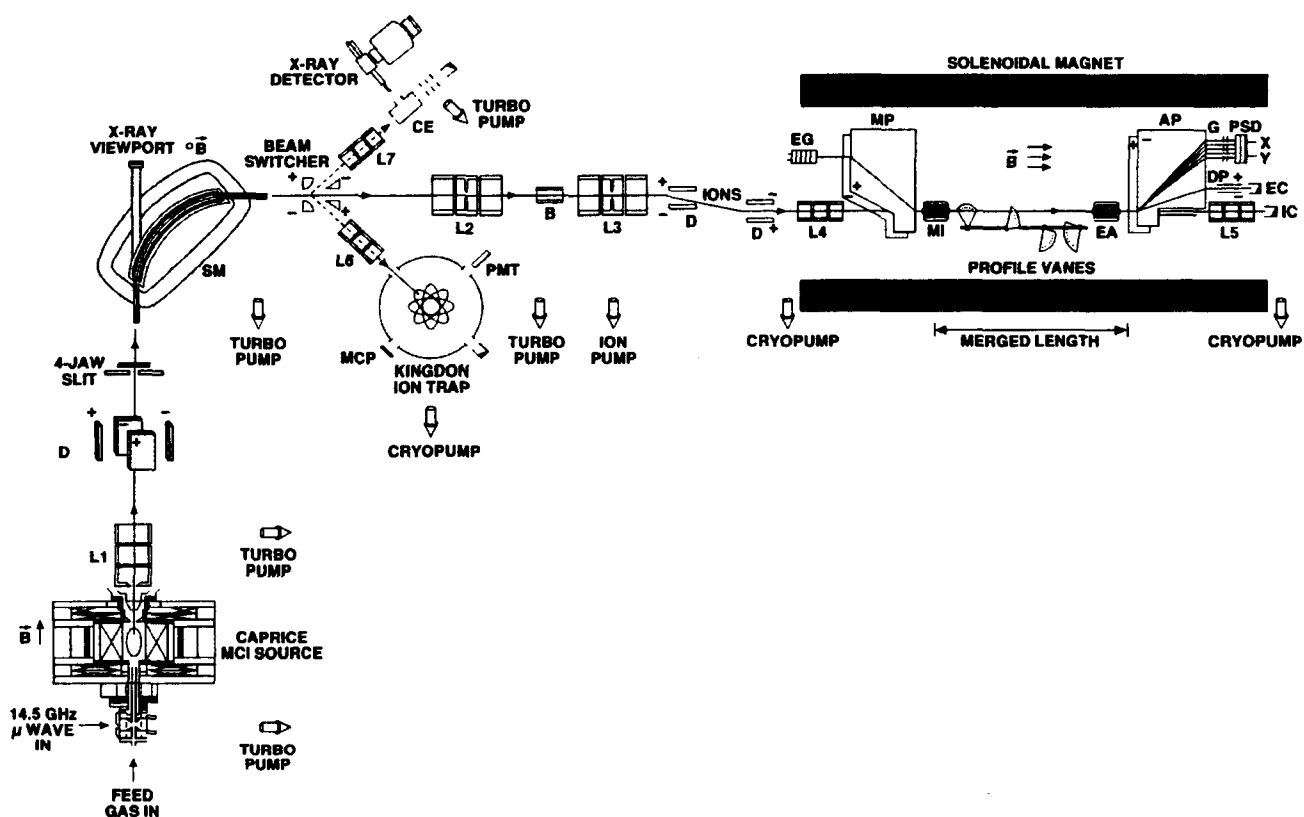
Figure 1. Experimental arrangement of the JPL Highly-Charged Ion Facility (HCIF). (L1-L7) three-element focusing lenses, (SM) mass/charge selection magnet, (B) differential pumping baffle, (D) deflector plates, (MP) electron-merging trochoidal plates, (AP) electron-analyzing trochoidal plates, (MI) electron mirror to reflect backward-scattered electrons, (EA) electronic aperture to discriminate against elastically-scattered electrons (DP) trochoidal plates to deflect parent electron beam out of the scattering plane, (PSD) position-sensitive detector, (G) electron-retarding grids for discrimination against elastically-scattered electrons, (EC) electron Faraday cup, (IC) ion Faraday cup, (CE) charge-exchange cell, (MCP) microchannel plate, (PMT) multiplier phototube. The three beam lines after the switcher are for excitation, metastable lifetimes, and charge-exchange/ experiments.

Emission lines in Fe IX-Fe XIV are detected in stellar and solar spectra [11]. The fine-structure line at λ 6376 Å in Fe^{9+}, the so-called coronal red line, corresponds to the forbidden transition $2s^2 2p^5 \ ^2P^o_{3/2} \rightarrow 3s^2 3p^5 \ ^2P^o_{1/2}$. Examples of its use in astrophysical diagnostics can be found in Ref. [12]. Recent HCIF results are shown in Fig. 3, with comparison to results in a 49-state Breit-Pauli theory. These are the first measurements of an absolute excitation cross section in an iron ion. Comments in (a)-(d) above apply here. The strong resonance at 4.35 eV (theory) is seen at 4.6 ± 0.1 eV (experiment). This agreement is resonable, given the error in the energy scale, and effects in the calculation (number and type of bound and continuum orbitals, electron correlation and relativistic effects etc.) that can shift the resonance-peak by tenths of an eV. The impressive return of high-resolution X-ray spectra from the Chandra and Newton telescopes has revealed the rich X-ray life of the Universe. Iron emission lines are a major contributors to the spectra, but high charge states of C, N, O, Mg, Si, S, rare gases, etc. are also detected. Almost all quantities in these HCIs, especially collision strengths, are calculated, with few comparisons to experiment. The JPL HCIF will measure critical collision strengths in these ions.
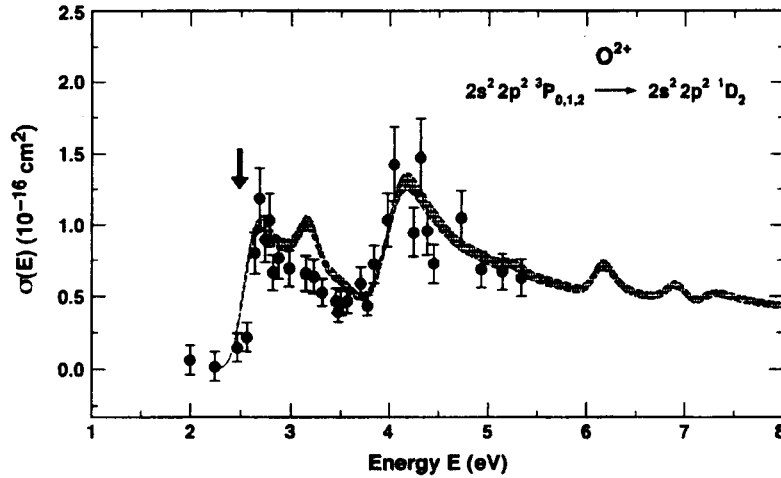
Figure 2. Comparison of experimental absolute excitation cross sections for the $2s^2 2p^2\ ^3P \rightarrow 2s^2 2p^2\ ^1D_2$ transitions in O^{2+} (solid circles) [4], with theoretical results in the 26-state R-matrix calculation [10]. The sharp resonance structures in the calculation have been convoluted with an energy-dependent resolution, as given by experimental conditions (3). These results are drawn with a 5% "theoretical accuracy" error band. Experimental error limits are shown at the 1.7σ (90%) confidence level. The arrow indicates the energy threshold of this transition.
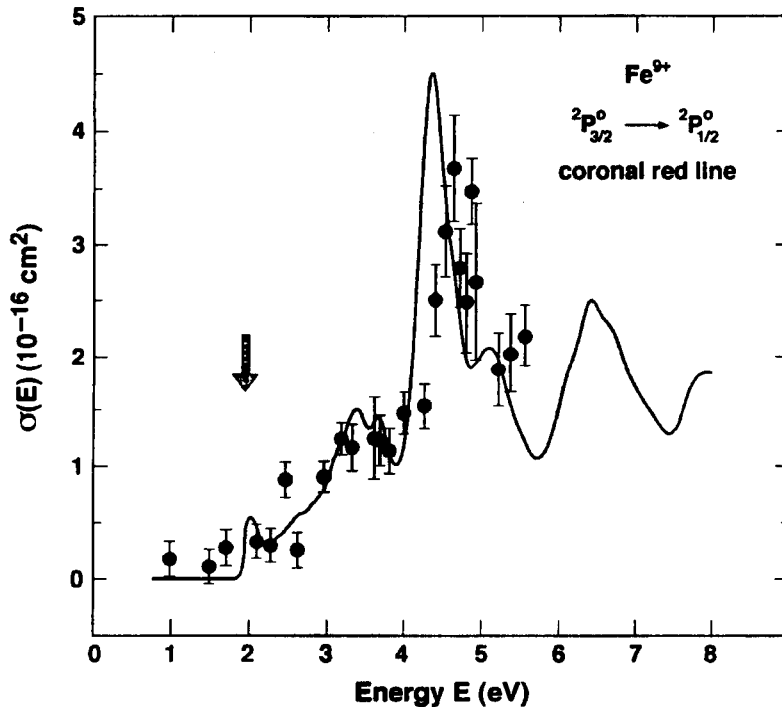
Figure 3. Comparison of the convoluted 49-state Breit-Pauli R-Matrix results (solid line) and measured absolute experimental cross sections (solid circles) for the Fe^{9+} coronal red-line transition (λ 6376 Å) [7]. Experimental errors are shown at the 1.7σ (90%) confidence level [18% or less, depending on the number of measurements (1-5) of each cross section]. The energy scale is accurate to 0.1 eV, and the vertical arrow denotes the transition threshold at 1.945 eV.

Acknowledgments

REFERENCES

[1] "Collision Phenomena Involving Highly-Charged Ions in Astronomical Objects," A. Chutjian, *The Physics of Multiply* and Highly Charged Ions (Kluwer Academic, 2002) (in press).

[2] A. Chutjian, J. B. Greenwood, and S. J. Smith, in *Atomic Processes in Plasmas* (eds. E. Oks and M. S. Pindzola, Am. Inst. Phys., New York, 1998).

[3] J. B. Greenwood, S. J. Smith, A. Chutjian, and E. Pollack, *Phys. Rev.A* **59**, 1348 (1999).

[4] M. Niimura, S. J. Smith, and A. Chutjian, *Ap. J.* **565**, 645 (2002).

[5] J. Lozano, M. Niimura, S. J. Smith, A. Chutjian, and S. S. Tayal, *Phys. Rev. A* **63**, 042713 (2001).

[6] J. B. Greenwood, S. J. Smith, A. Chutjian, and S. S. Tayal, *Ap. J.* **541**, 501 (2000).

[7] M. Niimura, I. Cadez, S. J. Smith, and A. Chutjian, *Phys. Rev. Lett.* **88**, 103201 (2002).

[8] S. J. Smith, I. Cadez, A.Chutjian, and M. Niimura, "Measurement of the Metastable Lifetime for the $2s^2 2p^2$ ^1So Level in O^{2+}," Ap. J. (in press).

[9] J. B. Greenwood, I. D. Williams, S. J. Smith, and A. Chutjian, *Phys. Rev. A* **63**, 062707 (2001).

[10] K. M. Aggarwal and F. P. Keenan, *Ap. J. Suppl. Ser.* **123**, 311 (1999).

[11] E. Behar, J. Cottam, and S. M. Kahn, *Ap. J.* **548**, 966 (2001); S. M Kahn, *et al.*, Astron. Astrophys. **365**, L312 (2001).

[12] H. E. Mason, At. Data Nucl. Data Tables **57**, 305 (1994).

A National Facility for Astrophysical Atomic Data Needs

Gary J. Ferland

Physics Department, University of Kentucky, Lexington, KY

David R. Schultz

Physics Division, Oak Ridge National Laboratory, Oak Ridge, TN

Abstract

Nearly all astronomical environments are far from equilibrium. As a result, the emission we observe is sensitive to details within the source that created it. This is why spectroscopy is such a powerful tool for understanding the physics of the cosmos, but it also presents a challenge because the spectrum is sensitive to the atomic processes that determine its emission. Although some of the needed atomic data can be provided by existing theory codes, much must be studied experimentally, especially those involving collisions. Currently no national US facility exists for such investigations. NASA researchers currently must look to Europe for such facilities. We propose a coordinated program, based at Oak Ridge National Laboratory (ORNL), which would provide a national focus for efforts to generate the needed atomic data. The central facility would be a storage ring that would directly measure the needed processes. A data center and internet-based community of astrophysical modelers would be associated with the facility and provide both dissemination of data and guidance in future data needs. The Center could build upon ORNL resources that fall within its current fusion program and so accomplish its goals at relatively modest cost.

1. Introduction

Astrophysics is an observational rather than experimental science. We can observe the cosmos in every way possible with our technology, but must infer what is happening in front of our telescopes by indirect means, most often by reference to computer simulations. The best quantitative information comes from spectroscopy - nearly all current and future NASA missions have a major spectroscopic component, often at wavelengths that are not observable at the Earth's surface. These missions, and the astrophysical problems they investigate, need to maximize the information gained from spectroscopic observations to fulfill their potential. Investigation of interstellar, intergalactic, and circumstellar matter, with absorption or emission lines, is commonly a major mission theme because these are the sites of our origins. These environments are far from thermodynamic equilibrium because of their low density. As a result, the physical conditions, and the spectrum we observe, are determined by a balance between microphysical processes. The state of the gas, and its observed properties, are best determined by reference to large-scale plasma simulations which include these as their foundation. This is an example of the "inverse problem" - we know the answer (the spectrum of a distant object) and are working backwards to understand the question (what happened there, to produce the light we receive here). As participants in an observational science, astronomers know the frustration of being passive observers, unable to directly solve a problem. Our ability to unravel the message in a spectrum is mainly mitigated by uncertainties in the basic atomic and molecular parameters. But this uncertainty is not fundamental and can be removed by laboratory studies. The last section in this paper outlines a key facility which could go a long way to solving these problems.

2. The Most Important Problems in Plasma Astrophysics

Star birth - HII Regions, PDRs (SIRTF, SOFIA, Herschel, NGST) New stars form in the vicinity of the molecular clouds. Ionizing radiation from the hottest stars produces an ionized layer on the surface of the cloud, a "blister" H II region. An atomic region, "PDR", lies between the IIII region and the molecular cloud. In the case of starburst galaxies, or distant objects within our own galaxy, these are mainly detectable in the infrared. The central questions concern the creation of the heavy elements, galactic abundances gradients, primordial helium abundance (one of the three tests of the Big Bang), and star formation.

Star death - planetary nebulae and supernova remnants (XMM Newton, Chandra, FUSE, HST, SIRTF, SOFIA) Stars return some fraction of their mass into the interstellar medium at the end of their lives. This matter, enriched in heavy elements by nuclear processing, is used in forming later generations of stellar systems. The effects of nuclear processing by massive stars can be directly observed in supernova remnants like the Crab Nebula. Planetary nebulae are produced by lower mass stars like the sun, as a gentle wind rather than a violent explosion. In each case, the continuum emitted by the central star, a neutron star or white dwarf, photoionizes the ejected material. Spectroscopy allows direct measurement of the composition and mass of the ejecta, thus testing models of stellar evolution and synthesis of elements.

The interstellar and intergalactic media (Chandra, XMM Newton, FUSE, HST, SIRTF, SOFIA, Herschel, NGST) Matter fills the space between the stars and galaxies and is most easily detected with absorption lines superimposed on the spectra of more distant object. Investigations determine the chemical composition, level of ionization, and kinematics. Studies of the interstellar medium reveal the structure and dynamics of the solar, while intergalactic medium investigations determine how the chemical evolution of the universe changes across cosmic time, the formation of structure at high redshift, and the form and luminosity of the cosmic background radiation that ionizes the clouds.

Active Galactic Nuclei (AGN) (Chandra, XMM Newton, FUSE, HST, SIRTF, SOFIA, NGST) These are the most distant objects for which it is now possible to obtain spectra, and are thought to be energetic events that occur during the formation of the most massive galaxies. Emission lines have been detected from gas close to the central energy source, serving as probes of events that occur near the very centers of young massive galaxies and tracing the first generations of stellar evolution. Chandra and XMM have detected high speed winds that carry nuclear processed material from the inner regions into the IGM, and, most surprisingly, carry even more kinetic energy than the radiative energy that first distinguished them. The central questions include understanding the evolution of central regions of the first galaxies and their effect on the chemical enrichment of the universe.

3. Astronomical plasmas

All of the environments described above share a central theme- the spectrum we observe is formed in tenuous plasma, often the result of photoionization by an energetic continuum. The plasma is far from thermodynamic equilibrium because timescales for collisions to share thermal energy among constituents are much longer than timescales for other changes. Every state of every ion would be characterized by a different temperature, so this concept is seldom used. Electrons are an exception - elastic collisions between them are the fastest collisional process that occur, so their velocity distribution can often be represented by a Maxwell-Boltzmann distribution. Two classic texts review these environments.[1,2] Physical conditions within the gas, and its observed spectrum, will be set by the

balance between a host of microphysical processes. These include the atomic processes that ionize a species, or allow it to recombine, as well as those that cause levels to be excited or allowed to decay. The formation of the spectrum of a non-equilibrium plasma is complicated because it is sensitive to these details, but this is also an asset - the spectrum is also sensitive to many of the details that we want to measure, such as its composition or hydrodynamic state of the gas. Because of these complexities, plasma is most often analyzed by reference to large-scale numerical simulations. GJF has been developing such a code, *Cloudy*, which is widely used ($\sim$100 papers annually) in interpreting astronomical spectra.[1] It is actively used to investigate all of the topics discussed above. The code occupies the middle ground between atomic and molecular data, which forms the foundation of the simulations, and observations made with NASA's observatories, its main application.

4. The Major Uncertainties

All of astronomical spectroscopy rests on a foundation of atomic and molecular data. The shear amount of data needed poses a major problem - literally millions of cross sections and transition probabilities go into a single plasma simulation. It is not practical to experimentally measure this quantity of data - rather large theory codes, such as the Belfast/UCL R-Matrix suite, are used to generate millions of cross sections or rates, which are then verified by a few careful experiments. This approach has been successfully followed for the cases of transition probabilities, collision rates, and photoionization cross sections. These plasmas present a special challenge because most collisional interactions occur at energies that are small compared with the ionization potential of the species that are present. This is because the electron kinetic energy is established by the balance between heating, due to residual energy of a photoelectron, and cooling, inelastic collisions between electrons and other constituents. Most of a photoelectron's energy goes into ionization rather than heating because the photoionization cross section is largest near threshold, where the number of photons is also largest. As a result the electrons will have energies that are typically 10–20% of the ionization energy of the species present, and most collisional processes occur near threshold. It is difficult for atomic theory to predict cross sections at these energies, and experiments have only become possible in recent years. In recognition of the importance of the problems herein described, NASA supported the 2000 Lexington Meeting on photoionized plasmas, at which atomic data needs, plasma modeling techniques, and other astrophysical questions were discussed. [3] The main atomic physics issues addressed include the following:

Dielectronic Recombination (DR) DR is the dominant recombination process for a broad range of plasmas. The theory goes back many decades, but recent experiments [4] show that theory can only produce experimental rates to within a factor of two. The question boils down to the position of autoionizing resonances, which can't be predicted with precision without experimental guidance; experiments must take the lead here.

Charge transfer (CT) This process involving a collisional between a neutral atom and lower stages of ionization of the heavy elements. Although it occurs within an ionized plasma, it is essentially a molecular process since the electron exchange occurs when the atom and ion reach the avoided crossing in the internuclear potential. Theory is possible, but difficult, and experiments are now possible.

---

[1]Available at: www.pa.uky.edu/ gary/cloudy; the web site provides references for the articles along with documentation, source, and atomic data base for the code.

Inner shell processes X-Ray missions observe lines that are emitted as an atom relaxes following removal of an inner-shell electron. Most calculations are now based on the tables published by Kaastra and Mewe [5] - these were often extrapolations from laboratory data obtained for solids, because no other data exist. Photoabsorption by inner shell resonance lines has recently been shown to be an important ionization process [6] although oscillator strengths for this process have only been calculated. Little work has been done on Auger processes following removal of an inner electron.

5. A Cross Disciplinary Approach

The atomic data needs of astrophysical spectroscopy are vast. Collisional interactions, including such processes as dielectronic recombination, charge transfer, and surface chemistry on grains, constitute a common thread running through the multi-mission research fields described above. These processes present difficult problems best addressed through a closely coupled effort involving atomic experiments, theoretical calculations, data collection and evaluation, and astrophysical plasma modeling (and thereby, space- and ground-based observation programs). Toward this end, the extensive and critical atomic and molecular data needs should be addressed by increased support for laboratory astrophysics broadly and, importantly, through support for a focused astrophysical atomic data facility. NASA would be particularly well-served by establishing a facility, constituted along the lines of this tightly coupled, multi-disciplinary model, to serve its many missions obtaining spectroscopic observations. The program's cost would be minimized by taking advantage of an existing facility such as that at ORNL. The ORNL facility lies at the interface between the atomic and molecular physics and fusion energy communities. This existing paradigm consists of a multicharged ion research facility capable of measuring both electron and heavy particle collision cross sections, a theory group to compute the large number of data that cannot be measured experimentally, and a data center to collect, evaluate, and disseminate the data to the community. The data center also serves as an interface to the national fusion modeling programs, taking feedback for requests for needed data, data formats, and priorities. The astrophysical atomic data facility would augment such an existing program and would consist of the following closely interacting components:

A national-use storage ring facility Storage rings make it possible to study collisional processes at energies of astrophysical interest. An electrostatic storage ring would allow study of collisions involving electrons, atoms, ions, and molecular ions, including very large species such as PAHs, at a construction cost of $1-2 million. It would provide a new and highly capable device for collisional and spectroscopic data production that would be a focal point for astrophysical atomic studies nationally. A magnetic storage ring would be capable of studying needed low collision energy electron- impact processes involving atomic ions and small molecular ions and would have a construction cost of $10-20 million. NASA presently supports several programs that utilize foreign storage rings because none are available in the US.

An experimental and theoretical infrastructure A national facility would require an experimental and theoretical staff appropriate to its mission as well as the equipment and apparatus required to perform the range of data production, as well as to design, construct, and operate the storage-ring facility. Leveraging existing human resources and investment in experimental infrastructure at a suitable facility such as ORNL would require only about three to four new staff members at an annual cost, including operating funds, of under $1 million.

An atomic data center The experimental and theoretical data produced by the facility and through all other world-wide efforts must be collected, evaluated, and consolidated into a single data base if these are to be used by the general astronomical community and available over the web in the appropriate format. A relatively modest expansion (one staff member at $\sim$ \$300 thousand annually) of the data center program at ORNL would enable this element of the integrated process.

A virtual community of astrophysical modelers The output of the database will enable the astrophysical plasma modeling required to interpret space-based observations. Modelers, who perform the numerical simulations that combine basic data to compare with observations, will open the two-way communication between the astrophysics and the atomic physics communities necessary to insure production of the required data as astrophysical knowledge evolves. The nucleus provided by the facility and data center can then be leveraged into an internet-based consortium of modelers and others interested in these basic data. This would establish a community of people who share a common interest, something now critically lacking. NASA missions requiring atomic data for their fullest interpretation cost many hundreds of millions of dollars and therefore the modest investment in a national astrophysical atomic data facility is both crucial and tremendously enabling. Furthermore, implementing the program outlined would cost far less than a new stand-alone program by building within an existing infrastructure. The DOE national labs represent an excellent opportunity because of their deep interest in collision processes that are closely related to those that occur in cosmic plasmas. A joint program would serve both communities at a fraction of the cost of an independent program.

REFERENCES

[1] Osterbrock, D. E. 1989, *Astrophysics of Gaseous Nebulae & Active Galactic Nuclei*, (Mill Valley; University Science Press).

[2] Spitzer, L. 1978, *Physical Processes in the Interstellar Medium*, (New York: Wiley).

[3] Ferland & Savin, eds., 2001, *Spectroscopic Challenges of Photoionized Plasmas*, (ASP Conference Series, Vol 247), on the web at http://nimbus.pa.uky.edu/plasma2000/

[4] Savin, D.W., *et al.*, 2002, *ApJS*, **138**, 337.

[5] Kaastra, J.S., & Mewe, R., 1993, *A&AS*, **97**, 443.

[6] Behar, E., & Netzer, H., 2002, *ApJ*, **570**, 165.

Microscopic Processes in X-Ray Modulated Star Formation

A.E. Glassgold[1]

Astronomy Department, University of California, Berkeley, CA

Abstract

Charge transfer processes accompanying X-ray irradiation are important for understanding protostellar jets.

1. Introduction

The outflows accompanying star formation are usually explained in terms of magneto-centrifugal wind models, e.g., the X-wind model of Shu and collaborators (2000). The iso-density contours of the X-wind collimate towards the axis and are suggestive of a jet. In order to establish whether the X-wind is capable of emitting optical forbidden lines, Shang, Glassgold. Shu, and Lizano (2002, henceforth referred to as SGSL) integrated the ionization and heat equations along the X-wind streamlines using appropriate ionization and heating agents. Although the processes that determine the ionization of atomic hydrogen at 1 eV are well known, there are changes for the flow of a partially ionized gas. First, the gas may not be in a local steady state. Second, adiabatic cooling is so strong that conventional heating mechanisms, including ambipolar diffusion, have difficulty competing. Third, the ionization fraction required to explain the observed forbidden lines cannot be achieved by stellar photoionization or collisional ionization.

SGSL proposed that dissipation of the flow kinetic energy heats the jet since observations indicate that the jets are time-dependent. In a time-dependent jet, shock waves and turbulence are generated when fast fluid elements catch up with slower ones. Dimensional reasoning suggests the form,

$$\Gamma_{mech} = \alpha\, \rho \frac{v^3}{s},$$

where ρ and v are density and speed of the flow, and s is the distance along the streamline. The temperature of the wind close to the axis approaches 10,000 K if α is $\sim 10^{-3}$.

2. $H^+ + H$ Scattering and Ambipolar Diffusion Heating

The heating rate due to ambipolar diffusion (see Appendix D of SGSL) is inversely proportional to the ambipolar diffusion coefficient γ, which is the sum over the rate coefficients for momentum transfer in ion-neutral collisions. Each rate coefficient is a double integral over the assumed thermal equilibrium velocity distributions (Draine 1986). The most abundant ion-neutral pair in a warm cosmic plasma is $H^+ + H$. Osterbrock (1961) discussed the momentum transfer cross sections in terms of the leading $1/r^4$ potential at large distances r. In the semi-classical limit, this leads to a $1/v$ cross section and a constant Langevin rate coefficient.

---

[1] Also Physics Dept., New York University, New York

He pointed out that shorter range interactions play a role at high enough energies, and others represented them by a constant cross section of the order of $10^{-15}\,\text{cm}^2$ [2]. The II_2^+ potential energy curve is the oldest and best studied in molecular physics, and good theoretical calculations of the H$^+$ + H cross sections have been available since 1977 (Hunter & Kuriyan 1977) for the energy range from $10^{-4} - 10\,\text{eV}$. They were recalculated by Kristić and Schultz (1998), along with those for H$^+$ + He and for H$^+$ + H$_2$, and close agreement is obtained. The theoretical cross sections are also in good agreement with experiments. The H$^+$ + H momentum transfer cross section oscillates below 10 eV, and it is hard to recognize the Langevin $E^{-1/2}$ behavior at low energies except in some average sense. There is a definite change in the energy dependence above 0.01 eV, where the cross section, averaged over small oscillations, varies weakly with energy as $E^{-1/8}$. The momentum transfer cross section is approximately $2 \times 10^{-14}\,\text{cm}^2$ at the break point near 0.01 eV, an order of magnitude larger than many guesses in the literature. To calculate the rate coefficient, SGSL fitted the average H$^+$ + H momentum transfer cross with power laws in energy,

$$\sigma_{\text{mt}} = \sigma(0.01\text{eV})\,(E/0.01\text{eV})^p,$$

with $p = -1/2$ for $E < 0.01\,\text{eV}$ and $p = -1/8$ for $E > 0.01\,\text{eV}$, and obtained values significantly larger than found in the literature, e.g., $\gamma(10^4\,\text{K}) \sim 8 \times 10^{13}\,\text{cm}^3\text{s}^{-1}\text{g}^{-1}$.

This new large coefficient means that the ambipolar diffusion heating rate, which varies inversely with γ, is reduced relative to earlier calculations. When the heat and ionization equations are intgerated along the X- wind streamlines with the new γ, only a thin inner layer of the X-wind jet is heated well enough to emit the forbidden lines; the emission from the bulk of jet is too weak to observe. Thus, ambipolar diffusion cannot account for jet temperatures in the X-wind model. This is to be contrasted with the conclusions of Safier (1993) and Garcia *et al.* (2001) for self-similar disk winds. Some of the discrepancy may be attributed to their use of γ coefficients that are too small, and the rest to differences between the magnetic field of the X-wind and self-similar disk winds.

3. Jet Diagnostics: Charge Transfer and the Sulfur Ions

The calculated physical properties of the flow and the built-in cylindrical collimation of the X-wind provide the basis for an explanation of the jets observed in active young stellar objects. In addition to the spatial variation of intensities and line ratios, the theory must also be able to predict absolute levels of the intensities. Reasonable agreement with observation is obtained for O. In this case, we can reliably estimate the amount of O$^+$ since its abundance is determined by fast forward and backward charge exchange with hydrogen; only about 5% of the oxygen is in O$^+$. The case for S II is less clear and deserves special attention because it requires presently unavailable atomic data. The problem with sulfur is obvious when we recall the large difference between the ionization potential of S (10.36 eV) and of O (13.60 eV). This means that the backward (S$^+$ + H) and forward (H$^+$ + S) reactions proceed at very different

---

[2] In contrast, Draine (1980) actually used theoretical calculations of high energy cross sections.

rates, even at 10,000 K, so that S^+ and H^+ are less likely to be in equilibrium than are O^+ and II^+. Furthermore, the existing calculations of the rate coefficients are probably not definitive. For example, the calculations of Kimura et al. (1997) lead to a rate coefficient for the forward reaction of $k(H^+ + S) \sim 10^{-10}\,\mathrm{cm^3 s^{-1}}$ at 10,000 K, and they give a rough estimate of the backward reaction rate coefficient of $k(S^+ + H) \sim 10^{-15}\,\mathrm{cm^3 s^{-1}}$. If the latter value is correct, then destruction of S^+ by charge exchange with H is weaker than destruction by radiative recombination, and the chemical timescale of S^+ will be long compared to the dynamical timescale. Consequently, the rate equation for S^+ would have to be integrated along the streamlines, just like the equation for the total ionization. In a jet irradiated with hard X-rays, ions up to S^{6+} are produced. Presumably, the ions with charge greater than 2 or 3 rapidly charge exchange with H to produce S^{2+} (see Stancil 2001 for calculations of $S^{4+} + H$), but the charge exchange of S^{2+} with H is problematic (e.g., Butler & Dalgarno 1980). If this charge exchange reaction is really weak, then S^{2+} will decay slowly, and its rate equation would also need to be integrated along the streamlines. In any case, calculations of charge exchange of sulfur ions with H at energies of 1 eV and below are badly needed, as are charge exchange cross sections of S and S^+ with the ions and atoms of the abundant heavy elements.

4. Conclusions

Two types of charge transfer processes play an important role in the physics of the jets of young stellar objects. The first is $H^+ + H \rightarrow H + H^+$, and we showed how good calculations that agree with laboratory measurements allow us to make a definitive calculation of the coefficient of ambipolar diffusion heating for warm atomic regimes and to eliminate this process for heating the X-wind and similar protostellar jets. In the second example, we noted the lack of good low-energy cross sections for sulfur ions, $S^{n+} + H \rightarrow H^+ + S^{(n-1)+}$. Especially urgent are the rate coefficients for the singly and doubly-ionized ions. In addition, charge exchange rates are needed for S^+ with C, Si, and other atoms with smaller ionization potentials, and for H^+, O^+, and C^+ with S. Without this information, the abundance of S II cannot be determined reliably. This reservation applies to other atoms and ions with astrophysically useful diagnostic lines, especially in problems with short dynamical time scales, but also in interstellar clouds.

Acknowledgments

REFERENCES

Butler, S.H. & Dalgarno, A. 1980, *A&A*, **85**, 144.

Draine, B. 1986, *MNRAS*, **220**, 133.

Draine, B. 1980, *ApJ*, **241**, 1021.

Garcia, P.J.V. 2001, Ferreira, J., Cabrit, S., & Binette, L., *A&A*, **377**, 589.

IIunter, G. & Kuriyan, M. 1977, *Proc. Roy. Soc.*, **A353**, 575.

Kimura, M., Gu, J.P., Hirsch, G., & Bunker, R.J. 1997, *Phys. Rev.*, **A55**, 2778.

Krstić, P.S. and Schultz, D. 1998, *Atomic and Plasma-Material Data for Fusion*, **8**, 1.

Osterbrock, D. 1961, *ApJ*, **134**, 270.

Safier, P. 1993, *ApJ*, **408**, 115.

Shang, II., Glassgold, A.E., Shu, F.II., & Lizano, S. 2002, *ApJ*, **564**, 853.

Shu, F.H., *et al.* 2000, in *Protostars and Planets IV*, eds. V. Mannings, A.P. Boss, & S. Russell, University of Arizona, p. 789.

Stancil, P.C., *et al.* 2001, *J. Phys.*, **B34**, 2481.

Improved Simulations of Astrophysical Plasmas: Computation of New Dielectronic Recombination Data

T. W. Gorczyca, K. T. Korista, and O. Zatsarinny

Department of Physics, Western Michigan University, Kalamazoo, MI

N. R. Badnell

Department of Physics and Applied Physics, University of Strathclyde, Glasgow, UK

D. W. Savin

Columbia Astrophysics Laboratory, Columbia University, New York, NY

Abstract

Here we recap the works of two posters presented at the 2002 NASA Laboratory Astrophysics Workshop. The first was *Shortcomings of the R-Matrix Method for Treating Dielectronic Recombination.* The second was *Computation of Dielectronic Recombination Data for the Oxygen-Like Isoelectronic Sequence.*

1. Introduction

Most hard astrophysical numbers come from the quantitative analysis and interpretation of spectra, frequently of emitting plasmas that are at extremely low density by laboratory standards, and as a result the gas is in a profoundly non-equilibrium state. The physical conditions and the resulting spectrum cannot be predicted by analytical theory, and large-scale numerical simulations must be done instead. The results can be directly compared with a broad range of X-ray, UV, and IR observations, but rely on a vast sea of basic atomic and molecular cross sections and rates.

We have initiated a program to carry out detailed theoretical calculations for dielectronic recombination (DR) of specific 2nd, 3rd, and 4th row ions. These are investigated using a radiation-damped R-matrix approach as well as the perturbative AUTOSTRUCTURE package. These independently-determined DR rates are benchmarked against each other and, where possible, against experimental results. Here we detail two projects along these lines. First, a comparison between R-matrix, perturbative, and experimental results is made for DR of Fe XVIII, where certain shortcomings of these and other R-matrix methods are discovered. Second, we have used the perturbative program AUTOSTRUCTURE to compute DR and radiative recombination (RR) data along the entire O-like sequence, giving a single table of fitting coefficients.

2. Shortcomings of the R-Matrix Method for Treating Dielectronic Recombination

By performing new radiation-damped R-matrix scattering calculations for the photorecombination of Fe XVIII forming Fe XVII, we have demonstrated the difficulties and fundamental

inaccuracies associated with the R-matrix method for treating dielectronic recombination (DR). Our new R-matrix results (Gorczyca et al. 2002) have significantly improved upon earlier R-matrix results (Pradhan et al. 2001; Zhang et al. 2001) for this ion. However, we have shown theoretically that all R-matrix methods are unable to account accurately for the phenomenon of radiative decay followed by autoionization. For Fe XVIII, we have demonstrated numerically that this results in an overestimate of the DR cross section at the series limit, which tends to our analytically predicted amount of 40%. We have further found the need for fine resonance resolution and the inclusion of radiation damping effects. Overall, slightly better agreement with experiment (Savin et al. 1999) is still found with the results of perturbative calculations, which are computationally more efficient than R-matrix calculations by more than two orders of magnitude.

3. Computation of Dielectronic Recombination Data for the Oxygen-Like Isoelectronic Sequence

We have systematically calculated rate coefficients for dielectronic recombination (DR) along the oxygenlike sequence. A recent benchmarking of DR resonance strength and energies between our theoretical techniques and the experimental results from the Test Storage Ring in Heidelberg has already shown fairly good agreement for the most highly-ionized oxygen-like system we consider here, DR of Fe XIX forming Fe XVIII (Savin et al. 2002). At the low-charge end of this isoelectronic sequence, we benchmark our results using F II DR data which are determined from measured neutral fluorine photoionization measurements and the principle of detailed balance. To assess the reliability of our calculations for intermediate oxygenlike ionization stages, we compare between theoretical R-matrix and perturbative results. All calculations have been performed in intermediate-coupling, so that fine structure effects are incorporated. Furthermore, both $\Delta n = 0$ and $\Delta n > 0$ core transitions are included in order to span a higher temperature range. Final-state-resolved rate coefficients and total rate coefficients have been tabulated, and these data are available in either format from our web site (http://homepages.wmich.edu/~gorczyca/drdata).

Acknowledgments

REFERENCES

Gorczyca, T. W., Badnell, N. R., & Savin, D. W. 2001, Phys. Rev. A, 65, 062707.

Pradhan, A. K., Nahar, S.N., & Zhang, H. L. 2001, ApJ, 549, L268.

Savin, D. W., et al. 1999, ApJS, 123, 687.

Savin, D. W., et al. 2002, ApJS, in press.

Zhang, H. L., Nahar, S. N., & Pradhan, A. K. 2001, Phys. Rev. A, 64, 032719.

Laboratory Measurements of Charge Transfer
on Atomic Hydrogen at Thermal Energies

C. C. Havener, C. R. Vane, and H. F. Krause

Oak Ridge National Laboratory, Physics Division, Oak Ridge, TN

P. C. Stancil

Department of Physics and Astronomy, University of Georgia, Athens, GA

T. Mroczkowski and D. W. Savin

Columbia Astrophysics Laboratory, Columbia University, New York, NY

Abstract

We describe our ongoing program to measure velocity dependent charge transfer (CT) cross sections for selected ions on atomic hydrogen using the ion-atom merged-beams apparatus at Oak Ridge National Laboratory. Our focus is on those ions for which CT plays an important role in determining the ionization structure, line emission, and thermal structure of observed cosmic photoionized plasmas.

1.   Introduction

We are carrying out charge transfer (CT) measurements for selected ions on atomic hydrogen using the ion-atom merged-beams apparatus (Havener 1997) at the Oak Ridge National Laboratory (ORNL) Multicharged Ion Research Facility. Our focus is on those ions for which CT is known to play an important role in determining the ionization structure, line emission, and thermal structure of observed cosmic plasmas. Objects for which these measurements are important include active galactic nuclei (AGN), galactic halos, H II regions, the intergalactic medium (IGM), planetary nebulae (PNe), and shocks in supernova remnants and Herbig-Haro objects. Our work is relevant to the past and present NASA flight missions IUE, HST, FUSE, ISO, Chandra/LETG and the upcoming missions GALEX, SIRTF, SOFIA, FIRST, and NGST. The ORNL merged-beams apparatus is the only apparatus in the world currently capable of measuring CT cross sections with H at the thermal energies important for interpreting spectra from photoionized cosmic plasmas such as those found in AGN, the IGM, H II regions, and PNe.

Our measurements are used to produce accurate CT rate coefficients and to benchmark state-of-the-art theoretical techniques. An example is given by our merged-beams measurements and rate calculations for C^+ + H (Stancil et al. 1998). Using these results the rate coefficient for the reaction H^+ + C was also calculated and found to differ from previous calculations by orders of magnitude (Stancil et al. 1998). The majority of thermal CT rates used in astrophysics are from Landau-Zener (LZ) calculations (Kingdon & Ferland 1996). These calculations are inapppropriate for collisions at eV energies and serve only as estimates, reliable, at best, to only a factor of three.

2. Merged-Beams Technique

At ORNL, an ion-atom merged-beams apparatus is used to study charge transfer by multicharged ions from ground-state H or D atoms at collision energies from 20 meV/amu to 5000 eV/amu. Relatively fast (keV) beams are colinearly merged producing low energy collisions in a moving center-of-mass frame. A 6-8 keV neutral hydrogen (deuterium) beam is produced via photodetachment of a H^- (D^-) beam as it passes through the inner cavity of a YAG laser. The neutral beam is electrostatically merged with an intense multicharged $q \times (8-25)$ keV ion beam from an Electron Cyclotron Resonance (ECR) ion source. Absolute charge transfer cross sections are determined at each collision energy directly from experimental parameters that include the primary beam intensities, beam-beam overlap or form factor, beam-beam signal rate, merge path length, and velocities of the beams.

3. Measurements

Figure 1 shows our merged-beams data for Si^{4+} (Pieksma *et al.* 1996), C^{4+} (Bliek *et al.* 1997), and N^{4+} (Folkerts et al. 1995) ions on H(D) with an energy scale from 10^{-2} to 10^3 eV/amu. As can be seen in the figure, at the higher energies all three ions have approximately the same cross section, agreeing to within 25% of the experimentally observed (Phaneuf *et al.* 1982) empirical scaling formula $q \times 10^{-15}$ cm^2. At lower energies (eV/amu), the cross sections vary by more than an order of magnitude. No simple scaling law is known that can predict the charge transfer cross section at eV/amu energies. Landau-Zener calculations can be used to estimate the energy dependence of the cross section but are not considered accurate.
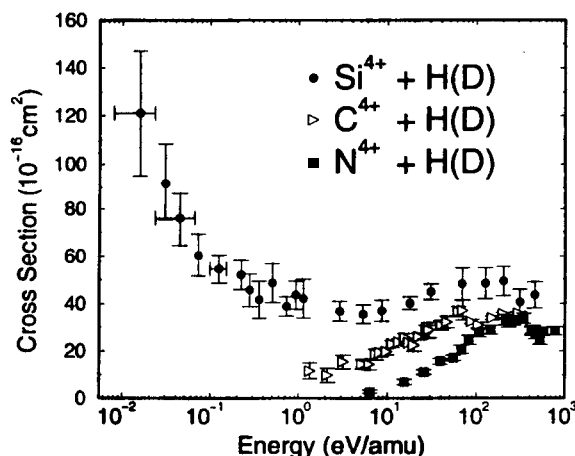
Fig. 1.— ORNL ion-atom merged-beams data for various quadruply- charged ions with H (D). The error bars correspond to the relative error at a level of two standard deviations. The decrease in the error bars for the C^{4+} data are in part due to improvements to the apparatus and an improvement in the intensity and quality of the beams produced by the ECR ion source. The absolute uncertainty is typically 15% at a level of two standard deviations.

Coupled-channel molecular-orbital fully-quantal calculations (Stancil et al. 1998; Gargaud & McCarroll 1988) are considered most appropriate at these energies but are difficult to perform. At energies below 10 eV/amu the Si^{4+} cross section is seen to increase as $1/v$, where v is the relative collision velocity, due to trajectory effects arising from the ion-induced dipole attraction. These measurements (which below 10 eV/amu had to be performed with D due to the limited dynamic energy range of the ECR source) agree with MOCC calculations (Pieksma et al. 1996) for Si^{4+} + D. Our measurements verify the accuracy of the theory for this system. The MOCC calculation (Gargaud & McCarroll 1988) for collisions with H when compared to the calculation with D, predict a strong isotope effect for this collision system. The theoretical cross section for H is predicted to be 1.9 times that for D at the lowest energies.

Acknowledgments

REFERENCES

Blick, F. W., Hoekstra, R., Bannister, M. E., & Havener, C. C. 1997, *Phys. Rev. A*, **56**, 426.

Folkerts, L., Haque, M. A., Havener, C. C., Shimakura, N., & Kimura, M. 1995, *Phys. Rev.*, **A51**, 3685.

Gargaud, M. & McCarroll 1988, R., *J. Phys. B*, **21**, 513.

Havener, C. C. 1997, in *"Accelerator Based Atomic Physics Techniques and Applications"*, ed. by S. Shafroth and J. Austin, (Woodbury New York: AIP Press), p. 117-145.

Kingdon, J. B., & Ferland, G. J. 1996, *ApJS*, **106**, 205.

Phaneuf, R. A., Alvarex, I., Meyer, F. W., & Crandall, D. H. 1982, *Phys. Rev. A*, **26**, 1892.

Pieksma, M., Gargaud, M., McCarroll, R., & Havener, C. C. 1996, *Phys. Rev. A*, **54**, R13.

Stancil, P. C., et al. 1998, *ApJ*, **502**, 1006.

Charge Transfer Collisions in Ionospheres, Exospheres, and Interstellar Clouds

David L. Huestis

Molecular Physics Laboratory, SRI International, Menlo Park, CA

Jeffery A. Spirko and A. Peet Hickman

Department of Physics, Lehigh University, Bethlehem, PA

The ionization potentials of $O(^3P_1)$ and H atoms are equal to within the current experimental uncertainty. This means that the charge transfer reactions

$$O + H^+ \leftrightarrow O^+ + H$$
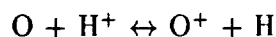
have very large cross sections in both directions, and thus play central roles in interactions with the solar wind and atomic escape in the exospheres of Venus, Earth, and Mars, as well as in interstellar clouds. We are performing *ab initio* electronic structure calculations [1] and quantum mechanical coupled channels calculations, including spin-orbit coupling, of differential and momentum transfer cross sections for charge exchange and fine structure excitation in this system. The work builds on previous theoretical [2-5] and photodissociation spectroscopy studies [3,6,7] of the OH^+ molecule and parallels our previous calculations on collisions of O^+ with O [8,9]. For several transitions, collision mechanisms based on curve crossings have been identified. The results indicate that long range coupling terms in the OH^+ potentials (internuclear distances of 10-15 a_0) contribute to the cross sections.

In interstellar clouds O/H charge exchange is an important step in formation of the OH radical. It also influences the ratio of $[O^+]/[O]$ versus $[H^+]/[H]$. At low temperature all the $O(^3P_J)$ population is in the $O(^3P_2)$ sublevel and the reaction of $O(^3P_J)$ with H^+ becomes much slower than $O^+(^4S_{3/2})$ with H, thus breaking the equillibrium relationship of $[O^+]/[O]$ with $[H^+]/[H]$. The relative reaction and production rates of $O(^3P_J)$ modify the distribution of population in the sublevels, thus changing the relative intensities of 63 μ and 145 μ atomic oxygen emissions.

II$^+$ in the solar wind collides with O atoms in the upper atmospheres of Venus, Earth, and Mars. On Venus and Mars this is the origin of about 10% of the exospheric ionization. Other effects include production of hot H atoms; facilitating upward flow of H, H^+, O, and O^+, as well as interhemispheric transport of hydrogen; transfering kinetic energy to O and O^+; mediating magnetosphere-ionosphere coupling; and modifying the $[O^+]/[O]$ and $[H^+]/[H]$ ratios versus altitude.

For many applications the key parameters are the state-to-state reaction rate coefficients (k) or total charge transfer cross sections (σ). Several laboratory measurements and theoretical calculations of these quantities exist, although significant uncertainties remain. However, modeling of kinetic energy transfer, transport, and magnetosphere-ionosphere coupling requires

differential cross sections $(d\sigma/d\Omega)$ for which theoretical tools exist, but no experimental or theoretical results are available.

The absolute magnitude of the total and differential cross sections is dominated at low energy by the long-range behavior of the matrix element between $|O(^3P_1)H^+{:}^3\Sigma^->$ with $|O^+(^4S_{3/2})H{:}^3\Sigma^->$. Our recent calculations [1] show that Stark mixing of the $O(2p^43s)$ configuration significantly increases the magnitude of the charge-transfer matrix element, moving the critical region to larger internuclear distance, and increasing the cross sections.

Additional information about the long range potential energy curves and coupling matrix elements can be obtained from analysis of experimental spectroscopy studies [3,6,7] of the energies, widths, and dissociation products of quasibound rovibrational levels of photoexcited OH^+ molecules. For example, the recent experiments in the Heidelberg heavy-ion storage ring [6,7] find expectedly high and narrow predissociating levels for low rotational quantum numbers, suggesting that the calculated [2-5] potential energy curves are too attractive at long range.

Acknowledgments

REFERENCES

[1] J. A. Spirko, J. T. Mallis, and A. P. Hickman, *J. Phys. B*, **33**, 2395–2407 (2000).

[2] G. Chambaud, J. M. Launay, B. Levy, P. Millie, E. Roueff, and F. T. Minh, *J. Phys. B*, **13** 4205–4216 (1980).

[3] H. Helm, P. C. Cosby, and D. L. Huestis, *Phys. Rev. A*, **30**, 851–857 (1984).

[4] R. P. Saxon and B. Liu, *J. Chem. Phys.*, **85**, 2099–2104 (1986).

[5] P. C. Stancil, D. R. Schultz, M. Kimura, J.-P. Gu, G. Hirsch, and R. J. Buenker, *Astron. Astrophys. Supp. Ser.*, **140**, 225–236 (1999).

[6] U. Hechtfischer, "Near Threshold Photodissociation of Cold CH^+ and OH^+ Molecular Ions," Thesis (U. Heidelberg, 1998).

[7] J. Levin, U. Hechtfischer, L. Knoll, M. Lange, G. Saathoff, R. Wester, A. Wolf, D. Schwalm, and D. Zajfman, *Hyperfine Interactions*, **127**, 267–270 (2000).

[8] A. P. Hickman, M. Medikeri-Naphade, C. D. Chapin, and D. L. Huestis, *Geophys. Res. Lett.*, **24**, 119 122 (1997).

[9] A. P. Hickman, M. Medikeri-Naphade, C. D. Chapin, and D. L. Huestis, *Phys. Rev. A*, **56**, 4633 4643 (1997).

Emission Line Spectra in the Soft X-ray Region 20 – 75 Å

J. K. Lepson

Space Sciences Laboratory, University of California, Berkeley, CA

P. Beiersdorfer and H. Chen

Dept of Physics & Advanced Technology, Lawrence Livermore National Laboratory

E. Behar and S. M. Kahn

Columbia Astrophysics Laboratory, Columbia University, New York, NY

Abstract

As part of a project to complete a comprehensive catalogue of astrophysically relevant emission lines in support of new-generation X-ray observatories using the Lawrence Livermore electron beam ion traps EBIT-I and EBIT-II, emission lines of argon and sulfur in the soft X-ray and extreme ultraviolet region were studied. Observations of Ar IX through Ar XVI and S VII through S XIV between 20 and 75 Å are presented to illustrate our work.

1. Introduction

Satellite observations in the soft X-ray and extreme ultraviolet region provide important diagnostic opportunities for astronomers. The region between 20 and 80 Å has received scant attention, however, even in solar measurements. Observations in the soft x-ray region by the *Chandra X-ray Observatory* and *XMM-Newton* are now providing high-resolution measurements, which have far outpaced available databases. There are many more lines in these spectra than can be currently identified, as is illustrated by Chandra spectra of Capella (Brinkman 2000) and Procyon (Raassen *et al.* 2002).

Long-term exposures of HR 1099 have shown a wealth of weak lines that cannot be identified with available databases. These weak lines raise the "background" level for the brighter, known lines and add uncertainty to their interpretation. Contributions to these unidentified lines are thought to come from argon, sulfur, silicon, magnesium, calcium, iron, and nickel. Calculations are helpful to predict emissions from these elements. However, a major problem is that the wavelengths are frequently unreliable, given the high density of unidentified lines in this region. This is because the structure of the intermediate ionization stages of all high-Z ions of astrophysical interest are significantly affected by electron-electron interactions, and these ionization stages must be calculated in intermediate coupling. Wavelength errors of a few percent are not uncommon, and no *ab initio* code can calculate wavelengths to better than a quarter percent for mid-Z L-shell or M-shell ions.

Laboratory measurements are thus essential to locate the lines and to correlate them with the proper charge state. We are undertaking a concerted effort to identify all important lines from all relevant elements and ionization stages in this wavelength region (e.g, Lepson *et al.* 2000, 2002). Here we present spectroscopic measurements of argon and sulfur. These measurements were taken on the Lawrence Livermore electron beam ion trap EBIT-II. We also have performed new calcululations using of the Hebrew University - Lawrence Livermore Atomic Code HULLAC, which were used for comparison.

2. Spectroscopic measurements

EBIT-II has been operating since January 1990. It is the second electron beam ion trap to be put into operation, following the device's development at the Lawrence Livermore National Laboratory in 1986. It is particularly well-suited for spectral investigations because it can be operated at the low voltages (100–1,000 eV) necessary to produce the appropriate charge states. Moreover, different charge states can be produced simply by changing the voltage of the electron beam. As the voltage increases, higher charge states appear when their ionization potentials are exceeded; by systematically recording spectra at different energies and observing the rise and relative decline of different charge states, it is possible to determine which emission lines belong to which charge state.

Spectra were measured with a grazing-incidence spectrometer (Utter *et al.* 1999). Readouts were taken with a back-illuminated, liquid nitrogen-cooled CCD camera with a one inch square array of 1,024 × 1,024 pixels. Figure 1 shows a representative spectrum of argon taken on EBIT-II at a beam energy of 900 eV, with the strongest argon lines labeled by charge state. Note that charge states from Ar IX through Ar XVI are present. The charge states were identified by comparing spectra taken at different beam energies (cf. Lepson *et al.* 2000). This spectrum was chosen to show all the charge states we investigated; lower energy spectra have fewer charge states present. Figure 2 shows a spectrum of sulfur taken at a beam energy of 600 eV. Emission lines from charge states S VII through S XIV are identified. We also constructed synthetic spectra derived from our HULLAC calculations. A sample synthetic spectrum is shown in Fig. 3; this spectrum has been made to emulate Fig. 2, and includes S VII through S XIV. The synthetic HULLAC spectra were intensity corrected for our detector response to be directly comparable with our measurements and to assist in line identification.

3. Summary

Our work is an ongoing effort to catalogue all astrophysically relevant lines in the soft X-ray and extreme ultraviolet region (25 – 140 Å). Our laboratory measurements and spectral modeling represent a synergistic approach to build up such a catalogue. In this setting, most strong lines and some weaker lines can be identified with confidence. We will continue these studies until all important lines are identified. The L-shell spectra of silicon, for example, are currently being measured, and results will be available in the near future.

Acknowledgments

REFERENCES

Brinkmann, A. C., *et al.*, 2000, *ApJ*, **530**, L111.
Dere, K. P., *et al.*, 1997, *A&AS*, **125**, 149.
Dere, K. P., *et al.*, 2001, *ApJ*, **134**, S331.

Kaastra, J. S., & Mewe, R. 1993, *Legacy*, **3**, 6.

Lepson, J. K., *et al.*, 2000, *Rev. Mexicana Astron. Astrofis. Ser. de Conf.*, 9, 137.

Lepson, J. K., *et al.*, 2002, *ApJ*, in press.

Mewe, R., Kaastra, J. S., & Liedahl, D. A. 1995, *Legacy*, **6**, 16.

Raassen, A. J. J., *et al.*, 2002, *A&A*, in press (astro-ph/0204385).

Smith, R. K., & Brickhouse, N. S., 2000, *Rev. Mex. Astron. Astrofis. Ser. de Conf.*, 9, 134.

Utter, S. B., *et al.*, 1999, *Rev. Sci. Instrum.*, **70**, 284.
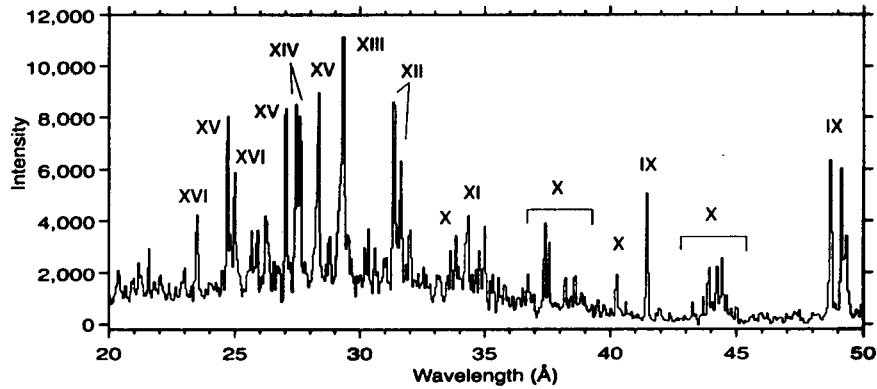
Fig. 1.— Spectrum of argon taken on EBIT-II at a beam energy of 900 eV, with Ar IX through Ar XVI present. Major peaks are labelled for each charge state.
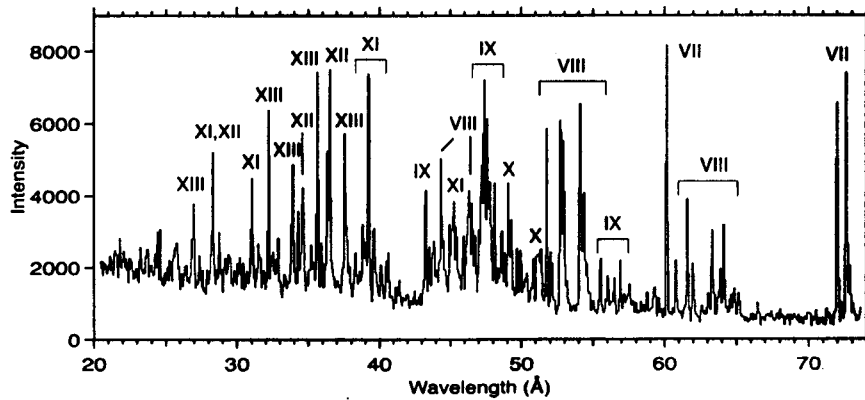
Fig. 2. Spectrum of sulfur taken on EBIT-II at a beam energy of 600 eV, with S VII through S XIV present. Major peaks are labelled for each charge state.
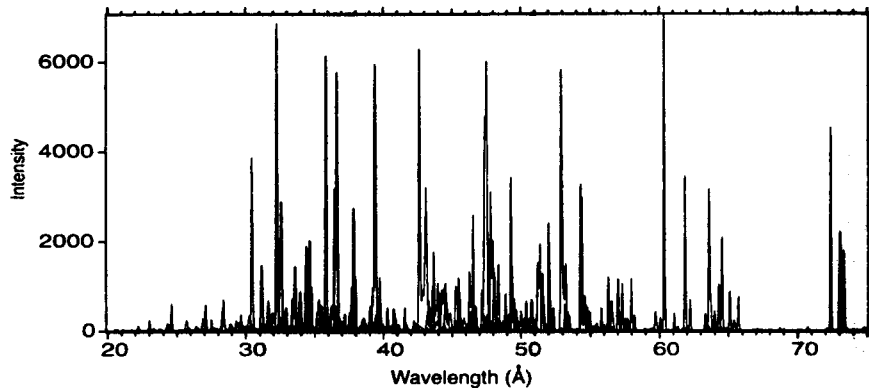
Fig. 3.— Synthetic spectrum of sulfur calculated with HULLAC. Spectrum includes S VII through S XIV, and has been intensity corrected for the detector response to be directly comparable to the EBIT-II data. Relative peak sizes were adjusted between data and calculations to match for the highest peak in each charge state.

Interchannel Coupling in the Photoionization
of Atoms and Ions in the X- Ray Range

Steven T. Manson

Georgia State University

Himadri S. Chakraborty

Kansas State University

Pranawa C. Deshmukh

Indian Institute of Technology-Madras, India

Photoionization cross sections of atoms and ions are of great importance in astrophysical modeling. Since experimental cross sections for most species of astrophysical interest are not yet available, a great deal of effort has gone into the calculation of these cross sections and the associated ionization rates, e.g., the Opacity Project [1], using highly sophisticated theoretical methodologies which include extensive accounting for electron-electron correlation effects. These efforts are confined almost exclusively to outer and near-outer shells of the relevant atoms and ions; the inner shell photoionization data complilations are primarily results of using very much simpler independent particle model (IPM) calculations [2]. This is the data base used in connection with the virtually laboratory-quality data in the x-ray region produced by the recently-launched CHANDRA mission, and other x-ray astronomy missions. Of significance in this regard, however, it has been recently shown that electron- electron correlation is not unimportant for photoionization at x-ray energies or for inner shells [3,4]. In fact it has been found that electron-electron correlation, in the form of interchannel coupling [5], is important for most subshells, of most atoms, at most energies [6]. Basically what is found is that when there is a photoionization channel with a large cross section degenerate with a channel with a small cross section, interchannel coupling can modify the cross section of the channel with the smaller cross section significantly. Electron-electron correlation in atoms and ions is a result of the Coulomb interaction between the pairs of atomic/ionic electrons. With increasing stage of ionization, however, this interelectron Coulomb interaction becomes increasingly less important as compared to the nuclear Coulomb interaction.

To understand how this interchannel coupling, so important in neutral atoms, applies to positive ions, a research program has been initiated to deal with this question, i.e., a program to quantify the effects of interchannel coupling in ionic photoionization, thereby assessing existing photoionization data bases in the x-ray region. To accomplish this task, we have employed the Relativistic Random-Phase-Approximation (RRPA) methodology [7,8] which includes significant aspects of electron-electron correlation, including interchannel coupling. The RRPA methodology has been found to produce excellent agreement with experiment for neutral Ne at photon energies in the 1 keV range [3]. Specifically, it was found the the ratio of the 2s to 2p photoionization cross sections is altered by interchannel coupling as much as about 40% for 1.5 keV photons as compared to a similar calculation that ignored interchannel coupling. In the keV energy region the 2s cross section is significantly larger than the 2p since the 2s

cross section falls off with energy much more slowly than the $2p$ [9]. The "real" wave functions for the $2p$ photoionization channels contains a small admixture of the wave functions of the $2s$ photoionization channels. And, since the $2s$ cross section dominates here, this small admixture leads to a significant alteration of the $2p$ cross section, producing the results discovered earlier [3]. It is also worthwhile to point out that the Ne I calculation showed that the cross section ratio calculated with fully coupled channels, as compared to the result which omits channel coupling, diverge from each other with increasing energy. In other words, the effect seen for Ne I in the 1 keV photon energy region becomes more and more pronounced with increasing energy.

Calculations have been performed on the neon isoelectronic sequence as a test case to illustrate the behavior of interchannel coupling with increasing stage of ionization. Specifically, we have investigated every member of the sequence form neutral Ne I to neon-like Fe XVII. Photon energies from the first $2p$ threshold to at least 25 times the threshold energy were considered; this meant going up to over 30 keV in Fe XVII. In each case two calculations were performed, as was done previously for neutral Ne [3]. In one calculation, a full RRPA was done, with all of the channels coupled. In the second, the coupling among channels arising from different subshells, $2p$, $2s$ and $1s$ for the case of neon-like systems, was omitted to spotlight the effect(s) of this coupling.

The results show that at the higher energies, the interaction of the larger $2s$ cross section with the smaller $2p$ cross section modifies the former by a factor of about 1.4 in neutral neon. Along the isoelectronic sequence, the calculation shows that this modification decreases monotonically to about 1.1 in neon-like iron at the highest energies considered. However, in each case, the fully coupled ratios are diverging from the ratios calculated without channel coupling with increasing energy, just as was the situation for Ne I. It is interesting to note that the influence of correlation upon many other ionic properties does not decrease smoothly as a function of the stage of ionization [10,11] as it appears to here. In any case, based upon these results, our preliminary conclusion is that interchannel coupling must be taken into account for the photoionization of neutral and low-charge ions, and becomes less and less important as the ionic charge increases, but more and more important with increasing photon energy. Several other cases need to be investigated before we can confirm this tentative conclusion. Such studies are in progress.

Finally, it is worthwhile to point out how this results affect the modelling of astrophysical plasmas. It is clear from the above discussion that the coupling of channels can strongly affect the photoionization cross sections of weak channels that are degenerate with cross sections from much stronger channels. Since it is only the small cross sections that are significantly affected, the total photoionization cross section is not changed very much by this interchannel coupling effect. But, for inner shell photoionization, the response to the creation of an inner shell vacancy of an ion in an astrophysical plasma, e.g, x-ray or Auger electron emission, depends critically upon the specific subshell in which the vacancy is created. Thus, small cross sections become important because they populate different states, and produce differing x-ray energies, from their larger counterparts. Furthermore, this alteration of cross sections has an equal effect of

the astrophysically-important inverse process, radiative recombination; both the probability of producing certain recombined states, as well as the details of the recombinationation radiation in the x-ray region, can be significantly affected. Thus, to understand the basic physics of the astrophysical plasma, as regards the x-ray region, a quantitative understanding of all inner shell photoionization cross sections of any reasonable size is required, not just the largest ones, particularly as the higher x-ray energies become important in a particular astrophysical situation.

Acknowledgments

REFERENCES

[1] *The Opacity Project* (Institute of Physics Publishing, Bristol and Philadelphia, 1995).

[2] R. F. Reilman and S. T. Manson, *Ap. J. Supp.*, **40**, 815 (1979); D. A. Verner and D. G. Yakovlev, *Astron. Astrophys. Supp.*, **109**, 125 (1995).

[3] E. W. B. Dias, H. S. Chakraborty, P. C. Deshmukh, S. T. Manson, O. Hemmers, P. Glans, D. L. Hansen, H. Wang, S. B. Whitfield, D. W. Lindle, R. Wehlitz, J. C. Levin, I. A. Sellin and R. C. C. Perera, *Phys. Rev. Letters*, **78**, 4553 (1997).

[4] H. S. Chakraborty, D. L. Hansen, O. Hemmers, P. C. Deshmukh, P. Focke, I. A. Sellin, C. Heske, D. W. Lindle and S. T. Manson, *Phys. Rev. A*, **63**, 042708 (2001).

[5] U. Fano and J. Cooper, *Rev. Mod. Phys.*, **40**, 441 (1968).

[6] D. L. Hansen, O. Hemmers, H. Wang, D. W. Lindle, I. A. Sellin, H. S. Chakraborty, P. C. Deshmukh and S. T. Manson, *Phys. Rev. A*, **60**, R2641 (1999).

[7] W. R. Johnson and C. D. Lin, *Phys. Rev. A*, **20**, 964 (1979).

[8] W. R. Johnson, C. D. Lin, K. T. Cheng and C. M. Lee, *Phys. Scr.*, **21**, 409 (1980).

[9] M. Ya. Amusia, N. B. Avdonina, E. G. Drukarev, S. T. Manson and R. H. Pratt, *Phys. Rev. Lett.*, **85**, 4703 (2000).

[10] S. T. Manson, C. E. Theodosiou, and M. Inokuti, *Phys. Rev. A*, **43**, 4688 (1991).

[11] H. S. Chakraborty, P. C. Deshmukh, W. B. Dias, and S. T. Manson, *Ap. J.*, **357**, 1094 (2000).

Empirical Near-UV Line Parameters from Hubble Spectroscopy

Ruth C. Peterson,[1] Bruce W. Carney[2], Ben Dorman[3], Elizabeth M. Green[4],
Wayne Landsman[5], James Liebert[6], Robert W. O'Connell[6], and Robert T. Rood[6]

1) University of California Santa Cruz

2) University of North Carolina

3) L-3Com Analytics Corp.

4) University of Arizona

5) Science Systems & Applications, Inc.

6) University of Virginia

Abstract

Laboratory astrophysics is critical to our Hubble Treasury program GO-9455, whose goal is to characterize the age and metallicity of old stellar systems. We are calculating from first principles[1] the near-UV spectra for a wide variety of old stars, and coadding these using weights derived from stellar isochrones to model mono-age, mono-metallicity composite systems. However, our calculations do not match near-UV spectra of solar-type stars, for which laboratory identifications of atomic lines become incomplete. We will continue our empirical pseudo-identifications of these unknown near-UV lines using observed echelle spectra of individual stars. A much better solution would be additional near-UV laboratory identifications for neutral and first-ionized species of iron-peak elements.

Characterizing the age and metallicity of spatially unresolved systems older than a few billion years is the goal of our Hubble Treasury program GO-9455. We are calculating a set of theoretical stellar spectra covering 2280 – 3120 Å for main-sequence turnoff stars, whose light dominates this spectral region in an old globular cluster or elliptical galaxy, plus red giants, blue stragglers, and hotter evolved blue horizontal branch stars, whose contribution must also be evaluated. The calculations are coadded to represent the integrated light of a simple composite system. Its age is inferred from the temperature of the main-sequence turnoff stars giving the best match, and metallicity from their line strengths.

However, the calculations do not yet match solar-metallicity stars well enough. The weak-lined pseudo-continuum regions that best fix the temperature show greater absorption than predicted in the near-UV spectra of solar-type stars with metal abundances above one-fifth solar, [Fe/H] > −0.7. As described by Peterson, Dorman, & Rood (2001, *ApJ*, **559**, 372), this is because lines are missing from our calculations, lines too weak to have been identified in the laboratory but strong enough to appear in solar-metallicity spectra.

We model such lines by comparing against a group of observed spectra, in an iterative bootstrap procedure. We estimate an identification based on the change in the strength of a

---

line from one star to another of different temperature but similar line strength. We guess a wavelength and transition probability, recalculate the relevant spectra, and adjust as necessary. We match the weakest-lined stars first, then proceed to stronger-lined ones.

The limited success of this procedure is illustrated in the figures. Each plot shows comparisons for seven stars of an observed near-UV spectrum (heavy line) versus a model calculation (light line). Calculations in Fig. 1 use the unmodified Kurucz line list for atomic lines identified in the laboratory, downloaded from http://cfaku5.harvard.edu. Calculations in Fig. 2 are based on this line list modified as described as above. Each pair of spectra is offset vertically for clarity; the tick marks are separated by 10% of the full scale of each plot. The HD number or other identification of the observed star is given on the right. Below are the parameters of the model used in the calculations. The effective temperature, log gravity, [Fe/H] and microturbulent velocity are followed by the logarithm of the abundance enhancement of O, Mg, Si, Ca, and Ti with respect to iron. For the top spectrum, of the blue horizontal branch star 2206 in the globular cluster NGC 6752, an ATLAS 12 model with zero microturbulent velocity was used to model its near-solar iron-peak abundances.

The unmodified line list can match only the extremely weak-lined spectra. In the comparison shown at the bottom, its calculations overestimate the flux level between 2650 – 2700 Å for α Cen A by a factor of three. With the modified line list, only for [Fe/H] $\geq$ −0.6 are significant discrepancies seen in this region. Our Treasury program first seeks to remedy this by obtaining echelle spectra of high S/N and resolution for several stars of one-fifth solar to solar metallicity, to fill in the remaining gaps. The calculations will then be extended to hotter and cooler stars, and tested with observations of main-sequence turnoff stars and blue stragglers in the open clusters M 67 and NGC 6791 and five Andromeda globular clusters. All our observations will become public immediately, and our calculations will be made public as they are completed. For more information and tables of targets, see the Spring 2002 Newsletter of the Space Telescope Science Institute, at http://sco.stsci.edu/newsletter.

The true remedy is more extensive laboratory identifications. Laboratory astrophysicists suggest that most of our missing lines arise from the neutral species of iron-peak elements, with some contribution from first-ionized species. We urge the relevant laboratory studies to identify at least the wavelength and species of as many such near-UV lines as possible.

FIGURE 1 - Using an Unmodified Kurucz Laboratory Line List

6752-2206
11000 4.0 -1.50 A12

19445
6050 4.5 2.00 1.0
0.8 MgSiCaTi.35

94028
6050 4.2 -1.40 1.3
0.5 Mg.35SiCaTi.3

128167
6850C4.3 -0.35 2.0
0.0 MgSiCaTi.0

201891
5900C4.1 -1.00 1.0
0.2 Mg.25SiCaTi.2

184499
5750C4.0 0.60 1.2
0.1 Mg.3 SiCaTi.25

128620
5800C4.3 0.15 1.0
0.0 MgSiCaTi.0
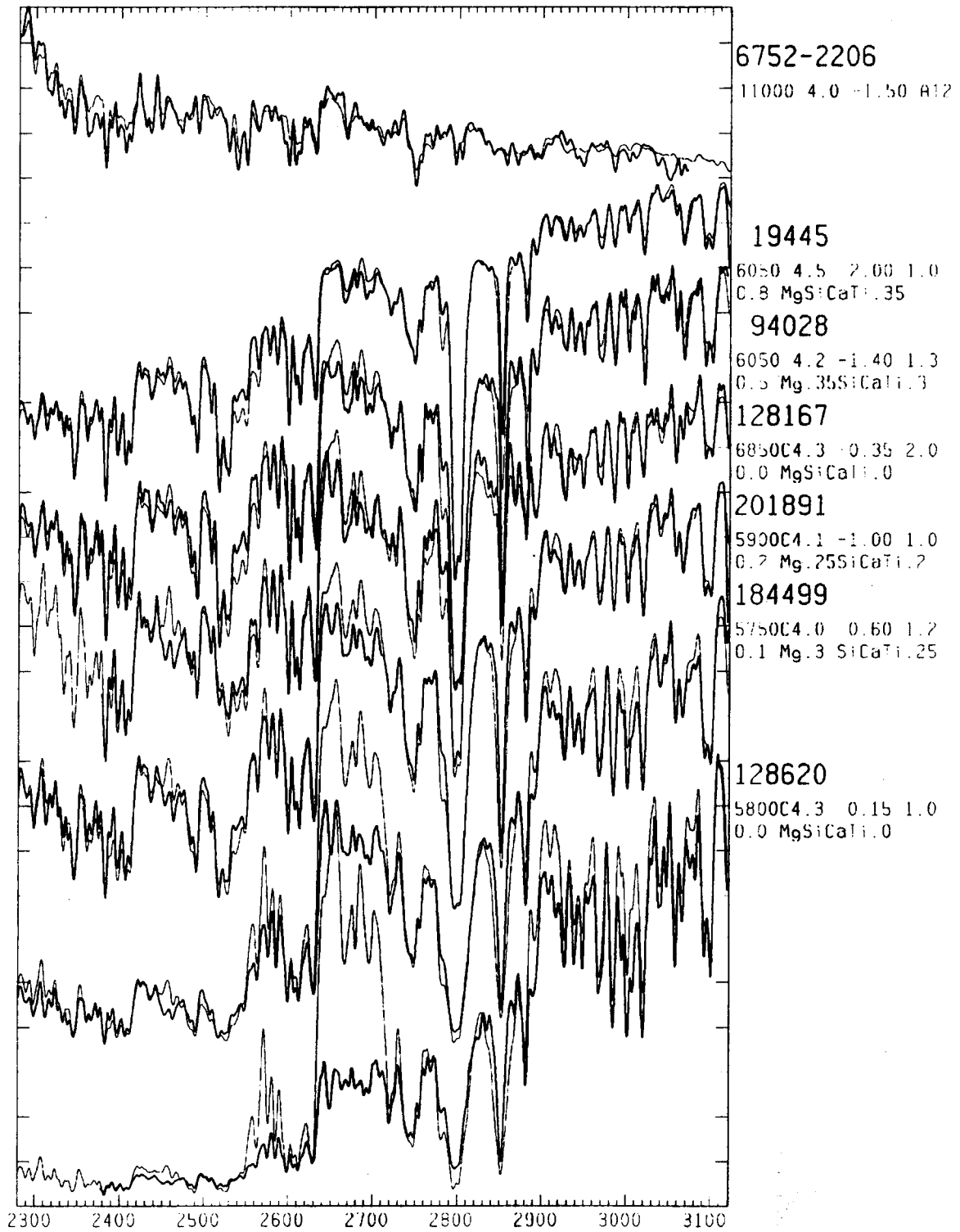
FIGURE 2 - Using the Modified Kurucz Laboratory Line List

6752-2206
11000 4.0 1.50 A12

19445
6050 4.5 2.00 1.0
0.8 MgSiCaTi.35

94028
6050 4.2 -1.40 1.3
0.5 Mg.35SiCaTi.3

128167
6850C4.3 0.35 2.0
0.0 MgSiCaTi.0

201891
5900C4.1 -1.30 1.0
0.2 Mg.25SiCaTi.2

184499
5750C4.0 0.60 1.2
0.1 Mg.3 SiCaTi.25

128620
5800C4.3 0.15 1.0
0.0 MgSiCaTi.0
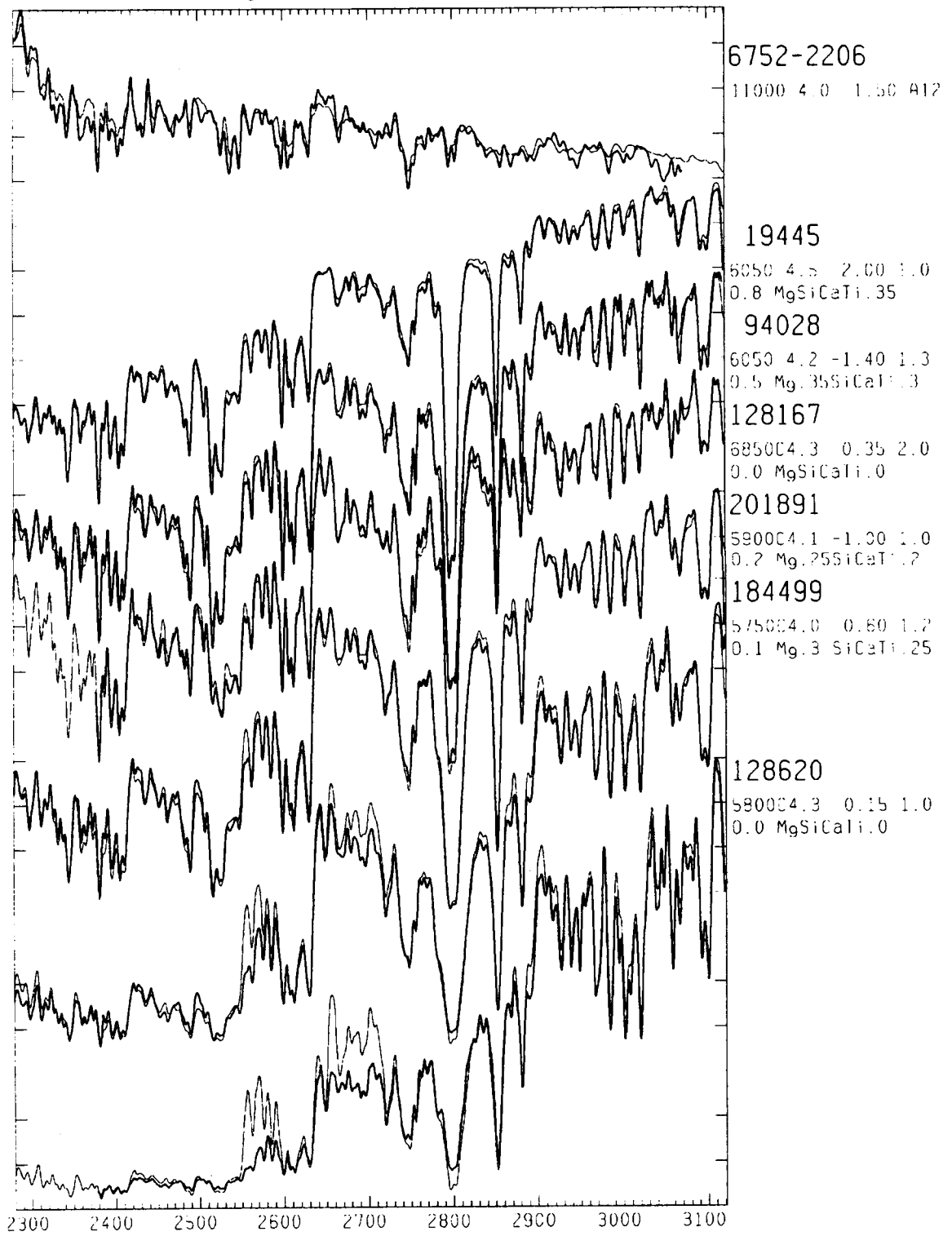
Laboratory Astrophysics and High Resolution Atomic Spectroscopy with the Imperial College Fourier Transform Spectrometer

Juliet C. Pickering, Anne P. Thorne and Richard Blackwell-Whitehead

Blackett Laboratory, Imperial College, London

Abstract

We report work, both recently completed and still in progress, on significant improvements to wavelengths, energy levels and oscillator strengths of neutral and singly ionised atoms of astrophysical importance, mainly in the iron group, carried out by means of high resolution Fourier transform spectroscopy from the near infrared to the vacuum ultraviolet regions. In some cases hyperfine structure has also been analysed. We also report highly accurate measurements of absolute wavelengths of certain transitions relevant to studies of possible variation of the fine structure constant.

1. Introduction

For several years the Imperial College (IC) Fourier transform spectrometry group has been focusing on improvements in the laboratory atomic and molecular data base needed by astrophysicists. Fourier transform (FT) spectrometry is ideal for this work because it combines high resolution, broad spectral range, high absolute wavenumber accuracy and good optical throughput (Pickering 1999). Improvements in the quality of astrophysical spectra observed with high resolution spectrographs on both ground and space-based telescopes have shown up the inadequacy of the laboratory data base needed to interpret the observations.

The FT spectra yield lines with very accurate wavenumbers (better than $1: 10^7$). The line lists are valuable in themselves and are also used for large scale term analyses, from which the accuracy of known energy levels is improved, usually by an order of magnitude, and new levels are identified. These in turn make possible the prediction of lines that may not be observable in the laboratory. Measurement of the line intensities leads to the determination of branching ratios and hence to transition probabilities. In addition, the high resolution makes it possible to analyse hyperfine structure (hfs), which has proved to play an essential role both in abundance studies and in the unravelling of blends.

2. Experimental

Most of the spectra were recorded at IC with our visible/ultraviolet FT spectrometers (Thorne *et al.* 1987), one of which uses a MgF_2 beamsplitter to extend the spectral range down to 140 nm (Thorne 1996). Where infrared spectra are required for completeness, as in large-scale spectral analysis and in some of the branching fraction measurements, we have recorded spectra with the high resolution IR FT spectrometer at NIST or, in some cases, used the archive from the FT spectrometer on the McMath telescope at Kitt Peak National Observatory. The instrumental resolution in all spectra was sufficiently high that the line width was determined by Doppler broadening in the source. A sufficient number of interferograms were co-added to reach acceptable signal-to-noise ratios. The light source in most cases was a

water-cooled hollow cathode discharge run in argon or neon at a few mbar pressure at currents up to 600 mA. A Penning discharge lamp at currents up to 2 A was used to excite the higher energy levels for the work on branching ratios in the Fe II spectrum.

3. Large scale term analyses, branching ratios and transition probabilities

Most of our effort has been directed at the neutral and singly ionised spectra of the iron group elements because of their importance in stellar atmospheres. The results for Fe I, Ni I, Co I and Co II were published some years ago, and we are currently working on Mn I, Cr I and V I and II. In all cases the accuracy of wavenumbers and energy levels should improve by an order of magnitude.

The state of the atomic data base for oscillator strengths (f-values) is even less satisfactory than for wavelengths. Much reliance has to be placed on calculations, which are frequently good for strong lines but notoriously unreliable for weak lines. Relative oscillator strengths (f-values) for lines starting from the same upper level are found experimentally from their relative intensities (branching ratios). If all significant transitions are included (frequently covering a wide spectral range), the ratios can be normalized to become branching fractions, and the relative f-values are made absolute if the lifetime of the level is measured or calculated. Calculated lifetimes are usually acceptable when there are no measurements available because lifetime is determined predominantly by the generally reliable strong transitions.

We have recently completed (Pickering *et al.* 2001) extensive branching ratio measurements in Ti II, resulting in f-values for 328 lines from levels with measured lifetimes and a further 335 lines from levels with liftimes calculated by Kurucz (Kurucz 2001). Typical uncertainties are 7% for strong lines and better than 20% for the majority of weaker lines.

Despite the attention that has been paid to determining f-values in iron, there is a serious lack of accurate experimental values for Fe II in the ultraviolet spectral region. Weak lines are especially important because the strong lines are frequently saturated in the astrophysical spectra and cannot be used in abundance determinations or as a probe of physical conditions. As part of the FERRUM project, we have measured branching ratios for sets of lines from seven energy levels. Combined with recently measured lifetimes (Sikstrom *et al.* 1999; Li *et al.* 2000), these give absolute f-values for 100 lines. Comparison of our measurements with the theoretical calculations of Kurucz (Kurucz 2001), Raassen (Raassen 1999) and Nahar (Nahar 1995) for transitions from four $3d^6(a^3F)4p$ levels shows good agreement for the stronger lines, particularly with Raassen. The much greater scatter for the weaker transitions emphasizes the need for experimental data for the latter.

4. Hyperfine structure studies

Following an extensive analysis of hfs in Co I (Pickering 1996), we are working on the other odd-Z iron-group spectra Mn I, Mn II, V I, V II and Co II, with the aim of obtaining magnetic dipole hfs splitting factors A for a large number of levels (the electric quadrupole splitting factors B are mostly too small to derive reliably in this group of elements).

We have completed the first extensive measurements of hfs in Ta II, using FT spectra over the range 10000–53000 cm^{-1} (1000–187 nm). Computer fits to several hundred line profiles have yielded A-values of 88 energy levels with an uncertainty between 0.5% and 10% for the majority. Approximate values for the electric quadrupole hfs factor B were also found for 73 levels (Zilio & Pickering 2002). No previous measurements are known for most of these levels.

5. Atomic data for studies of the time variation of the fine structure constant

High resolution spectroscopy in the visible region of distant gas clouds seen against quasars yields accurate wavelengths for atomic transitions at high red shifts. Comparison of these with the rest wavelengths seen in the ultraviolet in the laboratory can provide constraints on space-time variations of the fine structure constant α (Webb et al. 2001). Certain sets of lines which have different dependencies on α are particularly suitable for the comparison, but it is still necessary to measure the absolute values of the laboratory wavelengths to a few parts in 10^8. We have used our FT spectrometer to make these measurements on particular lines of Cr II, Mg I, Mg II, Ni II and Zn II (Pickering et al. 1998; Pickering et al. 2000). The latest results of the comparison appear to indicate a small but statistically significant time variation (Webb et al. 2001).

Acknowledgments

REFERENCES

J. C. Pickering 1999, *Physica Scripta*, **T83**, 27.

A. P. Thorne, C. J. Harris, I. Wynne- Jones, R. C. M. Learner & G. Cox 1987, *J. Phys. E.*, **20**, 54.

A. P. Thorne 1996, *Physica Scripta*, **T65**, 31.

J. C. Pickering, A. P. Thorne and R. Perez 2001, Astrophys. *J. Supp. Series*, **132**, 403.

R. L. Kurucz 2001, http//cfaku5. harvard.edu/.

C. M. Sikstrom et al. 1999, *J. Phys. B*, **32**, 5687.

Z-S. Li et al. 2000, *J. Phys. B*, **33**, 5593.

A. J. J. Raassen 1999, ftp://ftp. wins. uva. nl/pub/orth/iron.

S. Nahar 1995, *Astron. & Astro.*, **293**, 967.

J. C. Pickering 1996, *Ap. J. Supp. Ser.*, **107**, 811.

V. Zilio and J. C. Pickering 2002, *Mon. Not. R. Astr. Soc.*, in press.

J. K. Webb et al. 2001, *Phys. Rev. Lett.*, **87**, 091301.

J. C. Pickering, A. P. Thorne and J. K. Webb 1998, *Mon. Not. R. Astron. Soc.*, **300**, 131.

J. C. Pickering, A. P. Thorne, J. E. Murray, U. Litzén, S. Johansson and J. K. Webb 2000, *Mon. Not. R. Astron. Soc.*, **319**, 163.

NIST Databases on Atomic Spectra

Joseph Reader, Wolfgang L. Wiese, William C. Martin, Arlene Musgrove, and Jeffrey R. Fuhr

National Institute of Standards and Technology, Gaithersburg, MD

Scientists at the National Institute of Standards and Technology (NIST) have critically compiled and published atomic spectroscopy data since 1945. Their data volumes have become classic reference books, used all over the world. Until the early 1990s, the data tables were all issued as hardcover books, but since then much of this material, including more recent compilations, has been made available on the World Wide Web through the NIST Physics Laboratory home page [1]. In addition to the large, comprehensive "Atomic Spectra Database" which will be discussed below, the NIST website contains complementary databases on Ground Levels and Ionization Energies for the Neutral Atoms, a Bibliographic Database on Atomic Transition Probabilities, a Bibliographic Database on Atomic Spectral Line Broadening, an Electron-Impact Ionization Cross Section Database, and a database on the Spectrum of Platinum Lamp for Ultraviolet Spectrograph Calibration.

The latest version (2.0) of the principal spectroscopic database at NIST, the Atomic Spectra Database (ASD) was released in March 1999. It contains critically evaluated compiled reference data for 900 spectra and includes at least some data on all natural elements as well as some man-made elements, from Hydrogen (atomic number $Z = 1$) through Einsteinium ($Z = 99$). Specifically, it contains 70000 energy levels, 91000 wavelengths of lines ranging from about 1 Å to 2000 μm, and 45000 transition probabilities (oscillator strengths). Wavelengths for prominent observed transitions are included for all 99 elements. Classified lines with transition probabilities are included for most spectra of H through Ni ($Z = 1-28$). For heavier elements, wavelengths and transition probabilities are given for prominent lines of the neutral atoms and the first four ions. Rather comprehensive lists of the wavelengths of observed lines are included for all spectra of Mg, Al, S, Sc, plus Be I, O II and Ne I. Energy level data are presented for most spectra of Hydrogen through Krypton ($Z=1-36$), plus the first five spectra of the lanthanides ($Z=57-71$).

The Atomic Spectra Database has been set up specifically to handle queries on energy levels and transitions (lines), and it offers a large range of options and selections to be specified by the user. Thus, for queries on spectral lines, the transitions may be arranged by wavelength or in multiplet order, they may be listed in Angstrom units or nanometers, and given in air or vacuum. The transition strength may be displayed by any combination of oscillator strength (or f-value), log gf, transition probability and line strength, and an estimated uncertainty is presented. Energy level information may be either included or suppressed with the line data. Of course, energy level data may also be displayed separately. ASD includes a comprehensive bibliography of the original literature sources used for the data tables, and it also includes an extensive help file with a compendium on atomic spectroscopy. A sample data page is shown in Figure 1.

DATA ——————— INFORMATION ——————————

NIST Atomic Spectra Database Lines Data (Wavelength Ordered)
Wavelength=2900 Å, ± 100   Mg I
16 Lines of Data Found (page 1 of 2)

Wavelength Air (Å)	Rel. Int.	A_{ki} (10^8 s^{-1})	Acc.	E_i (cm^{-1})	E_k (cm^{-1})	Configurations	Terms	J_i-J_k	Type	TP Refs.	Line Refs.
2 809.756	3			47 957.045 -	83 536.84	3s3d - 3p3d	^{3}D - ^{3}D°	3-3			R1
2 811.048	2bl			47 957.027 -	83 520.47	3s3d - 3p3d	^{3}D - ^{3}D°	2-2			R1
2 811.780	1			47 957.058 -	83 511.25	3s3d - 3p3d	^{3}D - ^{3}D°	1-1			R1
2 846.7167	12	1.5e-01	D-	21 850.405 -	56 968.271	3s3p - 3s5d	^{3}P° - ^{3}D	0-1		ls	R1
2 848.344		1.1e-01	D-	21 870.464 -	56 968.271	3s3p - 3s5d	^{3}P° - ^{3}D	1-1		ls	
2 848.3456	14	2.1e-01	D-	21 870.464 -	56 968.248	3s3p - 3s5d	^{3}P° - ^{3}D	1-2		ls	R1
2 851.652		7.6e-03	E	21 911.178 -	56 968.271	3s3p - 3s5d	^{3}P° - ^{3}D	2-1		ls	
2 851.654		6.8e-02	D-	21 911.178 -	56 968.248	3s3p - 3s5d	^{3}P° - ^{3}D	2-2		ls	
2 851.6562	16	2.7e-01	D-	21 911.178 -	56 968.218	3s3p - 3s5d	^{3}P° - ^{3}D	2-3		ls	R1
2 852.1261	50g	4.95e+00	B	0.000 -	35 051.264	3s^2 - 3s3p	^{1}S - ^{1}P°	0-1		3,4,5	R1

Fig. 1.— Sample ASD output of transition data from a single spectrum, in wavelength order. A detailed explanation of the symbols, code letters, etc. is given in the Help page of ASD [1].

The data are displayed in formats similar to those in the NIST reference data books on energy levels [2], spectra [3] and transition probabilities [4]. It should be emphasized that the NIST Atomic Spectra Database is a tabulation of critically evaluated reference data. For each spectral line and its strength and for each energy level, the database contains only one "best" value, which is determined from the critical assessment of all available literature data. This best value either may be from a single source or may be the average of several sources. Furthermore, the restriction to "reference" data means that only data fulfilling certain quality requirements are included. This is especially important for transition probabilities (or oscillator strengths), which are in many cases still rather uncertain. Only data with uncertainties estimated not to exceed ± 50% are normally included. The data evaluation process is necessarily time consuming and involves a detailed analysis of all pertinent literature sources. An elaborate scheme for the critical assessment has been established and is consistently being followed. A key ingredient are technique- specific critical factors that need to be considered for each numerical determination of oscillator strengths. Reference [5] contains a detailed discussion of these factors. It should be noted that the general goal of the NIST atomic spectroscopy data center is to provide critically evaluated tables of reference data to the U.S. industry and to the scientific community in general. While NIST does provide internal support, this support is focused on assisting US industry and technology, and it is not adequate to provide for the

large and ever increasing needs of astronomy. In recent years the NASA has not been able to maintain the needed supplemental funding for astronomical data needs. If this trend continues, the NIST database may not be able to continue to serve as a viable resource for astronomy.

REFERENCES

(1.) URL address: http://physics.nist.gov/asd.

(2.) See for example, Sugar, J., and Corliss, C. H., *J. Phys. Chem. Ref. Data*, **14**, Suppl. 2, 1985.

(3.) See for example, Reader, J., Corliss, C. H., Wiese, W. L., and Martin, G. A., "Natl. Stand. Ref. Data Ser., Natl. Bur. Stand." U.S. **68**, 1980.

(4.) See for example, Wiese, W. L., Fuhr, J. R., and Deters, T. M., *J. Phys. Chem. Ref. Data*, Monograph 7, 1996.

(5.) Wiese, W. L., and Kelleher, D. E., "The Critical Assessment of Atomic Transition Probabilities," in Atomic and Molecular Data and Their Applications (ICAMDATA 97), edited by P. J. Mohr and W. L. Wiese, AIP Conference Proceedings 434, 1998, pp. 105-118.

Ion Storage Ring Measurements
of Low Temperature Dielectronic Recombination Rate Coefficients
for Modeling X-Ray Photoionized Cosmic Plasmas

D. W. Savin

Columbia Astrophysics Laboratory and Department of Physics,
Columbia University, New York, NY

G. Gwinner, D. Schwalm, and A. Wolf

Max-Planck-Institut für Kernphysik, Heidelberg, Germany
and Physikalisches Institut der Universität Heidelberg, Heidelberg, Germany

A. Müller and S. Schippers

Institut für Kernphysik, Strahlenzentrum der Justus-Liebig-Universität, Giessen, Germany

1. Reliable DR Data Needed

Low temperature dielectronic recombination (DR) is the dominant recombination mechanism for most ions in X-ray photoionized cosmic plasmas. Reliably modeling and interpreting spectra from these plasmas requires accurate low temperature DR rate coefficients. Of particular importance are the DR rate coefficients for the iron L-shell ions (Fe XVII-Fe XXIV). These ions are predicted to play an important role in determining the thermal structure and line emission of X-ray photoionized plasmas, which form in the media surrounding accretion powered sources such as X-ray binaries (XRBs), active galactic nuclei (AGN), and cataclysmic variables (Savin *et al.*, 2000).

The need for reliable DR data of iron L-shell ions has become particularly urgent after the launches of *Chandra* and *XMM-Newton*. These satellites are now providing high-resolution X-ray spectra from a wide range of X-ray photoionized sources. Interpreting the spectra from these sources requires reliable DR rate coefficients. However, at the temperatures relevant for X-ray photoionized plasmas, existing theoretical DR rate coefficients can differ from one another by factors of two to orders of magnitudes.

2. New Program at Max-Planck-Institute

To address the need for accurate low temperature DR rate coefficients of the iron L-shell ions, we have initiated a program of measurements for DR via $2 \rightarrow 2$ core excitations using the heavy-ion Test Storage Ring located at the Max-Planck-Institute for Nuclear Physics in Heidelberg, Germany. To date measurements have been carried out for Fe XVIII (Savin *et al.*, 1997, 1999), Fe XIX (Savin *et al.*, 1999), Fe XX (Savin et al 2002), Fe XXI, Fe XXII, and Fe XXIV. A detailed discussion of our results can be found in the references cited.

Acknowledgments

REFERENCES

Savin, D. W., *et al.*, 1997, *ApJ*, **489**, L115.

Savin, D. W., *et al.*, 1999, *ApJS*, **123**, 687.

Savin, D. W., *et al.*, 2000, in *Proceedings of the 12th APS Topical Conference on Atomic Processes in Plasmas*, Reno Nevada, ed. R. C. Mancini (New York: American Institute of Physics), p. 267.

Savin, D. W., *et al.*, 2002, *ApJS*, **138**, 337.

EMILI - An Aid to Emission Line Identification in Emission-Line Regions

Brian Sharpee and Jack Baldwin

Dept of Physics and Astronomy, Michigan State University, East Lansing, MI

Robert Williams

Space Telescope Science Institute, Baltimore, MD

Peter van Hoof

Queen's University Belfast, Belfast, Northern Ireland

Abstract

We present results from EMILI, our software optimized to identify weak emission lines in planetary nebulae and H II regions. We discuss the steps carried out by the code to arrive at identifications, and planned future improvements.

1. Introduction

High resolution and signal-to-noise emission spectra of planetary nebulae and H II regions reveal large numbers of weak emission lines. Identifying these lines is both difficult and time consuming, given the large number of atomic transitions which could be responsible. Model spectra require precise information about atomic parameters, such as collision strengths, recombination coefficients, and spontaneous emission coefficients, information which is not always available for the wide variety of possible transitions that could be associated with such lines. Our code, EMILI for Emission Line Identifier, is specifically tailored to help identify such lines, by using a minimum of such information, and by providing easy to interpret results.

2. Calculation Steps

A user submits a list of unidentified lines and their measured parameters (wavelength, between 3000-11000Å, and associated measurement error, flux with respect to Hβ, and FWHM), and supplies estimates for the temperature and electron density of the object from which the spectra and its lines are drawn, as well as a value for the instrumental resolution. Optionally, a list of pre-identified lines can be used by the code to correct for the systemic velocity and any ionization energy dependent velocity structure within the spectra. Using default solar abundances, or a user supplied abundance table, the code calculates ionic abundances for all elements $Z \leq 30$. These abundances use a set of ionization correction factors that are either reasonable default values, or are calculated from the strengths of certain lines in the user-supplied pre-identified list.

For each unidentified line a transition database (Atomic Line List v2.04, van Hoof 2001, http://www.pa.uky.edu/~peter/atomic) is searched for nearby lines. The wavelength of the

unidentified line is then corrected for the systemic velocity and for any ionization energy dependent velocity structure present that is appropriate for the ion producing the transition. Only transitions where the residual wavelength difference between the corrected observed wavelength and the laboratory wavelength are within a few observed wavelength measurement error sigma, are retained.

For surviving transitions, a *template flux* is calculated utilizing a simplified one temperature/density zone model of the object, a two-level atom, the specified nebular attributes, calculated ionic abundances, and assumed generic values of the atomic parameters appropriate for the type of transition (electric dipole, quadrupole, magnetic dipole). Each calculation includes contributions from collisionally excited and recombination populated origin levels, regardless of transition type. The transitions with template fluxes within the top 3 decades, among all transitions for which the flux was calculated, are retained under the assumption that they are the most likely to be seen in the actual spectrum.

For transitions reaching this stage, the code endeavors to find additional *multiplet lines*, if any, that could correspond to other unidentified lines in the submitted list. A match is considered "found" if the relative observed flux of the line currently being tested, to the flux for the one considered as a match for the other multiplet line, is roughly equal to the ratio of the products of the statistical weight and spontaneous transmission coefficient for each of the respective multiplet lines, or within an order of magnitude if the coefficients are not available. Furthermore, the residual wavelength differences between the observed lines and the respective laboratory wavelengths for their associated transitions must be nearly the same, to reflect that all multiplet lines come from the same region of the object and are produced by the same excitation mechanism.

Finally, the code sorts the remaining transitions, using a simple ranking mechanism which employs the relative amounts of residual wavelength differences, the relative strengths of the template fluxes, and the results of the multiplet checks, to provide a ranking and a quality of identification "score" for each unidentified line. The user may interpret these results to select a probable line identification.

3. Sample Results

Figure 1 is a segment of our recently obtained, resolution=30000 (10 km/sec), spectrum of IC 418 (Sharpee *et al.* 2002, in preparation). Figure 2 is an EMILI identification of a weak line at 4641.45 Å marked in Figure 1. EMILI suggests N III λ4640.46 Å is the most likely ID, as indicated by a low number/score in column G of Figure 1 for this transition as compared to the other suggested alternate IDs. EMILI arrives at this conclusion by noting: 1) The residual wavelength difference (in km/sec, column E) between the corrected observed wavelength (column A) and the laboratory wavelength for the transition (column B) is fairly small. 2) The template flux (column D) is the largest among all the potential IDs, and fairly close to the observed value. 3) The multiplet check indicates that another observed line from the same line list matches well with another transition belonging to the same multiplet as N III

$\lambda 4640.46$ Å, with a similar residual wavelength difference (column H). EMILI indicates that it found one of two multiplet lines with strengths predicted to be strong enough to observe (column F) if this ID is really the correct ID, which are better statistics than for any other alternate ID in the list.

EMILI provides a similar group of possible identifications for every observed line submitted by the user. For the 500+ lines in the full spectrum to which Figure 1 belongs, a standard desktop computer requires approximately 5-6 minutes to process them all.
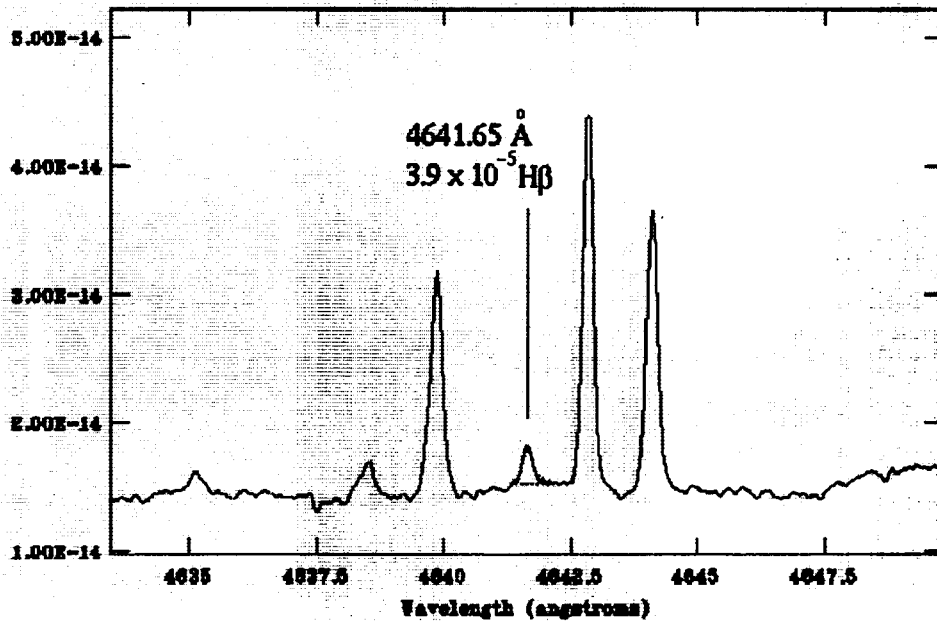
Fig. 1.— A section of our recently obtained, high resolution and signal-to-noise spectra of IC 418. Indicated is a weak line at 4641.65 Å. The EMILI derived identification list for this line is shown in **Figure 2**.

```
Observed Line:   4641.65   3.9E-05   S/N:      23.35 FWHM:   15.9
        4640.57 |  4640.47  Fe II]  8.0E-07    5.9 4/0 8
     +  4640.61 |  4640.54  Ni II   4.4E-06    4.6 4/0 6D
     +  4640.60 |  4640.59  Fe III  6.4E-05    0.6 5/0 4B
     +  4640.60 |  4640.64  N  III  2.0E-04   -2.5 2/1 2A 4634.12  -2.6
        4640.57 |  4640.66  Cr I    2.5E-07   -6.3 7/0 8
        4640.61 |  4640.73$ Ni II   3.9E-06   -7.4 0/0 5C
        4640.60 |  4640.75  S  IV   4.3E-05   -9.6 3/0 7

         A          B         C        D       E F G     H
```

Fig. 2.— The EMILI identification list for the line at 4641.65 Å indicated in Figure 1. An explanation of these results is given in the text.

4. Future Directions

To improve the existing code we plan on making two major modifications. The first involves cross correlations between IDs in separate lines, beyond the multiplet check, which have the same source ion and excitation mechanism. This is to see if they have roughly the expected relative strengths and residual wavelength differences, and to look for patterns that could provide further corroborating evidence for a group of possible IDs for different lines. Secondly, we plan on making the code iterative, using the best IDs from an initial run to recalculate and improve the accuracy the ionic abundances and velocity structure corrections, for use in successive runs. A preliminary version of the code is now available at:

http://www.pa.msu.edu/people/sharpee/emili.html

New Atomic Data for Doubly Ionized Iron Group Atoms by High Resolution UV Fourier Transform Spectroscopy

Peter L. Smith
Harvard–Smithsonian Center for Astrophysics

Juliet C. Pickering and A. P. Thorne
Blackett Laboratory, Imperial College, London

Abstract

Currently available laboratory spectroscopic data of doubly ionized iron-group elements were obtained about 50 years ago using spectrographs of modest dispersion, photographic plates, and eye estimates of intensities. The accuracy of the older wavelength data is about 10 mÅ at best, whereas wavelengths are now needed to an accuracy of 1 part in 10^6 to 10^7 (0.2 to 2 mÅ at 2000 Å). The Fourier transform (FT) spectroscopy group at Imperial College, London, and collaborators at the Harvard College Observatory have used a unique VUV FT spectrometer in a program focussed on improving knowledge of spectra of many neutral and singly and doubly ionized, astrophysically important, iron group elements. Spectra of Fe II and Fe III have been recorded at UV and VUV wavelengths with signal-to-noise ratios of several hundred for the stronger lines. Wavelengths and energy levels for Fe III are an order of magnitude more accurate than previous work; analysis is close to completion. f-values for Fe II have been published.

1. Introduction

Improvements in the quality of astrophysical spectra obtained using high resolution spectrographs on ground and satellite telescopes have highlighted inadequacies in the laboratory atomic data base needed to interpret these observations, especially in the ultraviolet (UV) wavelength region. In these spectra of hot stars, lines from doubly and singly charged species dominate. Wavelengths accurate to a few parts in 10^7 are required to allow unambiguous identification and modeling of all spectral features in highly blended spectra; transition probabilities and hyperfine structure (hfs) are also needed.

The laboratory spectroscopic database for doubly charged members of the iron group is based on measurements with spectrographs of modest dispersion. The literature covering the third spectra (*i.e.*, the spectra, denoted "III," of doubly charged ions) comprises roughly a score of papers with an average age of about forty years. Some generalizations are possible:

- the accuracy of the old data is about 10 to 20 mÅ at best, whereas wavelengths are now needed to an accuracy of 1 part in 10^6 to 10^7 (0.2 to 2 mÅ at 2000 Å).
- there are no measured intensities other than eye estimates of photographic blackening;
- there are no accurate data on hyperfine structure.

The strongest transitions in these doubly ionized spectra lie in the UV. However, it is not only the UV region that has need of improvement:

- there are no data at wavelengths longer than 2675 Å for Cr III;
- until our work on Fe III there were no data longer than 2105 Å for Fe III;
- only 2 % of the known lines of Co III are at wavelengths longer than 3000 Å.

The lack of data is not a consequence of atomic structure: Ti III, the simplest ion in the set being discussed, should have ~500 lines with $3000 < \lambda[\text{Å}] < 9300$ resulting from allowed transitions between known levels.

Hfs is significant in astrophysically important odd-Z third spectra because the contribution of a transition to an absorption feature is strongly dependent on whether the line is single or the absorption is distributed among many components. Some existing data, on Mn III for example, indicate that the vast majority of the lines are either diffuse (**h**) or wide (**w**). This notation reaches near farce with some lines being noted as **hhww**! This is not the quality of data needed for modern astrophysical observations.

2. Apparatus

The Fourier transform (FT) spectrometer that we use (see Thorne *et al.* 1987, 1994) holds the world short wavelength record (~1350 Å) for high resolving power spectroscopy. FT spectrometry using hollow cathode discharges in the laboratory has provided wavelengths with the accuracy required in modern astrophysics for neutral atoms and singly charged ions (Pickering 1999; Nave *et al.* 1999), but application of this method to doubly charged ions has been hindered because such ions are not efficiently created and excited in d.c. hollow cathode discharges.

Third spectra and the higher levels of second spectra have hitherto been excited only with pulsed hollow cathodes, sliding sparks, etc. The poor 'shot-to-shot' reproducibility of such sources makes them unacceptable for high quality measurements with either a scanning grating or an FT spectrometer, so most laboratory spectroscopy on pulsed sources has been done using photographic plates, which have low signal/noise ratio and poor photometric and wavelength accuracies relative to those required to support modern astronomy.

We have resolved this source/spectrometer incompatibility with the identification and construction, with support of NASA, of a light source based on a d.c. Penning discharge originally developed and studied as a VUV radiometric standard. Our preliminary studies (Smith *et al.* 1998) using it and the VUV FT spectrometer at Imperial College (IC), showed that this source strikes easily, operates steadily and reproducibly for significant periods of time (10 to 15 hours), and can be quickly refurbished for reuse. We have since used the Penning discharge and the IC FT spectrometer to improve wavelength and f-value data for Fe II and Fe III.

3. Fe II and Fe III Wavelengths and f-values

We have used our Penning discharge source to obtain high signal/noise ratio Fe III spectra for the 175 nm to 210 nm region (see Fig. 1). The data analysis procedure used the wavelengths of Nave *et al.* (1997) and Ekberg (1993) for identification of Fe II and Fe III lines, respectively. Because the wavelengths of Nave *et al.* (1997) are very accurate, our new wavelengths for the ~ 400 lines identified as Fe III have uncertainties of about 0.2 mÅ (about one part in 10^7). They therefore supplant those of Ekberg (1993) for the needs of modern high resolution astronomical spectroscopy.

Fe III (Fe^{2+}) UV FT emission spectrum
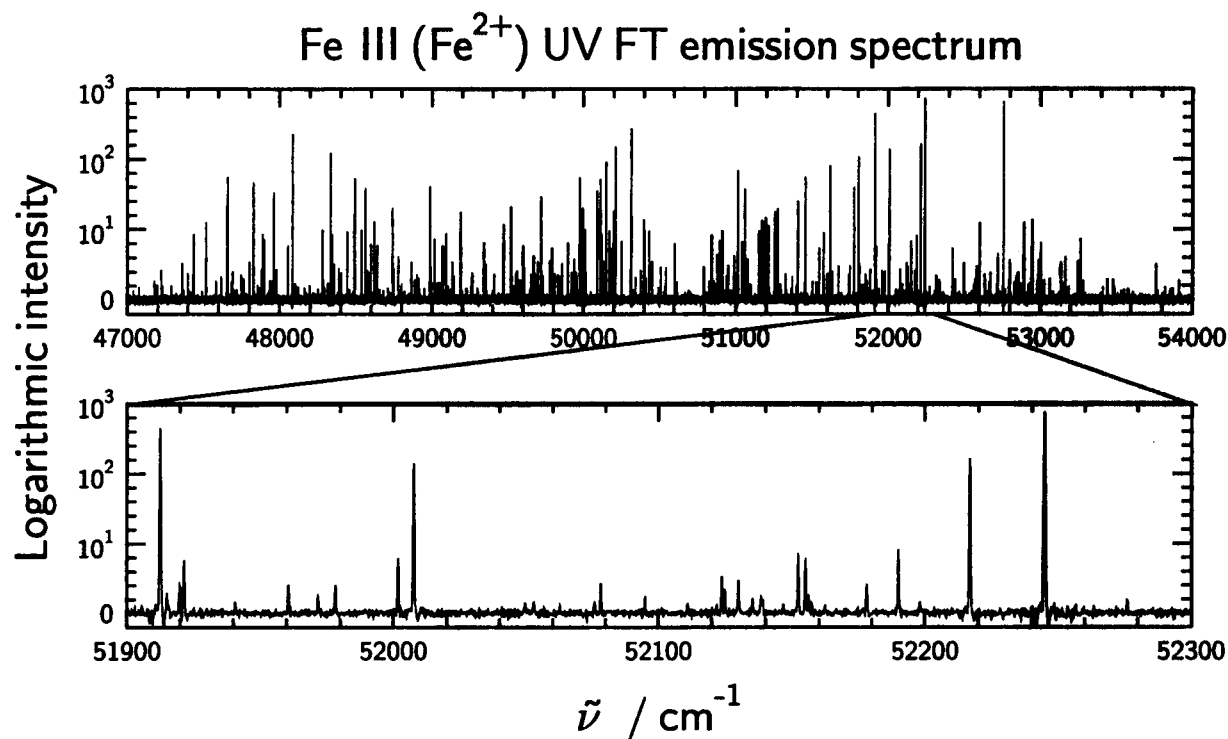
Fig. 1.— Top: Spectrum from 1851.8 to 2127.7 Å;
Bottom: A 15 Å portion of the spectrum centered at ~1919 Å.

Our measurements of the spectrum of Fe III have been accompanied by contemporaneous determinations of the radiometric response of the FT spectrometer. Thus, branching fractions are determined and A-values could be calculated if lifetimes were available.

The hollow cathode discharges used for the precision spectroscopy of Fe II (Nave et al. 1997) do not excite the higher-lying levels of Fe II. However, our Penning discharge does and we have taken advantage of this feature to make new measurements of A-values for Fe II (Pickering et al. 2001). This work required determining the responsivity of the FT spectrometer using a standard D_2 emission source, so that accurate branching fractions, and thus relative f-values, can be derived from the spectral data.

When the Fe III work is complete, we will extend our efforts to other doubly charged ions of the iron group, initially Co III and then Cr III, Ni III, and Mn III. All three ions have spectra that are significant components of data obtained by *GHRS*, *STIS*, and *FUSE*. The second spectra of these atoms may also be worthy of additional study. For example, we believe that the Penning discharge will excite levels in Co II that were not observed by Pickering et al. (1998), and, therefore, that additional wavelengths and f-values can be measured.

Acknowledgments

REFERENCES

Ekberg, J. O., 1993, *A&AS*, **101**, 1.

Nave G., S. Johansson & A. P. Thorne, 1997, *JOSA B*, **14**, 1035.

Pickering, J. C., 1999, *Physica Scripta*, **T38**, 27-34.

Pickering, J. C., A. J. J. Raassen, P. H. M. Uylings & S. Johansson, 1998, *ApJS*, **130**, 541.

Pickering, J. C., S. Johansson & P. L. Smith, 2001, *A&A*, **377**, 361.

Smith, P. L., *et al.*, 1998, in *Improved VUV Spectroscopy of Doubly Ionized Atoms*, APS Conf. Ser. **143**, 395.

Thorne, A. P., C. J. Harris, I. Wynne-Jones, R. C. M. Learner & G. Cox, 1987, *J. Phys. E.*, **20**, 54.

Thorne, A. P., G. Cox, P. L. Smith & W. H. Parkinson, 1994, *Proc. SPIE*, **2282**, p.58.

Measurement of Metastable Lifetimes of Highly-Charged Ions

Steven J. Smith, A. Chutjian, and J. Lozano

Jet Propulsion Laboratory, California Institue of Technology, Pasadena, CA

The present work is part of a series of measurements of metastable lifetimes of highly-charged ions (HCIs) which contribute to optical absorption, emission and energy balance in the ISM, stellar atmospheres, *etc.* [1]. Measurements were carried out using the 14-GHz electron cyclotron resonance ion source (ECRIS) at the JPL HCI facility. The ECR provides useful currents of charge states such as $C^{(1-6)+}$, $Mg^{(1-6)+}$ and $Fe^{(1-17)+}$. In this work the HCI beam is focused into a Kingdon electrostatic ion trap [2] for measuring lifetimes *via* optical decays. A schematic diagram of the beamline is given in Fig. 1. After extraction the ions are directed into one of three beam lines for excitation, charge-exchange/X-ray emission, and lifetime measurements. A description of data acquisition procedures has been given in Refs. [1,3].
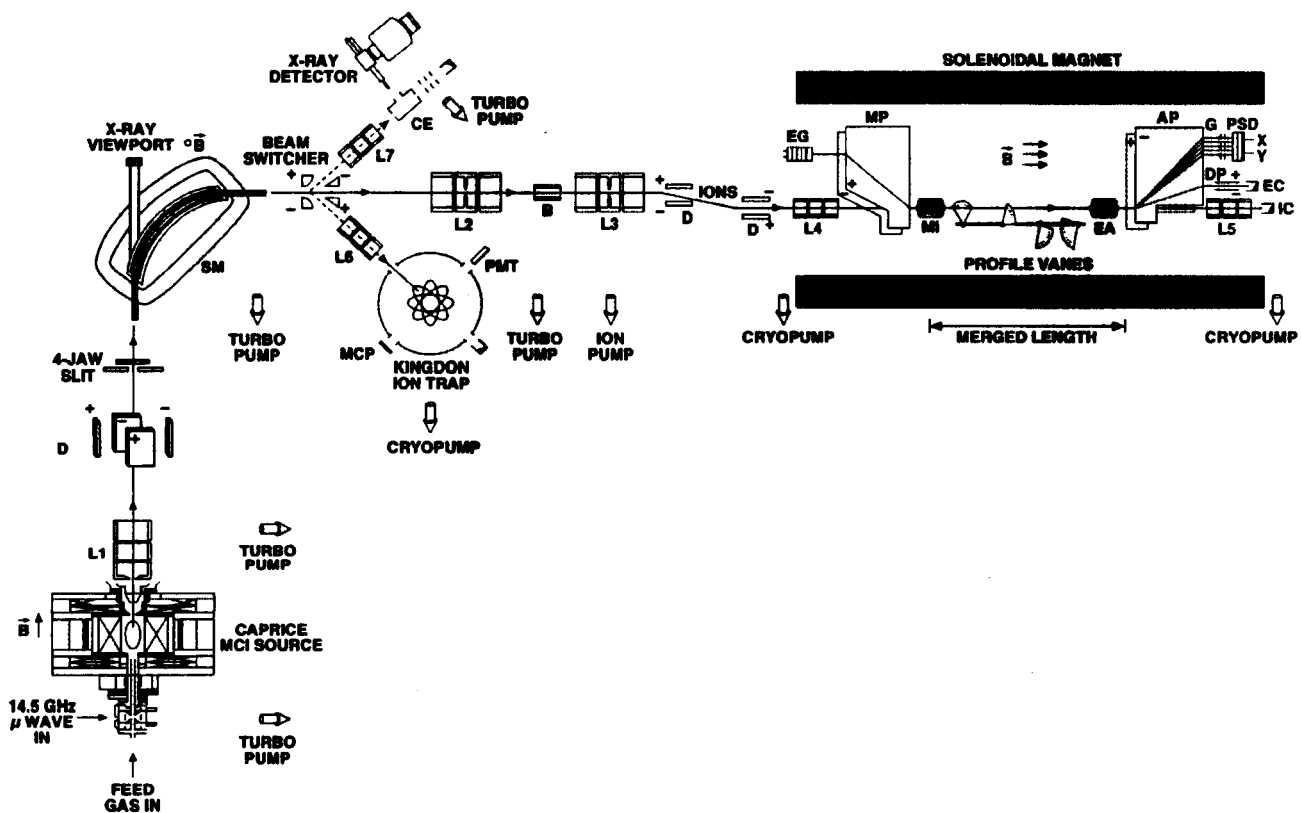
Fig. 1. Experimental set-up of JPLs Highly-Charged Ion Facility (HCIF). (L1-L7) three-element focusing lenses, (SM) mass/charge selection magnet, (B) differential pumping baffle, (D) deflector plates, (MP) electron-merging trochoidal plates, (AP) electron-analyzing trochoidal plates, (MI) electron mirror to reflect backward-scattered electrons, (EA) electronic aperture to discriminate against elastically-scattered electrons, (DP) trochoidal plates to deflect parent electron beam out of the scattering plane, (PSD) position- sensitive detector, (G) electron-retarding grids for discrimination against elastically-scattered electrons, (EC) electron Faraday cup, (IC) ion Faraday cup, (CE) charge-exchange cell, (MCP) microchannel plate, (PMT) multiplier phototube. The three beam lines after the switcher are for excitation, meta- stable lifetimes, and charge-exchange/X-ray measurements.

Ions are focused into the trap, after which the central wire is rapidly pulsed to a low voltage. Trapped ions orbit the center wire where they emit radiation at the wavelength corresponding to the energy of the transition, and (in the absence of cascading into the upper level) at a decay rate given by the inverse lifetime of the upper level. Observed decay channels include intercombination, E2, M1 and 2E transitions. Ion population is also lost *via* collisional-quenching, charge-exchange collisions of the HCI with the background gas, and by collisions with the trap and walls. The UV emissions are detected by an interference filter and phototube using a UV grade optical system. For wavelengths less than 180 nm, a cesium-iodide coated microchannel plate, enhanced for UV performance, is used. The output of the photomultiplier (pulse-counting mode) is coupled to a multichannel scaler having a variable time resolution of 0.1-10 ms/channel. The range of lifetimes that can be measured is determined, at the short end, by the time it takes for ions to settle into stable orbits (1-2 ms); and at the long end by the various trap loss mechanisms (1.5 s). The stored ion cloud is estimated to extend over a diameter of 5-10 mm. This is much smaller than the diameter of the trap (100 mm), hence wall collisions are minimized.

We have published measurements of the lifetimes of the $^2P^o_{1/2,3/2} \rightarrow\ ^4P_{1/2,3/2,5/2}$ intersystem transitions of C^+ at 232.5 nm [1]. Results are in good agreement with other experiments and theoretical calculations [4,5]. Reported herein is the measurement of the lifetime of the $2s^2 2p^2$ $^1S_0$ level in O^{2+} at 232.17 nm [6]. These transitions are detected in diffuse nebulae- H II regions, planetary nebulae, in our own Sun, and in the Io plasma torus. The data, when combined with absolute excitation cross sections for O^{2+} [7] provide benchmark values for assessing results of astrophysical line-intensity ratio calculations. The interference filter was centered at 232 nm, with a 12 nm (FWHM) bandwidth. The filter rejected emissions lines for the transition $^1S_o \rightarrow$ $^1D_2$ at 436.4 nm, and the transition $^5S^o_2 \rightarrow\ ^3P_{1,2}$ at 166 nm. The latter rejection was aided by the fact that the light path to the UV phototube and interference filter is exterior to the (fused quartz) window of the vacuum chamber. Hence the path was partly through the absorbing atmosphere. The photon-decay is shown in Fig. 2. As in the C^+ work, because of the low pressure in the trap during operation (3×10^{-10} torr), there is negligible loss of population of the emitting state by ion-gas collisions. The trap decay rate is measured by using the microchannel plates exterior to the trap. The ion population is monitored as the trap is emptied after different elapsed trapping times, up to a maximum trapping time of 1.5 s. In addition, the photomultiplier signal is monitored over a longer (1.5-2.0 s) time interval. This longer-term signal arises from ion-central wire, ion-trap wall, and ion-lens surface collisions. Results of both techniques give a minimum trap lifetime of 1.1 s. The trapped O^{2+} ions may also decay by collisions with the background gas. The JPL measured lifetime of the $^1S_0$ level was found to be 541 $\pm$ 40 ms at the 1σ limit of error. Theoretical values range from 392 ms to 1333 ms [8-12], factors of 0.7 to 2.5 times the experimental values. The present compares well with an ion-storage ring experimental measurement of 530 $\pm$ 25 ms [13]. The spread in theoretical results points out the difficulty of using theoretical data. Additional lifetime measurements have been made for $Fe^{9,10,13+}$ and Mg^{6+} and are in the preparation/submission stage.
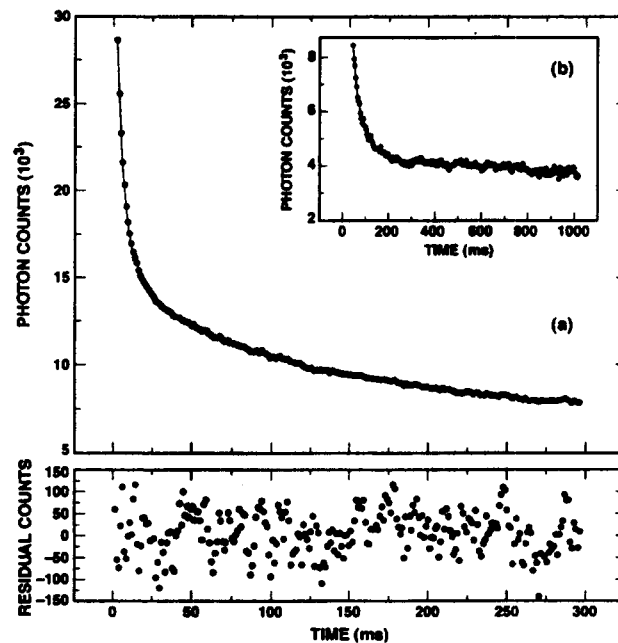
Fig. 2.— Comparison of experimental absolute excitation cross sections for the 2s2 2p2 3P0,1,2 (2s2 2p2 1D2 transitions in O2+ (solid circles) [4], with theoretical results in the 26-state R-matrix calculation [10]. (Photon-decay signal for the M1 232 nm decay branch in the 2s2 2p2 1S0 3P1 transition of O2+. Shown are the decay in the range 0-300 ms (a) and the 0-1000 ms range (b). The data fit is shown by the thin solid line through the points. The lower figure shows the residuals of the data fit throughout the 0-300 ms portion of the decay.)

Acknowledgments

REFERENCES

[1] J. B. Greenwood, S. J. Smith, A. Chutjian, and E. Pollack, *Phys. Rev. A* **59**, 1348 (1999).

[2] L. Yang and D. A. Church, *Phys. Rev. Lett.* **70**, 3860 (1993).

[3] D. P. Moehs, D. A. Church, and R. A. Phaneuf, *Rev. Sci. Instr.* **69**, 1991 (1998).

[4] D. J. Lennon et al., *Ap. J.* **294**, 200 (1985).

[5] Z. Fang, et al., *Phys. Rev. A* **48**, 1114 (1993).

[6] S. J. Smith, I. Cadez, A. Chutjian, and M. Niimura, "Measurement of the Metastable Lifetime for the $2s^2 2p^2$ $^1S_0$ Level in O^{2+}," *Ap. J.* (in press).

[7] M. Niimura, S. J. Smith, and A. Chutjian, *Ap. J.* **565**, 645 (2002).

[8] A. K. Bhatia, G. A. Doschek, and U. Feldman, *Astron. and Astrophys.*, **76**, 359 (1979).

[9] K.-T. Cheng, Y.-K. Kim, and J. P. Desclaux, *At. Data Nucl. Data Tables* **24**, 111 1979.

[10] K. M. Aggarwal and F. P. Keenan, *Ap. J. Suppl. Ser.* **123**, 311 (1999).

[11] C. Froese Fischer and H. P. Saha, *Phys. Scr.*, **32**, 181 (1985).

[12] H. Nussbaumer and C. Rusca, *Astron. and Astrophys.* **72**, 129 (1979).

[13] E. Träbert, et al., *Phys. Rev. A*, **62**, 022507 (2001).

X-ray Spectroscopy of Trapped Ions with a Microcalorimeter on the NIST Electron Beam Ion Trap

E. Takács[1,2], J.D. Gillaspy[1], L. Ratliff[1], K. Makónyi[1,2], M. Laming[3], E. Silver[4],
H. Schnopper[4], M. Barbera[5], J. Beeman[6], E. Haller[6], N. Madden[6]

1) Massachusetts Institute of Technology, Cambridge, MA
2) National Institute of Standards and Technology, Gaithersburg, MD
3) Naval Research Laboratory, Washington, DC
4) Harvard-Smithsonian Center for Astrophysics, Cambridge, MA
5) INAF - Osservatorio Astronomico di Palermo G.S. Vaiana, Palermo, Italy
6) Lawrence Berkeley National Laboratory, Berkeley, CA

1. Introduction

The electron beam ion trap (EBIT) was invented about 15 years ago (?). Judging from the wide range of experiments performed on the machine since its inception, EBITs have become one of the most successful devices to produce, trap, and study the structure and interactions of highly charged ions. Today, EBITs exist in several different laboratories around the world and are used in a variety of fields of research where multiply charged ions are relevant. Recent astrophysical missions by NASA and ESA targeting the x-ray wavelength range of the electromagnetic spectrum opened up a new direction for EBIT research. Efforts at two U.S. EBIT sites, the Lawrence Livermore National Laboratory (LLNL) in Livermore and the National Institute of Standards and Technology (NIST) in Gaithersburg, have provided highly charged ion data for astrophysical applications. This report, summarizes some recent NIST results.

2. Electron Beam Ion Traps

In simple terms, an EBIT can be considered to be a sophisticated x-ray source. The spectral lines are emitted by highly charged ions that are trapped and excited in a well-defined volume of space under controlled and easily variable conditions. There are several key features to the machine that can be most appreciated by understanding the operation of the device. In the heart of the EBIT there is a high current (up to 150 mA), high current density ($> 10^3$ A/cm^2) electron beam traveling along the axis of a homogenous 3 T magnetic field. (The operating parameter values and limits that we list here correspond to those of the NIST EBIT and can be different in the different EBIT implementations.) The ion trap consists of electrostatic and magnetic components. Axially, the ions are trapped by potential biases applied to a three-piece cylindrically symmetric drift tube structure. The radial confinement is maintained by the space charge of the magnetically compressed electron beam and the magnetic field itself. The magnetic field is produced by a pair of superconducting Helmholtz coils situated around the trap region. Both the cooling of the superconducting magnet and the ultrahigh vacuum conditions are implemented by the use of cryogenic liquids (liquid helium and liquid nitrogen). The ions to be investigated are injected into the trap region in the form of low charge ions or neutral atoms. Intersecting the electron beam, they quickly become highly ionized and their motion becomes tightly confined near the electron beam. Adjusting the voltage applied to the middle drift tube can be used to optimize the presence of the desired charge states. Excited ionic states can be accessed by electron impact excitation and the resulting electromagnetic radiation can be detected through side observation ports around the trap region.

One of the most appealing features of EBITs for astrophysical applications is that all the charge states of all the astrophysically important elements are accessible for spectroscopic studies. With a narrow energy distribution electron beam, specific slices of astrophysical conditions can be investigated, providing key information (e.g. line positions, cross sections etc.) for modelers. In this paper, a few examples of our recent results are presented to highlight the capabilities of an EBIT for astrophysical research.

3. X-ray Microcalorimeter

Since highly charged ions mostly radiate in the x-ray region of the electromagnetic spectrum, EBITs have typically been equipped with crystal spectrometers and solid-state detectors. At NIST, we have used such instruments for a variety of investigations ranging from precision wavelength determinations to electron-ion recombination studies (2). The Livermore group has pioneered the use of such instruments for EBIT studies that are relevant to laboratory astrophysics (3). Recently, we introduced a high energy-resolution, broadband x-ray microcalorimeter to our suite of x-ray instruments. This instrument, developed at the Harvard-Smithsonian Astrophysical Observatory (SAO) (4), operates with close to 100% quantum efficiency. It is able to cover the 0.2 keV to 10 keV x-ray energy range with a 4.5 eV - 6.0 eV energy resolution throughout. The operating principles of the Harvard-SAO microcalorimeter have been described elsewhere (4). Fig. 1 is an example, which demonstrates the capabilities of the EBIT-microcalorimeter combination for astrophysical applications. The lefthand portion of Fig. 1 is the predicted spectrum of the Perseus Cluster with a Harvard-SAO microcalorimeter in the focus of a Constellation-X type telescope. The righthand part of Fig. 1 shows a spectrum of highly ionized Fe taken at the NIST EBIT (22). Detailed analysis of the comparison indicates that the charge state distributions and line intensity ratios are very similar in the two spectra.

4. Surveying the Capabilities

Fig. 2 provides four representative examples of x-ray spectra obtained using our EBIT. Hydrogen-like and helium-like lines of O, N, and Ne are among the most useful diagnostic tools for astrophysical plasmas with temperatures of a few million kelvin and electron densities of 10^9 cm^{-3} to 10^{12} cm^{-3}. Figs. 2a and 2b show emission lines from these ions obtained with the Harvard-SAO microcalorimeter on the NIST EBIT. Systematic study of the He-like lines in Ne (Fig. 2b) is underway to improve our understanding of the ion cloud dynamics inside the EBIT and make astrophysically important studies more reliable (5).
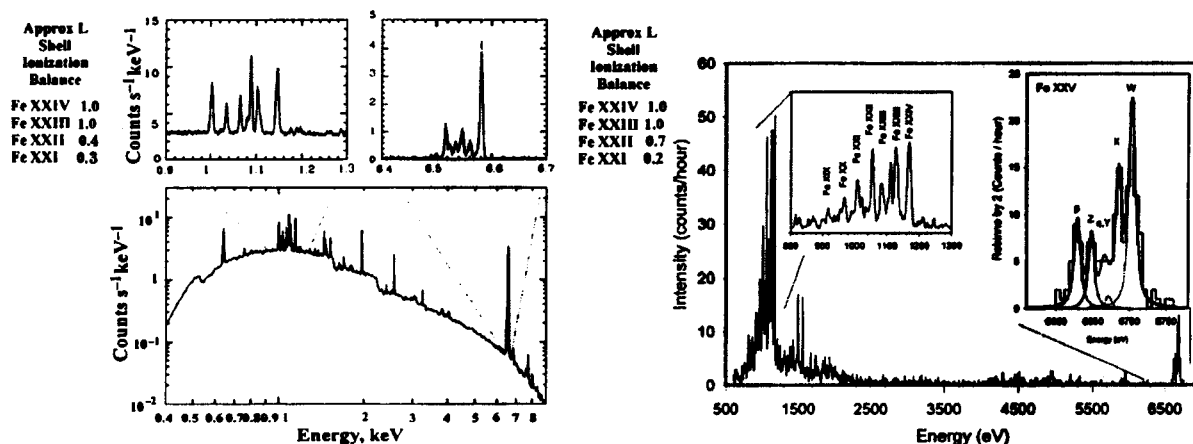
Fig. 1.— Left: Simulated spectrum of the Perseus cluster with the SAO microcalorimeter at the focus of a CON-X type telescope. The L and K lines of Fe are seen red-shifted. Right: L and K specra of Fe obtained with the microcalorimeter on the NIST EBIT.

Apart from the in-trap studies, the NIST EBIT is also equipped with an ion beam extraction and transport system capable of delivering highly charged ion beams into external experimental setups. Fig. 2c shows an example of such an experiment. In this case, hydrogen-like argon ions were collided with a solid target and the resulting x-rays were detected by the x-ray microcalorimeter. These types of collisions have been studied in the investigation of "hollow atoms" (6), mainly using crystal spectrometers as shown in the comparison in Fig. 2c, but they can also have relevance in astrophysical situations (e.g., the interaction of solar or stellar wind ions with solid surfaces or small particle clusters). Fig. 2d also represents an experiment that was done using an extracted highly charged ion beam. The x-ray spectrum was produced in the interaction of bare Kr^{36+} ions with a jet of neutral Ar atoms in a crossed beam arrangement (7). This avoids the effects of the EBIT magnetic field on the neutral atom or molecule collision partners, in contrast to "magnetic trapping" experiments (17). External target and "magnetic trapping" (internal target) experiments are thus complementary, having different types of potential systematic errors. At gas jet pressures, where single collision conditions are maintained, elementary atomic collision processes can be studied and compared with theoretical calculations. The calculations are relevant in modeling the interaction of solar wind ions with cometary and planetary atmospheres (8) and thus to recently discovered x-ray radiation from these sources (9). This experiment will be greatly improved if the solid-state Ge detector now in use (7) is replaced with the x-ray microcalorimeter used for the other spectra in Fig. 2.

5. Line Intensity Ratios in Ne-like Fe^{16+}

Fe^{16+} is one of the most dominant ions forming line spectra in astrophysical plasmas with temperatures around 5×10^6 K. The six strongest lines originate from transitions between the $2p^6$ $^1S_0$ ground state and the $2p^63s$ $^1P_1$, $^3P_1$, $^3P_2$, and $2p^63d$ $^1P_1$, $^3D_1$, $^3P_1$ excited states. Although these lines could offer excellent electron temperature diagnostics (10), observations of solar flares (11) and astrophysical sources (12) have pointed to discrepancies involving the obtained intensity ratios. Recently, both the LLNL (13) and the NIST EBIT groups (14) have made lab observations, and improved theoretical calculations became available (15; 16; 18). However, it seems fair to say that a number of issues require further work to resolve. One of the discrepancies in astrophysical observations is related to the intensity of $2p^63d$ $^1P_1$ line relative to other features in the spectra. Since this line originates from a transition with large oscillator strength it has been suggested (18) that resonance scattering may be removing a significant number of photons from the line of sight. Tokamak measurements (19) and observations by the LLNL EBIT group (13), under conditions where optical thickness is negligible, showed that opacity issues in the Sun are less significant than previously thought, but can still be relevant elsewhere. Recent broadband comparison of Chandra spectra from Xi Uma and Capella also seem to support this assessment (19). The strongest $2p^63d$ $^1P_1$ line is diminished in the optically thicker Xi Uma, while other features show similar relative intensity ratios in the two spectra. The second set of line intensity ratio problems lies in the relative ratio between the $2p^63s$ $^1P_1$, $^3P_1$, $^3P_2$ and $2p^63d$ $^1P_1$, $^3D_1$, $^3P_1$ groups of lines. In particular the summed intensity of the lines originating from the $2p^63s$ configurations appears enhanced relative to the summed intensity of the lines from $2p^63d$ configurations (20). Recent calculations show that resonance excitations in Maxwellian plasmas can help resolve this problem (15), but a firm quantitative conclusion has not yet been reached. That the problem still persists in recent observations is shown by the fact that the aforementioned Xi Uma and Capella observations by Chandra (Drake) both give about 1.5 – 2 for the $2p^63s$ – $2p^63d$ ratio, whereas in the XMM spectra (21) of the hot star Z Puppis and Chandra spectra of alpha Cen B the ratio is unusually low, ~ 0.7. Fig. 3a shows the NIST EBIT measurements of both groups of lines in Fe^{16+}. In Fig. 3b the astrophysical observations are compared with our experimental data and
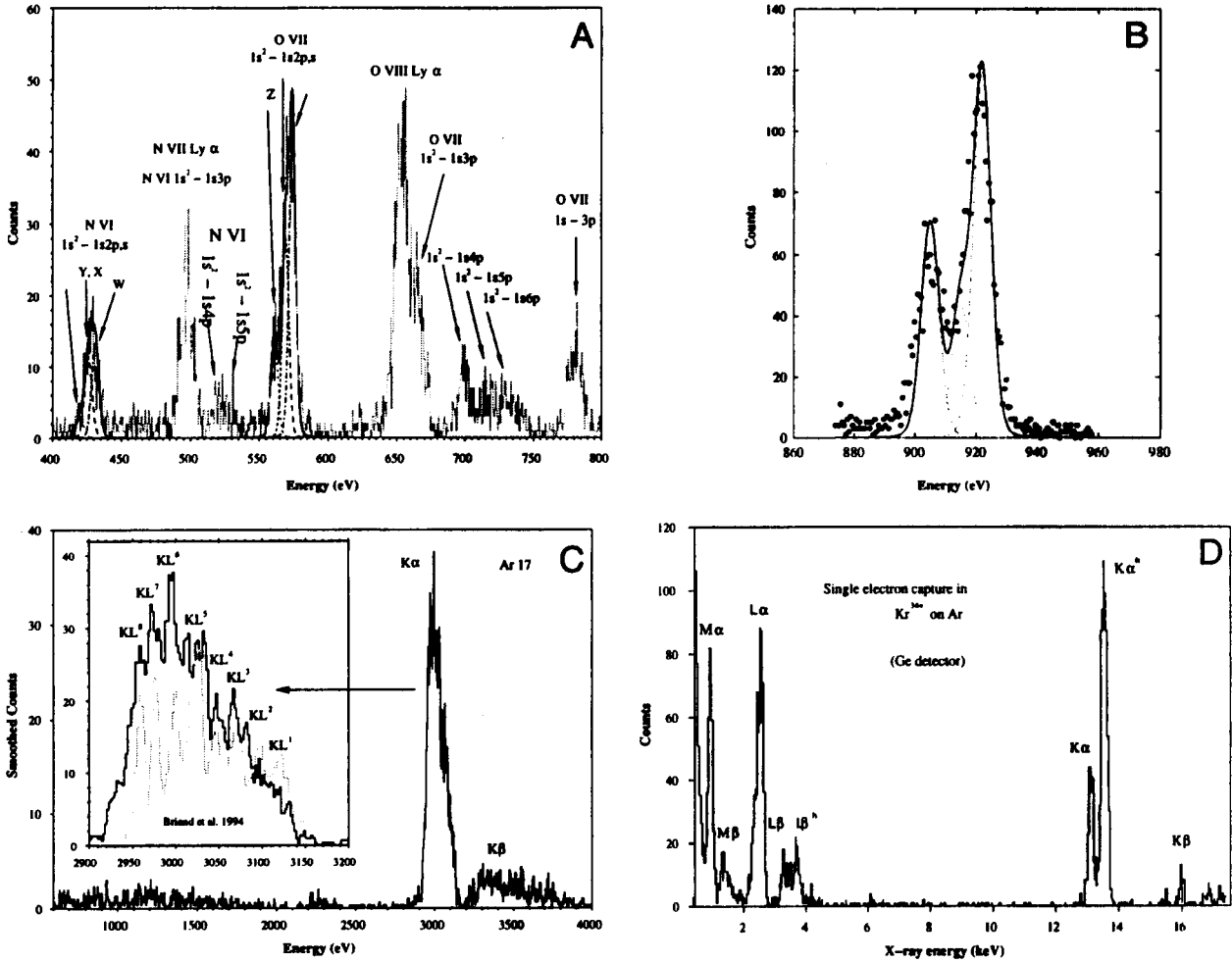
Fig. 2.— A: Microcalorimeter spectrum of H-like and He-like O and N. (23) B: Resonance, intercombination, and forbidden lines of He-like Ne (5) C: Microcalorimeter X-ray spectrum obtained from Ar^{17+} ions impacting on an Al surface with a velocity of 8×10^7 cm/s. For comparison a crystal spectrometer spectrum from (6) is shown. D: K, L, and M spectral lines from the interaction of bare Kr^{36+} ions with neutral Ar atoms. The spectrum was taken with a pure Ge solid state detector.
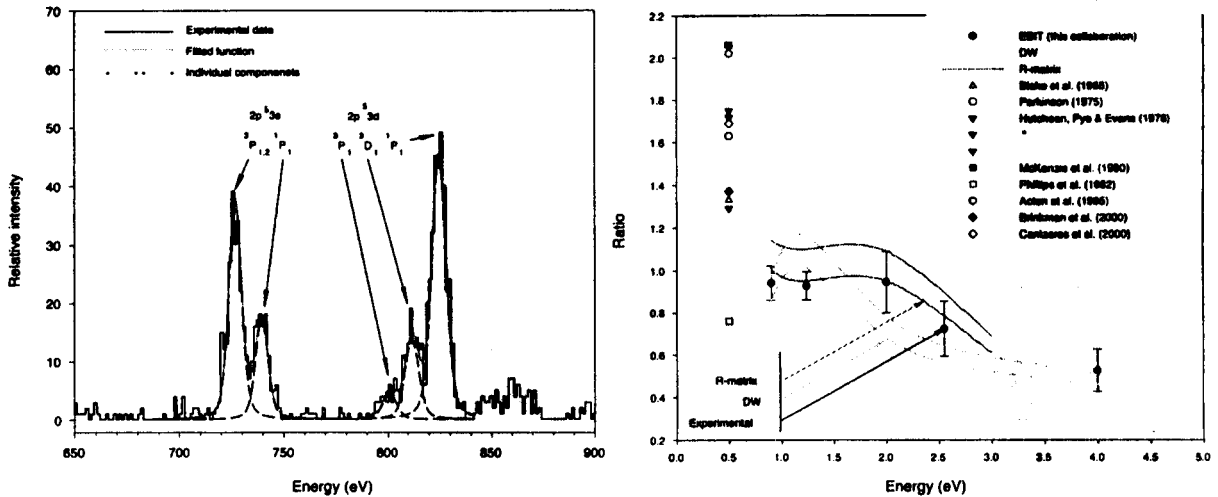
Fig. 3.— Left: Fit to the strong Fe XVII lines recorded at an electron beam energy of 900 eV. Right: The intensity ratios of the $2p^5 3s$ to the $2p^5 3d$ lines is compared with astrophysical and solar observations and with theory (14)

with calculations. Distorted wave (16) and R matrix (18) calculations that do not include resonance excitation of the excited levels agree with our measurements. Due to the monoenergetic electron beam, resonant excitations can mostly be avoided in EBIT compared to astrophysical sources where the electron energy distribution is broad. In astrophysical observations, depicted in the lefthand side of Fig. 3b resonant effects need to be taken into account in a fashion similar to (15). The inclusion of these effects tends to increase the $2p^63s$ to $2p^63d$ ratio producing a qualitative understanding of the scattered experimental and astrophysical values. Further experimental and theoretical work is needed to fully understand the physics of x-ray line production in Fe^{16+}.

6. Conclusion

Electron beam ion traps are ideal laboratory devices to support present and future x-ray astrophysical missions. Apart from providing test sites for advanced x-ray instruments like microcalorimeters, they also provide valuable laboratory data on the structure and interactions of highly charge ions that are found in a wide variety of astrophysical environments.

REFERENCES

(1) Levine, M. A., et al. (1988), Phys. Scr, **T22**, 157-163.

(2) C. T. Chantler, et al. (1999) Phys. Scr., **T80**, 440 and E. Takács, et al. (1996) Phys. Rev. A54, **1342**, 23.

(3) Brown, G. V., et al. (1998), ApJ, **502**, 1015 (erratum 532, 1245 (2000)).

(4) E. Silver, et al., (2000), Nucl. Instrum. Meth. Phys. Res. A, **444**, 156.

(5) M. Matranga, et al., to be published.

(6) J. P. Briand et. al., (1994) Nucl. Instrum. Meth. Phys. Res. B, **87**, 138.

(7) H. Tawara, et al., to be published.

(8) T. Cravens, (2002), Science, **296**, 1042.

(9) Lisse, C.M., et al., (1996), Science, **274**, 205.

(10) Raymond, J. C., & Smith, B. W. (1986) ApJ, **306**, 762.

(11) Schmelz, J. T., Saba, J. L. R., & Strong, K. T. (1992), ApJ, **398**, L115.

(12) Brinkman, A. C., et al. 2000, ApJ, 530, L111 and Canizares, C. R., et al. (2000), ApJ, **539**, L41.

(13) G.V. Brown, et al. (2001) Phys. Scr, **T92**, 130.

(14) J.M. Laming, et al. (2000), ApJ, **545**, L161-L164 (2000).

(15) R. Doron and E. Behar (2002), ApJ, **574**, 518.

(16) Bhatia, A. K., & Doschek, G. A. (1992), At. Data Nucl. Data Tables, **52**, 1.

(17) P. Beiersdorfer, et al., (1999) Phys. Scr, **T80** 121.

(18) Mohan, M., Sharma, R., & Eissner, W. (1997), ApJS, **108**, 389.

(19) Phillips, K. J. H., et al., (1997), A&A, **324**, 381.

(20) Jeremy Drake, unpublished.

(21) Liedahl, D. A., Kahn, S. M., Osterheld, A. L., & Goldstein, W. H. (1990), ApJ, **350**, L37.

(22) Kahn et al., (2001), A&A, **365**, L312.

(23) E. Silver, et al., Proc. XXII Intl. Conf. on Photonic, Electronic, and Atomic Collisions, Santa Fe, NM, 2001, (J. Burgdörfder, et al., eds., Rinton Press, 2002) p. 312.

(24) E. Silver, et al., (2000), ApJ, **541** 495.

Charge Transfer Calculations and Database for Astrophysics

J. G. Wang and P. C. Stancil

Dept. of Physics Astronomy; Ctr. for Simulational Physics, Univ. of Georgia, Athens, GA

M. Raković and D. R. Schultz

Physics Division, Oak Ridge National Laboratory, Oak Ridge, TN

B. Zygelman

Dept. of Physics, Univ. of Nevada, Las Vegas, NV

Abstract

A variety of theoretical approaches, having different but overlapping energy ranges of applicability, are applied to investigate charge transfer processes for collisions of atomic ions with atoms and molecules. The methods include quantal molecular-orbital close-coupling, classical trajectory Monte Carlo, and continuum distorted wave methods. Recent collision systems studied include $S^{4+} + H$, $S^{4+} + He$, $N^{7+} + He$, H_2O, CO, and CO_2, $O^{q+}(q = 1 - 8) + H$, H_2, and $S^{q+}(q = 1 - 16) + H_2$. The database effort is concentrating on astrophysically important reactions of atomic ions $X^{q+}(X$=H–Zn, q=1–4, and selected higher charges) with H, He, various metal atoms, H_2, and other selected molecular targets. Existing data, much of it produced by us, have been compiled and critically evaluated. Data for many reactions missing in the literature are estimated using the multichannel Landau-Zener approximation. Fits to cross sections and rate coefficients using standard functions are provided as well as tabulations of the raw data. The database is available on the World Wide Web at cfadc.phy.ornl.gov/astro/ps/data.

1. Introduction

Charge transfer, occuring in a very large range of astrophysical environments, can be decisive in establishing ionization structure, energy transfer, and inducing IR to x-ray radiative relaxation. However, little comprehensive data exist for complex projectile ions or targets more complex than atomic hydrogen. Therefore, to aid in the remediation of this situation, we are engaged in two efforts: (i) the calculation of charge transfer cross sections and rate coefficients using a variety of modern theoretical methods and (ii) the development of an on-line database of charge transfer reactions.

2. Theoretical Methods

To perform calculations for charge transfer, we use a variety of theoretical methods. Each method has its own advantages as well as disadvantages which can be classified according to the nature of the projectile ion and neutral target, the relevant energy range, the type and number of channels, and the degree of computational difficulty. For low-energy collisions, we employ the quantal molecular-orbital close-coupling (QMOCC) method. Radial, and often rotational, couplings are included in our QMOCC approach. For molecular targets, orientation and vibrational excitation of the target are also considered. The classical trajectory Monte
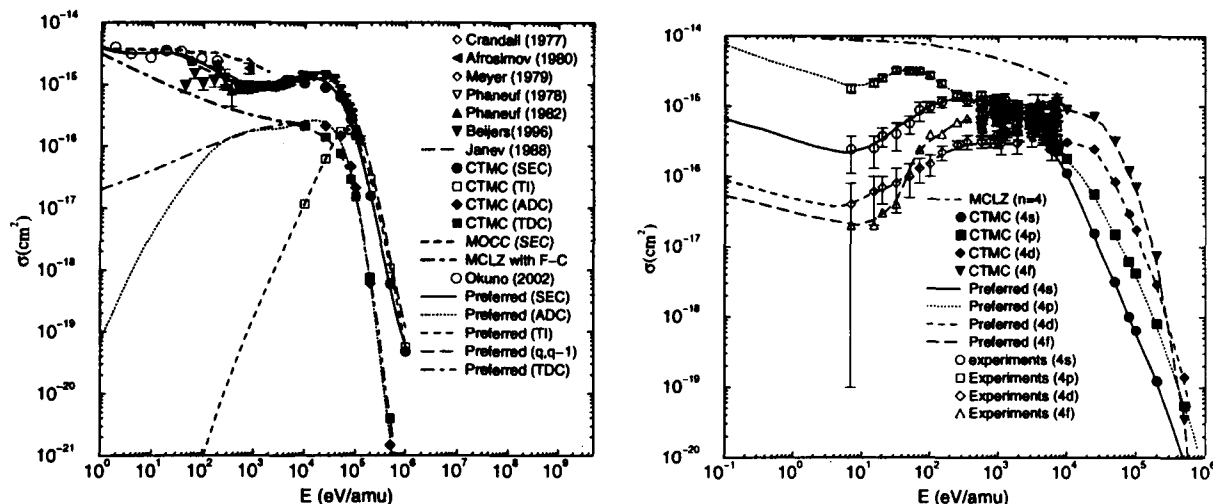
Fig. 1.— (a) Total cross sections for O^{3+} + H_2. (b) SEC state-selective cross sections for O^{6+} + H_2.

Carlo (CTMC) method is applied to collision problems at intermediate energies. For multi-electron targets such as He and H_2, CTMC has the advantage of providing data, in addition to single-electron capture (SEC), on multielectron processes such as true double-electron capture (TDC), transfer ionization (TI), and double-electron capture followed by autoionization (ADC). For relatively high collision energies, the continuum distorted wave (CDW) method can be used, but we apply it only for SEC calculations. A method which has been routinely used for astrophysical applications is the Landau-Zener (LZ) aproach. We use a multichannel (MCLZ) variant and for molecular targets, Frank-Condon ionization factors are used to treat the vibrational states of the product ion for SEC. We have also developed a method to treat total double capture (the sum of ADC and TDC) with the MCLZ approach.

3. Database

For our database effort, we i) collect existing experimental and theoretical data from the literature, ii) where data for a reaction is missing from the literature, cross sections and rate coefficients are computed using one or more of the methods described above, iii) all data are compiled and evaluated, and iv) the resulting preferred cross sections and rate coefficients are fit to standard functions (e.g. Chebychev polynomials).

4. Representative Results

A number of individual calculations have been completed as well as compilations and fittings for a series of collision systems. For example, for $O^{q+}(q = 1 - 8)$ + H_2, we considered charge transfer for all accessible final states with $n \leq 10$ for all four possible channels (SEC, TDC, TI, and ADC), which gives: 32 total, about 320 n-selective, and about 1760 n, l-selective cross sections. The cross sections were obtained and fitted over a large energy range from at least 1 eV/u to 10 MeV/u. A few examples are shown in figures 1-3. All of the results will be available on the ORNL/UGA Charge Transfer Database for Astrophysics.
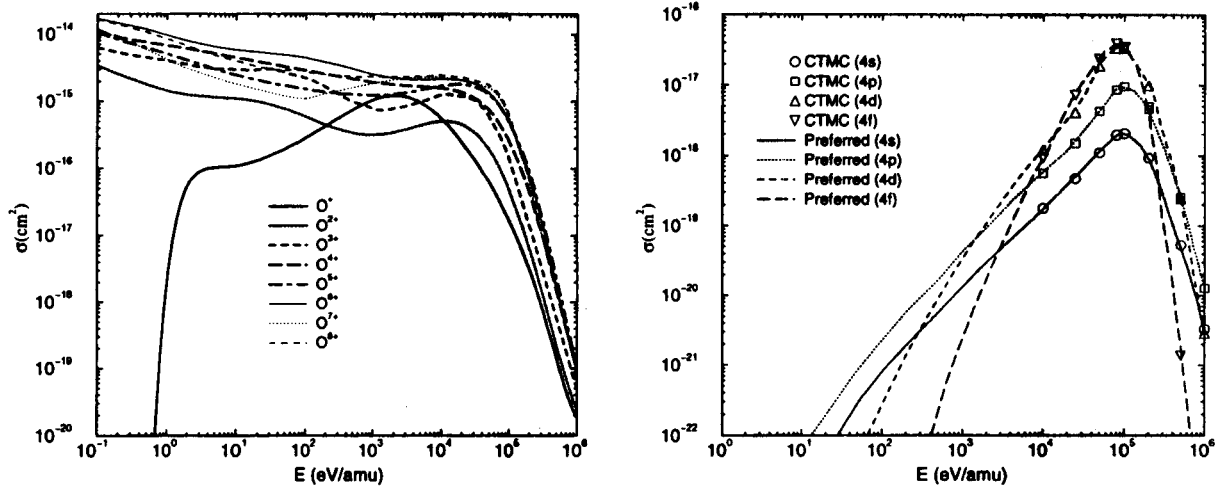
Fig. 2.— (a) The preferred total SEC cross sections for $O^{q+}(q = 1 - 8)$ + H_2. (b) Tl state-selective cross sections for O^{5+} + H_2
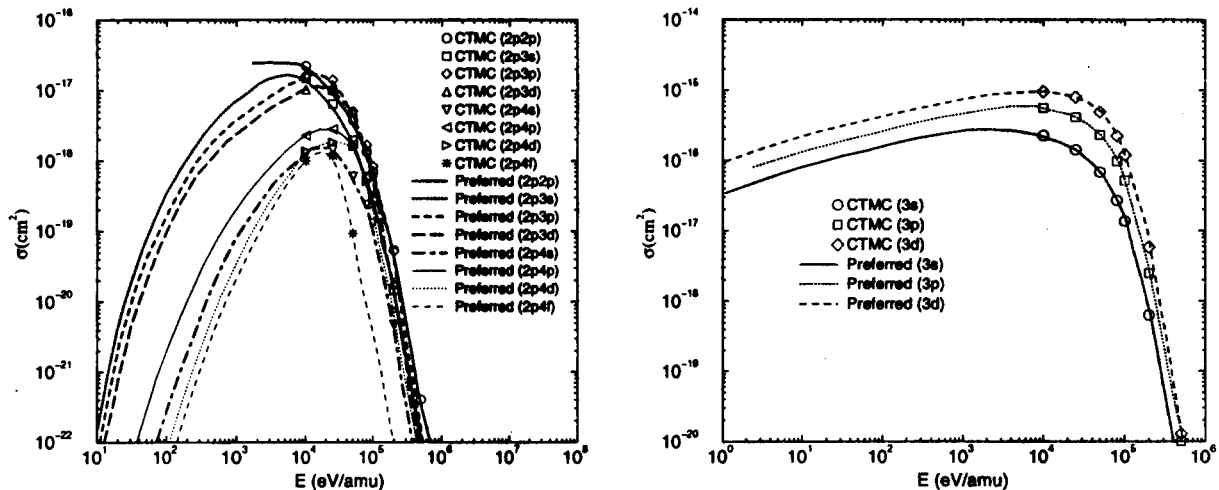
Fig. 3.— TDC state-selective cross sections for O^{2+} + H_2. ADC state-selective cross sections for O^{7+} + H_2.

Acknowledgments

REFERENCES

K. Okuno, private communication (2002).

R. A. Phaneuf et al., Phys. Rev., 26, 1892 (1982).

J. P. M. Beijers et al., J. Phys. B, 29, 1397 (1996).

D. H. Crandall et al., Phys. Rev. A, 15, 61 (1977).

F. W. Meyer et al., Phys. Rev. A, 19, 515 (1979).

V. V. Afrosimov et al., Sov. Phys.-JETP Lett., 31, 600 (1980).

R. A. Phaneuf et al., Phys. Rev. A, 17, 534 (1978).

R. K. Janev et al., At. Data Nucl. Data Tables, 40, 249 (1988).

Atomic Oscillator Strengths
by Emission Spectroscopy and Lifetime Measurements

W. L. Wiese and U. Griesmann
National Institute of Standards and Technology, Gaithersburg, MD

R. Kling
Inst. für Atom and Molekülphysik, Abteilung Plasmaphysik, Universität Hannover, Germany

J. Musielok
Institute of Physics, Opole University, Opole, Poland

Over the last seven years, we have carried out numerous oscillator strength measurements for some light and medium heavy elements (Musielok *et al.* 1995, 1996, 1997, 1999, 2000; Veres & Wiese 1996; Griesmann *et al.* 1997; Bridges & Wiese 1998; Kling *et al.* 2001; Kling & Griesmann 2000; Bridges & Wiese to be published). Most recently we have determined numerous transitions of Mn II (Kling *et al.* 2001; Kling & Griesmann 2000) and are now working on Cl I (Bridges & Wiese to be published). See the summary statement at the end of the text. For the emission measurements, we have applied either a high-current wall-stabilized arc (described for example, in Musielok *et al.* (1999)), or a high-current hollow cathode, or a Penning discharge. The latter two sources were used for branching ratio measurements from common upper levels, while the wall-stabilized arc was operated at atmospheric pressure under the condition of partial local thermodynamic equilibrium, which allows the measurement of relative transition probabilities. Absolute data were obtained by combining the emission results with lifetime data measured by other research groups, especially the University of Hannover, with which we have closely collaborated. This group uses the laser induced fluorescence (LIF) technique. Our emission spectra were recorded for the light elements with a 2 m grating spectrometer, or, for Mn II, with an FT 700 vacuum ultraviolet Fourier transform spectrometer. The radiometric calibration was carried out with a tungsten strip lamp for the visible part of the spectrum and with a deuterium lamp for the ultraviolet. All measurements were made under optically thin conditions, which was checked by doubling the path length with a focusing mirror setup. Typical uncertainties of the measured oscillator strengths are estimated to be in the range 15%–20% (one-standard deviation). However, discrepancies with advanced atomic structure theories are sometimes much larger. In Tables 1–3 and Fig. 1, we present some sample comparisons, mainly with such advanced calculations.

Summary of Elements and Spectra Covered

C I (Musielok *et al.* (1997, 2000)), N I (Musielok *et al.* (1995, 2000)), O I (Bridges & Wiese (1998)), F I (Musielok *et al.* (1999))

N II (Musielok *et al.* (1996)), O II (Veres & Wiese (1996)), Ne II (Griesmann *et al.* (1997))

Cl I (Bridges & Wiese (to be published))

Mn II (Kling *et al.* (2001); Kling & Griesmann (2000))

Table 1: A case of strong cancellation in the transition integral: two weak O I multiplets (A-values in 10^5 s^{-1})

			3s ^{3}S^o–4p ^{3}P (436.8 nm)	3s ^{5}S^o–4p ^{5}P (394.7 nm)
Calculations:				
Hibbert et al. (1991) (CIV3)	length	(ℓ)	5.86	5.06
	velocity	(v)	9.48	3.92
Bell & Hibbert (1990) (R matrix)		ℓ	10.1	4.10
		v	2.52	0.542
Pradhan & Saraph (1977) (R matrix)		ℓ	11.2	4.67
Seaton (1995) (R matrix)		ℓ	9.01	4.55
Experiments:				
Solaraki & Wiese (1964)			6.55	
Veres & Wiese (1996)			7.58	
Bridges & Wiese (1998)			7.62±7.5%	3.64±7.7%

Table 2: Comparison of some NIST experimental data with advanced calculations (A-values in 10^6 s^{-1}) for Ne II (F-sequence); IC=intercombination line

		NIST(expt.)[a]	CIV(th.)[b]	MCDF(th.)[c]	MCHF(th.)[d]
3p ^{4}P$^o_{5/2}$–3d ^{4}D$_{7/2}$		270	302	306	273
^{4}D$^o_{5/2}$–3d ^{4}D$_{7/2}$		1.08	3.22	2.88	2.36
^{4}D$^o_{7/2}$–3d ^{4}D$_{7/2}$		85.8	89.4	91.8	89.3
3p ^{4}P$^o_{5/2}$–3d ^{2}F$_{7/2}$	IC	1.33	4.11	4.83	2.08
^{4}D$^o_{5/2}$–3d ^{2}F$_{7/2}$	IC	111	189	173	161
^{4}D$^o_{7/2}$–3d ^{2}F$_{7/2}$	IC	8.46	18.6	16.0	16.4
^{2}D$^o_{5/2}$–3d ^{2}F$_{7/2}$		112	149	164	
3p ^{2}D$^o_{5/2}$–3d ^{4}F$_{7/2}$	IC	120	178.9	160	161
^{4}D$^o_{5/2}$–3d ^{4}F$_{7/2}$		85.6	149.4	166	169
^{4}D$^o_{7/2}$–3d ^{4}F$_{7/2}$		7.74	15.8	16.6	16.1

[a] Griesmann et al. (1997)   [b] Godefroid & Hibbert (2000)
[c] Fischer & He (1999)   [d] Fritzsche (unpublished)

Table 3: Comparison of lifetime data (in ns) for Mn II

Level	Martinson et al. 1973 (beam foil)	Pinnington et al. 1974, 1992 (beam foil)	Schnabel et al. 1995 (LIF)	NIST & Hannover 2001 (LIF)
3d^{5}4p ^{7}P$_2$	4.4	3.66[a]	3.89	3.67
3d^{5}4p ^{7}P$_3$	4.4	3.60[a]	3.62	3.61
3d^{5}4p ^{7}P$_4$	4.7	3.54[a]	3.58	3.68
3d^{5}4p ^{5}H$_7$			3.93	4.01
3d^{5}4p ^{5}F$_5$	4.1	4.0[b]		2.66
3d^{5}4p ^{5}F$_4$		4.5[b]		2.7

[a] Pinnington et al. (1992)   [b] Pinnington & Lutz (1974)
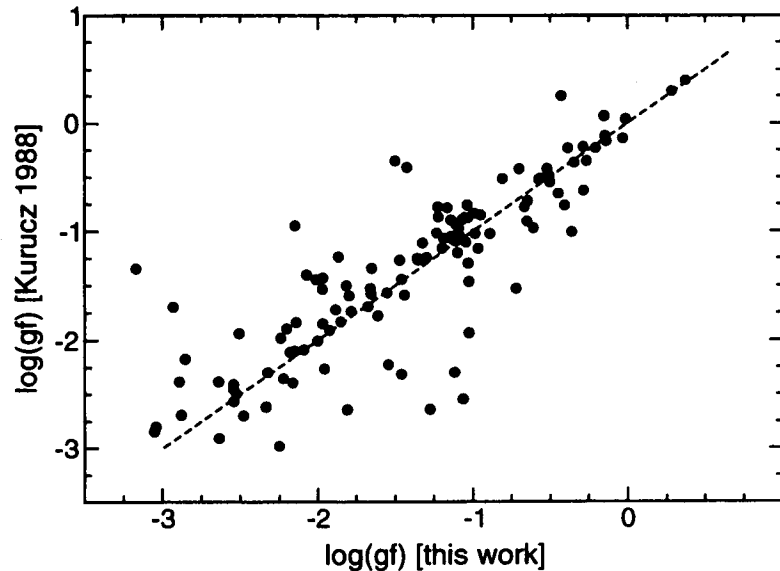
Fig. 1.— Comparison of NIST experimental oscillator strengths for Mn II(expressed as $\log gf$, from Kling *et al.* (2001)) with those calculated semiempirically by Kurucz (1988). The dashed line marks the identity.

REFERENCES

Bell, K. L., & Hibbert, A. 1990, *J. Phys.*, **B**, **23**, 2673.

Bridges, J. M., & Wiese, W. L. 1998, *Phys. Rev. A*, **57**, 4960.

Bridges, J. M., & Wiese, W. L. (to be published).

Froese Fischer, C., & He, X. 1999, *Can. J. Phys.*, **77**, 177.

Fritzsche, S. (unpublished).

Godefroid, M. R., & Hibbert, A. 2000, *Mol. Phys.*, **98**, 1099.

Griesmann, U., Musielok, J., & Wiese, W. L. 1997, *J. Opt. Soc. Am. B*, **14**, 2204.

Hibbert, A., Biemont, E., Godefroid, M., & Vaeck, N. 1991, *J. Phys. B*, **24**, 3943.

Kling, R., & Griesmann, U. 2000, *ApJ.*, **531**, 1173.

Kling, R., Schnabel, R., & Griesmann, U. 2001, *ApJS*, **134**, 173.

Kurucz, R. L. 1988, in *Trans. IAU*, ed. M. McNally (Dordrecht, Kluwer), **20B**, 168.

Martinson, I., Curtis, L. J., Brzozowski J., & Buchta, R. 1973, *Phys. Scr.*, **8**, 62.

Musielok, J., Bridges, J. M., Djurovic S., & Wiese, W. L. 1996, *Phys. Rev. A*, **53**, 3122.

Musielok, J., Bridges, J. M., Fuhr, J. R., & Wiese, W. L. 2000, *Phys. Rev. A*, **61**, 044502.

Musielok, J., Pawelec, E., Griesmann, U., & Wiese, W. L. 1999, *Phys. Rev. A*, **60**, 947.

Musielok, J., Veres, G., & Wiese, W. L. 1997, *J. Quant. Spectrosc. Radiat. Transfer*, **57**, 395.

Musielok, J., Wiese, W. L., & Veres, G. 1995, *Phys. Rev. A*, **51**, 3588.

Pinnington, E. H., Gou, B., Ji, Q., Berends, R. W., Ansbacher, W., & Biemont, E. 1992, *J. Phys. B*, **5**, L475.

Pinnington, E. H., & Lutz, H. O. 1974, *Can. J. Phys.*, **52**, 1253.

Pradhan, A. K., & Saraph, H. E. 1977, *J. Phys. B*, **10**, 3365.

Schnabel, R., Bard, A., & Kock, M. 1995, *Z. Phys. D*, **34**, 223.

Seaton, M. J. 1995, *The Opacity Project*, Vol. 1 (IOP, Bristol).

Solarski, J. E., & Wiese, W. L. 1964, *Phys. Rev.*, **135**, A1236.

Veres, G, Musielok, J., & Wiese, W. L. (unpublished).

Veres, G., & Wiese, W. L. 1996, *Phys. Rev. A*, **54**, 1999.

~ ~ *INVITED* ~ ~

Missing Pieces in Our Understanding of Astrochemistry: The Answers are in the Lab

Edwin A. Bergin and Gary J. Melnick

Harvard-Smithsonian Center for Astrophysics, Cambridge, MA

Abstract

Recent SWAS results demonstrate the importance of including gas- grain interactions for interstellar chemistry. This paper highlights areas where lab astrophysics can greatly increase our understanding of astrochemistry.

1. SWAS and Oxygen Bearing Molecules in the ISM

SWAS is a complete radio telescope in space, capable of observing the ground state transition of o-H_2O and a low-lying transition of O_2 (Melnick *et al.* 2000). At the time of launch, the primary mission goals were to answer these important questions: (1) Where is all of the oxygen in the dense interstellar medium (and, in particular, are H_2O and O_2 major reservoirs of oxygen)?, and (2) Are H_2O and O_2 significant gas coolants?

During the baseline mission SWAS succeeded in answering these questions. In particular, SWAS has shown that H_2O is a major repository of oxygen in warm ($T \gtrsim 300$ K), dense ($n(H_2) \gtrsim 10^3$ cm^{-3}) gas as well as a major gas coolant – in accord with model predictions. However, within cold ($T \lesssim 30$ K), dense clouds the abundance of gaseous H_2O is between 100 and 1000 times below the predictions of gas-phase chemical models (see Fig. 1) and the O_2 abundance is at least 100 times below predictions. As a result, gaseous H_2O and O_2 are neither significant reservoirs of elemental oxygen in cold gas nor are they important gas coolants in such clouds. Within cold, but diffuse ($n(H_2) < 10^3$ cm^{-3}), gas there is limited evidence that the H_2O abundance is higher than in the cold dense gas, but O_2 remains undetected. The 20 August 2000 issue of *Ap.J. Letters*, which was dedicated to early SWAS results, summarizes many of these findings.

These results highlighted the need to construct a new model of interstellar chemistry, consistent with the broad range of SWAS-inferred abundances. The model developed by the SWAS team to account for this discrepancy combines pure gas-phase chemistry with the chemical effect of depletion onto cold dust grains, along with the possibility of reactions also occurring on the surface (Bergin *et al.* 2000). Fig. 2a shows a model of pure-gas phase chemistry, which predicts higher water abundances at $t > 10^3$ years than observed. In Fig. 2b we show a gas-grain chemical model which includes the formation of water on grain surfaces via hydrogenation of atomic oxygen. In this model the near total freeze-out of oxygen in the form of water on grain surfaces effectively removes the fuel that forms gaseous H_2O and O_2, lowering the abundance to match observed values (Bergin *et al.* 2000; Viti *et al.* 2001; Charnley *et al.* 2001).
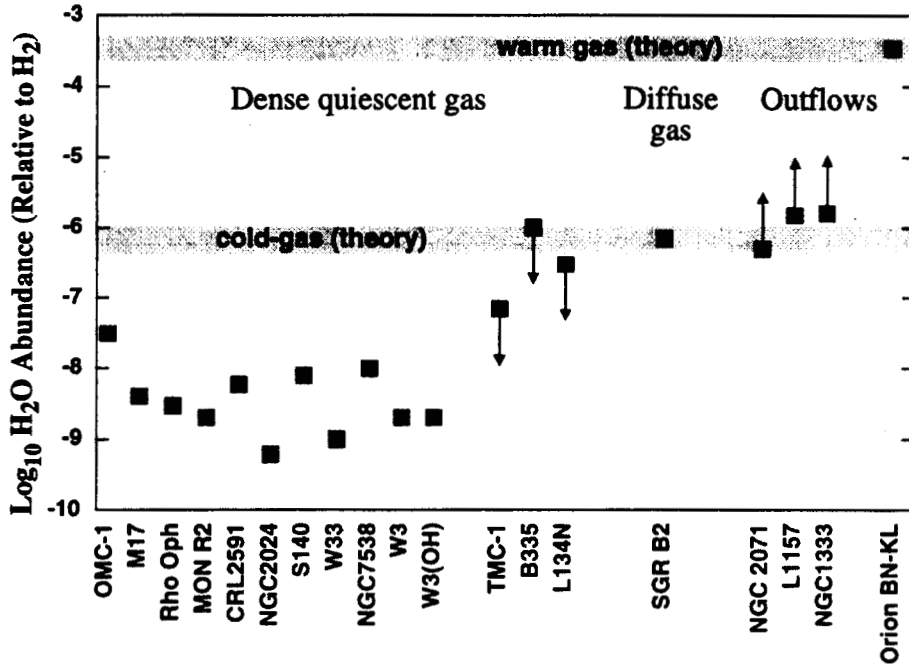
Fig. 1.— SWAS H_2O abundance results obtained during the baseline mission toward a sample of sources. The equilibrium H_2O abundances predicted by pure gas-phase chemical models is shown as grey bands for both cold- and warm-cloud conditions (see text).
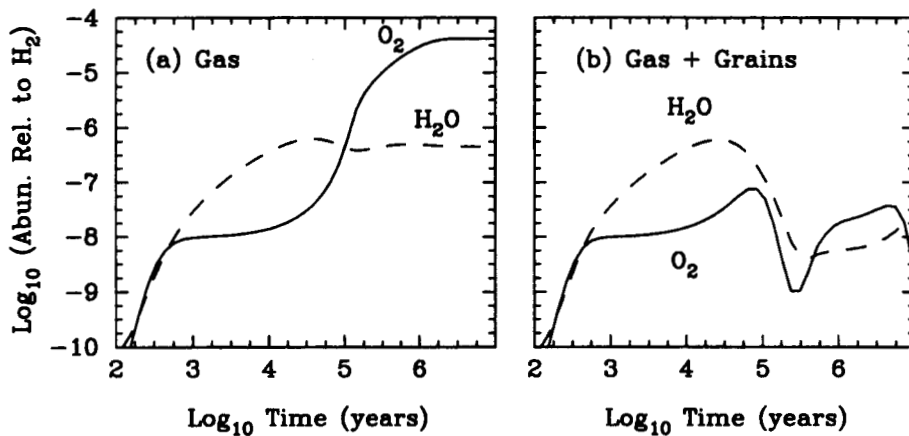
Fig. 2.— (a) Theoretical predictions of the H_2O and O_2 abundance (relative to H_2) from a pure gas-phase chemical model using representative physical conditions for a star forming cloud ($n_{H_2} = 10^5$ cm^{-3}, T = 20 K, and $A_V = 20$ mag). (b) Same as (a) but from a model that includes gas phase atoms and molecules interacting with grain surfaces. Adapted from Bergin et al.(2000).

2. Gas-Grain Chemistry and Laboratory Astrophysics

For chemical theory to account for the low H_2O and O_2 abundances crucial assumptions must be made. To examine whether these assumptions are correct we must continue to draw upon the important relationship between laboratory astrophysics and astrochemistry. Below we suggest several areas where attention can be focused which would allow for continued progress in our understanding of the chemistry associated with the formation of stars and planetary systems.

1. Dissociative Recombination: Rate coefficients and branching ratios for the dissociative recombination reactions of several molecular ions are available; however, for H_2O there persist discrepancies in the measured values (e.g., Vejby-Christensen *et al.* 1997; Williams *et al.* 1996). Characterizing this process for numerous molecules is necessary because many species are theorized to form via this process.

2. Molecular Photodissociation: The photodestruction of molecules subject to the local radiation field may also contribute to the low measured abundance of H_2O and O_2 (e.g., Spaans & van Dishoeck 2001). To properly study these effects requires an accurate determination, with sufficient spectral resolution, of the UV photodissociation cross-sections of important molecules.

3. Binding Energy: The bond between molecules and grain surfaces occurs via van der Waals interactions, with the strength of this bond effectively determining the energy required to remove a molecule from the grain (and place it into the gas phase). Chemical models which include desorption processes require estimates of these values, which have only been determined for a handful of molecules (Sandford & Allamandola 1990; Fraser *et al.* 2001).

4. Grain Surface Chemistry: The type and rate of catalytic chemical reactions on the surfaces of dust grains are among the greatest unknowns in astrochemistry. The topic has recently received attention from laboratory astrophysicists (e.g., Pirronello, Liu, Shen, & Vidali 1997), though more work needs to be done. Specifically, important questions remain in H_2 formation as well as reactions between various species with oxygen atoms.

5. Grain Thermal Properties: The residence time of molecules on grain surfaces relies not only on the bond strength, but also on how the grain responds to energy deposited by cosmic rays and X-rays. In particular, the thermal conductivity and specific heats of amorphous solids are both quantities that play a significant role in determining how heat is dissipated throughout a grain. The past decade has led to important advances in our understanding of these properties, recently summarized by Pohl (1998). However, laboratory work has shown that these properties depend on the sample size. Most work to date has been done on bulk samples and as such there is little information on the thermal properties of small particulate material that could be representative of the small 1000 Å grains found in the interstellar medium.

REFERENCES

Bergin, E. A. *et al.* 2000, *ApJ*, **539**, L129

Charnley, S. B., Rodgers, S. D., & Ehrenfreund, P. 2001, *A&A*, **378**, 1024

Fraser, H. J., *et al.* 2001, *MNRAS*, **327**, 1165

Melnick, G. J. *et al.* 2000, *ApJ*, **539**, L77

Pirronello, V. *et al.* 1997, *ApJ*, **475**, L69

Pohl, R. O. 1998, *Encyclopedia of Applied Physics*, **23**, 223

Sandford, S. A., & Allamandola 1990, *Icarus*, **87**, 188

Spaans, M. & van Dishoeck, E. F. 2001, *ApJ*, **548**, L217

Vejby-Christensen, L. *et al.* 1997, *ApJ*, **483**, 531

Viti, S. *et al.* 2001, *A&A*, **370**, 557

Williams, T. L. *et al.* 1996, *MNRAS*, **282**, 413

Gas Phase Spectroscopy of Cold PAH Ions: Contribution to the Interstellar Extinction and the Diffuse Interstellar Bands

L. Biennier, F. Salama, and L.J. Allamandola

NASA Ames Research Center, Space Science Division, Moffett Field, California

J.J. Scherer and A. O'Keefe

Los Gatos Research, Mountain View, California

1. Introduction

Polycyclic Aromatic Hydrocarbon molecules (PAHs) are ubiquitous in the interstellar medium (ISM) and constitute the building blocks of interstellar dust grains. Despite their inferred important role in mediating the energetic and chemical processes in the ISM, their exact contribution to the interstellar extinction, and in particular to the diffuse interstellar bands (DIBs) remains unclear. The DIBs are spectral absorption features observed in the line of sight of stars that are obscured by diffuse interstellar clouds. More than 200 bands have been reported to date spanning from the near UV to the near IR with bandwidths ranging from 0.4 to 40 Å (Tielens & Snow 1995). The present consensus is that the DIBs arise from free flying, gas-phase, organic molecules and/or ions that are abundant under the typical conditions reigning in the diffuse ISM. PAHs have been proposed as possible carriers (Allamandola *et al.* 1985; Léger & D'Hendecourt 1985). The PAH hypothesis is consistent with the cosmic abundance of Carbon and Hydrogen and with the required photostability of the DIB carriers against the strong VUV radiation field in the diffuse interstellar clouds. A significant fraction of PAHs is expected to be ionized in the diffuse ISM.

2. Laboratory Approach

Extensive laboratory efforts have been engaged in the last decade to evaluate the potential of neutral and ionized PAHs as DIB carriers using Matrix Isolation Spectroscopy (MIS) (Salama 1999). In MIS, PAHs are isolated in a solid rare gas matrix at very low temperature and submitted to VUV radiation to mimic the ISM conditions. However even in the least perturbing media (neon matrices) the interaction of the trapped PAHs with the rare gas atoms of the solid lattice induces a frequency shift and a broadening of the band profile precluding thus a decisive comparison with astronomical data. MIS surveys over a broad spectral range are critical however for the pre-selection of the most promising candidates. To properly address the issue of the identification of the DIBs, astronomical observations must be compared to laboratory spectra that are measured in an astrophysically relevant environment i.e., with the molecules/ions isolated, cold and in the *gas phase*. This task represents a serious experimental challenge because PAHs are large, non-volatile molecules that need to be vaporized and ionized. Furthermore, due to the ultra-fast non-radiative processes of internal electronic conversion that

take place in these large molecular systems, detection by laser-induced fluorescence or by multiphoton excitation cannot be employed. Because of all these technical limitations, it was only very recently that two groups were able to measure the absorption spectra of cold PAH ions in the gas-phase (Romanini et al. 1999; Bréchignac & Pino 1999). The approach followed by Bréchignac et al. is an indirect method based on the messenger method that measures the photodissociation spectrum of the rare gas – aromatic ion complex formed by two photons two colors photoionization (Bréchignac & Pino 1999). Our approach is a direct method, that relies on the association of a cold plasma source (pulsed discharge nozzle) with a high sensitivity direct absorption technique (cavity ring down spectroscopy or CRDS) and led to the first detection of the naphthalene ion in the gas phase (Romanini et al. 1999). This versatile method possesses the advantage of being independent of inter- and intra- molecular processes. Following the pioneering scheme of Nesbitt et al. (Davis et al. 1997), the pulsed discharge nozzle combines a supersonic slit jet (Liu et al. 1996) that cools down the Ar carrier gas seeded with aromatics ($\sim$ 1%), with two electrodes that produce a discharge in the stream of the planar expansion to ionize the mixture. The PAH vapor pressure is increased by heating a pick-up cell that contains the sample upstream the Ar flow. A cavity ringdown spectrometer probes the expansion several mm downstream with sub-ppm absorption sensitivity (Biennier et al. 2002).

3.   Experimental Results

We report the preliminary experimental results regarding the electronic spectroscopy of several cold PAH cations in the gas phase that have been obtained with this new instrument (Biennier et al. 2002). The electronic spectrum of the cold naphthalene ion ($C_{10}H_8^+$) was first measured in order to compare directly with the results obtained during the feasibility phase (Romanini et al. 1999) and because MIS (Salama & Allamandola 1991) and gas-phase molecular depletion experiments (Pino et al. 1999) were already available. We have measured the first four strongest absorption bands at 670.70, 648.89, 612.52 and 593.35 nm (Fig. 1) two of which are reported for the first time. The bands correspond to the vibrational progression of the $^2B_{3g}(D_2) \leftarrow X^2A_u(D_0)$ electronic system of Np$^+$ ($C_{10}H_8^+$). There is an excellent agreement with the band positions measured in the previous gas- phase experiments confirming the 0.5% redshift observed in the band positions when the species is trapped in a solid neon matrix. The four bands are broad and without any substructure, a characteristic of non-radiative intramolecular relaxation processes that explains the UV photon pumping mechanism that occurs in the ISM and the observations of the UIR emission by radiative cascade. Detailed analysis of the band profile leads to the determination of a FWHM of 25 cm^{-1}. This value corresponds to an ultra fast relaxation time of 220 fs and is very close to the value found by molecular depletion experiments in which they measure the intrinsic band profile. We can therefore conclude that the discharge does not affect the vibrational temperature of the aromatic ions formed in the cold plasma expansion.
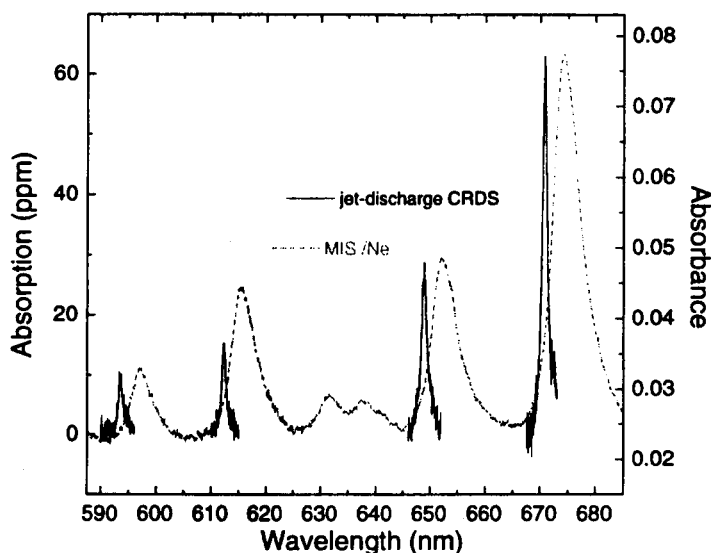
Fig. 1.— Comparison of CRDS (Biennier *et al.* 2002) and MIS/Ne (Salama & Allamandola 1991) spectra. The interactions of the trapped Np$^+$ with the atoms of the solid neon matrix induce a frequency shift and a spectral broadening of the electronic spectrum. This figure illustrates dramatically the need for gas-phase experiments for a decisive, unambiguous, identification of the DIBs. MIS remains however critical for the pre-selection of potential candidates.

The acenaphthene ion ($C_{12}H_{10}^+$) was chosen for the next step. Acenaphthene belongs to the class of hydrogenated PAHs that are also thought to be present in the ISM. We have measured for the first time in the gas phase the absorption spectrum of the cold Acenaphthene ion (Ac$^+$). In this preliminary work, we report the vibration-less (0-0) $B_1(D_2) \leftarrow XA_2(D_0)$ electronic absorption spectrum of Ac$^+$ that peaks at 646.31 nm. The fitting of the profile results in a bandwidth of 2.3 nm (54 cm^{-1}) that is twice broader than the corresponding value for the naphthalene ion and that corresponds to a 100 fs relaxation time. Based on unpublished results from the NASA-Ames group, the Ac$^+$ molecular ion electronic absorption band is redshifted by 0.3% (or -42 cm^{-1}) when it is trapped into a Neon matrix (648.1 nm) and its width is about 3.9 nm (92 cm^{-1} or 1.7 times the gas phase value) (Halasinski & Salama 2002). This might be explained by the increased rigidity induced in Ac by the additional three C–C bonds, making less vulnerable to the matrix-induced cage effect as compared with Np.

The study has now been extended to the pyrene ion ($C_{16}H_{10}^+$). Ionized pyrene derivatives are considered as good candidates for the carrier of the strong 4430 Å DIB (Salama & Allamandola 1992). We report the vibration-less (0-0) $^2A_u(D_5) \leftarrow {}^2B_{3g}(D_0)$ electronic transition. The band centered at 436.6 nm reveals an extremely large width (3.6 nm or about 190 cm^{-1}) slightly smaller than its solid-phase value (about 4 nm in a neon matrix). This value provides a value of 30 fs for the relaxation time from D_5 to D_4 through electronic internal conversion. The peak position of the electronic spectrum of the free flying pyrene cation is blue shifted by 0.6 % compared to its value when trapped in a neon matrix.

4. Perspectives and Conclusion

These preliminary results strongly validate our original experimental approach associating a cold plasma source with a cavity ringdown spectrometer. These experiments provide first hand data on the spectroscopy and on the molecular dynamics of *free, cold* large carbon-containing molecules and ions in the gas phase. We are now, for the first time, in the position to directly compare laboratory spectral data on free PAH ions with astronomical observations in the UV-NIR range. Work is currently under progress in collaboration with J. Krelowski to assess the naphthalene ion as carrier for two newly detected large DIBs centered at 6704 and 6486 Å. This new phase offers tremendous opportunities for the data analysis of current and upcoming space missions (e.g., HST data and the COS instrument).

Acknowledgments

REFERENCES

Allamandola, L. J., Tielens, A. G. G. M., & Barker, J. R. 1985, *ApJ*, **290**, L25

Biennier, L., Salama, F., Allamandola, L., Scherer, J., & O'Keefe, A. 2002, submitted to *J. Chem. Phys.*

Bréchignac, P. & Pino, T. 1999, *A&A*, 343, 49.

Davis, S., Anderson, D. T., Duxbury, G., & Nesbitt, D. J. 1997, *J. Chem. Phys.*, **107**, 5661.

Halasinski, T. & Salama, F. 2002, in preparation.

Léger, A. & D'Hendecourt, L. B. 1985, *A&A*, 146, 81.

Liu, K., Fellers, R. S., Viant, M. R., McLaughlin, R. P., Brown, M. G., & Saykally, R. 1996, *Rev. Sci. Instrum.*, 67, 410.

Pino, T., Boudin, N., & Bréchignac, P. 1999, *J. Chem. Phys.*, **111**, 7337.

Romanini, D., Biennier, L., Salama, F., Allamandola, L. J., & Stoeckel, F. 1999, *Chem. Phys. Lett.*, **303**, 165.

Salama, F. 1999, in Solid Interstellar Matter: The ISO Revolution (France: EDP Sciences), 6587.

Salama, F. & Allamandola, L. J. 1991, *J. Chem. Phys.*, **94**, 6964.

—. 1992, *Nature*, **358**, 42.

Tielens, A. G. G. M. & Snow, T. P., eds. 1995, The Diffuse Interstellar Bands (Dordrecht, the Netherlands: Kluwer Academic Publishers).

Laboratory Measurements of Solar-Wind/Comet X-Ray Emission and Charge Exchange Cross Sections

A. Chutjian, I. Čadež, J. B. Greenwood, R. J. Mawhorter, S. J. Smith, and J. Lozano

Jet Propulsion Laboratory, California Institute of Technology, Pasadena, CA

The detection of X-rays from comets such as Hyakutake, Hale-Bopp, d'Arrest, and Linear as they approach the Sun has been unexpected and exciting [1,2]. This phenomenon, moreover, should be quite general, occurring wherever a fast solar or stellar wind interacts with neutrals in a comet, a planetary atmosphere, or a circumstellar cloud. The process is, $O^{8+} + H_2O \rightarrow O^{7+*} + H_2O^+$, where the excited O^{7+*} ions are the source of the X-ray emissions. Detailed modeling has been carried out of X-ray emissions in charge-transfer collisions of heavy solar-wind HCIs and interstellar/interplanetary neutral clouds [3]. In the interplanetary medium the solar wind ions, including protons, can charge exchange with interstellar H and He. This can give rise to a soft X-ray background that could be correlated with the long-term enhancements seen in the low-energy X-ray spectrum of ROSAT. Approximately 40% of the soft X-ray background detected by Exosat, ROSAT, Chandra, etc. is due to CXE [3]: our whole heliosphere is glowing in the soft X-ray due to CXE.

Comet-modeling calculations to date have (a) used an approximate, over-barrier expression for the charge-exchange (CXE) cross section, (b) assumed a flat energy dependence of cross section, and (c) neglected multiple charge exchanges. To understand the intensity and spatial extent of the X-ray emissions, X-ray emission cross sections and absolute CXE cross sections for process such as defined in Eq. (1) have been measured using the charge-exchange beam line at the JPL Highly-Charged Ion Facility (HCIF) [4]. The projectiles have been partially- and fully-stripped H, He, C, N, O, Ne, and Fe ions interacting with the comet molecules He, H_2, CO, CO_2, and H_2O. Absolute CXE cross sections have been measured, and normalized X-ray emission cross sections reported for the major HCI components of the solar wind [5-8]. The heavier HCI components will produce high-energy X-rays. Data have been acquired on $Fe^{(5-13)+}$ [9].

A schematic of the CXE beam line is shown in Fig. 1. Experimental details are given in Refs. [7,8]. Briefly, the HCI beam enters the gas collision cell through a series of beam-collimating apertures **A**. Charge exchange takes place, and the charges of the exiting ions are analyzed using a retarding potential- difference method with the grids **RA**. Absolute CXE cross sections are obtained by knowledge of the incident and transmitted beam currents, the gas density in the cell (with corrections for effusion from the cell's entrance and exit apertures, and thermal transpiration), and the effective cell length. Checks are made to ensure full angular collection of the retarded ion beams by varying aperture sizes in **RA**; and for the presence of metastable levels in the incident HCI beam by carrying out CXE measurements with quenching gas in the beam line. Recent experimental results [6] for CXE of H^+, He^+ and He^{2+} on H_2O are shown in Fig. 2.
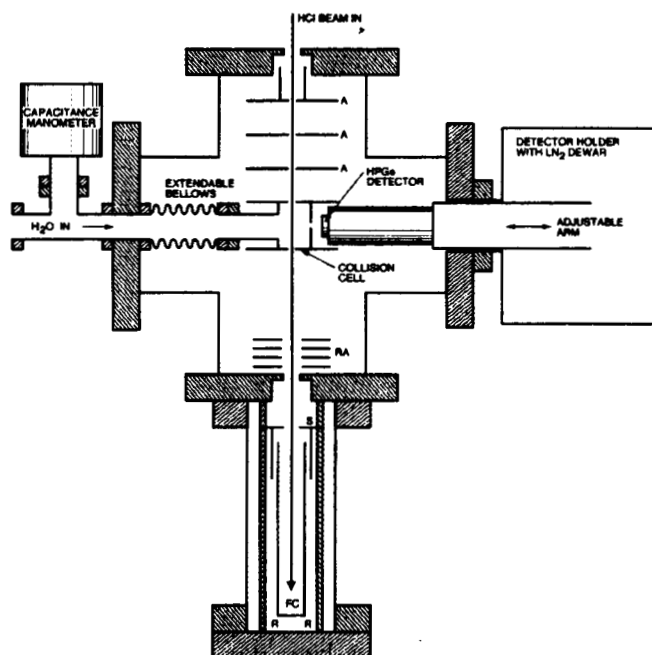
Figure 1. Detail of the JPL HCIF charge-exchange beamline. The legend is: (A) input HCI beam-defining apertures, (RA) retarding-field apertures, (S) secondary electron shield, (FC) Faraday cup, (R) support rods, (LN$_2$) liquid nitrogen cooling for the HPGe detector crystal.
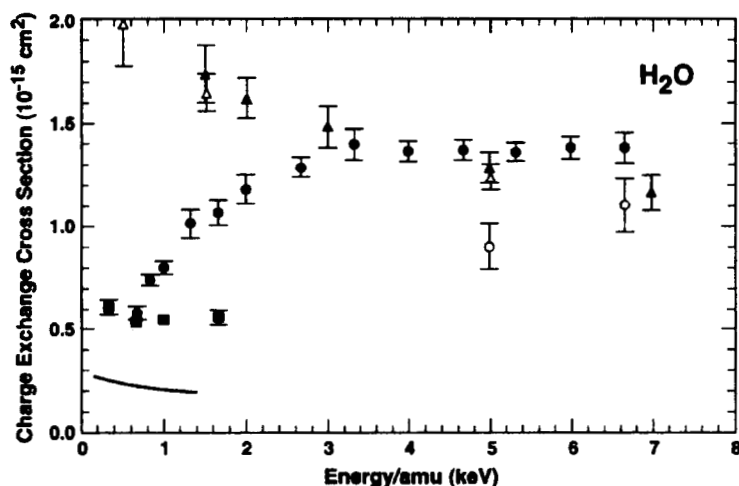
Figure 2. Absolute single charge exchange cross sections of H$^+$ (▲), He$^+$ (■), and He^{2+} (●) in H$_2$O. Data by others are given for H$^+$ (△ and ▬) and for He^{2+} O). See Ref. [6] for details.

Placed orthogonal to the incident HCI beam direction is an HPGe X-ray detector which views the X-ray emissions from the gas cell. Gaussian profiles centered on the known transition energies are fitted to the observed spectra. The estimated FWHM of these fits is 102 ± 2 eV, which is narrower than the 170 eV width of Si-Li detectors used in other measurements. A series of X-ray spectra for the collisions of O^{7+}, O^{8+}, Ne^{9+}, and Ne^{10+} with H$_2$O is shown in Fig. 3. Spectra for collisions of Ne^{10+} with He, H$_2$, CO$_2$, and H$_2$O are shown in Fig. 4. Prominent in the spectra are the Lyman transitions $np \rightarrow 1s(n = 2 - 5)$ which are important contributors to the observed cometary X-ray emissions. Future work will be extended to Mg^{q+} charge states, and include as well II and NH$_3$ as targets.
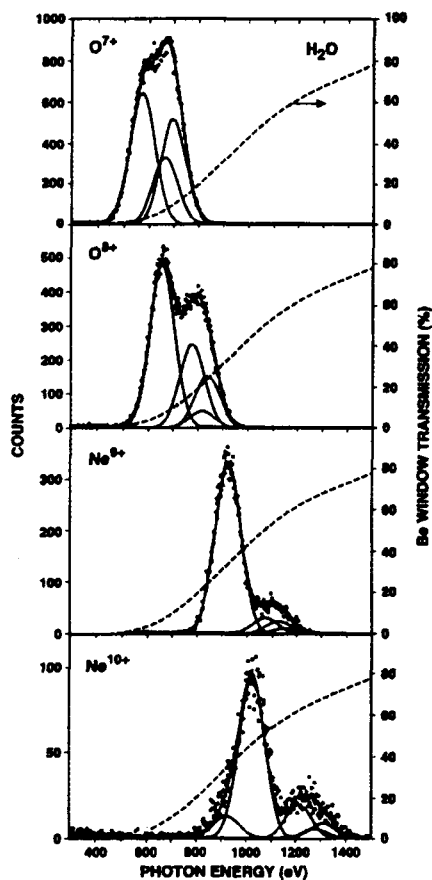
Figure 3. X-Ray emission spectra for the collision of the indicated ions with H_2O at energies of 70 keV. Data are uncorrected for the Be window transmission, shown by the dashed line (– – –). The underlying curves are the Lyman transitions np $\rightarrow$ 1s (n=2-4 and 5).
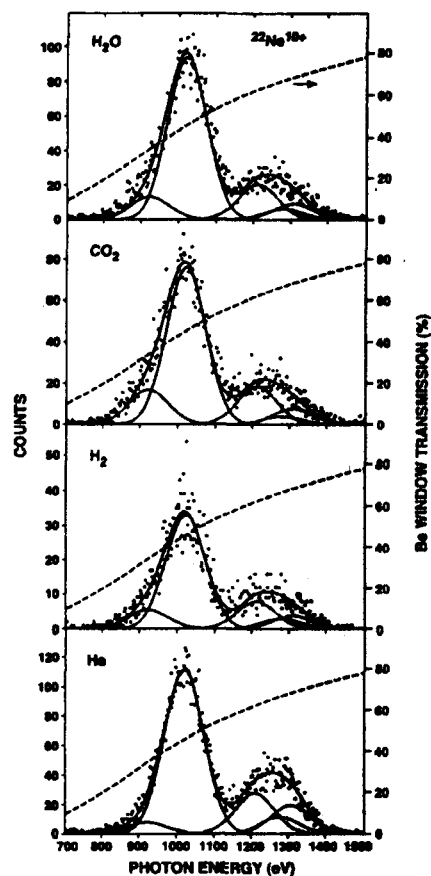
Figure 4. X-Ray emission spectra for the collision of $^{22}Ne^{10+}$ ions with He, H_2, CO_2, and H_2O at 70 keV energy. Data are uncorrected for the Be window transmission, shown by the dashed line (– – –). The underlying curves are the Lyman transitions np $\rightarrow$ 1s (n=2-5).

REFERENCES

[1] C. M. Lisse *et al.*, *Science* **274**, 404 (1996); C. M. Lisse *et al.*, *Science* **292**, 1343 (201).

[2] V. A. Krasnopolsky and M. J. Mumma, *Ap. J.* **549**, 629 (2001).

[3] T. E. Cravens *Ap. J.* **532** L153 (2000); N. A. Schwadron and T. E. Cravens, *Ap.J.* **544**, 558 (2000); T. E. Cravens et al., *J. Geophys. Res.* **106**, 24883 (2001).

[4] A. Chutjian, *et al.*, in *Atomic Processes in Plasmas* (eds. E. Oks and M. S. Pindzola, Am. Inst. Phys., NY, 1998); A. Chutjian, *et al.*, in *Applications of Accelerators in Research and Industry* (eds. J. L. Duggan and I. L. Morgan, Am. Inst. Phys., NY, 1999) p. 881.

[5] J. B. Greenwood, I. D. Williams, S. J. Smith, and A. Chutjian, *Ap. J. Lett.* **533**, L175 (2000).

[6] J. B. Greenwood, A. Chutjian and S. J. Smith, *Ap. J.* **529**, 605 (2000).

[7] J. B. Greenwood, I. D. Williams, S. J. Smith, and A. Chutjian, *Phys. Rev. A* **63**, 062707 (2001).

[8] I. Čadež, J. B. Greenwood, A. Chutjian, S. J. Smith, and M. Niimura, "Absolute Cross Sections for Single and Double Charge Exchange in $^3He^{2+}$ Impact on CO," *J. Phys. B*(in press).

[9] J. B. Greenwood, I. D. Williams, S. J. Smith, and A. Chutjian, *Phys. Scr.* **T92**, 150 (2001).

[10] I. Čadež, S. J. Smith, M. Niimura, J. B. Greenwood, and A. Chutjian, "Measurements of Absolute Electron Capture Cross Sections for 7q keV Fe^{q+} Ions in Collisions with CO," *J. Phys. B* (in preparation).

Laboratory Anion Chemistry: Implications for the DIBs, and a Potential Formation Mechanism for a Known Interstellar Molecule

B. Eichelberger[1], C. Barckholtz[1], M. Stepanovic[1], V. Bierbaum[1], and T. Snow[2]

University of Colorado, Boulder, CO

1) Department of Chemistry and Biochemistry

2) Center for Astrophysics and Space Astronomy

Abstract

Due to recent interest in molecular anions as possible interstellar species, we have carried out several laboratory studies of anion chemistry. The reactions of the series C_n^- and C_nH^- with H and H_2 were studied to address the viability of such species in the diffuse interstellar medium and to address their ability to be carriers of the DIBs. These same molecules were also reacted with N and O to show possible heteroatomic products. C_mN^- was a particularly stable product from the reaction of C_n^- + N. C_3N^- was further reacted with H to study chemistry that could produce HC3N, a known interstellar species. The reactions were done in a flowing afterglow selected ion flow tube apparatus (FA-SIFT). The anions were generated in an electron impact or cold cathode discharge source and the anion of interest was then selected by a quadrupole mass filter. The selected ion was then reacted with the atomic or molecular species in the flow tube and products were detected by another quadrupole. While the C_n^- species do not appear to be viable DIB carriers, their possible presence could provide a mechanism for the formation of known heteroatomic neutral molecules detected in the ISM.

1. Introduction

The reactions of negative-ions with atoms have historically received little attention, in part due to the limited and unusual environments in which such reactions would have significance. The first anion-atom studies provided insight into the ion chemistry of the lower ionosphere (Fehsenfeld et al. 1966). More recently, it has been suggested that there may be negative ions in the interstellar medium (ISM), where it is known that atomic species are abundant. Specifically, some carbon chain species have been cited as possible carriers of some of the unidentified visible absorption features known as the diffuse interstellar bands (DIB)(Fulara et al. 1993; Tulej et al. 1998). Some neutral carbon chain species, C_n (n = 2,3,5), HC_n (n = 2-8), and C_nH_2 (n = 2,3,4,6), have been positively identified in the ISM by radio techniques, but the presence of their negative ion counterparts remains undetermined (Thaddeus et al. 1998; Blanksby et al. 1999). The most abundant atomic species in the ISM is H atom, followed by N and O atoms. Recently, the reactions of organic cations, including small hydrocarbons (McEwan et al. 1999; Scott et al. 1998; Scott et al. 1999; Scott et al. 1999; Scott et al. 2000) and polycyclic aromatic hydrocarbons (LePage et al. 1997, 1999a, 1999b; Snow et al. 1998) with H, N, and O atoms have been investigated to elucidate the chemistry of planetary atmospheres and the ISM. Also detected in the ISM by radio astronomy are heteroatomic species containing carbon and either N or O (C_nO (n = 1,2,3), C_nN (n = 1,3,4), and HC_nN (n = 1,2,3,5,7,9,11)). In some regions of the ISM, it is possible that reactions of carbon chain anions serve as precursors to these species. In the present work, we report the results of FA-SIFT experiments that explored the reactivity of C_n^- (n = 2,4-7) and HC_n^- (n = 2,4,6,(7)) with H, N and O and describe and addition to the Langevin theory that accounts for this unique case.

2. Experimental Procedures

The experiments were carried out using a FA-SIFT apparatus that has been discussed in detail elsewhere (Van Doren et al. 1987). The C_2^- and HC_n^- species were generated using electron impact on acetylene and the C_n^- (n > 2) were generated using a cold cathode discharge source (Leopold et al.). Atomic hydrogen was produced using a thermal dissociator on H_2 (Barckholtz et al.). Atomic nitrogen was produced using a microwave discharge on N_2 and oxygen atoms were produced as a product of the quantitative reaction of NO with N.

3. Chemical Results

The rate constants and efficiencies for the reactions of H, N and O with C_n^- are reported in Tables 1, 2, and 3 and reactions with HC_n^- are reported Table 4. H atom reacts quickly and the reaction is primarily associative detachment, producing neutrals of the form C_nH and C_nH_2. O atom reacts quickly and produces CO and C_{n-1}^- or HC_n^- as well as C_nO^- and H for reactions with HC_n^-. N atom reacts more slowly with C_n^- and produces C_nN^- where n is odd as well as C_{n-1}^- with CN. The rapid reaction of these species with H atom suggests the carbon chain anions are unlikely carriers of the unidentified DIBs. Of interest, though, is the number of neutral species produced in these reactions that have been detected in the ISM by radio astronomy. Specifically, CO, CN, HCCN, HCCH, C_3, C_5, C_6H_2, and C_nH where n is 2,4,5,6,7 and 8 are generated in these reactions and are neutrals detected in the ISM through radio astronomy. In the O atom reactions, it was found that the reaction was rapid, and in the case of C_5^- + O, the efficiency of the reaction, which is defined as the reaction rate constant (k_{exp}) divided by the theoretical collisional rate constant as predicted by Langevin theory (k_L), was greater than 1. This gave rise to new considerations in the potential that describes the collision.

Table 1. Reactions of C_n^- with H atom

(C_n^-)	k_{exp} (cm^3/sec x 10^{-10})	k_{exp}/k_L	k_{exp}/k_{ODPI}
2	7.7 (±0.9)	0.39	0.32
4	6.2 (±1.9)	0.32	0.25
5	6.2 (±0.9)	0.32	0.25
6	6.1 (±1.0)	0.32	0.22
7	6.9 (±0.6)	0.36	0.25
8	7.3 (±1.3)	0.38	0.25
9	7.2 (±1.6)	0.37	nodata
10	7.5 (±0.8)	0.39	nodata

Table 2. Reactions of C_n^- and C_nH^- with N atom

(C_n^-)	k_{exp} (cm^3/sec x 10^{-10})	k_{exp}/k_L	k_{exp}/k_{ODPI}
2	2.3 (±0.4)	0.28	0.24
4	2.0 (±0.7)	0.27	0.22
5	2.7 (±0.5)	0.37	0.30
6	1.5 (±0.4)	0.21	0.15
7	2.2 (±0.4)	0.31	0.22

Table 3. Reactions of C_n^- and C_nH^- with O atom

(C_n^-)	k_{exp} (cm^3/sec x 10^{-10})	k_{exp}/k_L	k_{exp}/k_{ODPI}
2	5.8 (±1.3)	0.84	0.70
4	5.6 (±0.7)	0.92	0.73
5	6.4 (±1.0)	1.09	0.86
6	4.7 (±0.7)	0.80	0.56
7	5.3 (±0.5)	0.92	0.65

Table 4. Reactions of C_n^- with H atom

n (C_nH^-)	Atom	k_{exp} (cm^3/sec x 10^{-10})	k_{exp}/k_L	k_{exp}/k_{ODPI}
2	H	16 (±3)	0.82	0.72
	N	0.5 (±0.2)	0.06	0.05
	O	6.2 (±1.7)	0.93	0.82
4	H	8.3 (±2.1)	0.43	0.35
	N	~0.06	0.008	0.007
	O	5.3 (±0.2)	0.88	0.72
6	H	5.0 (±0.7)	0.26	0.18
	N	~0.1	0.02	0.01
	O	5.4 (±0.3)	0.93	0.65
7	H	7.4 (±1.3)	0.39	nodata

4. Theoretical Adjustment to the Langevin Rate

In 1905, Langevin first described the potential between an ion and a polarizable neutral (Langevin 1905). The potential had two parts, a centrifugal part based on the relative collisional energy (E) and the impact parameter (b) and an attractive part based on the polarizability of the neutral (α_n). From this potential, Langevin derived a rate constant that depended exclusively on α_n. The potential took the form:

$$V_L(r) = E\frac{b^2}{r^2} - \frac{1}{2}\frac{\alpha_n e^2}{r^4}$$

This theory works well to describe the rate of collision in most ion-neutral cases, but in a few cases, significant deviation can be observed. The modification of the theory due to a permanent dipole has been described in detail (Hsieh and Castleman 1981) and has been parameterized for easy use by experimentalists (Su and Bowers 1973; Su and Chesnavich 1982). In our case, the deviation comes not from the non-point nature of the neutral, but from the non-point nature of the ion. These carbon chain anion-atom systems have two major factors that contribute to this deviation. First, the negative ions have large, diffuse electronic clouds and are Π-conjugated molecules that facilitate movement of the electrons within the molecule and specifically along the axis of the molecule. Second, the atoms have relatively low polarizabilities. This effectively lowers the Langevin rate constant making a deviation due to the ionic polarizability more apparent. Due to these factors, terms need to be added to the existing Langevin potential. The new terms are added in the following fashion:

$$V_{eff}(r) = V_L + V_\alpha$$

where V_α is the potential term that arises from the induced dipole-induced dipole interaction between the ion and the neutral. The effect of this potential term is studied in two forms. The first is assuming the ion is a point-polarizable ion (PPI) such that the orientation of the ion with respect to the neutral is not considered. The first form of this potential term, where EA is the electron binding energy of the ion, IP is the ionization potential of the neutral and α_{ion} is the polarizability of the ion, is (Karplus and Porter 1970):

$$V_{PPI} = -\frac{3}{2}\left(\frac{EA \times IP}{EA + IP}\right)\frac{\alpha_{ion}\alpha_n}{r^6}$$

The second form was an orientation dependent polarizable ion (ODPI) where the axis of the molecule creates an angle with the approach vector of the neutral, as shown in figure 1. Here, where $\alpha_{parallel}$ and $\alpha_{perpendicular}$ are with respect to the long axis of the molecule, the potential takes the form:

$$V_{ODPI}(r) = -\frac{3}{2}\left(\frac{EA \times IP}{EA + IP}\right)\frac{(\alpha_{parallel}\cos\theta + \alpha_{perpendicular}\sin\theta)\alpha_n}{r^6}$$

Using calculated values for the polarizabilities of the ions, the rate constants are derived in a similar fashion as the original theory. The results are listed in Table 5 and show significant deviation in the rate constant as chain length increases as well as a significantly larger effect generated by ODPI over PPI in this case. Calculations were also done for the benzene cation and significant deviation was seen there as well, suggesting that large PAH cations collisions would be affected by the additional potential term.
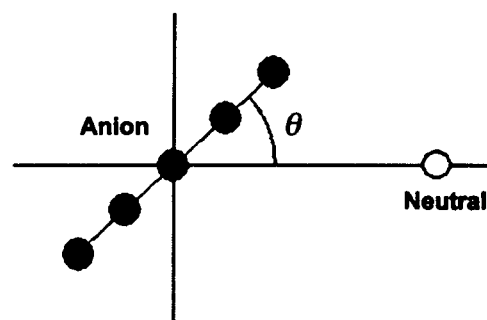
Fig. 1.— C_5^- has some orientation with respect to the approaching atom. This orientation is specified by the angle θ

Table 5. Deviations of k_{PPI} and k_{ODPI} from k_L - C_n^- + O

n (C_n^-)	%Deviation (PPI from Langevin)	%Deviation (ODPI from Langevin)
2	20.43	21.15
4	19.22	25.72
5	19.50	26.36
6	29.77	39.64
7	30.88	41.26
8	36.67	48.76

5. Future Work

Current modeling suggests that larger PAH cations would be likely candidates for the unidentified DIB carriers. We plan to study the reaction of PAH cations (carbon number 30 - 60) with H atom to address the viability of these species in the ISM.

Acknowledgments

REFERENCES

Fehsenfeld, F. C., Ferguson, E. E., Schmeltekopf 1966, J. Chem. Phys., 45, 1844- 1845.

Fulara, J., Lessen, D., Freivogel, P., Maier, J. P. 1993, Nature, 366, 439-441.

Tulej, M., Kirkwood, D. A., Pahckov, M., Maier, J. P. 1998, ApJ, 506, L69-L73.

Thaddeus, P., et al. 1998, Faraday Discuss., 109, 121-135.

Blanksby, S. J., Bowie, J. H. 1999, Mass Spectrom. Rev., 18, 131-151.

McEwan, M. J., et al. 1999, Astrophys. J., 513, 287-293.

Scott, G. B. I., et al. 1998. J. Chem. Phys., 109, 9010-9014.

Scott, G. B. I., et al. 1999, J. Phys. Chem. A, 103, 1073-1077.

Scott, G. B. I., et al. 1999, J. Phys. Chem. A, 103, 7470-7473.

Scott, G. B. I., et al. 2000, J. Chem. Phys., 112, 4959-4965.

Le Page, V., Keheyan, Y., Bierbaum, V. M., Snow, T. P. 1997, J. Am. Chem. Soc., 119, 8373- 8374.

Snow, T. P., Le Page, V., Keheyan, Y., Bierbaum, V. M. 1998, Nature, 391, 259-260.

Le Page, V., Keheyan, Y., Snow, T. P., Bierbaum, V. M. 1999, J. Am. Chem. Soc., 121, 9435- 9446.

Le Page, V., et al. 1999, Intl. J. Mass Spectrom., 185/186/187, 949-959.

Van Doren, J. M., et al. 1987, Intl. J. Mass Spectrom. Ion Processes, 81, 85- 100.

Leopold, D. G., Ho, J., Lineberger, W. C. 1987, J. Chem. Phys., 86, 1715-1726.

Barckholtz, C., Snow, T. P., Bierbaum, V. M. 2001, Astrophys. J. Lett., 547, L171-174.

Langevin, P. 1905, Ann. Chem. Phys., 5, 245.

Hsieh, E. T., Castleman, Jr. A.W. 1981, Intl. J. Mass Spectrom., 40, 295-329.

Su, T., Bowers, M. T. 1973, Intl. J. Mass Spectrom., 12, 347-356.

Su, T., Chesnavich, W. J. 1982, J. Chem. Phys., 76, 5183-5185.

Karplus, M., Porter, R. N. 1970, Atoms and Molecules, W. A. Benjamin Inc., New York, p. 267.

Near Infrared Emission of Highly Electronically Excited CO: A Sensitive Probe to Study the Interstellar Medium??

Murthy S. Gudipati [1,2]

Institute of Physical Sciences and Technology, University of Maryland, College Park, MD

Abstract

Among the various spectroscopic features of the second most abundant molecule in the space, CO, "the triplet – triplet transitions involving the lowest triplet state $a^3\Pi$ and the higher-lying $a'\,^3\Sigma^+$, $d\,^3\Delta$, $e\,^3\Sigma^-$ states spanning near-UV to mid-IR spectral range" have so far not been explored in astrophysical observations. The energies of these transitions are highly sensitive to the surroundings in which CO exists, i.e. gas-phase, polar or non-polar condensed phase. It is proposed here that these triplet-triplet emission / absorption bands can be used as a sensitive probe to investigate the local environments of CO, whether in the planetary atmosphere, stellar atmosphere or interstellar medium.

1. Introduction

Carbon monoxide (CO) is the second most abundant species in the Space. Due to its almost ubiquitous presence in stars, stellar objects and interstellar mater, CO has been one of the most extensively observed and tagged molecules as a remote-sensor of the local environments. Most commonly used spectroscopic signatures of CO are the vibrational fundamental at 4.7 μm (Boogert *et al.* 2002) and its overtones at 2.35 (Schreiber 2000) and 1.56 μm (Lançon and Wood 2000). Light emission or absorption due to electronic transitions in CO has also been utilized for remote-sensing purposes, for example in Red Rectangle and its central star HD 44179. The relevant electronic states of CO are given in Figure 1. Vacuum UV emission due to the fourth positive system of CO involving the $A^1\Pi - X^1\Sigma^+$ transition has been observed using GHRS on the HST (McMurry and Jordan 2000; Glinski *et al.* 1997). Cameron emission from the $a^3\Pi$ state to the ground-state is also extensively used in astrophysical observations (Yan *et al.* 2000, for example). We may also note that CO is also a major constituent in the atmospheres of Satellites like Triton (Lellouch 1994; Tryka *et al.* 1993; Young *et al.* 2001) in our own solar system.

Given the importance of CO in astrophysical studies mentioned above, to our surprise, so far there has been no mention of other emission lines of CO in astrophysical literature (to the best of our knowledge) involving the triplet electronic states $a'\,^3\Sigma^+$, $d\,^3\Delta$, $e\,^3\Sigma^-$, and $a\,^3\Pi$. Emission from the a', d and e states to the a state, which is both spin and symmetry allowed, occurs when CO is electronically excited into the A-state or higher excited states (8 eV or above). The wavelength-region of this *triplet-triplet* emission can span between 0.3 to

---

3 μm. The only comprehensive compilation to date on the astrophysical relevance of the electronic states and the electronic spectra of CO (Morton and Noreau 1994) does not include the triplet-triplet transitions. As will be discussed below, NIR emission of CO can be used as a remote spectroscopic sensor that is sensitive for the local environments, wherever light with photon energies >8 eV (<0.16 μm) is present. We may also note that having a dedicated NIR monochromator (NICMOS) launched on the HST reflects the importance of NIR astrophysical observations and the complementary laboratory measurements.

2. Laboratory Studies

A few years ago we have discovered that NIR emission spectrum of CO isolated in Argon (Ar) matrices at 15 K (Gudipati and Kalb 1998) is entirely different compared to the gas-phase emission spectrum published in literature only once so far (Effantin et al. 1982). While the gas-phase spectrum is dominated by the $a' - a$ transition (Asundi system), in the condensed phase low-temperature Ar matrices, emission from all the three a', d and e upper states to the a state has been observed. As mentioned earlier, the triplet-triplet emission from the a', d and e states to the a state (Figure 1) spans 0.3 to 3 μm region and the intensity of these emission lines are stronger in the NIR region. A complete set of optical excitation and emission spectra of CO in low-temperature Ar matrices is also summarized in Figure 1. Spectra measured in the NIR region from CO in Ar matrices are expanded in Figure 2.

Due to the fact that the transitions from the a', d and e states to the a state are both spin and symmetry allowed, both emission and absorption involving the three upper a', d and e states and the lower a state should have strong features that are purely dictated by the Franck-Condon factors (FCFs) in collision-free gas-phase very low-density conditions. If, on the other hand, collisions become important like in high-density molecular clouds or if CO exists in condensed phase, then it turns out that in addition to the FCFs, the energy gap between any given vibrational level of the a', d and e states and the immediate energetically low-lying vibrational level of the a state is also crucial (Gudipati and Kalb 1998). Smaller the energy gap, faster will the nonradiative vibrational relaxation of the particular level of the a', d and e states. When the energy gap turns out to be large, of the order of several hundred wavenumbers, these vibrational levels undergo radiative decay. Such electronic levels are known as *bottlenecks* and emission occurs from these vibrational levels.

The surrounding medium of CO also influences whether or not bottlenecks are formed at certain vibrational levels, because, the vibrational levels of the a', d and e states shift energetically to different degree in different directions with respect to the a state based on the polarization and dipole moment of the surrounding medium. This happens because of the fact that each of the electronic states of CO has different inherent dipole moments, as for example, X (-0.12 D), A (0.15 D), a (0.84 D), a' (-2.49 D), and d (-2.31 D) (Lynch et al. 1982). Consequently, through shifting the sets of vibrational levels of different electronic states against each other, some bottlenecks disappear and others appear. Accordingly, the emission spectra change. As an example, the energy level diagram of the triplet states of CO in the gas-phase and in Ar matrices is shown in Figure 2. As a consequence, the transition energies and the corresponding

wavelengths change significantly between gas-phase and Ar matrices. For example, a blue shift of the 1.05 μm band by $\sim$200 cm^{-1} (Figure 2) is an enormous magnitude, compared to the changes in the ground-state vibrational frequencies of CO under similar circumstances ranging only less than 10 cm^{-1} (Elsila et al. 1997).

The ground-based or satellite-based NIR spectroscopic measurements on CO need to be carried out along with detailed laboratory investigations on the spectroscopic nature of CO in different environments. These studies may lead to a better understanding of the ISM containing CO. The objects that emit VUV and UV light due to $A \rightarrow X$ and Cameron emission of CO should also show the NIR absorption / emission features.
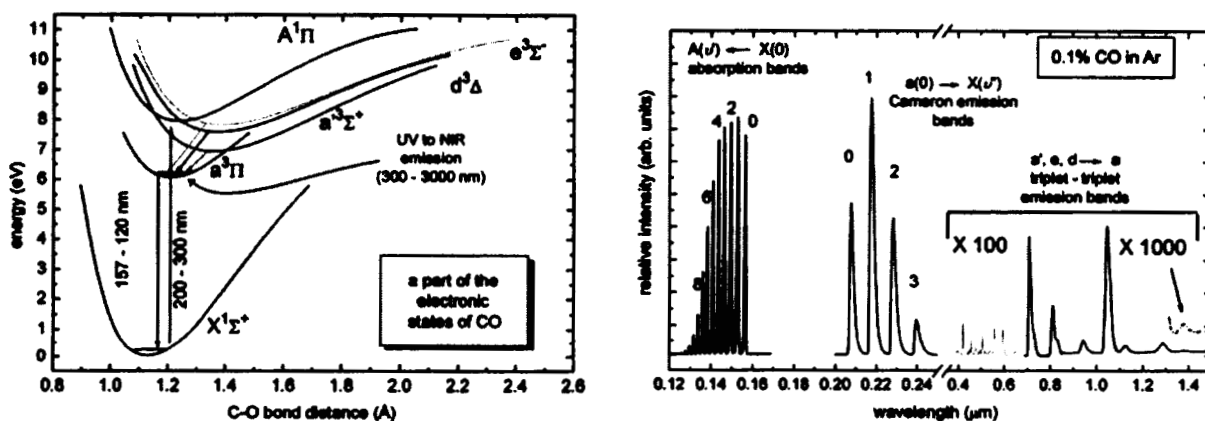
Fig. 1.— A part of the electronic states (left) and electronic spectra (right) of CO. The energies are given in eV (left). Vibrational levels of the final states are numbered accordingly (right).
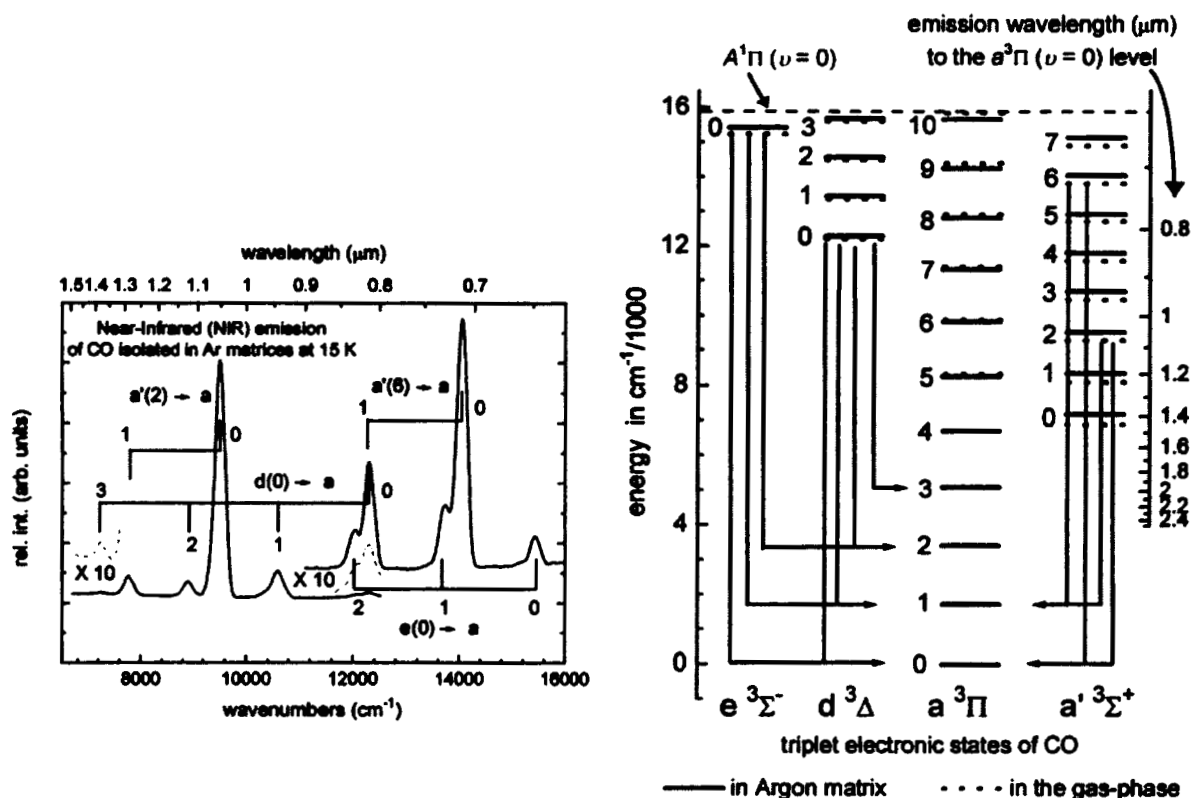
Fig. 2.— Near infrared emission from CO in Ar matrices (left) and shifts in the energies of the vibronic levels of the triplet states from the gas-phase to Ar-matrices (right).

Acknowledgments

REFERENCES

Boogert, A. C. A., Hogerheijde, M. R., and Blake, G. A. 2002, *ApJ*, **568**, 761-770.

Elsila, J., Allamandola, L. J., and Sandford, S. A. 1997, *ApJ*, **479**, 818-838.

Effantin, C., Michaud, F., Roux, F., D'Incan, J., and Verges, J. 1982, *J. Mol. Spectr.*, **92**, 349-362.

Gudipati, M. S., and Kalb, M. 1998, *A&A*, **329**, 375-379.

Glinski, R. J., Lauroesch, J. T., Reese, M. D., and Sitko, M. L. 1997, *ApJ*, **490**, 826-834.

Lançon, A., and Wood, P. R. 2000, *A&AS*, **14**, 217-249.

Lellouch, E. 1994, *ICARUS*, **108**, 255-265.

Lynch, D., Herman, M. F., and Yeager, D. L. 1982, *Chem. Phys.*, **64**, 69-81.

McMurry, A. E., and Jordan, C. 2000, *MNRAS*, **313**, 423-432.

Morton, D. C., and Noreau, L. 1994, *ApJS*, **95**, 301-343.

Schreiber, N. M. F. 2000, *ApJ*, **120**, 2089-2100.

Tryka, K. A., Brown, R. H., Anicich, V., Cruikshank, D. P., and Owen, T. C. 1993, *Science*, **261**, 751-754.

Yan, M., Dalgarno, A., Klemperer, W., and Miller, A. E. S. 2000, *MNRAS*, **103**, L17-L18.

Young, L. A., Cook, J. C., Yelle, R. V., and Young, E. F. 2001, *ICARUS*, **153**, 148-156.

The Submillimeter-wave Rotational Spectra
of Interstellar Molecules

Eric Herbst, Frank C. De Lucia, R. A. H. Butler, and M. Winnewisser
Department of Physics, The Ohio State University, Columbus, OH

G. Winnewisser and U. Fuchs
I. Physikalisches Institute, University of Cologne, Cologne, Germany

P. Groner
Department of Chemistry, University of Missouri-Kansas City, Kansas City, MO

K. V. L. N. Sastry
Department of Physics, University of New Brunswick, Fredericton, New Brunswick, Canada

Abstract

We discuss past and recent progress in our long-term laboratory program concerning the submillimeter-wave rotational spectroscopy of known and likely interstellar molecules, especially those associated with regions of high-mass star formation. Our program on the use of spectroscopy to study rotationally inelastic collisions of interstellar interest is also briefly mentioned.

1. Introduction

More than 120 molecules have been discovered in interstellar and circumstellar clouds by the methods of high resolution spectroscopy. Although most of these molecules are unsaturated (hydrogen-poor), saturated and near-saturated molecules can be found in regions of star formation, especially those associated with high-mass stars. These hydrogen-rich molecules are especially prominent in so-called hot cores, which are quiescent regions at densities ($\approx 10^6$ cm^{-3}) and temperatures (100-300 K) higher than standard values in dense interstellar clouds. Some well-studied hot cores are the Hot Core and Compact Ridge in Orion, and the molecular heimat source Sgr B2(N-LMH) in Sagittarius B2. It is generally thought that the saturated molecules are formed via a two-stage process in which the first stage occurs at low temperatures before the onset of star formation. In this stage, the molecule CO is hydrogenated on grain surfaces to form formaldehyde (H_2CO) and methanol (CH_3OH), which develop large abundances in grain mantles. As temperatures begin to rise during star formation, the grain mantles evaporate and the particularly high abundance of methanol makes it an important precursor of still larger saturated organic molecules that form from it via gas-phase chemical processes (Millar & Hatchell 1998).

Many if not most of the saturated organic molecules in hot cores have complex rotational spectra due to a large-amplitude motion known sometimes as torsion and sometimes as internal rotation. This motion is most prominent in methyl (-CH$_3$) groups; the hydrogens of a methyl group rotate around the bond connecting the carbon to another heavy atom. The rotation

is not free, but is constrained by a potential of three-fold symmetry. If one considers torsion as a one-dimensional motion, one can easily determine the energy levels and eigenstates of the system. The torsional levels are typically separated by ≈ 100 K, and each level is split into two sublevels, characterized by the letters A and E. Molecules with two rotating methyl groups have torsional sublevels characterized by two letters, e.g. AA, AE, etc. In any case, rotational transitions occur within each torsional sublevel. Since the rotational constants are not the same for different torsional levels, there are more rotational spectral lines than in rigid molecules of the same size. Moreover, torsional and rigid (end-over-end) rotational motions interact with one another, making the quantum mechanics of the overall system rather complex, especially for molecules such as methanol with rather small barriers against torsional motion. The result is that the laboratory analysis of common internal rotors such as methanol and methyl formate has taken long periods of time to be even partially understood. Neverthless, we have managed to study and analyze the spectra of a long list of internal rotors up to frequencies of 500 GHz - 1 THz. The molecules include: methanol (CH_3OH) and several of its isotopomers ($^{13}CH_3OH$, CH_3OD, CH_2DOH, and CHD_2OH), methyl mercaptan (CH_3SH), acetaldehyde (CH_3CHO), methyl formate ($HCOOCH_3$) and one of its isotopomers ($DCOOCH_3$), ethanol (CH_3CH_2OH), dimethyl ether (CH_3OCH_3), and acetone (CH_3COCH_3). In addition to these internal rotors, we have studied a number of more rigid species detected in hot cores, including ethyl cyanide (C_2H_5CN), ethylene oxide (C_2H_4O), and glycolaldehyde (CH_2OHCHO).

2. Laboratory Program

The microwave laboratory at the Ohio State University, which moved from Duke University more than a decade ago, has long been involved with the extension of rotational spectroscopy of gas-phase species into the millimeter-wave and submillimeter-wave regions of the electromagnetic spectrum. We currently have a variety of spectrometers that operate at frequencies through 1 THz. In addition, a close collaboration with the spectroscopy group in Cologne, Germany, allows us to utilize their spectrometers at frequencies to 2 THz. One of the more exciting recent developments in our laboratory at Ohio State has been a fast-scan spectrometer with the acronym of FASSST (Fast Scan Submillimeter-wave Spectroscopic Technique) (Petkie et al., 1997). With this technique, a frequency range of 100 GHz can be swept in a matter of seconds, and a large number of spectral lines recorded. The rate-limiting step in the analysis of the spectrum then becomes the determination of the quantum numbers for each transition and the fitting of the frequencies of the assigned spectral transitions to calculated values obtained with an effective Hamiltonian. Such a Hamiltonian normally contains a number of adjustable parameters, known as rotational and distortion constants, which multiply assorted kinetic and potential operators. For molecules that undergo internal rotation, these sets of constants are joined by constants relating to the torsional motion and its interaction with the end-over-end rigid-body rotation (De Lucia et al., 1989). Once a large number of spectral lines are fit to an effective Hamiltonian, one can obtain their intensities, normally in the form of transition strengths, and one can predict frequencies for many lines not measured or assigned in the laboratory (Groner et al., 1998).

At the current time, we are studying rotational-torsional spectra of the molecules *trans*-ethyl methyl ether ($CH_3OC_2H_5$) and methyl carbamate ($H_2NCOOCH_3$). Neither of these species has been detected in hot cores, possibly because their millimeter-wave spectra have not yet been measured. Since dimethyl ether has a high abundance in hot cores, it is likely that methyl ethyl ether, the next member of the ether series, is also detectable. Methyl ethyl ether possesses two rotating methyl groups and these groups are not in similar environments. Such a situation is rather complex spectroscopically, and the analysis of the spectrum is taking some time to complete. Methyl carbamate is being studied because it is an isomer of glycine, the simplest amino acid. Although glycine has not been detected in space, methyl carbamate may be much more abundant since it is a simple derivative of the abundant methyl formate.

3. Inelastic Collisions

We also use submillimeter-wave spectroscopy to monitor rotationally inelastic collisions by pressure-broadening experiments and by pump-probe double-resonance studies. Astronomers need cross sections for inelastic collisions to analyze spectral lines excited collisionally under non-LTE conditions. Since our laboratory studies cannot be undertaken under all conditions relevant to astronomy, they are also are used to constrain intermolecular potentials so that detailed quantum mechanical calculations can be undertaken for the conditions not studied in the laboratory. Examples of collisional systems studied under this program are $CO + H_2$, $H_2CO + H_2$, and $HDO + H_2$, as well as the ion-molecule system $HCO^+ + H_2$ (Oesterling *et al.*, 2001).

4. Some Future Spectroscopic Plans

Our future spectroscopic plans include the study of newly detected interstellar molecules such as ethylene glycol and vinyl alcohol, both of which were identified on the basis of lines not measured in the laboratory, as well as the study of common internal rotors in excited torsional states, since these states are at energies relevant to warm star-formation regions. Finally, we plan to push our spectral studies to higher frequencies so that the future analysis of Herschel data will be feasible.

Acknowledgments

REFERENCES

De Lucia, F. C., Herbst, E., Anderson, T., & Helminger, P. 1989, *J. Mol. Spec.*, **134**, 395.

Groner, P., Albert, S., Herbst, E., & De Lucia, F. C. 1998, *ApJ*, **500**, 1059.

Millar, T. J., & Hatchell, J. 1998, *Faraday Discuss.*, **109**, 15.

Oesterling, L. C., De Lucia, F. C., & Herbst, E. 2001, *Spectrochim. Acta A*, **57**, 705.

Petkie, D. T., Goyette, T. M., Bettens, R. P. A., Belov, S. P., Albert, S., Helminger, P., & De Lucia, F. C. 1997, *Rev. Sci. Instrum.*, **68**, 1675.

Infrared Emission From Interstellar PAHs,
New Probes of the Interstellar Medium

D. M. Hudgins and L. J. Allamandola

Astrochemistry Laboratory, NASA Ames Research Center, Moffett Field, CA

Tremendous strides have been made in the understanding of interstellar material over the past twenty years thanks to significant, parallel developments in two closely related areas: observational IR astronomy and laboratory astrophysics. Twenty years ago the composition of interstellar dust was largely unknown and the notion of abundant, gas phase, polycyclic aromatic hydrocarbons (PAHs) anywhere in the interstellar medium (ISM) considered impossible. Today the dust composition of the diffuse and dense ISM is reasonably well constrained and the spectroscopic case for interstellar PAHs, impossibly large molecules by early interstellar chemistry standards, is very strong. PAH spectral features are now being used as new probes of the ISM. PAH ionization states reflect the ionization balance of the medium while PAH size and structure reflect the energetic and chemical history of the medium. Aromatic carbon-rich materials ranging in size from PAHs and PAH nanoclusters, to sub-micron and micron-sized dust grains represent an important component of the ISM. These species: (1) dominate the heating and cooling of interstellar clouds via energetic photoelectron ejection and infrared (IR) emission; (2) moderate the ionization balance in photodissociation regions and molecular clouds; (3) moderate the composition of the gas phase and play an important role in determining the chemistry of the ISM; (4) contribute to the interstellar extinction in the near IR, visible, and UV spectral regions; and (5) convert UV, visible, and near-IR radiation to mid- and far-IR radiation in the ISM and, as such, are responsible for the well known, widespread family of mid-IR emission features with major components near 3.3, 6.2, 7.7, 8.6, and 11.3 μm.

Over the past two decades, PAH molecules have gained recognition as an important, ubiquitous component of interstellar dust (Duley and Williams 1981; Leger and Puget 1984; Allamandola, *et al.* 1985; Dwek *et al.* 1997; Draine and Li 2001, Li and Draine, 2001). Current estimates are that PAHs of 15-500 carbon atoms comprise 5 to 15% of all of carbon in the galaxy (Allamandola, *et al.* 1989; Dayal *et al.* 1998), implying that PAHs are more abundant than the other known interstellar, gaseous, polyatomic molecules. For comparison, the diaotmic CO comprises 10-20% of the elemental cosmic carbon. The proposed ubiquity and abundance of PAHs in the ISM explains their impact on so many interstellar processes. The fundamentals of the interstellar PAH model can be found in Allamandola *et al.* (1989) and Puget and Leger (1989). The power of the PAH model and the breadth and depth of the possible applications of combining laboratory data with astronomical observations and theory can be found in: Bakes *et al.* (2001a,b) and Pech, Joblin, Boissel (2002). Progress in the area of interstellar PAHs has been rapid in recent years. The launch of ISO in 1995 opened up the mid-IR window to systematic and coherent investigations of objects in the Solar neighborhood. These studies showed that the detailed profiles and relative strengths of the PAH emission features vary between sources, and these variations correlate with the characteristics of the astronomical sources. Clearly, the carriers are sensitive to the local physical conditions (Bakes *et al.* 2001a,b; Pech, Joblin, Boissel 2002). Extensive lab studies at NASA Ames and elsewhere (Piest *et al.* 1999a,b; and references therein), combined with quantum chemical calculations,

have pinpointed the origin of variations in the changing size, charge state, molecular structure, substitution, and clustering of the PAHs responsible. Table 1 lists the types of PAHs in the Ames IR spectral database.

There have been many comparisons between PAH spectra and the interstellar spectra over the years. As observational tools became more sensitive and lab techniques more appropriate to the interstellar case, the correlations have revealed more about PAH populations in different regions increasing insights into conditions in the emitting regions.

Figure 1 compares the spectrum produced by a mixture dominated by PAH cations and the 5-14 μm spectrum from the Orion ionization ridge. In objects with more benign radiation fields, neutral PAHs play a larger role (Allamandola et al. 1999). Analysis of the complete interstellar spectrum with laboratory and theoretical studies has shown that the 3.3 μm CH stretching band is dominated by neutral and negativley charged PAHs and the 6.2 and 7.7 μm CC stretching bands are dominated by PAH cations. Hence, the interstellar emission spectrum provides a measure of the degree of PAH ionization and this, in turn, is a measure of the flux, the exciting ionizing UV field, and the electron density (e.g., Hudgins and Allamandola, 1999b; Allamandola et al. 1999; Bakes et al. 2001 a,b; Draine and Li, 2001; Li and Draine, 2001).

Development of a database of astrophysically relevant data, spurred efforts to construct comprehensive astrophysical models (Bakes et al. 2001 a,b; Li and Draine 2001; Draine and Li, 2001). Initial applications of the the Bakes et al. and Draine and Li models have already demonstrated their effectiveness in addressing such characteristics of the emitting PAH population as charge state, size distribution, molecular structure, degree of hydrogenation, and UV-Vis-Near IR absorption properties. Bakes et al. (2001) investigated the spectral variations of a PAH population at the surface of the Orion photodissociation region (PDR) and have found the IR spectrum of a PAH population varies dramatically as a function of depth (or radiation field) through the PDR. Figure 2 illustrates the modeled evolution of the PAH emission from the ionization ridge as a function of depth (radiation field) into the molecular cloud.

This revolution in our understanding of interstellar PAHs and the many roles they play in the ISM reflects a breakthrough in the IR spectral range. The Infrared Space Observatory (ISO) spectral archives are now publicly available, but are limited to the local Solar neighborhood. SIRTF will soon be launched and will provide observations in the mid- and far-IR with exceptional sensitivity allowing studies of the IR spectral characteristics of the whole local group of galaxies. Monitoring when the PAH features appear as a function of galactic metallicity is an important goal of the SIRTF mission. The laboratory data will aid in identifying the types, sizes, and charge states of PAHs present as a function of metallicity. Galactic spectra vary from one place to another. Our laboratory and theoretical program aims to understand the relationship between the conditions in galactic sources and the emitted spectra, and apply this understanding to other regions, galactic and extragalactic. Thus, measuring the differences in the PAH spectra between objects can be used as a new tool to probe the local environmental conditions. Lastly, all of these detailed spectral studies using template galaxies of the local universe, will facilitate the interpretation of the broad band data for the weaker, most distant galaxies.

Formula	Name	Ion State
C9H7N	quinoline	o
	isoquinoline	o
C10H8	naphthalene	o,+
C12H8	acenaphthylene	o
C13H9N	acridine	o,+
	7,8-benzoquinoline	o,+
	phenanthridine	o,+
C14H10	anthracene	o,+
	phenanthrene	o,+
C14H11N	2-aminoanthracene	o,+
C15H9N	9-cyanoanthracene	o,+
C15H12	1-methylanthracene	o,+
	9-methylanthracene	o,+
C16H10	fluoranthene	o,+
	pyrene	o,+
C16H12	4,5-dihydropyrene	o
C16H16	1,2,3,6,7,8-hexahydropyrene	o
C18H10	benzo[ghi]fluoranthene	o
C17H11N	1-azabenz[a]anthracene	o,+
	2-azabenz[a]anthracene	o,+
	1-azachrysene	o,+
	2-azachrysene	o,+
	4-azachrysene	o,+
C18H12	1,2-benzanthracene	o,+
	chrysene	o,+
	tetracene	o,+
	triphenylene	o
C19H14	7,8-dihydro-9H-cyclopenta[a]pyrene	o
C20H12	benzo[a]fluoranthene	-,o,+
	benzo[b]fluoranthene	o,+

Formula	Name	Ion State
C20H12	benzo[j]fluoranthene	-,o,+
	benzo[k]fluoranthene	o,+
	benzo[a]pyrene	o,+
	benzo[e]pyrene	o,+
	perylene	o
C20H14	7,8-dihydrobenzo[a]pyrene	o
	9,10-dihydrobenzo[e]pyrene	o,+
C21H13N	dibenz[a,h]acridine	o,+
	dibenz[a,j]acridine	o,+
C22H12	benzo[ghi]perylene	o,+
C22H14	pentacene	-,o,+
C22H16	7,14-dihydrodibenz[a,h]anthracene	o
C24H12	coronene	o,+
C24H14	dibenz[a,e]pyrene	o,+
	dibenz[a,l]pyrene	o,+
	naphtho[2,3:a]pyrene	o,+
C36H16	3,4;5,6;7,8;12,13-tetrabenzoperopyrene	o,+
	3,4;5,6;10,11;12,13-tetrabenzoperopyrene	o,+
C40H18	dipyreno-(1',3';10,2),(1",3";5,7)-pyrene	o,+
C40H22	dianthraceno-(2',3';3,4),(2",3";9,10)-pyrene	o,+
C42H18	1,12;2,3;4,5;6,7;8,9;10,11-hexabenzocoronene	o,+
C42H22	1,18;4,5;9,10;13,14-tetrabenzoheptacene	o,+
C44H20	2,3;12,13;15,16-tribenzoterrylene	o,+
	1,2;3,4;5,6;7,8;9,10;12,13-hexabenzoperopyrene	o,+
C48H20	dicoronylene	-,o,+

Table 1 The Ames-Astrochemistry Lab PAH IR Spectral Database (Hudgins et al. 1994 - 1999.)
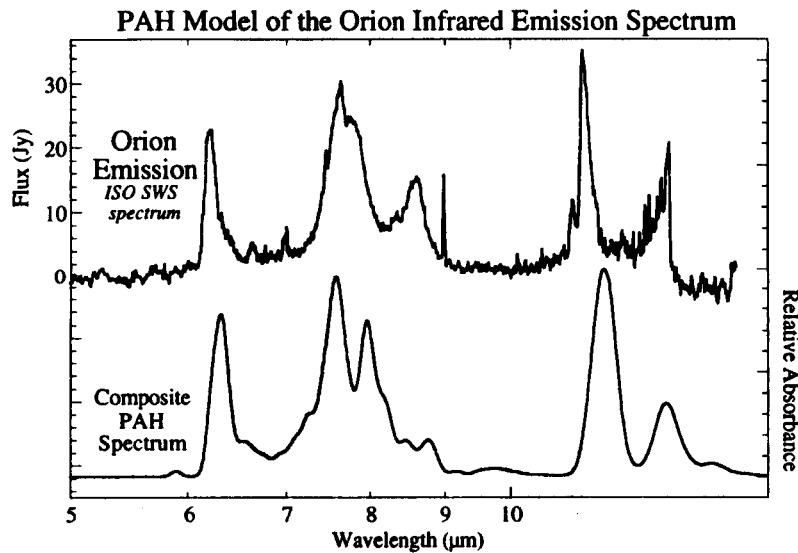
Figure 1. The 5 - 14 µm ISO SWS spectrum (top) from the Orion ionization ridge compared with (bottom) the composite absorption of a mixture of PAHs produced by coadding laboratory spectra of 11 different PAH cations (Peeters et al. 2002, in press).
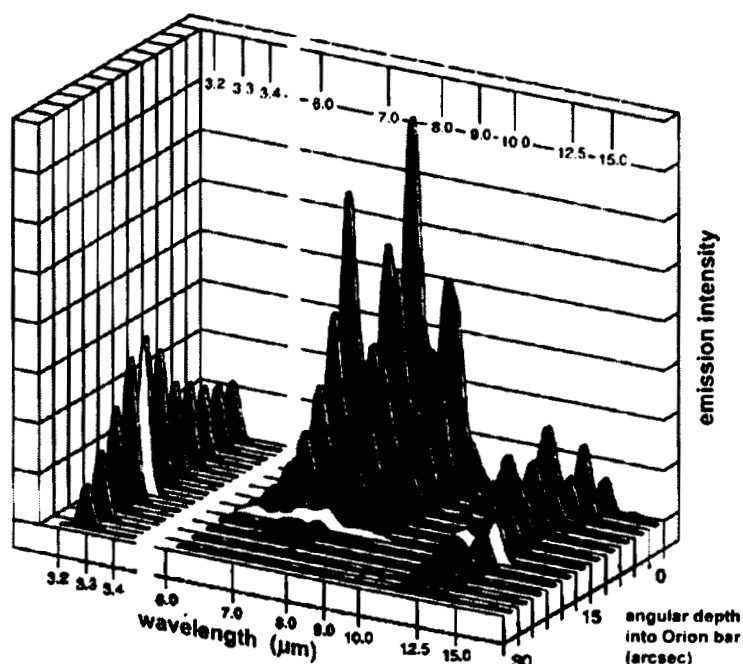
Figure 2. PAH emission spectral evolution predicted from the Orion ionization bar into the Orion molecular cloud utilyzing the model of Bakes, Tielens and Bauschlicher (2001a).

REFERENCES

Allamandola, L.J., Tielens, A.G.G.M., and Barker, J.R. (1985). *Ap. J. (Letters)* **290**, L25.

Allamandola, L.J., Hudgins, D.M., and Sandford, S.A., (1999). *ApJ. (Letters)* **511**, L115.

Bakes, E.L.O.; Tielens, A.G.G.M.; Bauschlicher, C. W., Jr. (2001a). *ApJ* **556**, 501.

Bakes, E.L.O., *et al.*, (2001b). *ApJ.* **560**, 261.

Dayal, A., *et al.*, (1998). *ApJ.* **492**, 603.

Draine, B.T., and Li, A. (2001). *ApJ.* **551**, 807.

Duley, W.W., and Williams, D.A. (1981). *Mon. Not. R. Astr. Soc.* **196**, 269.

Dwek *et al.*, (1997). *ApJ.* **475**, 565.

Hudgins, D.M., Sandford, S.A., and Allamandola, L.J. (1994b). *J. Phys. Chem.* **98**, 4243.

Hudgins, D.M. and Allamandola, L.J. (1995a). *J. Phys. Chem.* **99**, 8978.

Hudgins, D.M. and Sandford, S.A., (1998a). *J. Phys. Chem.* **102**, 329.

Hudgins, D.M. and Allamandola, L.J., (1999a). *ApJ (Letters)* **513**, L69.

Leger, A., and Puget, J.L. (1984). *A&A* **137**, L5.

Li, A., Draine, B.T. (2001). *ApJ.* **554**, 778.

Pech, C.; Joblin, C.; Boissel, P. (2002). *A&A* **388**, 639.

Peeters, E., *et al.*, (2002). *A&A* in press.

Piest., J.A., von Helden, G., and Meijer, G. (1999a). *J. Chem. Phys.* **110**, 2010.

Puget, J.L., and Leger, A. (1989). *Ann. Rev. Astr. Ap.* **27**, 161.

Infrared Spectroscopy of Matrix-Isolated Polycyclic Aromatic Nitrogen Heterocycles (PANHs)

A.L. Mattioda, D.M. Hudgins, C.W. Bauschlicher, and L.J. Allamandola

NASA Ames Research Center, Moffett Field, CA

C. D. Biemesderfer

National Optical Astronomy Observatories, Tucson, AZ

M. Rosi

Chemistry, University of Perugia, Italy

Abstract

The mid-infrared spectra of the nitrogen-containing heterocyclic polycyclic aromatic compounds 1-azabenz[a]-anthracene; 2-azabenz[a]anthracene; 1-azachrysene; 2-azachrysene; 4-azachrysene; 2-azapyrene, and 7,8 benzoquinoline in their neutral and cation forms were investigated. The spectra of these species isolated in an argon matrix have been measured. Band frequencies and intensities were tabulated and these data compared with spectra computed using density functional theory at the B3LYP level. The overall agreement between experiment and theory is quite good, in keeping with earlier results on homonuclear polycyclic aromatic hydrocarbons. The differences between the spectral properties of nitrogen bearing aromatics and non-substituted, neutral polycyclic aromatic hydrocarbons will be discussed.

1. Introduction

The past decade has witnessed renewed interest in the molecular physics and infrared spectroscopic properties of polycyclic aromatic hydrocarbons (PAHs). Motivated in large part to understand the widespread interstellar infrared emission attributed to mixtures of neutral and ionized PAHs in different interstellar environments. The matrix isolation technique has also been particularly effective in providing the infrared An ongoing project at the NASA Ames Astrochemistry laboratory has combined matrix isolation spectroscopy of polycyclic aromatic hydrocarbons with theoretical computations using density functional theory to generate an infrared spectral database of neutral, cationic, and anionic PAHs. These data are available from our website at www.astrochem.org/pahdata/index.html. This database is expanded here with the first reported IR spectra of neutral and ionized, nitrogen substituted PAHs (aza-PAHs). The argon matrix isolated spectra of the nitrogen substituted PAHs (PANHs): 1-azabenz[a]anthracene; 2-azabenz[a]anthracene; 1-azachrysene; 2-azachrysene; 4-azachrysene; 2-azapyrene, and 7,8 benzoquinoline in their neutral and cation forms are discussed.

2. Experimental

The experimental technique will be described briefly, a detailed description of the procedure is available elsewhere [1, 2]. Samples were prepared by vapor co-deposition of the PAH/PANH of interest with an over abundance of argon onto a 14K CsI window suspended in a high-vacuum

chamber. In general, samples were vaporized from heated Pyrex tubes while argon was admitted through a length of liquid nitrogen cooled copper tubing. Such conditions yield an Ar/PANH ratio, in excess of 1000/1 [3]. Once a sufficient amount of material has been deposited, the infrared spectrum of the sample is recorded. Comparison of the original (neutral) spectrum to that obtained after the sample is exposed to ionizing radiation permits identification of PAH/PANH ion features, which appear upon photolysis. To distinguish between the bands of PAH/PANH cations and anions, as well as spurious photoproducts, experiments were conducted in which the argon matrix was doped with an electron acceptor, NO_2, at a concentration of approximately 1 part in 1000. The presence of an electron acceptor quenches the formation of PANH anions, permitting the unambiguous identification of PANH cations.

All calculations were performed using the Gaussian 98 computer code. For the species treated here, the geometries are optimized and the harmonic frequencies computed using density functional theory (DFT). Specifically, the hybrid [4] B3LYP [5] functional was utilized in conjunction with the 4-31G basis sets [6]. Calibration calculations, which have been carried out for selected systems, show that a single scale factor of 0.958 brings the B3LYP harmonic frequencies computed using the 4-31G basis set into excellent agreement with the experimental fundamental frequencies.

3. Results

This section presents a brief overview of the mid-infrared spectra of neutral PANHs (For a detailed analysis see; A. L. Mattioda, D. M. Hudgins, C. W. Bauschlicher, Jr., Rosi, M., L. J. Allamandola, J. Phys. Chem, submitted). As with all polycyclic aromatic species studied to date, the vibrations can be grouped into the following categories: CH stretching modes (centered near 3050 cm^{-1}), CC stretching and combinations between CC stretching and CH in-plane bending vibrations (between 1650 and 1100 cm^{-1}), and CH out-of-plane bending modes (between 900 and 500 cm^{-1}). However, for species as complex as these, the notion of a fundamental vibration involving only these separate motions is not strictly valid. Nonetheless these motions dominate the vibrations that give rise to the bands that fall in these regions and they can be used to understand the influence of nitrogen insertion as described below.

Nitrogen insertion induces several interesting new spectroscopic trends for this family of molecules. For the neutral species nitrogen inclusion causes unusual intensity enhancements for the different classes of vibration and induces significant, new IR activity for a specific mode. Computed dipole moments are also presented for these species in their neutral and ionized forms, enabling a search for individual interstellar PANHs. There are two features which set the spectra of nitrogen bearing aromatics apart from the general spectral properties of non-substituted, neutral polycyclic aromatic hydrocarbons. First, the addition of nitrogen induces a remarkable enhancement of the bands between 1650 and 1100 cm^{-1}, reminiscent of the changes which occur upon ionization [7,8]. The bands which are enhanced the strongest by nitrogen inclusion are those which involve the skeletal CC and CN stretching vibrations, those bands falling between 1600 and 1100 cm^{-1}. The second unique influence of nitrogen substitution is the appearance of a significant new band near 1400 cm^{-1} for 1-azabenz[a]anthracene, 4-azachrysene,

and 7,8 benzoquinoline. In most (not all) cases, this band is associated with structures in which the nitrogen is located in a pendant ring, at one of the vertices adjacent to the fused bond. A requirement for this feature to appear prominently is the presence of a hydrogen atom at the para-position to the nitrogen.

The overall calculated dipole moments for the neutral and cation forms of the PANH molecules are as follows: 7,8-benzoquinoline, 1.84 (2.38 for the cation) Debye; 2-azapyrene, 3.1597 (3.49 for the cation) Debye; 1-azabenz[a]anthracene, 1.66 (2.20 for the cation) Debye; 2-azabenz[a]anthracene, 3.00 (5.34 for the cation) Debye; 1-azachrysene, 2.43 (3.72 for the cation) Debye; 2-azachrysene, 3.37 (4.24 for the cation) Debye and 4-azachrysene, 1.88 (2.17 for the cation). This compares with 1.85 Debye for H_2O and 2.34 for H_2CO and indicates these molecules should be accessible to microwave or radio searches.

Acknowledgments

REFERENCES

[1] Hudgins, D.M., Sandford, S.A., Allamandola, L.J. 1994, *J. Phys. Chem.*, **98**, 4243.

[2] Hudgins, D.M., Allamandola, L.J. 1995, *J. Phys. Chem.*, **99**, 3033.

[3] Hudgins, D.M., Sandford, S.A. 1998, *J. Phys. Chem.*, **102**, 329.

[4] Becke, A.D., 1993, *J. Chem. Phys.* , **98**, 5648.

[5] Stephens, P.J., Devlin, F.J., Chabalowski, C.F., Frisch, M.J., 1994, *J. Phys. Chem.*, **98**, 11623.

[6] Frisch, M.J., Pople, J.A., Binkley, J.S., 1984, *J. Chem. Phys.* , **80**, 3265.

[7] Szczepanski, J., Vala, M., 1993, *Nature*, **363**, 699.

[8] Hudgins, D.M., Bauschlicher, C.W., Allamandola, L.J., 2000, *J. Phys. Chem.*, **104**, 3655.

Early Results from the APO Diffuse Interstellar Band Survey

B. J. McCall[1], J. Thorburn[2], L. M. Hobbs[2], D. E. Welty[2], T. P. Snow[3], B. L. Rachford[3],
P. Sonnentrucker[4], S. Friedman[4], and T. Oka[2], D. G. York[2]

1) Department of Astronomy, University of California at Berkeley

2) Department of Astronomy & Astrophysics, University of Chicago

3) Center for Astrophysics and Space Astronomy, University of Colorado at Boulder

4) Department of Physics & Astronomy, Johns Hopkins University

Abstract

The diffuse interstellar bands (DIBs) are absorption features observed in the visible spectra of nearly all reddened stars, and were first observed in the early decades of the 20th century when many lines in astronomical spectra were unassigned. As laboratory spectroscopy progressed, most of the stronger lines were identified with atomic or diatomic species — the DIBs are those lines (more numerous and generally broader) that remain unidentified.

Since the DIBs have remained unassigned for over 75 years despite extensive laboratory efforts, we are trying a new approach. Our goal is to obtain moderate resolution ($\lambda/\Delta\lambda \simeq 37,500$), high signal-to-noise spectra of a large sample of reddened stars. We are using the ARCES echelle spectrograph at the Apache Point Observatory, which offers complete spectral coverage from 3700–10,000Å. So far, we have taken data on 75 nights and have obtained S/N>1000 on 63 stars, and S/N>500 on 60 additional stars. Our hope is that this extensive DIB dataset, coupled with complementary measurements of known species at ultraviolet, visible, and infrared wavelengths, will yield new insights into the origin of the DIBs — this paper presents some of our early results.

1. DIB Correlation Studies

In looking through our dataset, we have discovered a new class of narrow DIBs that appear to be stronger, relative to many broader DIBs, in sightlines with above average C_2 column densities per unit E(B-V). Figure 1a depicts these bands, some of which were not identified in previous DIB surveys [e.g., (Tuairisg *et al.* 2000)]. This appears to be the first known set of DIBs which shows systematic line strength correlations with a known molecule. The "C_2 DIBs" will be discussed in more detail in an upcoming paper (Thorburn *et al.* 2002). Two of the stronger of these bands ($\lambda\lambda$ 4963, 4984) seem to be well correlated, suggesting that they may have carriers which are closely (chemically) related. It is also remarkable that many of these "C_2 DIBs" happen to occur in pairs with similar splittings of about 20 cm^{-1}. Based on the magnitude of this splitting, we conjecture that this splitting may be due to the spin-orbit interaction in a linear molecule. We have also examined the correlation coefficient of each DIB with H_2, versus that with H I, for all DIBs that have been measured in at least 20 stars where H I and H_2 have been measured. It is clear that most DIBs are better correlated with H I than with H_2. Our survey is designed to have complete overlap with the new H_2 measurements from the Far Ultraviolet Spectroscopic Explorer, so we should soon have even better statistics for these correlations.

We have also searched for "families" of DIBs whose intensities are tightly correlated from sightline to sightline: such correlations would suggest that those DIBs have the same (or closely chemically related) carriers. We have considered 1060 pairs of DIBs which are observed in at least 40 sightlines. The majority of the correlation coefficients are less than 0.8 (e.g., Figure 1b), and there are relatively few tightly correlated pairs (e.g., Figure 1c). However, we have tentatively identified one set of DIBs which all have $r > 0.94$ ($\lambda\lambda$ 5487, 5780, 6196, 6204, and 6613).
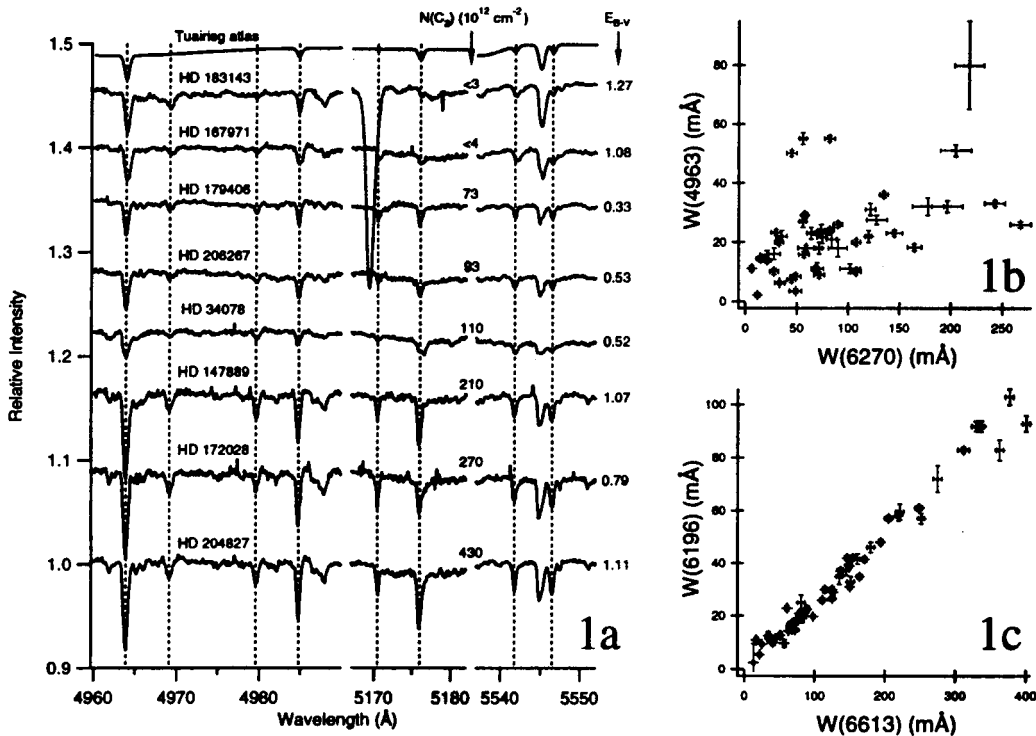
Fig. 1.— (a) The "C_2" DIBs; (b) Two DIBs with $r = 0.50$; (c) Two DIBS with $r = 0.99$

2. Comparisons with Laboratory Data

In 1998, J. P. Maier's group reported a possible match between the DIBs and the origin and four vibronic bands of the lowest electronic transition ($A^2\Pi_u \leftarrow X^2\Pi_g$) of C_7^- (Tulej et al. 1998). At the time, the match seemed plausible, given the uncertainties in both the laboratory and observational data (McCall, York, and Oka 2000). Subsequently, Lakin et al. (2000) revisited the C_7^- spectrum with considerably higher resolution and sensitivity. We have recently compared our observations of the $\lambda6270$ DIB with simulations of the C_7^- origin band at various temperatures (the simulations use the molecular constants derived by Lakin et al. (2000)) — and find that they do not agree in wavelength. Another of the proposed DIB matches with C_7^- ($\lambda5747$) turns out to be a stellar line. We also found that the DIB at $\lambda4963$, another proposed match with C_7^-, is completely uncorrelated with the supposed "origin band" $\lambda6270$. Altogether, we find no evidence supporting the hypothesis that C_7^- is a DIB carrier, as discussed in detail by McCall et al. (2001).

More recently, Maier's group suggested that the origin and three vibronic bands of the linear propadienylidene anion ℓ-$C_3H_2^-$ might match the DIBs (Güthe *et al.* 2001). We have performed detailed simulations of the expected spectrum of the ℓ-$C_3H_2^-$ origin band and compared them with the λ6993 DIB. Given the accuracy of the spectroscopic constants used in the simulations, the lack of wavelength agreement rules out ℓ-$C_3H_2^-$ as a carrier of λ6993. We find that there is also little evidence of a match with the vibronic bands. Overall, there seems to be no evidence to support the suggestion that ℓ-$C_3H_2^-$ is a DIB carrier, as discussed in more detail by McCall *et al.* (2002).

3. Other Results

The moderately reddened B5V star HD 62542 is known to have an unusual UV extinction curve of the type usually identified with dark clouds. The excitation of C_2 in this sightline suggests T $\sim$ 50 K and $n_H \sim$ 500–1000 cm^{-3}. The diatomic molecules CH, CN, and C_2 have high column densities, but the enigmatic CH$^+$ is not detected. We have observed HD 62542 (along with HD 215733) with UCLES at AAT, and compared these spectra with others from our APO survey. These spectra reveal that the typically strongest DIBs in our UCLES wavelength coverage ($\lambda\lambda$ 5780, 5797, 6270, 6284, and 6614) are essentially absent towards HD 62542. We interpret this as an extreme case of deficient DIB formation in a dense cloud whose more diffuse outer layers have been stripped away (Snow *et al.* 2002).

Another by-product of our survey has been the detection of the $A^1\Pi_u \leftarrow X^1\Sigma_g^+$ transition of C_3 at 4051.6 Å in 15 sightlines. Although the resolution of our spectrograph is not sufficient to resolve individual rotational lines, we clearly detect the central Q-branch. We also find that the C_2 and C_3 column densities are well correlated. Our C_3 detections will be discussed in detail in an upcoming paper (Oka *et al.* 2002).

In collecting our new database of DIBs and related interstellar quantities, we are encouraged by our ability to rule out specific laboratory candidates for the DIBs, to suggest physical associations (as in HD62542) of different DIBs with different types of interstellar clouds, to isolate at least some families of DIBs with high significance, and to discover, for the first time, associations of some DIBs with known small molecules.

Acknowledgments

REFERENCES

Güthe, F., Tulej, M., Pachkov, M. V., and Maier, J. P. 2001, *ApJ*, **555**, 466.
Lakin, N. M., *et al.* 2000, *J. Chem. Phys.*, **113**, 9586.
McCall, B. J., York, D. G., and Oka, T. 2000, *ApJ*, **531**, 329.
McCall, B. J., Thorburn, J., Hobbs, L. M., Oka, T., and York, D. G. 2001, *ApJ*, **559**, L49.
McCall, B. J., Oka, T., Thorburn, J., Hobbs, L. M., and York, D. G. 2002, *ApJ*, **567**, L145.
Snow, T. P., *et al.* 2002, *ApJ*, in press (astro-ph/0203254).
Tuairisg, S. Ó., Cami, J., Foing, B. H., Sonnentrucker, P., and Ehrenfreund, P. 2000, *A&AS*, **142**, 225.
Tulej, M., Kirkwood, D. A., Pachkov, M., and Maier, J. P. 1998, *ApJ*, **506**, L69.

Laboratory Astrophysics Needs of the Herschel Space Observatory

J. C. Pearson

Jet Propulsion Laboratory, California Insititute of Technology, Pasadena, CA

Abstract

The science teams of the Herschel Space Observatory have identified a number of areas where laboratory study is required for proper interpretation of Herschel observational data. The most critical is the collection and compilation of laboratory data on spectral line frequencies, transition probabilities and energy levels for the known astrophysical atomic and molecular species in 670 to 57 micron wavelength range of Herschel. The second most critical need is the compilation of collisional excitation cross sections for the species known to dominate the energy balance in the ISM and the temperature dependent chemical reaction rates. On the theoretical front, chemical and radiative transfer models need to be prepared in advance to assess calibration and identify instrument anomalies. In the next few years there will be a need to incorporate spectroscopists and theoretical chemists into teams of astronomers so that the spectroscopic surveys planned can be properly calibrated and rapidly interpreted once the data becomes available.

The science teams have also noted that the enormous prospects for molecular discovery will be greatly handicapped by the nearly complete lack of spectroscopic data for anything not already well known in the ISM. As a minimum, molecular species predicted to exist by chemical models should be subjected to detailed laboratory study to ensure conclusive detections. This has the greatest impact on any astrobiology program that might be proposed for Herschel. Without a significant amount of laboratory work in the very near future Herschel will not be prepared for many planned observations, much less addressing the open questions in molecular astrophysics.

1. Introduction

The Herschel Space Observatory is a far infrared observatory class mission scheduled for Ariane 5 launch in 2007. The observatory will reside at the second Lagrange point L2, where it is easy to shield the spacecraft from the sun as well as the Earth and Moon. The L2 environment allows for passive cooling of the cryostat shell and telescope on Herschel to below 80 Kelvin. The Herschel mission has three instrument mounted in a 2500 liter superfluid helium cryostat with helium vapor cooling providing temperature levels of approximately 4K and 15K. The silicon carbide telescope will be diffraction limited at 60 microns and have a 3.5 meter aperture. The nominal Herschel mission is for three years with a design goal of 5 years. Each instrument will be operated separately during observations. Two thirds of the observational time will be open time subject to a proposal process fully open to American and European observers.

The Herschel mission supports three instruments; the Photodetector Array Camera and Spectrometer (PACS), the Spectral and Photometric Imaging Receiver (SPIRE) and the Heterodyne Instrument for Far Infrared (HIFI). PACS is designed to perform two color imaging photometry in the 57-210 micron band or broadband spectroscopy with a grating spectrometer on two arrays of detectors at a resolution $\lambda/\Delta\lambda$ of approximately 1000. SPIRE is designed to perform three-color imaging photometry or broadband Fourier transform spectroscopy with at a resolution $\lambda/\Delta\lambda$ of 20-1000. HIFI is a seven channel dual polarization single pixel heterodyne receiver with 4 GHz of intermediate frequency bandwidth within each polarization in the 480-1250 or 1410-1910 GHz frequency range.

The Herschel Space Observatory is the first facility to cover the entire far infrared region and the only mission covering the 200-600 micron spectral range. The L2 environment provides a complete lack of atmospheric absorption and emission in a much lower thermal background environment than possible on the Earth.

2. Instruments and Science Objectives

The PACS instrument is designed to have a relatively large 1.75 by 2.5 field of view in photometry or a 50 by 50 field of view for spectroscopy. The PACS science program is focused on galaxies, with major observing programs planned for large area extragalactic surveys and follow up spectroscopy of distant galaxies. In our local galaxy, PACS will explore the initial mass function of cores and clusters as well as study HD and the galactic distribution of the D/H ratio as a probe of galactic evolution.

The SPIRE instrument, like PACS, is optimized to have a large field of view, 4 by 8 arcminutes in photometry and greater than 2 arcminutes for spectroscopy. The SPIRE science programs main target is also galaxies, with the major observing programs planned for large area extragalactic surveys. SPIRE will also perform spectroscopy of distant galaxies. In our local galaxy, SPIRE will explore the initial mass function of cores, clusters and star forming regions. Since SPIRE and PACS overlap very little in wavelength space, it is anticipated that the deep extragalatic surveys will be a joint science program with the 5 (or 6) available colors providing a great deal of spectral energy distribution information without further spectroscopy.

The HIFI instrument is optimized to return high R to 10^7 spectral data. As such HIFI is optimized to study the details of Doppler shifts, resolve close velocity groups, and perform complete chemical and dynamical inventories. The HIFI science program is divided into two key programs requiring large chunks of observing time and a number of topical core programs. The identified key programs are to perform complete spectral surveys of a significant number of objects ($\sim$ 30) and to study in detail the role of water in the universe. The core science programs are to study the interstellar medium in the Milky Way, the late stages of stellar evolution, solar system objects (several will probably be part of the spectral survey program), the interstellar medium in galaxies and star formation.

3. Instrument Laboratory Needs

The PACS instrument is optimized to study spectral energy distributions as well as strong Doppler broadened lines. As a result, the major laboratory needs are in the areas of Calibration sources, dust properties and models and radiative transfer models for complex sources. On orbit calibration of PACS requires a variety of continuum sources with a wide range of well-known flux levels in the 57-210 micron range. Spectroscopic frequency calibration requires the frequencies of bright emission lines. Pointing calibration requires bright stars in the far infrared with well-known astrometric positions. Proper interpretation of PACS data will require detailed models and measurements of dust spectral energy distributions as a function of chemical composition and conditions. Additionally, dust extinction as a function of conditions is also needed for the study of complex sources. Lastly full analysis of PACS data and early detection of instrument problems will require complete and tested radiative transfer models of complex sources. These

models must include gas, dust and 3-D morphology and be robust enough to cope with only a few lines and a continuum for distant object studies.

Since the SPIRE instrument is optimized to study spectral energy distributions as well as strong Doppler broadened lines, the laboratory needs are similar to PACS. However, SPIRE is really the first imaging instrument in the majority of its spectral range. Due to SPIRE new wavelength range the major laboratory need is in the areas of Calibration sources. SPIRE requires sources with known and modeled spectral energy distributions. SPIRE also needs a very precise model of Neptune and precise models of a number of asteroids in the 680-200 micron range. SPIRE also needs far infrared models of bright stars and a number of point-like objects in the 18 beam. Calibration sources are needed, which cover the entire dynamic range, are non-variable and distributed throughout the sky. For spectroscopic calibration sources with known low continuum levels, sources with known or well modeled line fluxes, which are non-variable, point like and have several observable non-blended lines. The line sources need to be distributed around the sky and cover the SPIRE dynamic range. For the proper interpretation of SPIRE data, good models of galaxy spectral energy distributions are needs as well detailed models and measurements of dust spectral energy distributions as a function of chemical composition and conditions. Additionally, dust extinction, as a function of conditions is also needed for the study of complex sources. Additionally, complete and tested radiative transfer models of complex sources. These models must include gas, dust and 3-D morphology and be robust enough to cope with only a few lines and a continuum for distant object studies.

The high spectral resolution, wide spectral coverage and high frequency of HIFI make it an enormous challenge for laboratory astrophysics. HIFI will return an enormous amount of highly detailed data, which will require several levels of laboratory data for analysis and finally interpretation. The basic analysis of HIFI data requires that the observed features be assigned to a transition in absorption or emission of an atom or molecule. For this to happen, the transition frequencies of all potential atoms and molecules must be known to better than HIFI's resolution. At a minimum this requires the rotational and low lying ro-vibrational spectra of all the known ISM molecular species be known and cataloged for use. Additionally the main isotopomers of ISM species must be known and cataloged for use. To take full advantage of HIFI, the transitions of potential molecules must be recorded and cataloged. All this must happen in the 480-1910 GHz frequency range. The next level of spectral data requires the transition strengths be precisely known. At this point the raw HIFI data is ready for interpretation, but interpretation requires several more layers of laboratory data.

Full interpretation of HIFI data requires collisional excitation parameters for each observed line, chemical reaction rates for all species related to those observed, chemical models including grain effects, detailed radiative transfer models including line transport and physical conditions. In the case of water, state-to-state excitation parameters are also necessary along with ratiative transfer models with simultaneous solution of statistical equilibrium and line transfer in the comoving frame including temperature, density and velocity gradients. The chemical reaction rates for gas phase, gas-dust, and on dust grain and collisional rates must also be cataloged in an easy to use format.

3.1. Laboratory Prospects

The Herschel space observatory represents a major challenge to the laboratory astrophysics community. Basic data such as the needed line intensities data can quickly exceed the current boundaries of fundamental physical knowledge. Similar problems arise in chemical data, chemical models, excitation cross sections, radiative transfer models and dust studies. Data catalogs only exist for reaction rates and spectral lines, however they are not close to comprehensive or complete. No catalog exists for excitation or dust chemistry. Astrophysics has in the past leveraged the state of the art chemical research techniques for long wave length astronomy. Unfortunately, the data now required for astrophysics is generally not at the cutting edge of chemical research funded by other interests, so astrophysics will have to support the programs it needs to interpret astrophysics data. The problem will further compound itself, since graduate programs and students currently have no incentive or long term prospects if they study in the areas of laboratory astrophysics. The problem is not unique to Herschel or long wavelengths and generally is shared by a number of missions so no one mission feels compelled (or is given the resources) needed to generate the required data. In the case of Herschel, responsibility for a laboratory program could just as easily be assigned to SOFIA or in many cases SIRTF or SWAS. As a result, a laboratory program is the responsibility of none. NASA, ESA, and a variety of national agencies in Europe are going to spend in excess of $1.5 billion for Herschel, but there is no specific budget or plan for performing the basic lab work necessary. The lack of a lab program is a major risk to the Herschel science return, because instrument anomalies will take longer to discover and correct, calibration will be problematic and will take more observing time, and complete interpretation of the data will not be possible, undermining the science. An identical statement could just as easily be made about a number of other astronomy instruments. None of this would be necessary with a proper lab program.

4. Conclusions

A number of steps urgently need to be taken prior to launch of Herschel. These include funding of basic laboratory and theoretical studies of line frequencies, transition moments, and collisional excitation cross sections. Chemical and radiative transfer models need to be prepared in advance and tested with ground based observations. Comprehensive catalogs of line frequencies, intensities, excitation cross sections, and temperature dependent chemical reaction rates need to be prepared. A comprehensive ground based program for calibration needs to established and funded, since no time allocation committee would normally grant proposals for calibration studies. NASA astrophysics has three choices in addressing Herschels lab needs. The existence of a lab data problem can be denied until after Herschel produces data, which defies scientific interpretation. The Herschel mission could be funded directly for lab support, or NASA could establish and fund a proper, focused lab program across missions. In theory, the current NASA system is designed for the latter, but in reality it is forever addressing data needs after the observations. In the case of Herschel the lab burden is shared with Europe, but it is not entirely Europe's burden either and NASA must contribute.

Acknowledgments

Microwave, Millimeter, Submillimeter, and Far Infrared Spectral Databases

J. C. Pearson, H. M. Pickett, B. J. Drouin, P. Chen and E. A. Cohen

Jet Propulsion Laboratory, California Insititute of Technology, Pasadena, CA

Abstract

The spectrum of most known astrophysical molecules is derived from transitions between a few hundred to a few hundred thousand energy levels populated at room temperature. In the microwave and millimeter wave regions, spectroscopy is almost always performed with traditional microwave techniques. In the submillimeter and far infrared microwave technique becomes progressively more technologically challenging and infrared techniques become more widely employed as the wavelength gets shorter. Infrared techniques are typically one to two orders of magnitude less precise but they do generate all the strong features in the spectrum. With microwave technique, it is generally impossible and rarely necessary to measure every single transition of a molecular species, so careful fitting of quantum mechanical Hamiltonians to the transitions measured are required to produce the complete spectral picture of the molecule required by astronomers. The fitting process produces the most precise data possible and is required in the interpret heterodyne observations.

The drawback of traditional microwave technique is that precise knowledge of the band origins of low lying excited states is rarely gained. The fitting of data interpolates well for the range of quantum numbers where there is laboratory data, but extrapolation is almost never precise. The majority of high- resolution spectroscopic data is millimeter or longer in wavelength and a very limited number of molecules have ever been studied with microwave techniques at wavelengths shorter than 0.3 mm. The situation with infrared technique is similarly dire in the submillimeter and far infrared because the black body sources used are competing with a very significant thermal background making the signal to noise poor. Regardless of the technique used the data must be archived in a way useful for the interpretation of observations.

The consequence to any archiving spectral database is that there is very limited high-resolution data available in the submillimeter and far infrared and the traditional infrared catalogs generally do not extend into the region. Additionally most astrophysical molecules are not very rigid further complicating the analysis and prediction of transitions. The JPL Submillimeter, Millimeter and Microwave Spectral line Catalog is an attempt to compile a complete and consistent set of spectroscopic data to support observations and observation planning.

1. Introduction

Atomic and molecular spectral line catalogs and databases facilitate the first step in reduction of astronomical spectra through the assignment of the observed spectral feature. The line strengths provided in many of the databases allows for determination of column density, effective temperature and when multiple transitions are observed the details on excitation conditions can be derived. The line shape allows for study of the local dynamics and provides some information on the line of sight. Since the molecular physics literature is well scattered in many journals and has many high quality publications prior to the electronic abstract data

base searches of today. As a result, it is critical to collect, compile and catalog the existing data in a form convenient for interpreting astrophysical observations.

There are four basic types of databases available. The microwave catalog database is where a set of rotational measurements is combined with a molecular Hamiltonian in least squares fitting procedure to predict all the unmeasured transitions. The second type is an infrared catalog where complete sets of high-resolution, rotationally resolved, infrared measurements are cataloged. The third type is an infrared database where low-resolution infrared measurements give the band structure and intensity, but provide no line resolution. The final type of database is the atomic line catalog where the transitions and transition moments of atoms and highly ionized atoms are recorded.

2. Microwave Catalogs

Microwave, Millimeter and Submillimter spectral line catalogs have greatly aided astronomy in the radio through submillimeter spectral region. Four different catalogs have been assembled and two, which use the same format, are active. The two inactive catalogs are the NIST Recommended Rest Frequencies for Observed Interstellar Molecular Microwave Transitions (Lovas 1992) and the Smithsonian Astrophysical Observatory Database SAO92 (Chance *et al.*, 1994). The two active catalogs JPL Submillimeter, Millimeter and Microwave Spectral Line Catalog (Pickett *et al.*, 1998) and the Cologne Database for Molecular Spectroscopy (Muller *et al.*, 2001) both employ an analysis program written by Herbert Pickett (1991). The use of one program to analyze the molecular data provides a consistent data format in a machine-readable form. It also assures the spin statistics, partition functions and line strengths are calculated in a consistent way. Combined there are over 150 molecules cataloged, however, this is only a subset of approximately 130 known interstellar molecules and both catalogs are very short on isotopic species and rotational states of vibrationally excited states. Additionally there are very few potentially detectable molecules and no attempt has been made to catalog the ro-vibrational or ro-torsional transitions sure to be observed in the far infrared.

3. Infrared Catalogs

Several infrared catalogs have been assembled, mostly to support atmospheric chemistry studies. These catalogs include HITRAN and HITEMP (Rothman *et al.*, 1998) and GEISA (Jacquinet-Husson *et al.*, 1999). Additionally a calibration catalog with heterodyne measurements in the infrared is maintained by NIST (Chu *et al.*, 1999). In these cases the number of species is rather limited with 37 molecules in HITRAN and HITEMP, slightly more than 40 molecules in GEISA and 5 molecules in NIST Wavenumber Calibration Tables from Heterodyne measurements. These catalogs are limited below 500 wavenumbers, generally only including microwave data. They are rotationally resolved, have measured line and band strengths and are generally accurate to 0.001 wavenumbers, especially below 3 microns. Unfortunately very few of the known astrophysical molecules are contained in either catalog and there is only a very limited effort to address this relative to molecules in the outer planets.

3.1. Infrared Database

A wide selection of Infrared Databases is available of analytical chemistry applications. These generally focus on gas or liquid phase low-resolution spectroscopy in the 400-4000 wavenumber spectral window. The free and easy to access databases include the NIST/EPA gas phase Infrared Database, the NIST Quantitative Infrared Database and the NIST Chemistry WebBook (all can be found from http://www.nist.gov). Another very complete system is the Integrated Spectral Database System for Organic Compunds, which has over 47,000 spectra available. Virtually every chemical company line Sigma-Aldrich or Sadtler has a available data base as do all the spectrometer makers Bio-rad, Bruker, Nicolet. The analytical chemistry Coblentz Society also has an Infrared database. These databases and spectra will provide band location, but they do not provide line resolved data and generally do not provide intensity data. As a result, they are only useful in potentially (not unambiguously) identifying spectral features like the 3 micron PAH feature.

3.2. Atomic Line Catalogs

The atomic physics community has several databases, mostly supporting plasma physics and observations in the UV and X-ray spectral regions. These catalog the observed and calculated atomic transitions for charged and uncharged atoms. The Harvard Center for Astrophysics web site http://cfa-www.harvard.edu/amdata provides links to a number of sites. The NIST Atomic Spectra Database has an easy to use access form. Collectively these databases are relatively complete, but are known to have some problems with intensities, transition frequencies. A major challenge remains the development of a complete catalog and keeping up with the rapid instrumental progress towards progressively wider wavelength coverage and higher resolution.

4. Conclusions

A great deal of atomic an molecular data has been collected and compiled in catalogs. Unfortunately only the Microwave Catalogs and some of the Atomic Line Catalogs were developed to support Astronomy. The catalogs supporting astronomy are generally not as complete as desirable or as easy to use as desirable. In the case of the microwave catalogs, may of the species missing pose significant theoretical challenges to calculating energy levels and transition strengths or significant challenges to collecting the fundamental data needed as an input to the database. As result, an enormous amount of work is required to upgrade the exiting databases to address the needs of missions like FUZE, Herschel or SOFIA. Ideally this should be done prior to launch, however it is all to often an afterthought once data arrives.

There are also some glairing holes in the available catalogs. These include little or no rotationally resolved data in the entire infrared region and no catalog of electronic transition of molecules in near infrared to UV. The infrared space observatory, ISO, has provided many wonderful spectra of the CH stretch band in the interstellar medium. Unfortunately, very few of the approximately 100 known molecules with a CH bond have line resolved infrared spectra

available or cataloged. As a result, not much can be concluded about the ISO CH stretch bands. Similar statements can be made about the diffuse interstellar bands. Ultimately the resolution of all these quandaries will require catalogs of line resolved atomic and molecular data.

Acknowledgments

REFERENCES

Chance, K., Jucks, K.W., Johnson, D.G. & Traub, W.A., 1994, *J. Quant. Spectrosc. Radiat. Transfer* **52**, 447.

Chu, P.M., Guenther, F.R., Rhoderick G.C. & Lafferty, W.J., 1999, *J. Res. Natl. Inst. Stand. Technol.* **105**, 59.

Jacquinet-Husson, N., *et al.*, 1999, *J. Quant. Spectrosc. & Radiat. Transfer.* **62**, 205.

Lovas, F.J., 1992, *J. Phys. Chem. Ref. Data* **21**, 181.

Muller, H.S.P., Thorwirth, S., Roth, D.A. & Winnewisser, G., 2001, *A&A* **370** L49.

Pickett, H.M., 1991, *J. Mol. Spectrosc.* **148**, 371.

Pickett, H.M., Poynter R.L., Cohen, E.A., Delitsky, M.L., Pearson, J.C., & Muller, H.S.P., 1998, *J. Quant. Spectrosc. & Radiat. Transfer* **60**, 883.

Rothman, L.S., Rinsland, C.P., Goldman, A., Massie, S.T., *et al.*, 1998, *J. Quant. Spectrosc. & Radiat. Transfer.* **60**, 665.

Laboratory Calibration Studies in Support of ORGANICS on the International Space Station: Evolution of Organic Matter in Space

R. Ruiterkamp,[1] P. Ehrenfreund,[1] T. Halasinski,[2] F. Salama,[2] B. Foing,[3] W. Schmidt[4]

[1] *Leiden Institute of Chemistry, Leiden, The Netherlands*

[2] *NASA-Ames Research Center, Space Science Division, Moffett Field CA, USA*

[3] *ESA RSSD, ESTEC/SCI-SR, Noordwijk, The Netherlands*

[4] *PAH Forschungs Institut, Greifenberg/Ammersee, Germany*

Abstract

This paper describes the scientific overview and current status of ORGANICS an exposure experiment performed on the International Space Station (ISS) to study the evolution of organic matter in space (PI: P. Ehrenfreund), with supporting laboratory experiments performed at NASA Ames. ORGANICS investigates the chemical evolution of samples submitted to long-duration exposure to space environment in near-Earth orbit. This experiment will provide information on the nature, evolution, and survival of carbon species in the interstellar medium (ISM) and in solar system targets.

1. Introduction

Understanding the chemical evolution of organic (carbon-based) matter in space is of great importance for the study of the origin of Life on Earth. Carbon- based molecules form a large fraction of the species detected in the interstellar medium (for recent reviews see Henning & Salama 1998; Ehrenfreund & Charnley 2000). The ORGANICS experiment has been selected by ESA for External Payload on the International Space Station for the study of the effects of near-earth space environment (VUV, vacuum, cosmic rays) on carbonaceous matter. Polycyclic Aromatic Hydrocarbons (PAHs) are observed in reflection and planetary nebulae, HII regions and external galaxies and are thought to be the most abundant free organic molecules and the carriers of some of the visible Diffuse Interstellar Bands (DIBs). PAHs have also been identified in meteorites, interplanetary dust particles (IDPs) and in comet Halley. In the ISM, PAHs can be neutral, ionized, partly dehydrogenated or even fragmented depending on the environment. Fullerenes, could also be important carriers of carbon in our Galaxy. C_{60} and larger fullerenes up to C_{240} have been detected in the Allende meteorite while C_{60}^+ might be associated with two DIBs in the NIR. Finally, Kerogen is a mixture of complex organic macromolecules. More than 90% of the carbon in meteorites is in the form of insoluble kerogen-type residues (Gardinier *et al.* 2000). By subjecting these molecules to near-earth orbit conditions we simulate the deep space conditions in terms of cosmic rays, space vacuum and ionizing radiation. An extensive laboratory simulation program is now in progress in support of this space experiment (Ruiterkamp *et al.* 2002).

2. Experimental Setup

The ORGANICS experiment is integrated in the multi-user facility EXPOSE that contains 9 experiments dedicated to astrobiology. Selected samples will be exposed to space environment

on the outside of the ISS. The samples will remain at least one year onboard the ISS before they are returned to Earth. The radiation dose that is collected by the samples during flight exceeds the limits for simulation in the laboratory and the results will greatly enhance our knowledge of the evolution of large organic molecules in space environment. Due to changes in the ISS external payload program, the mounting site of the EXPOSE experiment on board the ISS is currently not defined.

Sample Carriers: Samples are deposited in thin (~ 1 μm) films by spin coating on MgF_2 windows inside the sample cells (see Figure 1A). Dark samples on the Lower Sample Carrier are shielded from the UV photons and enable us to discriminate between the effects of exposure to photons and cosmic rays. Additional filters will enable us to select specific spectral regions for samples. The 1mm thick MgF_2 windows that hold the sample films are transparent well into the VUV.

Sample Tray: The sample carriers containing the different experiments of the EXPOSE facility are mounted in a sample tray (see Figure 1B). This tray is closed by MgF_2 windows and is equipped with shutters over some of the experiments. Passive and active heating keep the temperature in the 0-25 degree Celsius range. The design of the sample trays allows retrieval of the experiments without transporting the complete EXPOSE support structure. The particle and UV Radiation dose is monitored by the R3D dosimetry experiment situated at the sample level in one experiment tray. Thermocouples are installed at all experiments to monitor the temperature. The ORGANICS experiment will be situated in two compartments of the tray. One compartment will be closed from the external environment and one compartment will be vented to space.
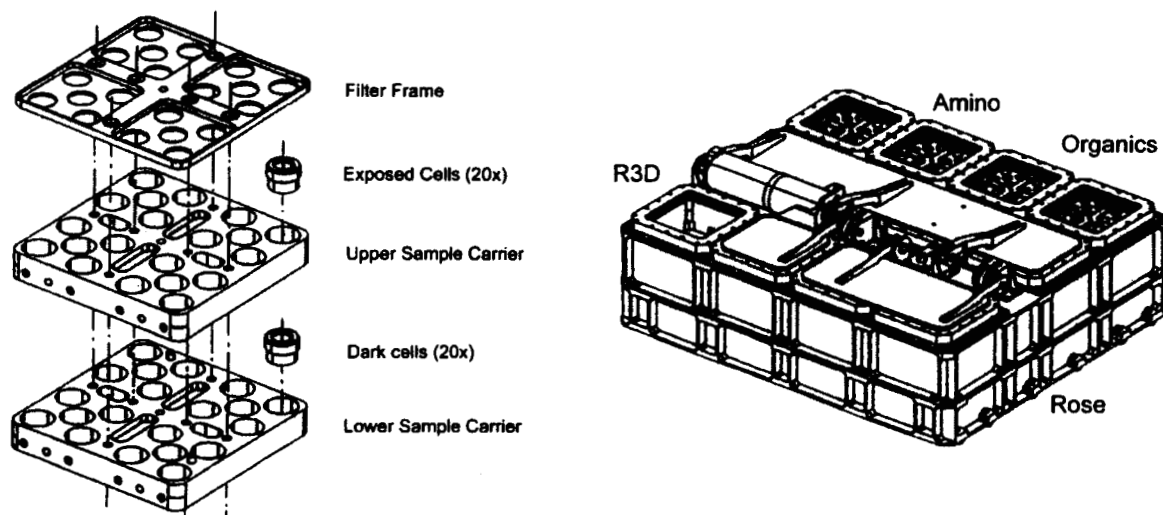
Fig. 1.— A. (left): Layout of the Sample Carriers used in the ORGANICS experiment. Samples are deposited on the inside of the MgF2 pellets that seal the sample cells. B. (right): Sample Tray of EXPOSE. The acronyms of the experiments are located at their assigned positions. The ORGANICS experiment consists of one sealed sample compartment and one vented to space.

3. Experimental Goals

The ORGANICS experiment will investigate the UV photochemistry of complex organic materials and study their evolution in space. It will provide better constraints on the composition and the survival rate of carbonaceous molecules in space (ISM and planetary/cometary surfaces). Matrix isolation spectroscopy of PAHs (Salama 1996) is performed as an integral part of the EXPOSE experiment. The laboratory simulations guides the selection of flight samples and provide an essential tool for the identification of the DIB carriers (Ruiterkamp et al. 2002). The results of this experiment will also be of relevance to planetary sciences and could help constrain the cosmic delivery of organics onto planetary surfaces, such as Earth and Mars (ten Kate et al. 2002).

4. Approach

Flight samples will be selected from a set of large PAH molecules, synthesized by the PAH Forschungs Institut. The sample selection will focus on large stable PAHs; aza-, oxo-, thio-PAHs; PAH isomers and potentially reactive PAH species (see Figure 2A).

The selection of large fullerenes depends on sample availability but will include C_{60}, C_{70} and C_{84}. The kerogen samples are of type III that most closely resembles the infrared spectrum of carbonaceous extracts of the Orgueil meteorite (Ehrenfreund et al. 1991).

Pre-flight analysis of the samples will consist of a combination of IR spectroscopy, fluorescence spectroscopy, UV/Visible spectroscopy, time-of-flight secondary ion mass spectroscopy, matrix isolation spectroscopy and isotopic analysis by the members of the team. The change in chemical composition resulting from the exposure of the samples on the Space Station Express Pellet will be evaluated with the same methods after retrieval. The EXPOSE platform is equipped with a dosimetry experiment that monitors the flux of radiation striking the sample tray. This will enable us to monitor the total energy input at the samples and to correlate with the spectral information.

5. Preliminary Results and Current Status

The selection and the calibration of the PAH and fullerene samples have been performed through Matrix Isolation Spectroscopy (MIS) studies (Ruiterkamp et al. 2002). In MIS, a gas mixture of PAHs highly diluted in Neon is frozen on a cold (5 K) substrate. The inert Ne matrix is transparent to UV. Irradiation with 10.2 eV photons from a hydrogen discharge lamp leads to the formation of PAH ions that are detected through their characteristic electronic spectra in the UV- Visible range (Salama 1996). This method has also been shown to be an effective tool for the preselection of promising species as potential diffuse interstellar band (DIB) carriers (Salama et al. 1999). Definitive detection can only be made, however, through free jet expansion (gas-phase) experiments (see e.g. Biennier et al. in this volume). In Figure 2B, the spectrum resulting from the 2B convolution of the MIS spectra of 10 PAH ions is compared to a synthetic DIB spectrum in an arbitrary scale. Although no definitive comparison can be made at this preliminary stage, a general overview of the spectral resemblance can be derived. The absence of spectral features toward the infrared of the DIB spectrum is due to the lack of astronomical data and not to a lack of features in this spectral region.
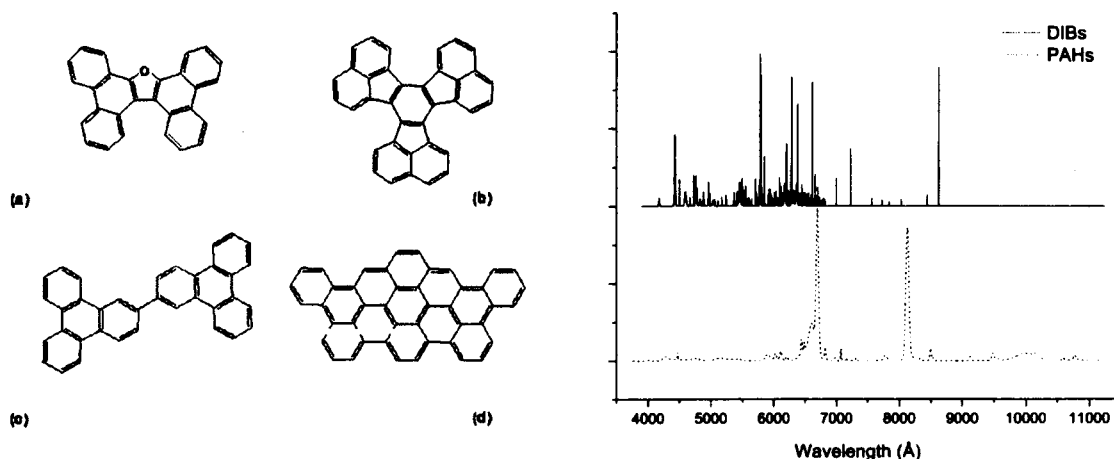
Fig. 2.— A. (left): Examples of Polycyclic Aromatic Hydrocarbons (PAHs) that will be used in the ORGAN-ICS experiment. (a) Diphenanthrofuran, (b) decacyclene, (c) (2,2')-bis-triphenylyl, (d) hexabenzoperopyrene. B. (right): Spectral comparison of a synthetic PAH spectrum composed of the Matrix Isolation spectra of 10 PAH ions and a synthetic DIB spectrum.

In preparation of the ORGANIC experiment on ISS we perform a short duration exposure experiment on BIOPAN. In this experiment the samples will be exposed to near earth orbit conditions for approximately two weeks. The BIOPAN experiment tray will be launched from Russia in October 2002 and the first results will be expected shortly thereafter. The current status of the EXPOSE platform on the ISS allows no definitive prediction of the launch date. In the mean time we will continue the chemical analysis of complex organic molecules and its implications for cosmo-chemistry.

Acknowledgments

REFERENCES

Ehrenfreund, P. & Charnley, S. B. 2000, ARA&A, 38, 427 and references therein.

Ehrenfreund P., Robert, F., d'Hendecourt L. and Behar, F. 1991, A & A 252, 712.

Gardinier, A., Derenne S., Robert F., Behar F., Largeau C., Maquet J. 2000, Earth Planet Sci Letters 184 9-21.

Henning, Th., and Salama, F., 1998, Science 282, 2204 and references therein.

ten Kate I. L., Ruiterkamp R., Botta O., Foing B.H., Ehrenfreund P., 2002, in preparation.

Ruiterkamp R., Halasinski T., Salama F., Foing B. H., Schmidt W., Ehrenfreund, P. 2002, A & A 390, 1153.

Salama, F., in LowTemperatureSpectroscopy, 483, R. Fausto ed., Kluwer, 169.

Salama, F., Galazutdinov, G. A., Krelowski, J. Allamandola, L. J. and Musaev, F. A. 1999, ApJ 526, 265.

The AstroBiology Explorer (ABE) MIDEX Mission:
Using Infrared Spectroscopy to Identify Organic Molecules in Space

S. A. Sandford

NASA Ames Research Center, Moffett Field, CA

Abstract

The AstroBiology Explorer (ABE) mission is one of four selected for Phase A Concept Study in NASA's current call for MIDEX class missions. ABE is a cooled space telescope equipped with spectrographs covering the 2.5-20 micron spectral range. The ABE mission is devoted to the detection and identification of organics and related molecular species in space. ABE is currently under study at NASA's Ames Research Center in collaboration with Ball Aerospace.

1. Introduction

One of the principal means by which organic compounds are detected and identified in space is by infrared spectroscopy. Past IR studies (telescopic and laboratory) have demonstrated that much of the carbon in the interstellar medium (ISM) is in complex organic species of a variety of types, but the distribution, abundance, and evolutionary relationships of these materials are not well understood. The Astrobiology Explorer (ABE) is a MIDEX mission concept designed to conduct IR spectroscopic observations to detect and identify these materials to address outstanding important problems in astrobiology, astrochemistry, and astrophysics. Systematic studies include the observation of planetary nebulae and stellar outflows, protostellar objects, Solar System Objects, and galaxies, and multiple lines of sight through dense molecular clouds and the diffuse ISM. ABE will also search for evidence of D enrichment in complex molecules in all these environments.

ABE is a cryogenically-cooled 60 cm diameter space telescope equipped with 3 cryogenic cross- dispersed spectrographs sharing a common slit. The spectrometers measure single spectral octaves (2.5-5, 5-10, 10-20 microns) and cover the entire range simultaneously. The spectrometers use state- of-the-art 1024x1024 pixel detectors, with a single InSb array for the 2.5-5 micron region and two Si:As arrays for 5-10 and 10-20 microns. The spectral resolution is >2000 across the entire spectral range. ABE would operate in a heliocentric, Earth drift-away orbit and will take maximum advantage of this environment for cooling, thermal stability, and mission lifetime. ABE's core science mission lasts ~1.5 years.

2. The Scientific Mission of the AstroBiology Explorer

In the course of its mission lifetime ABE will execute a focused series of observations designed to detect, identify, and determine the distribution of organics and related molecular species as they evolve through the cycle from stellar ejection, interstellar residence, and incorporation into forming stellar/planetary systems. The scientific tasks of the mission are described in the paragraphs that follow.

The Environments Surrounding Forming Stars. Independent of the formation site and interstellar evolution of cosmic organics, they must pass through dense clouds to end up on the surface of a planet. Thus, understanding the environment surrounding forming stellar systems is critical to addressing the role interstellar organics may play in the origin of life. Dense clouds are especially interesting because studies indicate that complex organic species are created in these environments (Dworkin et al., 2001) (Bernstein et al., 2002). ABE will greatly improve our understanding of the molecules in these environments by obtaining absorption spectra of embedded solar-mass protostars and background field stars probing lines of sight through nearby dense clouds in which star formation is occurring. ABE will be able to measure high signal-to-noise spectra from solar mass protostars, not just the high mass protostars previously observed (Gibb et al., 2000).

The Evolution of Complex Organic Molecules in the Interstellar Medium (ISM). Polycyclic aromatic hydrocarbons (PAHs) represent one of the main forms of molecular carbon in space. These molecules are thought to be produced in the outflows of late type carbons stars forming protoplanetary and planetary nebulae (PPN/PN). PAHs are detectable via their characteristic IR emission features (Allamandola et al., 1989). The PAH population evolves as it is subjected to the increasingly intense radiation field of their central star. ABE will study this evolution by examining the spectra of PPN and PN at different stages of evolution. In addition, the PAH population will be further modified in the ISM by the interstellar radiation field, supernovae shock waves, condensation and irradiation in ices in dense clouds, etc. Thus, ABE will also study PAH evolution by examining PAH emission spectra from HII regions and their boundaries with dense molecular clouds.

The Distribution of Organic Compounds in the Diffuse Interstellar Medium. On the basis of limited observations along a few lines of sight within our galaxy, it is known that about 10% of the cosmic abundance of carbon in the diffuse ISM is in the form of aliphatic hydrocarbons (Sandford et al., 1991) (Pendleton and Allamandola 2002). These materials appear to be associated with comparable or greater amounts of aromatic hydrocarbons. ABE will use field stars to probe for organic absorption bands along multiple sight lines through our galaxy to determine the composition, abundance, and distribution of this material.

Organics in the Solar System (comets, asteroids, planetary moons). Comets, asteroids, and the dust and meteoroids they produce are the principal bodies responsible for delivering interstellar materials to planetary surfaces (Chyba and Sagan 1992). Thus, understanding their organic contents is of direct interest to determining the role interstellar materials may have played in the origin of life. ABE will obtain spectra from a number of these objects, as well as from the surfaces of icy bodies in the outer solar system (KBOs, satellites of the gas giants, Pluto and Charon), objects that may either be repositories of interstellar organics or sites on which organics may be formed in situ.

The Cosmic History of Molecular Carbon. ABE will measure the spectra of galaxies to examine the relationships between the molecular component of galaxies as a function of type, composition, and cosmic distance. Spectral features such as the PAH emission bands and aliphatic absorption bands have both been seen in galaxies (Bridger et al., 1994) (Tran et

al., 2001). Targets include ultraluminous IRAS galaxies, Starburst galaxies, Seyfert galaxies, distant ULGs, and dwarf, S0, spiral, elliptical, and colliding galaxies. ABE will also do more detailed spectral mapping of a few nearby galaxies.

Tracing Deuterium Enrichments. In favorable cases, ABE will obtain spectra with sufficiently high S/N to detect, or derive meaningful upperlimits to, the D/H ratios of IS organics. A number of astrochemical processes enrich organics in D in the ISM (Sandford *et al.*, 2001) and the presence of D- enrichments in the organics in meteoritic materials provides the main proof that interstellar organics can survive incorporation into forming stellar systems and subsequent arrival on the surface of planets (Zinner 1997).

Guest Observations. ABE is prepared to carry out Phase F activities that would make approximately 20% of the missions total observing time available for a Guest Observer (GO) program. Time would be allocated to the general astronomical community on a competitive basis and would *not* be restricted to studies of direct interest to astrobiology. Thus, the capabilities of ABE could be used to address a wide variety of astrophysical issues that extend well beyond the central scientific goals of the ABE mission.

3. Additional Information

The Concept Study Reports for the current round of four MIDEX missions arc due on October 16, 2002. Final selection of the two missions to be flown is expected in March 2003. The selected missions will fly in 2007 and 2008. ABE data would be archived at IPAC and made public under a "rolling release" in which all the data would be available by mid 2010.

Information about the ABE mission can be found at http://www.astrochem.org/abe.html and in several SPIE publications (Ennico *et al.*, 2002) (Sandford *et al.*, 2000) (Sandford *et al.*, 2002). The most recent publications can be downloaded from the ABE website.

REFERENCES

Allamandola, Tielens, & Barker 1989, *ApJSS*, **71**, 733.

Bernstein, Dworkin, Sandford, Cooper, & Allamandola 2002, *Nature*, **416**, 401.

Bridger, Wright, & Geballe 1994, in *Infrared Astronomy with Arrays*, McLean, ed., Kluwer Academic, Netherlands, p. 537.

Chyba & Sagan 1992, *Nature*, **355**, 125.

Dworkin, Deamer, Sandford, & Allamandola 2001, *Proc. Nat. Acad. Sci. USA*, **98**, 815.

Ennico *et al.*, 2002, *Proc. SPIE*, **4495**, 273.

Gibb, *et al.*, 2000, *ApJ*, **536**, 347.

Pendleton & Allamandola 2002, *ApJSS*, **138**, 75.

Sandford, Allamandola, Tielens, Sellgren, Tapia, & Pendleton 1991, *ApJ*, **371**, 607.

Sandford, *et al.*, 2000, *Proc. SPIE*, **4013**, 604.

Sandford, Bernstein, & Dworkin 2001, Meteor. Planet. *Science*, **36**, 1117.

Sandford *et al.*, 2002, *Proc. SPIE*, **4495**, 170.

Tran, *et al.*, 2001, *ApJ*, **552**, 527.

Zinner 1997, in *Astrophysical Implications of the Laboratory Study of Presolar Materials*, eds. Bernatowicz & Zinner, Amer. Inst. Phys., Woodbury, NY, p. 3.

Molecular Carbon in the Galaxy:
New Laboratory and Observational Studies

Richard J. Saykally

Department of Chemistry, University of California, Berkeley, CA

The possible roles of two distinct forms of carbon in the ISM is being explored in our laboratories. Polycyclic Aromatic Hydrocarbon (PAH) molecules, proposed as UIR carriers [1] are studied in the gas phase by IR emission spectroscopy, while pure carbon clusters are studied by a combination of IR cavity ringdown spectroscopy, FIR laser spectroscopy, and observational FIR astronomy.

We have developed an infrared photon counting method [2] based on a blocked impurity band solid state photomultiplier (BIB-SSPM) for the purpose of measuring IR emission spectra of large PAH molecules under conditions approximating those in the Interstellar Medium. We have recently [3,4,5] used this new technique (single photon infrared emission spectroscopy, SPIRES) to measure gas phase IR emission from a number of UV laser-excited neutral PAHs over the entire spectral range of the UIRs. Apart from the 3.3 μm feature, no acceptable matches with UIR spectra were found. Here, we describe the extension of SPIRES to PAH cations, generated and observed in a well- characterized ion beam.

We have reported [6] the first observation of infrared emission from a gaseous polycyclic aromatic hydrocarbon ion (PAH$^+$), the pyrene cation, over the range of wavelengths spanned by the UIRs. The complete set of pyrene cation IR emissions is observed, with relative intensities consistent with astrophysical observations, thus supporting the proposal that ionized PAHs are major contributors to the UIR bands. Additionally, unidentified features possibly arising from dehydrogenated PAH species are noted in the spectrum.

Neutral carbon clusters as large as C_{13} have been studied in our laboratory by high resolution IR diode laser spectroscopy [7], and the vibration-rotation spectrum of the linear C_{10} cluster was analyzed and reported, in collaboration with the Cologne group [8,9] We have now developed a new high resolution pulsed IR cavity ringdown technique capable of higher sensitivity, much broader spectral coverage, and similar spectral resolution relative to a diode laser spectrometer, as demonstrated in a study of the C_9 cluster [10].

Meanwhile, our initial 1994 detection [11] of the C_3 molecule in the source Sg B2 was confirmed by the ISO study of Charnicharo *et al.* [12], demonstrating the general potential for detecting such nonpolar species via their low-frequency bending vibrations. This detection of C_3, as well as an expanded laboratory study of this molecule carried out in collaboration with the Cologne group, was subsequently described in detail [13].

REFERENCES

1. D.M. Hudgins, C.w. Bauschlicher, Jr., L.J. Allamandola, *Spectrochimica Acta Part A* **57**, 907-930 (2001).

2. S. Schlemmer, D.J. Cook, J.A. Harrison, B. Wurfel, W. Chapman, and R.J. Saykally, *Science* **265**, 1686 (1994).

3. D.J. Cook, S. Schlemmer, N. Balucani, D.R. Wagner, B. Steiner, and R.J. Saykally, *Nature* **380**, 227 (1996).

4. D.J. Cook, S. Schlemmer, N. Balucani, D.R. Wagner, J.A. Harrison, B. Steiner, and R.J. Saykally, *J. Phys. Chem. A* **102**, 1465 (1998).

5. D.R. Wagner, HS. Kim, and R.J. Saykally, *Astrophys. J.* **545**:854- 860 (2000).

6. H.-S. Kim, D.R. Wagner, and R.J. Saykally, *Phys. Rev. Lett. 8* **6**, 5691 (2001).

7. T.F. Giesen, A. Van Orden, H.J. Hwang, R.S. Fellers, R.A. Provencal, and R.J. Saykally, *Science* **265**, 756 (1994).

8. T.F. Giesen, U. Berndt, K.M.T. Yamada, G. Fuchs, R. Schieder, G. Winnewisser, R.A. Provencal, F.N. Keutsch, A. Van Orden, and R.J. Saykally, *ChemPhysChem* **4**, 242- 247 (2001).

9. T.F. Giesen, U. Berndt, G. Fuchs, G. Winnewisser, R.A. Provencal, F.N. Keutsch, A. Van Orden, and R.J. Saykally, *Proceedings of the Nobel Symposium* **117** *on The Physics and Chemistry of Clusters*, Visby, Sweden, E.E.B. Campbell and M. Larsson, eds.; pp. 309-310 (2001).

10. R.N. Casaes, R.A. Provencal, J.B. Paul, and R.J. Saykally, *J. Chem. Phys.* **116**, 6640- 6647 (2002).

11. A. Van Orden, J.D. Cruzan, R.A. Provencal, T.F. Giesen, R.J. Saykally, R.T. Boreiko, and A.L. Betz, *Proceedings of the 1994 Kuiper Airborne Astronomy Symposium, NASA- Ames Research Center, Moffett Field, CA, Astron. Soc. Pac. Conf. Ser.* **73**, 67- 70 (1995).

12. J. Chernicharo, J.R. Goicoechea, and E. Caux, *Ap. J.* **534**, L199 (2000).

13. T.F. Giesen, A.O. Van Orden, J.D. Cruzan, R.A. Provencal, R. Gendriesch, F. Lewen, G. Winnewisser, R.T. Boreiko, A.L. Betz, and R.J. Saykally, *Astrophys. J. Lett.* **551**:L181-L184 (2001).

UV photoabsorption cross sections of CO, N_2, and SO_2
for studies of the ISM and planetary atmospheres

Peter L. Smith, J. Rufus, K. Yoshino and W. H. Parkinson
Harvard–Smithsonian Center for Astrophysics

Glenn Stark
Physics Department, Wellesley College

Juliet C. Pickering and A. P. Thorne
Blackett Laboratory, Imperial College, London

Abstract

We report high-resolution laboratory measurements of photoabsorption cross sections of CO, N_2, and SO_2 in the wavelength range 80 to 320 nm. The motivation is to provide the quantitative data that are needed to analyze observations of absorption by, and to model photochemical processes in, the interstellar medium and a number of planetary atmospheres. Because of the high resolution of the spectrometers used, we can minimize distortion of the spectrum that occurs when instrument widths are greater than the widths of spectral features being measured. In many cases, we can determine oscillator strengths of individual rotational lines – a unique feature of our work. Abstract text here.

1. Carbon Monoxide (CO)

CO is the second most abundant interstellar molecule after H_2. Because CO is readily observed, it is used as a tracer of molecular material. However, estimates of abundances of CO are poorly determined observationally and not well understood theoretically. Incomplete or inconsistent molecular parameters contribute to many of the difficulties. Consequently, the acquisition of improved photoabsorption cross section and spectroscopic data for CO at VUV wavelengths has been a major focus of our research program in the past few years (Smith *et al.* 1994; Yoshino *et al.* 1995; Stark *et al.* 1999a).

Recently, we have studied the absorption spectrum of five weaker intersystem (spin-changing) bands in order to provide line oscillator strengths (*f*-values) for absorption features seen by Federman *et al.* (1994) and Sheffer *et al.* (2002). *f*-values can be difficult to calculate for these weak bands because each upper level is perturbed by a number of vibrational levels of the *A* state. Therefore, we have emphasized direct measurements with the 6.65-m 6VOPE normal-incidence spectrometer at the Photon Factory, a synchrotron radiation source in Tsukuba, Japan. This spectrometer has a resolving power of about 170,000 and an order-sorting predis-perser that greatly reduces spurious signal. An example of our data is shown in Figure 1; the instrument resolution was greater than the Doppler dominated width of the spectral lines, so the line shapes are somewhat distorted in this spectrum.

Our line *f*-values for the *d*(7)-*X*(0) and *e*(4)-*X*(0) bands are given by Stark *et al.* (2002). These are the first direct measurements of individual line *f*-values for an intersystem band of CO. Our measured values generally confirm the band simulations of Rostas *et al.* (2000) and those determined by Sheffer *et al.* (2002) from observations of interstellar absorption.
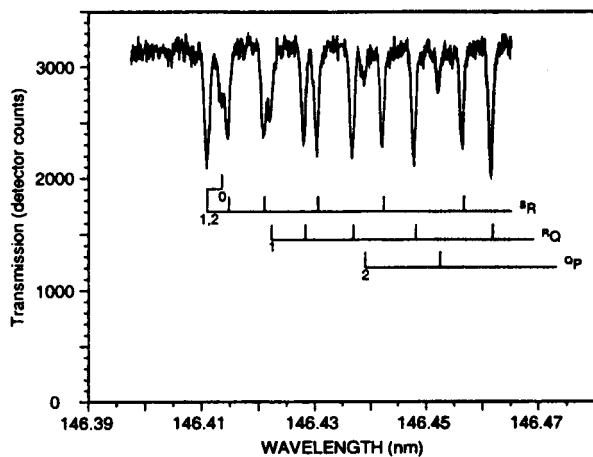
Figure 1. CO $d(7)$-$X(0)$ bandhead region.
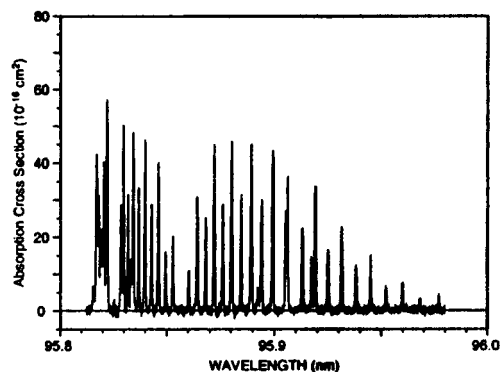
Figure 2. Measured photoabsorption
cross section for the $c'_4(0) - X(0)$ band of N_2.

2. Molecular Nitrogen (N_2)

The strongest band of N_2, $c'_4(0) - X(0)$ at 95.9 nm, is in the FUSE wavelength range and is not blended with CO or H_2 features. The most prominent EUV emission features in the airglows of Titan and Triton, where N_2 is the major atmospheric constituent, originate from the c'_4 $^1\Sigma_u^+(v' = 0)$ level. Like many of the VUV lines of N_2, those of the $c'_4 - X$ band are extremely sharp, with natural line widths much less than the Doppler widths. Line f-values cannot be reliably calculated from band f-values and Hönl-London factors because of perturbations: measurements are required. The highest possible resolving power is necessary to minimize distortions of the spectrum and concomitant obscuration of saturation effects.

We again used the 6.65-meter spectrometer at the Photon Factory. Data for the the $c'_4(0) - X(0)$ band of N_2 are shown in Figure 2. Our results (Stark et al. 2000) are the first measurements of individual line f-values for this band. Our data are available in our N_2 data archive at http://cfa-www.harvard.edu/amdata/ampdata/N2ARCHIVE/n2home.html. We have also measured band f-values and line widths for a number of the ~ 100 bands of N_2 in the 80 to 100 nm wavelength region. These bands are important for understanding the temperature-density profiles of the atmospheres of Titan and Triton. Analysis of these data is in progress.

3. Sulfur Dioxide (SO_2)

Analysis of the UV spectrum of Io and modelling of the chemical composition and photochemical processes in its atmosphere require knowledge of the photoabsorption cross section of SO_2 over a wide wavelength range at temperatures from 110 to ~500 K. Our laboratory program, which also supports HST observations of the atmosphere of Venus, is producing such data over the wavelength range 190 to 325 nm with orders of magnitude higher resolving power than previous work.

The ultraviolet spectrum of SO_2 is dominated by two broad regions of absorption: 175 to 230 nm, which is the stronger, and 250 to 320 nm. Because the upper electronic states participating in these transitions are strongly perturbed, no comprehensive rotational analyses exist or are likely in the near future. This means that the temperature dependence of the SO_2 absorption spectrum, needed for analyses of planetary atmospheres, cannot be reliably

modelled but must be measured. The region is exceedingly complex at room temperature; previous photoabsorption measurements have been unable to fully resolve it.

We used the VUV Fourier transform (FT) spectrometer at Imperial College, London (Thorne et al. 1987) for two sets of measurements. Cross section data for the 198 to 220 nm region have been published (Stark *et al.* 1999); results for the region 220 to 235 nm are reported here (see also Rufus *et al.* 2002). Figure 3 shows recent data plotted on linear and log scales; note that the structure (see inset) is essentially all real, *i.e.*, not noise. Our data are compared to those of Manatt & Lane (1993) and Wu *et al.* (2000) over a limited spectral region in Figure 4.
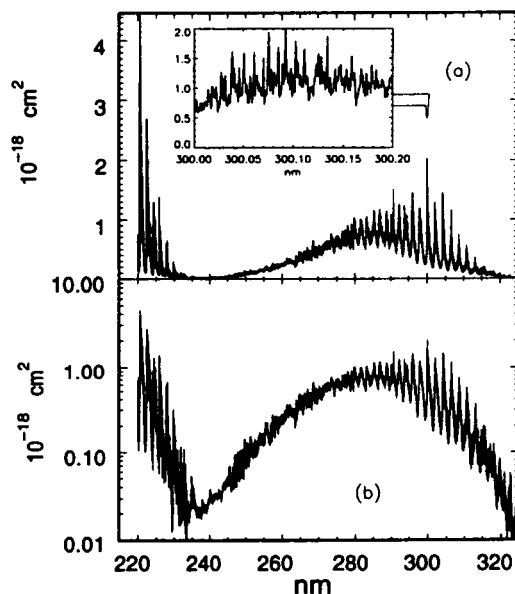
Figure 3. Photoabsorption cross section of SO_2 at 295 K measured with a resolution of 4 to 32 mÅ. Inset shows structure in a 0.2 nm region. Note that the *SNR* for this measurement was about 100, so the structure shown in the inset is real.
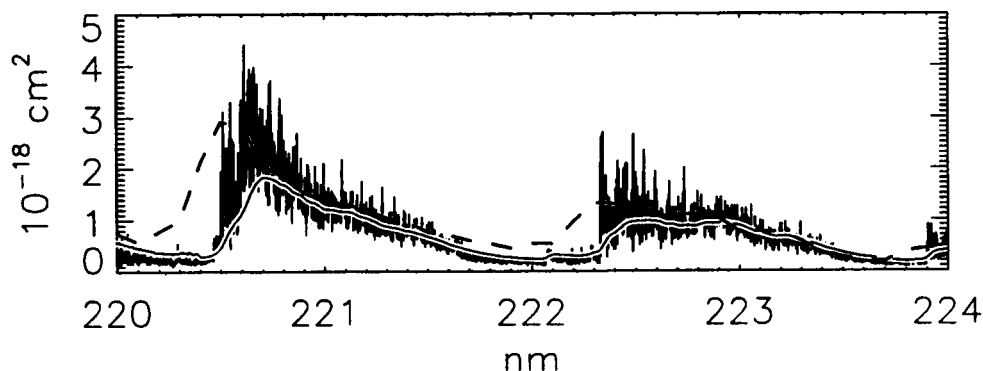
Fig. 4.— Comparison of our results (highly structured line) with those of Manatt and Lane [1993] (dashed line) and Wu et al. [2000] (smooth solid line with white border). Note that, on the average, the data roughly agree, but that our values for the peak cross sections are about a factor of two larger.

Acknowledgments

REFERENCES

Federman, S R, J A Cardelli, Y Sheffer, D L Lambert, & D C Morton 1994, 139.

Mannat, S L, A L Lane 1993, J. Quant. Spectrosc. Rad. Trans., 50, 267-276.

Rostas, F, M Eidelsberg, A Jolly, J L Lemaire, A Le Floch & J Rostas 2000, J. Chem. Phys. 112, 4591.

Rufus, J, G Stark, P L Smith, J C Pickering & A P Thorne 2002, JGR, submitted.

Sheffer, Y, S R Federman & D L Lambert 2002, ApJL, submitted.

Smith, P L, G Stark, K Yoshino & K Ito 1994, ApJL, 431, L143.

Stark, G, B R Lewis, S T Gibson & J P England 1999a, ApJ 520, 732.

Stark, G, P L Smith, J Rufus, A P Thorne, J C Pickering & G Cox 1999b, JGR 104, 16585.

Stark, G, K P Huber, K Yoshino, M-C Chan, T Matsui, P L Smith & K Ito 2000, ApJ 531, 321.

Stark, G, P L Smith, K Yoshino, J R Esmond & K Ito 2002, ApJS 138 305.

Yoshino, K, G Stark, J R Esmond, P L Smith, K Ito & T Matsui 1995, ApJ 438, 1013.

Wu, C Y R, B W Wang, F Z Chen, D L Judge, J Caldwell & L M Trafton 2000, Icarus 14, 289-296.

Dehydrogenated Neutral PAH Radicals as Carriers of the DIBs? Spectroscopy of the Fluorene-like $C_{13}H_9$ Radical

Martin Vala, Jan Szczepanski, John Banisaukas

Department of Chemistry, University of Florida, Gainesville, FL

So Hirata

Environmental Molecular Sci. Lab., Pacific Northwest Natl. Lab. Richland, WA

1. Introduction

Polycyclic aromatic hydrocarbons (PAHs), in their neutral, ionized, hydrogenated and dehydrogenated forms, have been proposed as possible carriers of the diffuse interstellar absorption bands (DIBs) and the unidentified infrared emission (UIR) bands. In this work, we suggest that a dehydrogenated PAH could be responsible for one of the DIBs.

It is general knowledge that neutral PAHs, upon ionization, shift their optical absorption bands to lower energy. We point out here that certain emphneutralPAHs may also shift their electronic transitions to the red when dehydrogenated. In particular, we show that when fluorene ($C_{13}H_{10}$) loses one hydrogen, its optical absorption shifts to the red and appears in the vicinity of a strong DIB band.

2. Computational Methods

Density functional theory (DFT) calculations (B3LYP/6-31G (d, p)) were used to Compute: 1) optimum geometries, 2) C-H bond energies and 3) ground state vibrational frequencies. Time-dependent DFT (TDDFT: B3LYP/6-31(2+, 2+) G (d, p)) calculations were also performed to predict the excited electronic states in the $C_{13}H_9$ radical.

3. Experimental Procedures

The $C_{13}H_9$ radical was produced from fluorene by UV photolysis (UVP) or low energy electron impact (EI). In the UVP approach, the parent fluorene, $C_{13}H_{10}$, was deposited in an Ar matrix at 12K and photolyzed with a 100W medium pressure Hg lamp ($h\nu < 5.5$ eV). In the EI approach, a mixed fluorene/Ar beam was crossed with an 300V electron beam with the resultant mixture deposited on a 12K Al-coated copper matrix block. Electronic absorption spectra were recorded in single beam mode through the sample/matrix on a BaF_2 window. Infrared spectra were recorded in the 700-4000 cm^{-1} region with a MIDAC FTIR spectrometer. Ar ion laser excitation into the strong $^2A_2(D_2) \leftarrow {}^2B_2(D_0)$ band of the $C_{13}H_9$ radical at 496.6 nm enabled Raman spectra to be recorded with a Spex double monochromator with photon counting.

4. Results

C-H Bond Energies. Using calculated optimized structures for the parent fluorene and the radical $C_{13}H_9$, the bond energy for the C-H bond at the sp³-hybridized carbon, was found to be 3.38 eV, compared to 4.79/pm 0.01 eV for the six- membered ring hydrogens. This leads to the conclusion that the H_9 is the first H lost upon photolysis. Interestingly, after this dehydrogenation, the C-H_9 bond becomes one of the strongest in the $C_{13}H_9$ radical.

Electronic Absorption. The electronic absorption of the fluorene- like $C_{13}H_9$ radical is shown in the figure.

Infrared Absorption. Infrared and UV/visible spectra were collected on the same $C_{13}H_9/C_{13}H_{10}$/Ar matrices. IR peaks due to $C_{13}H_9$ have been observed at 722.2, 780.9, 1239.5 and 1567.8 cm⁻¹. The intensities of these bands tracked each other and the UV/visible bands well under different experimental conditions (EI with different electron beam energies and UVP with different photon fluxes).

DFT calculations using B3LYP functionals and 6-31G (d, p) basis set (scaled by 0.978) predicted IR bands for $C_{13}H_9$ at 725 cm⁻¹[52 km/mol], 778 cm⁻¹ [44 km/mol], 1248 cm⁻¹ [10 km/mol], and 1580 cm⁻¹ [27 km/mol], in excellent agreement with the observed peaks.

Preresonance Raman Spectrum. The 496.4 nm Ar⁺ laser line falls just to the red of the 0-0 ²$A_2(D_2)$ ← ²$B_2(D_0)$ 0-0 band (cf, figure). The preresonance Raman spectrum recorded is shown in the figure. No peaks to higher wavenumbers than 1600 cm⁻¹ were observed. When compared with the observed peaks the agreement with the computed vibrational frequencies from DFT calculations is very good.

Possible DIB Carrier? The optical absorption of the $C_{13}H_9$ radical shows an intense, low energy peak at 494.6 nm with a shoulder on its red edge. If these two peaks are deconvoluted, the band width (FWHM) of the main 494.6 nm band is approximately 1.8- 2.0 nm. It is tempting to compare this peak with the DIB at 488.2 nm, which has a FWHM of 1.7 nm.

The gas-to-Ar matrix shift is 6.4 nm to lower energy. For comparison, the similarly-sized naphthalene cation absorbs at 670.65 nm in the gas phase and at 675.0 nm in Ar matrices, a gas-to-matrix red shift of 4.35 nm. The vibronic bands to higher energy of the origin band are only 10-12% of the intensity of the 0-0 band and therefore might be observationally difficult to find. A cold vapor phase spectrum of this species must be recorded before any definitive conclusions can be drawn.

If a close match is found, a clear observational test would be to search for transitions to the higher-lying electronic states (370.6, 353.2, and 283.1 nm). To date, no bands to the blue of the 443 nm DIB have been observed so this test might prove difficult, if not impossible.

The positions of the observed bands and the results of TDDFT calculations on the predicted excited electronic states of $C_{13}H_9$ are shown in Table 1 below. Quite good agreement can be seen.

Table 1. Calculated and observed electronic transitions from the $2B2$ ground state for $C_{13}H_9$.

State	Calc. Energy/eV	Calc. f_{TDDFT}	Expt. Energy/eV (nm)	Calc. f_{est}
$2A2$	2.75	0.0525	2.51 (494.6)	0.025
$2B2$	3.69	0.0153	3.34 (370.6)	>0.050
$2A2$	3.93	0.0359	3.51 (353.2)	<0.037
$2A2$	4.37	0.0154	4.38 (283.1)	>0.012
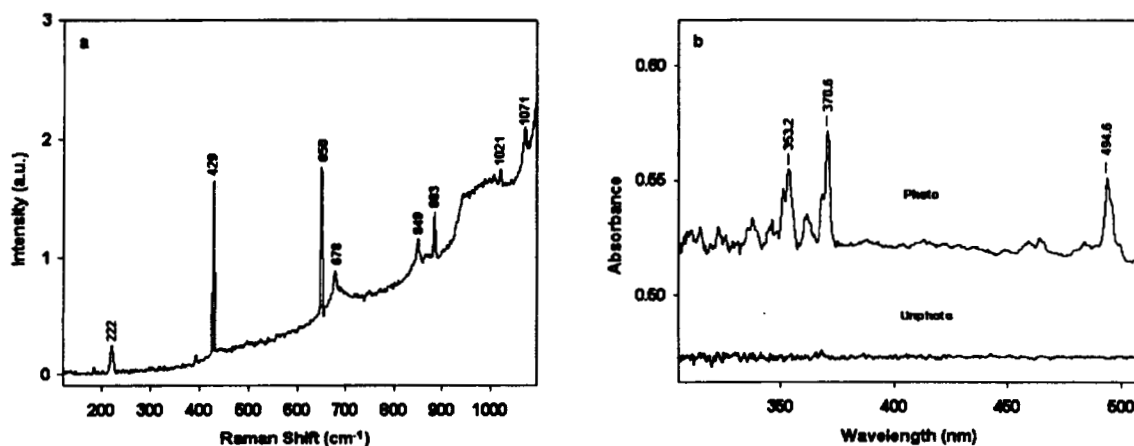
5. Conclusions

The first hydrogen lost from neutral $C_{13}H_{10}$ is most likely one of those attached to the sp^3 carbon in the five-membered ring, requiring 3.38 eV, according to theory. The preresonance Raman, IR, and vis/UV spectra of $C_{13}H_9$ were recorded for the first time. The observed vibrational frequencies match results of DFT calculations well. UV/vis bands reveal an electronic band in the vicinity of the 488.2 nm DIB. Neutral radicals, formed by photostripping hydrogen(s) from PAHs containing five-membered rings, probably shift their UV/vis spectra to the red. The energies required are less than needed for photoionization. This class of dehydrogenated compounds may give rise to some of the DIBs and is deserving of further study.

Molecular Line and Continuum Opacities for Modeling of Extrasolar Giant Planet and Cool Stellar Atmospheres

P. F. Weck, A. Schweitzer, P. C. Stancil, & P. H. Hauschildt

Dept. Physics & Astronomy; Ctr. for Simulational Physics, Univ. Georgia, Athens, GA

K. Kirby

ITAMP, Harvard-Smithsonian Center for Astrophysics, Cambridge, MA

Y. Yamaguchi & W. D. Allen

Ctr. for Computational Quantum Chem.; Dept. Chemistry, Univ. Georgia, Athens, GA

Abstract

The molecular line and continuum opacities are investigated in the atmospheres of cool stars and Extrasolar Giant Planets (EGPs). Using a combination of *ab inito* and experimentally derived potential curves and dipole transition moments, accurate data have been calculated for rovibrationally-resolved oscillator strengths and photodissociation cross sections in the B' $^2\Sigma^+ \leftarrow X$ $^2\Sigma^+$ and A $^2\Pi \leftarrow X$ $^2\Sigma^+$ band systems in MgH. We also report our progress on the study of the electronic structure of LiCl and FeH.

1. Introduction

The lack of accurate and complete molecular line and continuum opacity data has been a serious limitation to developing atmospheric models of cool stars and Extrasolar Giant Planets (EGPs). In fact, sophisticated modeling programs, such as the PHOENIX code (Hauschildt & Baron, 1999), require high quality opacity data in order to produce synthetic spectra and predict physical parameters (surface chemical composition, effective temperature, etc). Typically, atmosphere models include molecular bands with hundreds of millions of spectral lines, mostly derived from molecular band models. Moreover, few models consider the effect of molecular photodissociation processes which may play a role in the opacity at visible and UV wavelengths. In this work, we report our progress on the calculations of line and continuum opacities resulting from the presence of three molecules, MgH (Skory *et al.* 2002; Weck, Stancil, & Kirby 2002a; Weck *et al.* 2002b,c), LiCl and FeH.

2. Magnesium hydride

Accurate SDTCI potential-energy surfaces calculated by Saxon, Kirby & Liu (1978) have been used for the B' $^2\Sigma^+$, A $^2\Pi$ and X $^2\Sigma^+$ electronic states of ^{24}MgH, together with their connecting transition dipole moments, over the range $R = 2.2$ a_o to 9.5 a_o. For both the short- and long-range interactions, they have been extrapolated by an exponential fit. In Figure 1, the product of the rotational oscillator strengths $f_{v'J',v''J''}$ and the degeneracy factor $g_{J',J''}$ as a function of the absorbed photon energy is shown for the A-X bound-bound transitions. Our calculated spectrum appears to be more compact than the results of Kurucz (1993) obtained by extrapolation. In particular, the differences observed on the wavelength range

$19000 - 20500$ cm^{-1} may have significant consequences for high temperature studies (e.g., non-equilibrium chemistry models of M and L dwarf atmospheres). For the $B' - X$ bound-bound transitions, a good qualitative and quantitative agreement is observed with the results of Kurucz (1993).

The LTE rovibrationally-resolved photodissociation cross sections $\sigma_{v''J''}$ for the A-X transitions are presented in Figure 2 as functions of wavelength and temperature (Boltzmann distribution). Rotational cross sections are characterized by shape resonances arising from rotational predissociation of quasi-bound levels of the A $^2\Pi$ electronic state near threshold. The cross section from the ground RV level, $v'' = 0$, $J'' = 0$, is also represented for photodissociation through the B'-X transitions.
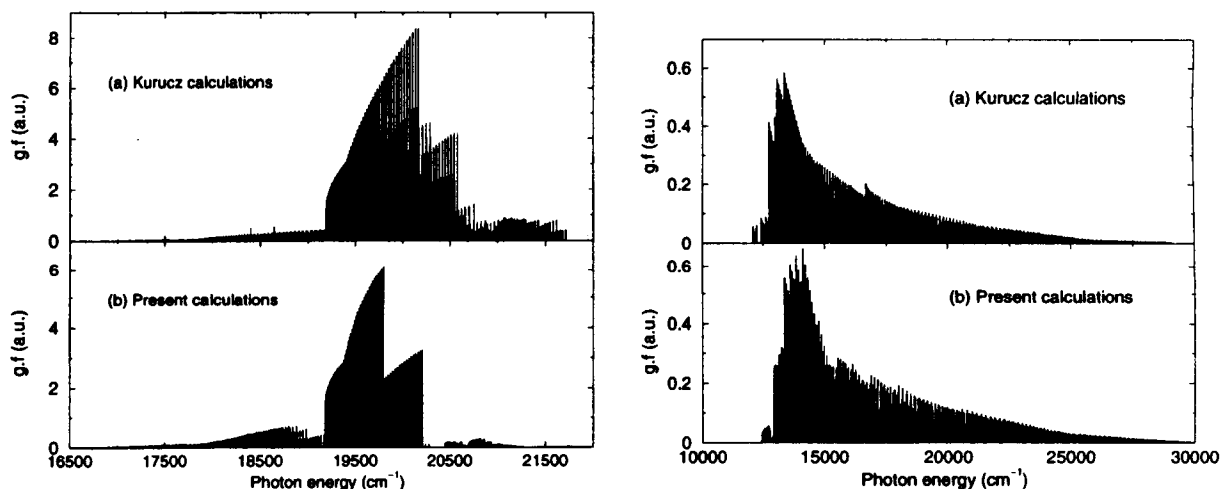
Fig. 1.— Product of the rotational oscillator strengths $f_{v'J',v''J''}$ and the degeneracy factor $g_{J',J''}$ as a function of the absorbed photon energy. Left: $A \leftarrow X$ trantsitions; right: $B' \leftarrow X$ trantsitions.
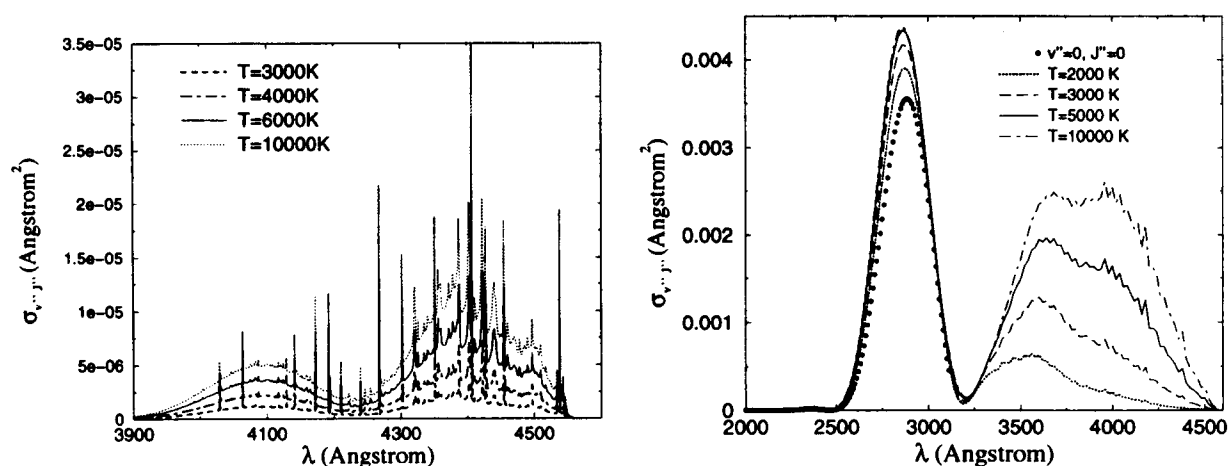
Fig. 2.— LTE photodissociation cross sections $\sigma_{v''J''}$ as functions of wavelength and temperature (Boltzmann distribution). Left: $A \leftarrow X$ trantsitions; right: $B' \leftarrow X$ trantsitions.

3. Lithium Chloride and Iron Hydride

From our *ab initio* SDCI calculations using the ALCHEMY code (Mc Lean *et al.* 1991), we have obtained five $^1\Sigma$ and five $^1\Pi$ electronic states, thus giving four additional electronic states than that calculated with a valence-bond method by Zeiri & Balint-Kurti (1983). Calculations to obtain the energy surfaces over a large internuclear distance range are underway. Calculations have been performed using the coupled cluster method (CCSD(T)) near the equilibrium distance r_e of the X $^4\Delta$ electronic state of FeH. Our results are presented in Table 1 together with the previous values obtained by Tanaka, Sekiya, & Yoshimine (2001) and by Langhoff & Bauschlicher (1990).

Table 1. Energy* values near the equilibrium distance† of X $^4\Delta$ of FeH

States	Present work		Langhoff *et al.*		Tanaka *et al.*		Experiment	
	E	r_e	E	r_e	E	r_e	E	r_e
X $^4\Delta$.....	0	2.964	0	3.001	0	3.016	0	3.002
A $^4\Pi$......	1309	2.917	1200	2.934	2010	2.933	930	···
a $^6\Delta$......	372	3.190	1290	3.199	2080	3.235	1970	3.34
b $^6\Pi$.......	2183	3.181	3244	3.197	3310	3.207	4010	···
c $^6\Sigma^+$.....	4249	3.203	3694	3.201	4600	3.190	4870	···

*Adiabatic term energy in cm^{-1}

†Equilibrium distance in a_o

4. Conclusion

Lines and photodissociation cross sections have been calculated for MgH using a full theoretical treatment, improving the previous extrapolated results. Progress has been made in the determination of *ab initio* potential energy surfaces for LiCl and FeH, in order to calculate for the first time complete absorption spectra of both molecules.

Acknowledgments

REFERENCES

Hauschildt, P. H., & Baron, E. 1990, *J. Comp. App. Math.*, **102**, 41.
Kurucz, R. L. 1993, CD-ROM No. 15. Diatomic molecular data for opacity calculations (Harvard-Smithsonian Center for Astrophysics).
Langhoff, S., & Bauschlicher, C. Jr. 1990, *J. Mol. Spec.*, **141**, 243.
Mc Lean, A. D., Yoshimine, M., Lengsfield B.H., Bagus P. S., & Liu B. 1991, *MOTECC*, **91**, E.Clementi Ed., Elsevier (Leiden).
Saxon, R. P., Kirby, K., & Liu, B. 1978, *J. Chem. Phys.*, **12**, 5301.
Skory, S., Stancil, P. C., Weck, P. F., & Kirby, K. 2002, *ApJS*, to be submitted.
Tanaka, K., Sekiya, M., & Yoshimine, M. 2001, *J. Chem. Phys.*, **115**, 10.
Weck, P. F., Stancil, P. C., & Kirby, K. 2002a, *ApJ*, submitted.
Weck, P. F., Schweitzer, A., Stancil, P. C., Hauschildt, P. H., & Kirby, K. 2002b, *ApJ*, submitted.
Weck, P. F., Schweitzer, A., Stancil, P. C., Hauschildt, P. H., & Kirby, K. 2002c, *ApJ*, submitted.
Zeiri, Y., & Balint-Kurti, G. 1983, *J. Mol. Spec.*, **99**, 1.

Sub-millimeter Spectroscopy of Astrophysically Interesting Metal-Containing Molecules

L. M. Ziurys, M. A. Brewster, P. M. Sheridan, C. Savage, D. T. Halfen and A. J. Apponi

Departments of Astronomy and Chemistry, The University of Arizona, Tucson, AZ

Abstract

With the advent of SOFIA and Herschel, new spectral windows will be opened for spectroscopy in the sub-millimeter region. To conduct science in this band, laboratory measurements must be carried out to provide accurate transition frequencies for molecular identification and physical interpretation. We are presently conducting such measurements using gas-phase submm direct absorption techniques. Of particular interest are simple molecules containing iron-peak elements, including carbides, and metal hydride ions (MH^+), both which possess favorable transitions at submm wavelengths.

1. Introduction

Various wavelength regions exist that are inaccessible by ground-based astronomy, but may contain important spectral information. For example, there are large gaps in the atmospheric windows from $\sim 525 - 575$ GHz, $725 - 775$ GHz, and upwards of 950 GHz. NASA has been developing SOFIA and Herschel for operation within these frequency ranges. The detector systems currently being constructed for these projects will have the necessary heterodyne capability for high resolution molecular spectroscopy. It is naturally assumed that new molecular discoveries will be made with these instruments; however, only with the necessary laboratory measurements will these expectations be realized.

The Ziurys group has been pursuing the measurements of rest frequencies for potentially new interstellar molecules for many years, in particular those containing a cosmically abundant metallic element (in the chemist's sense). Such species are relevant for astrophysical studies because many of them have relatively high cosmic abundances. Also, to date, eight metal-bearing molecules have been detected in the circumstellar gas of AGB stars such as IRC+10216, CRL2688 and CRL618. The species detected include AlNC (Ziurys *et al.* 2002), MgCN (Ziurys *et al.* 1995), MgNC (Kawaguchi *et al.* 1993; Highberger *et al.* 2001), NaCl, KCl, and AlF (Cernicharo & Guelin 1987; Ziurys, Apponi, & Phillips 1994; Highberger *et al.* 2001). Their appearance in these objects make them potential tracers of nucleosynthetic processes, as studies of the magnesium isotopes of MgNC have demonstrated (Guelin *et al.* 1995).

Interestingly, thus far such compounds have not been observed towards molecular clouds. Metallic elements are important components of the ISM, where they contribute to the electron density and hence the ionization balance, and where they are likely to form dust grains. On the other hand, they could also be contained in molecular form. The metal-bearing species AlNC, MgNC and MgCN, for example, are located in the outer circumstellar envelope of IRC+10216, where the gas is cold and dense. If there is a cold gas-phase refractory component in AGB shells, why not in molecular clouds?

2. Laboratory Molecular Spectroscopy

Submillimeter direct absorption spectroscopy is a relatively straightforward process in which radiation from a tunable source is focused through a reaction chamber and changes in power level due to absorption by molecules are measured with a detector. Currently, there are three operational systems in the Ziurys lab. The millimeter wave radiation sources used are Gunn oscillator/Schottky multiplier combinations that cover the range of 65 – 810 GHz. The gas cells are free-space chambers designed quasioptically, and the detectors are InSb hot electron bolometers. These systems are not commercially available.

Creation of metal-bearing molecules in the gas phase is not simple; these are highly reactive species whose physical properties are largely unknown. The technique used to sythesize these molecules is exotic: metal vapor is produced in a Broida-type oven and an appropriate precursor material is added, usually in the presence of a d.c. discharge. There is no guarantee that this method will work for any given molecule. Furthermore, large frequency ranges (30 – 60 GHz) must be scanned to identify the spectrum of a particular species.

Recently, metal bearing nitrides and carbides have been investigated in the Ziurys group. Metal nitrides are of interest because nitrogen is abundant, and molecules such as SiN and CN have been detected in the ISM. One of the radicals studied is CrN, which was produced by the reaction of chromium vapor and ammonia in a d.c. discharge. Nine rotational transitions were recorded in the frequency range 294 – 636 GHz, each consisting of four fine structure lines that compose an irregular quartet, consistent with a $^4\Sigma^-$ ground state. These data have been subsequently analyzed and rotational, spin-spin, and spin- rotation constants accurately determined (Sheridan, Brewster, & Ziurys 2002). The pure rotational spectrum of FeN ($X^2\Delta_i$) has also been recorded using a similar synthetic method. Eight transitions were measured for the lowest spin-orbit component, $\Omega = 5/2$, where no evidence of Λ-doubling was found. Again, highly accurate spectroscopic parameters were established from these data.

Metal carbides with the general formula MC are of interest because all metal- bearing molecules to data have been observed in circumstellar shells of <u>carbon-rich</u> stars. During the past two years, the Ziurys group has recorded the pure rotational spectrum of NiC and CoC, and very recently CaC. Each species was created by the reaction of the appropriate metal with CH_4 in a d.c. discharge. Four rotational transitions of CoC were measured, each consisting of 16 hyperfine components, while multiple transitions were obtained for both ^{60}NiC and ^{58}NiC (Brewster & Ziurys 2001). Highly accurate spectroscopic constants have been established for both species. In the case of CaC, eleven rotational transitions were recorded in which three fine structure components were resolved, as shown in Figure 1. Rotational, spin-spin, and spin-rotation parameters have been obtained from these measurements (Halfen, Apponi, & Ziurys 2002). This study is the first measurement of an alkaline earth carbide by <u>any</u> spectroscopic technique. The laboratory detection of CaC is thus a landmark experiment.

The work on CaC will hopefully lead to the discovery of other carbon-metal rings and chains, such as CaC_2, CaC_3, CaC_4, etc., in analogy to known silicon-carbon species. The magnesium and aluminum couterparts of these metal- carbon complexes are additionally of interest.

Finally, "first light" has been obtained with a new ion submm spectrometer, as evidenced by the observation of HCO$^+$ with this instrument. This system will be eventually used for the investigation of metal hydride ions with the formula MH$^+$. Some target molecules are shown in Table 1. Very little is known spectroscopically about these ions, including their ground electronic states, which is surprising. Any hydride molecule formed with a cosmically abundant element and hydrogen must be fundamental to interstellar chemistry. Metal hydride ions are particularly interesting since they are readily formed by ion-molecule reactions and may be the hidden carriers of metals in dense and diffuse clouds. Moreover, because of their small moments of inertia, hydrides have their rotational spectra entirely in the submm/infrared regions. They are thus critical targets for SOFIA and Herschel.

Table 1. Metal Hydride Ions of Submillimeter Interest

Species	Ground State	Estimated B (in GHz)	Production Method	Reference
MgH$^+$	$^1\Sigma$	188.0	Nozzle/ablation source, Mg + H$_2$	Balfour (1971)
AlH$^+$	$^2\Sigma$	201.9	Nozzle/ablation source, Al + H$_2$	Muller & Ottinger (1988)
KH$^+$	$^2\Sigma^+$	110.2	Nozzle/ablation source, K + H$_2$	Melius et al. (1979)
NaH$^+$	$^2\Sigma^+$	158.0	Nozzle/ablation source, Na + H$_2$	Melius et al. (1979)
CaH$^+$	$^1\Sigma^+$	138.2	Nozzle/ablation source, Ca + H$_2$	Canuto et al. (1993)
MnH$^+$	$^6\Sigma$	198.8	Nozzle/ablation source, Mn + H$_2$	Barone & Adamo (1997)
CrH$^+$	$^5\Sigma$	199.8	Nozzle/ablation source, Cr + H$_2$	Barone & Adamo (1997)
FeH$^+$	$^5\Sigma$	169.8	Nozzle/ablation source, Fe + H$_2$	Barone & Adamo (1997)
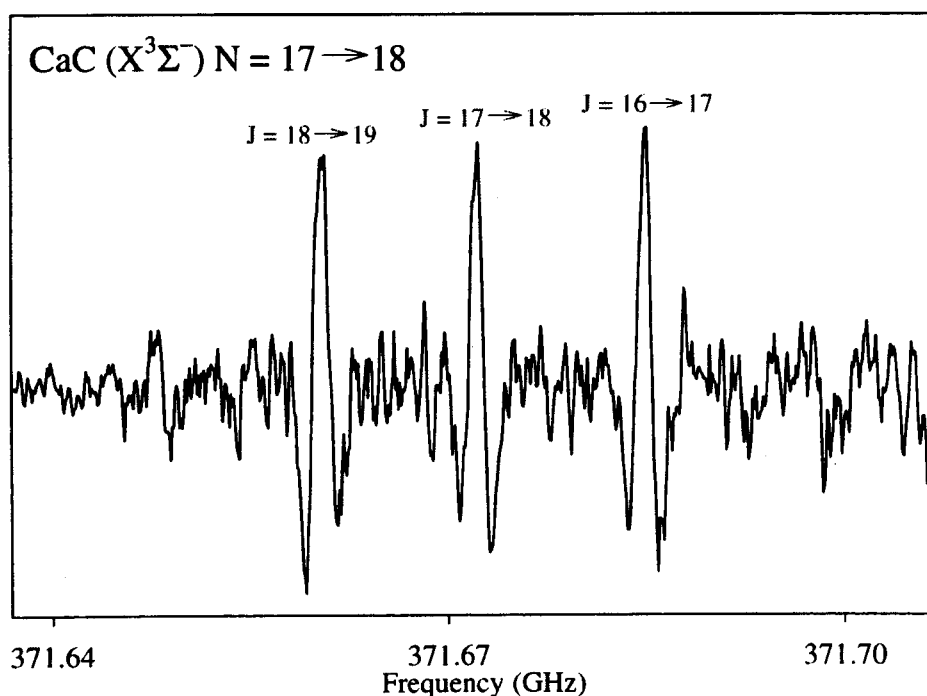
Fig. 1.— Spectrum of the $N = 17 \rightarrow 18$ transition of CaC in its $X^3\Sigma^-$ ground state.

Acknowledgments

REFERENCES

Balfour, W.J. 1972, *Can. J. Phys.*, **50**, 1082.

Barone, V. & Adamo, C. 1997, *Int. J. Quant. Chem.*, **61**, 443.

Brewster, M. A & Ziurys, L. M. 2001, *ApJ*, **559**, L163.

Canuto, S., Castro, M.A., & Sihha, K. 1993, *Phys. Rev. A.*, **48**, 2461.

Cernicharo, J. & Guelin, M. 1987, *A&A*, **183**, L10.

Guelin, M., *et al.* 1995, *A&A*, **297**, 183.

Halfen, D. T., Apponi, A. J., & Ziurys, L. M. 2002, *ApJ*, submitted.

Highberger, J. L., Savage, C., Bieging, J. H., & Ziurys, L. M. 2001, *ApJ*, **562**, 790.

Kawaguchi, K., Kagi, E., Hirano, T., Takano, S., & Saito, S. 1993, *ApJ*, **406**, L39.

Launila, O. & Lindgren, B. 1996, *J. Chem. Phys.*, **104**, 6418.

Melius, C.F., Numrich, R.W., & Truhlar, D.G. 1979, *J. Phys. Chem.*, **83**, 1221.

Müller, B. & Ottinger, C. 1998, *Z. Naturforsch. A.*, **439**, 1007.

Sheridan, P. M., Brewster, M. A., & Ziurys, L. M. 2002, *ApJ*, in press.

Ziurys, L. M., Apponi, A. J., & Phillips, T. G. 1994, *ApJ*, **433**, 729.

Ziurys, L. M., Apponi, A. J., Guelin, M., & Cernicharo, J. 1995, *ApJ*, **445**, L47.

Ziurys, L. M., Savage, C., Highberger, J. L., Apponi, A. J., Guélin, M., & Cernicharo, J. 2002, *ApJ*, **564**, L45.

~ ~ **INVITED** ~ ~

Nanoparticles in Space and the Laboratory

Th. Henning[1]

Max Planck Institute for Astronomy, Heidelberg, Germany

H. Mutschke

Astrophysical Institute and University Observatory, Laboratory Astrophysics, Jena, Germany

S. Schlemmer and D. Gerlich

University of Technology, Institute for Physics, Chemnitz, Germany

Abstract

Nanoparticles provide the largest fraction of solid surface in the interstellar medium. They are therefore of great importance as catalytic sites for chemical reactions. The very small grains have unique optical and radiation properties which deviate from those of bulk materials. This paper reviews observational evidence for such particles and summarizes the necessary steps to produce and characterize astronomically relevant materials in the laboratory.

1. Introduction

Small solid grains form an important component of our and other galaxies (Dorschner & Henning 1995). Although they are only a minor contributor to the total mass of these systems, they determine the thermal, dynamical, and chemical state of the cold and dense phases of the interstellar medium, thereby controlling the star formation process in molecular clouds and the mass loss from evolved stars. The coagulation of these particles in circumstellar disks is a first, but decisive step towards the formation of planetesimals.

From a chemical and physical point of view, the interstellar grains are a very interesting system of small and well-isolated particles interacting with radiation, other grains, and gas species at the low temperatures of interstellar space (Henning 1998). Therefore, many bridges to solid-state physics, quantum chemistry, and physical chemistry exist. The detection of novel forms of carbon was triggered by astrophysical studies and the investigation of polycyclic aromatic hydrocarbons (PAHs) got a new impetus from laboratory astrophysics. New computational and experimental methods for the investigation of the interaction of light with irregular, anisotropic, and fluffy grains were developed by astrophysicists.

The *Infrared Space Observatory* ISO demonstrated that the adequate interpretation of spectroscopic data of dusty objects in the universe requires the measurement of fundamental laboratory data of cosmic dust analogues (d'Hendecourt *et al.* 1999). The detection of widely distributed crystalline silicates was certainly unexpected and materials such as the Mg-rich end members of olivines and pyroxenes, forsterite and enstatite, were largely unknown to astronomers. The ISO observations and the analysis of "stardust" in meteorites and primitive

---

materials in interplanetary grains openend the new field of astromineralogy (Henning 2002). Furthermore, the presence of crystalline silicates points to annealing and mixing processes in protoplanetary disks and can be used to trace disk evolution (Bockelée-Morvan et al. 2002). SIRTF, SOFIA, Herschel and finally NGST will deliver infrared data of unprecedented sensitivity, spectral, and spatial resolution which cannot be fully exploited without laboratory data of cosmic dust analogues.

2. The Role of Nanoparticles in Space

The transition from the gas phase to solid dust grains in the interstellar medium results in the formation of solid surfaces. They provide important reaction sites for interstellar chemistry. In order to understand this phase transition, it is important to know how nanoparticles nucleate from the gas phase and grow. The formation of carbonaceous grains in space bears some similarity to soot formation by combustion processes (Frenklach & Feigelson 1997). In contrast, the formation routes of oxide particles under cosmic conditions are practically not understood.

In the interstellar radiation field, nanoparticles (in astrophysics often called "very small grains"), do not have an equilibrium temperature (Draine and Li 2001). They are stochastically heated because the time-averaged vibrational energy is smaller than the energy of the interstellar radiation field. The stochastic heating process leads to transient temperature spikes and infrared excess emission compared with larger grains of lower temperature.

Nanoparticles often have material properties different from those of bulk material. A simple example are metallic nanoparticles where the free mean path of the electrons is limited by the dimension of the grains. Surface structures are often more important for the optical behaviour of nanoparticles as this is the case for bulk materials. In addition, bulk materials with the same structure as the structure of the nanograins may not exist (and vice versa). This is especially important for carbonaceous grains where the concept of graphite nanoparticles makes no sense, but particles with graphitic basic structural units exist.

3. Observational Evidence for Nanoparticles

Direct evidence for the presence of nanoparticles comes from the analysis of primitive meteoritic material, where nanodiamonds have been found (see, e.g., Braatz et al. (2000)). Whether these particles indeed originate in the environment of evolved stars or supernovae or whether they are formed in the solar nebula remains an unsolved problem. Direct spectroscopic evidence for the presence of nanodiamonds in the environment of Herbig Ae/Be stars came from a comparison of ISO spectroscopy and laboratory data (Guillois et al. 1999).

The first observational proof for the presence of nanoparticles was already obtained by IRAS observations. The observations with this satellite led to the detection of mid-infrared excess emission in the IRAS 12, 25, and 60 μm bands which cannot be attributed to large grains which have typical temperatures of 20 K in the interstellar medium (Boulanger & Pérault 1988). In addition, the far-UV extinction is mainly attributed to scattering by nanoparticles.

On the basis of these observations, a comprehensive dust model for the ISM has been developed which includes very small grains (Desert *et al.* 1990).

Another line of evidence for the presence of nanoparticles in space comes from the analysis of spectroscopic features. The UV bump at 217.5 nm and the 3.4 μm absorption feature have been attributed to carbonaceous nanoparticles (Schnaiter *et al.* 1998, 1999), the Extended Red Emission to silicon nanoparticles (Witt *et al.* 1998; Ledoux *et al.* 2001), and the 21 μm feature, observed in the spectra of carbon-rich post-AGB stars, to TiC nanograins or clusters (von Helden *et al.* 2000).

4. Production and Characterization of Nanoparticles

Various techniques have been established to produce nanoparticles from the gas phase, from solid precursors or by sol-gel chemistry. These techniques have to be applied to astronomically relevant materials (see, e.g, Colangeli *et al.* (2002)). A particularly promising technique is laser pyrolyis which allows the production of size-selected nanoparticles of well-defined composition. Spectroscopy of the nanoparticles can be performed by conventional powder techniques, matrix isolation spectroscopy or with new intensive infrared light sources such as free electron lasers and synchrotron facilities. In addition, the luminescence properties of nanoparticles can be extremely important as it is the case for silicon nanoparticles. In order to reach a deeper understanding of the spectral behaviour of nanoparticles, a comprehensive analytic characterization of their internal structure by high-resolution electron microscopy and other techniques is absolutely necessary. This has been performed in many of the investigations of the Jena group (see, e.g., Jäger *et al.* (1999)).

5. Particles in Traps

Much of the present information on the role of dust as an active chemical component originates from bulk experiments. For example the interaction of gas phase species with grains is simulated by surface science experiments with macroscopic surfaces (Pironello *et al.* 1999). For experiments with grains, e.g. extinction measurements, large quantities of dust are necessary to obtain sufficient signal. Therefore most experimental results are congested by size and shape variations or variations in the chemical composition.

In order to overcome this problem and to characterize individual particles, a new approach has been developed in the Chemnitz group which uses the electrodynamical trapping technique. The benefit of the trapping device lies in the combination of the following features: (i) long time trapping of a single particle; (ii) isolation of the particle with respect to disturbing surfaces and gases, i.e., UHV and variable temperature conditions; (iii) very good localization (micrometre range) of the particle. The corresponding density can be as high as 10^{12} cm^{-3}, which makes it perfectly suited for optical experiments, and (iv) non-destructive and high resolution mass determination.

These features are operational in a 3D-quadrupole trap with an optical detection scheme for scattered light. The light signal is modulated by the particle's secular motion, the frequency of which is proportional to the particle's Q/M ratio. Frequency determination is achieved by Fourier analysis. A thorough description of the apparatus and first results have been published recently (Schlemmer et $al.$ 2001). Controlled charging/discharging of the particle in steps of single elementary charges leads to the determination of the absolute charge and thus also of the absolute mass. Presently a mass resolution ($\Delta m/m$) of about 10^{-4} for a single 500 nm SiO_2 particle in a 10 second measurement is routinely obtained. Integration over longer periods of time improve the resolution to the ppm regime.

Due to the long term stability of the rather robust experimental setup, the particle's Q/M ratio can be followed over weeks and makes the trap an ideal tool for systematic studies of the adsorption and desorption of molecules. As an example the adsorption of C_{60} molecules has been recorded with sub-monolayer resolution. Temperature programmed desorption (TPD) is a standard surface technique in order to determine the binding energies (or sublimation temperatures) of molecules to a surface (Fraser et $al.$ 2001). In the nanoparticle experiment TPD has been utilized by IR-laser heating of the trapped particle (Schlemmer et $al.$ 2002a).

The quadrupole trap for nanoparticles is more than just a scale. Thanks to the non-destructive high-resolution mass and charge determination, processes changing the mass as well as the charge can be monitored online. As a first example of such an experiment, the emission of secondary electrons upon electron bombardment of a 500 nm SiO_2 particle has been observed (Schlemmer et $al.$ 2002b). Future experiments make use of the good localization of the particle in the trap. Light scattering experiments on particles and agglomerates are presently performed in the Jena group. The interaction of particles with synchrotron radiation is studied in a new experiment. Light scattering in the VUV and soft X-ray regime from a well characterized trapped particle is one future objective. Fluorescence upon X-ray absorption (EXAFS and NEXAFS) will give information on the chemical and structural composition of the particle. Using short wavelengths Mie-scattering can be extended to much smaller particles and will reveal information on the size, shape and composition of dust particles.

6. Conclusions

The investigation of the spectral features of nanoparticles is a relatively new field in the context of astronomical missions with spectroscopic capabilities. It requires new initiatives to get the necessary fundamental data. An example is the identification of the ERE with silicon nanoparticles. This identification was recently questioned on the basis of the lack of observational evidence for a feature at 20 μm which would be produced by an oxide mantle around the silicon nanoparticles (Li & Draine 2002). However, the surface of silicon nanoparticles in space is more likely saturated by hydrogen atoms (no oxide feature) or the particles can be embedded in a larger matrix environment (no emission feature because of the lack of transient heating). In addition, it is not clear at all if the emission of the small oxide layer can be treated with

bulk optical properties. Progress in this area can only be reached with additional dedicated measurements.

The investigation of nanoparticles is a major future direction for quadrupole trapping. Production, isolation, trapping, and detection of very small particles is the technical challenge which has to be solved in coming years. One way of producing isolated carbon nanoparticles and measuring their optical emission was described in the pioneering work by Rohlfing (1988).

Acknowledgments

REFERENCES

Bockelée-Morvan, D., Gautier, D., Hersant, F., Huré, J.-M., Robert, F. 2002, *A&A*, **384**, 1107.

Boulanger, F., Pérault, M. 1988, *ApJ*, **330**, 964.

Braatz, A., Ott, U., Henning, Th., Jäger, C., Jescheke, G., *Meteoritics and Planetary Science*, **35**, 75.

Colangeli, L., Henning, Th., Brucato, J.R. *et al.* 2002, *Astron. Astrophys. Rev.*, in press.

Desert, F.-X., Boulanger, F., Puget, J.L., 1990, *A&A*, **237**, 215.

d'Hendecourt, L., Joblin, C., Jones, A. (eds.), 1999, *Solid Interstellar Matter: The ISO Revolution*, Berlin: Springer.

Dorschner, J., and Henning, Th. 1995, *Astron. Astrophys. Rev.*, 6, 271.

Draine, B.T., and Aigen Li, 2001, ApJ, **551**, 807.

Fraser, H.J., Collings, M.P., McCoustra, M.R.S., Williams, D.A. 2001, *MNRAS*, 327, 1165.

Frenklach, M., Feigelson, E., in: Pendleton, Y.J., Tielens, A.G.G.M. (eds.), 1997, *From Stardust to Planetesimals*, ASP Conf. Ser. 122, p.107.

Guillois, O., Ledoux, G., Reynaud, C., 1999, *ApJ*, **521**, L133.

Henning, Th. 1998, *Chem. Society Reviews*, **27**, 315.

Henning, Th. (ed.), 2002, Astromineralogy, Berlin: Springer, in preparation.

Jäger, C., Henning, Th., Schlögl, R., Spillecke, O., 1999, *J. Non-Cryst. Solids*, 258, 161.

Ledoux, G., Guillois, O., Huisken, F., Kohn, B., Porterat, D., Reynaud, C. 2001, *A&A*, **377**, 707.

Pironello, V., Liu, C., Roser, J.E., Vidali, G. 1999, *A&A*, **344**, 681.

Rohlfing, E.A., 1988, *J. Chem. Physics*, **89**, 8103.

Schlemmer, S., Illemann, J., Wellert, S., Gerlich, D. 2001, *J. Appl. Physics*, **90**, 5410.

Schlemmer, S., Wellert, S., Windisch, F., Gerlich, D., 2002a, *Appl. Phys. A.*, submitted.

Schlemmer, S., Illemann, J., Wellert, S., Gerlich, D., 2002b, in preparation.

Schnaiter, M., Mutschke, H., Dorschner, J., Henning, Th., Salama, F. 1998, *ApJ*, **498**, 486.

Schnaiter, M., Henning, Th., Mutschke, H., Kohn, B., Ehbrecht, M., Huisken, F. 1999, *ApJ*, **519**, 687.

Aigen Li, Draine, B.T. 2002, ApJ, **564**, 803.

von Helden, G., Tielens, A.G.G.M., von Heijnsbergen, D., Duncan, M.A., Hony, S., Waters, L.B.F.M., Meijer, G. 2000, *Science* **288**, 313.

Witt, A.N., Gordon, K.D., Furton, D.G. 1998, *ApJ*, **501**, L111

Laboratory Studies of the Optical Properties and Condensation Processes of Cosmic Dust Grains

M. M. Abbas[1], P. D. Craven[1], J. F. Spann[1], D. Tankosic[2], A. LeClair[2], E. West[1], R. Sheldon[2], W. K. Witherow[2], D. L. Gallagher[1], M. L. Adrian[1], G. J. Fishman[1], J. D. Fix[2], M. Horayani[3], I. Mann[4], D. A. Mendis[5], J. A. Nuth[6], and M. Rosenberg[5]

[1] *NASA-Marshall Space Flight Center, Huntsville, Alabama*
[2] *University of Alabama at Huntsville, Huntsville, Alabama*
[3] *University of Colorado, Boulder, Colorado*
[4] *Institut fr Planetologie and ESA Space Department, Mnster, Germany*
[5] *University of California, San Diego, California*
[6] *NASA-Goddard Space Flight Center, Greenbelt, Maryland*

1. Summary

A laboratory facility for conducting a variety of experiments on single isolated dust particles of astrophysical interest levitated in an electrodynamics balance has been developed at NASA/Marshall Space Flight Center. The objective of the research is to employ this experimental technique for studies of the physical and optical properties of individual cosmic dust grains of 0.1-100 micron size in controlled pressure/temperatures environments simulating astrophysical conditions. The physical and optical properties of the analogs of interstellar and interplanetary dust grains of known composition and size distribution will be investigated by this facility. In particular, we will carry out three classes of experiments to study the microphysics of cosmic dust grains. (1) Charge characteristics of micron size single dust grains to determine the photoelectric efficiencies, yields, and equilibrium potentials when exposed to UV radiation. (2) Infrared optical properties of dust particles (extinction coefficients and scattering phase functions) in the 1-30 micron region using infrared diode lasers and measuring the scattered radiation. (3) Condensation experiments to investigate the condensation of volatile gases on colder nucleated particles in dense interstellar clouds and lower planetary atmospheres. The condensation experiments will involve levitated nucleus dust grains of known composition and initial mass (or m/q ratio), cooled to a temperature and pressure (or scaled pressure) simulating the astrophysical conditions, and injection of a volatile gas at a higher temperature from a controlled port. The increase in the mass due to condensation on the particle will be monitored as a function of the dust particle temperature and the partial pressure of the injected volatile gas. The measured data will permit determination of the sticking coefficients of volatile gases and growth rates of dust particles of astrophysical interest. Some preliminary results based on measurements of photoelectric emission and radiation pressure on single isolated 0.2 to 6.6 micron size silica particles exposed to UV radiation at 120-200 nm and green laser light at 532 nm are presented.

2. Basic Equation of an Electrodynamic Balance

The electrodynamic balance, or a quadrupole trap, consists of a ring electrode kept at an alternating potential and two cap electrodes at opposite DC potentials. A charged particle in

the resulting electric field configuration is stably trapped and confined to the null point of the potential if the required stability conditions determined by the applied AC and DC potentials and the AC frequency are satisfied (e.g., Davis, 1985, Spann et al., 2001). For a stably trapped particle, the measurement of the DC potential required to balance the gravitational force, provides a measurement of the charge-to-mass ratio given by:

$$\frac{q}{m} = \frac{g z_o}{2 C_o V_{dc}}$$

With a single micron size charged particle stably trapped in the balance, evacuated to pressure of 10^{-5} to 10^{-6} torr, and cooled to astrophysical temperature, a variety of experiments may be conducted.

3. Dust Charging by Photoelectric Emissions

The dust grains in astrophysical environments are generally charged by electron/ion collisions or by photoemissions with UV radiation from nearby stars. Photon energies higher than the work function of the material are required for an electron to escape. In a photoemission process from solids, inelastic-scattering processes reduce the electron energy before the electron can escape. The interaction potential for a photoelectron from a grain is different from the corresponding potential of a grounded bulk sample.

Photoelectric efficiencies of particles, defined as the number of photoelectrons emitted/photons absorbed, and corresponding values of photoelectric yields for a neutral particle have been determined for individual negatively charged levitated silica particles of sizes of 0.2 to 6.62 μm size by exposing them to collimated beams of UV radiation of 120 to 160 nm wavelength (Figs. 1 - 2). These results remain to be compared with model calculations and with measurements for bulk materials.

Schematic of the Experimental Setup with Electrodynamic Balance
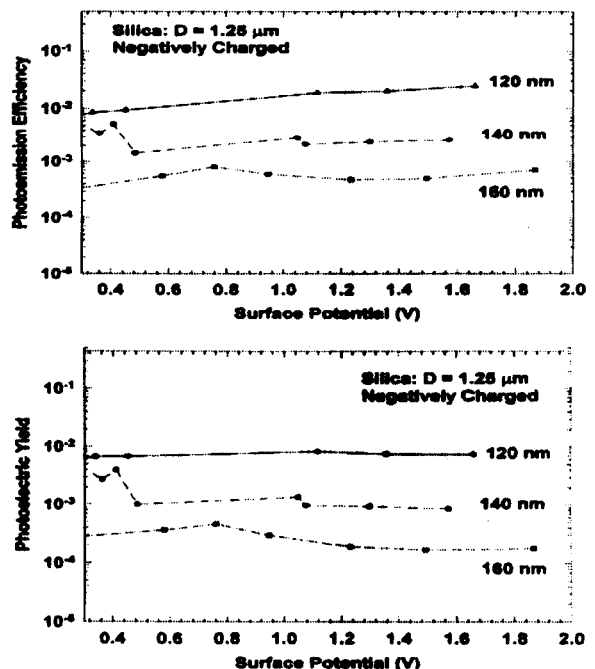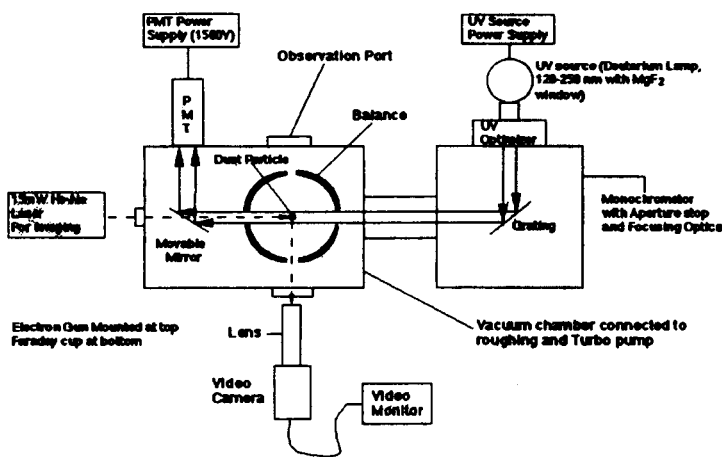
4.   Direct Radiation Pressure Measurements on Dust Particles

The electrodynamic balance provides a simple and accurate technique of measuring the radiation force F_rad on individual dust particles by balancing it with a change in the DC potential V_{dco} and calculating it with:

$$F_{rad} = F_g \frac{\Delta V_{dc}}{V_{dco}}, \quad (N)$$

where F_g of diameter D_d with an incident radiation power $P_m w$, and radiation pressure efficiency Q_e is:

$$F_{rad} = 3.33 \times 10^{-12} P_{mw} \frac{D_d^2}{D_B^2} Q_e$$

A comparison of the measured (dots) and calculated (solid line) values of the radiation pressure exerted by green laser light at 532 nm wavelength on silica particles of 1.5 μm and 3.0 μm is shown in Fig. 3).
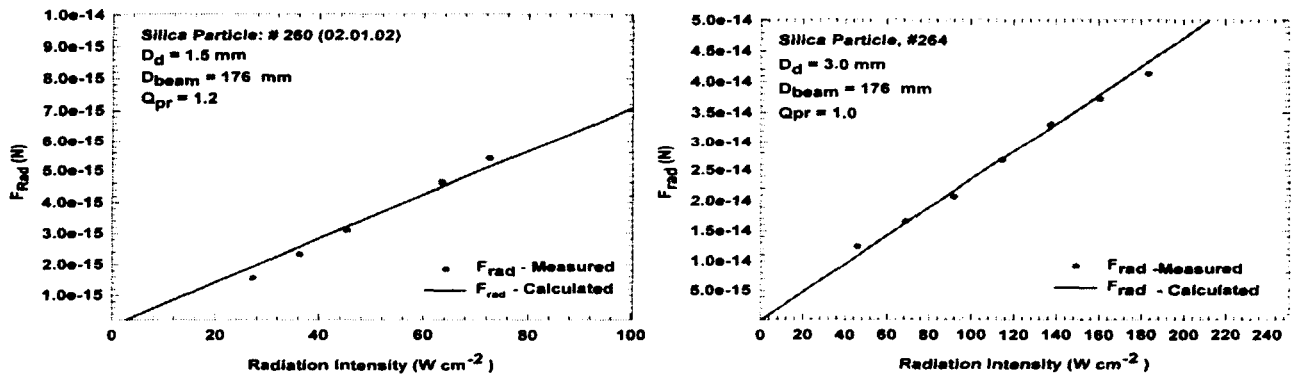
5.   Measurement of Infrared Optical Properties Individual Levitated Dust Grains

The physical nature and chemical composition of unprocessed interstellar dust grains can only be identified through their optical signatures and comparison with laboratory data. Laboratory data relating to the optical characteristics is generally based on measurements on bulk materials with the extinction coefficients obtained from theoretical calculations. The scattering phase function information, however, cannot be obtained from bulk material measurements. The laboratory technique considered here provides information about both the extinction coefficients and the phase function obtained from measurements made directly on individual dust grains and are expected to be a much more accurate description of the astrophysical environments. Specifically we will experimentally determine the complex refractive indices, the extinction coefficients, the scattering phase functions, and the polarization characteristics of isolated individual dust grains of interest in interstellar environments, in the infrared 1-25 μm spectral region (Figs.4- 5). The optical measurements will be made as condensation of ices on the core-mantle particles progresses with time. The spectral range will be extended to both shorter and longer wavelengths with the availability of suitable laser sources. The design and construction of the newly designed cryogenically cooled balance with the capability of making infrared scattering measurements is in progress and is expected to be completed in the near future.

6.   Measurement of Condensation of Ices on Individual Dust Grains

Theoretical and observational arguments indicate the cycling of dust between dense interstellar clouds where star and planet formation takes place, and the diffuse clouds in the interstellar medium. Small silicate particles that are blown out of cool evolved stars are believed to serve as condensate nuclei for volatile gases and organics in dense interstellar clouds leading to the formation of complex organic material. An understanding of the condensation processes is crucial to an increase in our knowledge of the evolution of the solar system bodies. Specifically, we will:

1. Investigate condensation processes in dense interstellar clouds by suspending single nucleus dust grains in the balance in simulated astrophysical environments, injecting volatile gases at a higher temperature, and monitoring the increase in the particle mass and the growth rate. Analogs of dust particles of astrophysical interest produced in the lab at GSFC will be used.

2. Investigate the growth rate of icy mantles on silicate grains of known composition and determine the sticking coefficients.

3. Compare the experimental measurements with calculations based on appropriate theoretical models, leading to a crucial increase in out knowledge of condensation processes in molecular clouds and formation of solar system bodies.
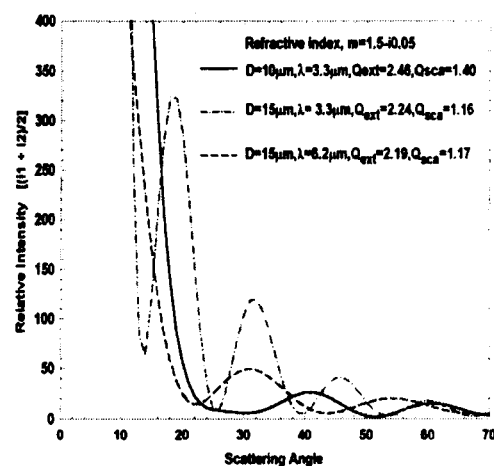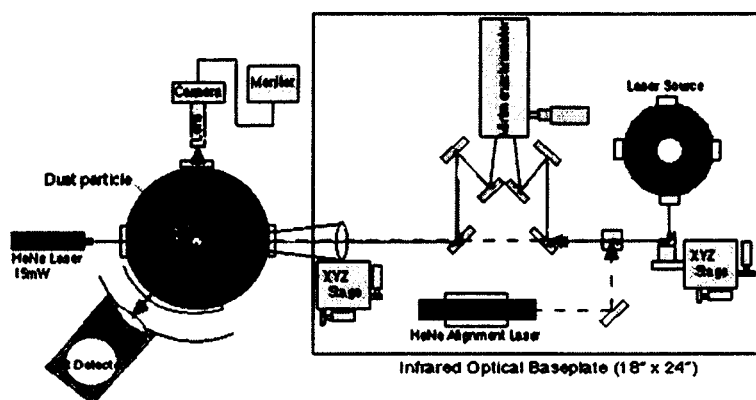
REFERENCES

Abbas, M., P. Craven, J. Spann, et al., Pysica Scripta, **T98**, 99-103, 2002.

Abraham, P., et al., Solid Interstellar Matter in the ISO Revolution, Ed., DHendecourt et al., Springer, 1995.

Allamandola, L. J., and A. G. G. M. Tielens, Ed., Interstellar Dust, Kluwer Academic Publishers, 1989.

Bernatowicz, T. J., and E. K. Zinner, (Eds.) Astrophysical Implications of the Laboratory Study of Presolar Materials, The American Institute of Physics, 1997.

Davis, E. J., Langmuir, **1**, 379-387 (1985).

DHendecourt, L., C. Joblin, A. Jones, in The ISO Revolution, Springer, 1996.

Draine, B. T., Ap. J. Suppl., **36**, 595-619, 1978, 2001.

Draine, B.T., and E. E. Salpeter, Ap. J., **231**, 77-94, 1979.

Giese, R., and E. Grun, in, Interplanetary Dust and Zodiacal Light, Ed., Elasser & Fechtig, Springer, 1976.

Goertz, C. K., Rev. Geophys., **27**, 272-292, 1989.

Greenberg, J. M., Ed., The Cosmic Connection, Kluwer Academic Publishers, 1996.

Henning, Th., in Solid Interstellar Matter in the ISO Revolution, Ed., DHendecourt et al., Springer, 1995.

Horanyi, M., Annu. Rev. Astron. Astrophys, **34**, 383-418, 1996.

Kimura, H., and I. Mann, *Ap. J.*, **499**, 454-462, 1998.

Levasseur-Regourd, A. C., and H. Hasegawa, Ed., *Origin and Evolution of Interplanetary Dust*, Kluwer, 1991.

Mann, I., H. Kimura, *J. Geophys. Res.*, **105**, No. A5, 10317, 2000.

Mathis, J. S, *J. Geophys. Res.* **105**, **No. A5**, 10269, 2000.

Mendis, D. A. and M. Rosenberg, *Ann. Rev. Astron. Astrophys.* **32**, 419-463, 1994.

Moore, M. H., in, Solid Interstellar Matter in the ISO Revolution, ED. DHendecourt *et al.*, Springer, 1995.

Nuth III, J. A., S. L. Hallenbeck, and F. J. M. Reitmeijer, *J. Geophys. Res.* **105**, **No. A5**, 10387, 2000.

Salama, F., in, *Solid Interstellar Matter in the ISO Revolution*, Ed., DHendecourt *et al.*, Springer, 1995.

Sedlmayer, E., and D. Kruger, in *Astrophysical implications of the laboratory study of presolar materials*, Ed. Bernatowicz and Zinner, The American Institute of Physics, 1997.

Schutte, W. A, in *Solid Interstellar Matter: The ISO Revolution*, Springer, 1996.

Spann, J.F., M.M. Abbas, C. C. Venturini, and R. H. Comfort, *Physica Scripta*, **T89**, 147-153, 2001.

Tielens, A. G. G. M., *Ap. J.*, **499**, 267-272, 1998.

Wiscombe, W. J., *Mie Scattering Calculations: Advances in Technique and Fast Vector Speed Computer Codes* (1979), Document PB301388, NTIS, Springfield, VA, 1979.

Weingartener, J. C., B. T. Draine, *Ap.J. Suppl.*, **134**, 263-281, 2001.

Influence of Impurities on the mm-Wave
Absorption in Amorphous Ice

N. I. Agladze, J. P. Wrubel and A. J. Sievers

Lab. Atomic and Solid State Physics & the Ctr. Radiophysics and Space Research

Cornell University, Ithaca, NY

Abstract

Mm-wave properties of both high and low density amorphous phases of ice are investigated as a function of impurities. Doping with ionic (LiCl) or molecular (methanol) impurities decreases the difference in the mm-wave absorption coefficient between the HDA and LDA ice phases so that the HDA spectrum can be used as an analog for impure ice.

1. Introduction

Both high density and low density amorphous ices can be found in the frost on interstellar grains depending on the environment and formation conditions (Jenniskens 1995). Since astrophysical ices are expected to be impure, this work investigates the effect of two different kinds of impurities (ionic and molecular) on the mm-wave spectral properties of the two amorphous ice phases.

In 1984, Mishima et al. established (Mishima 1985) that high density amorphous (HDA) ice can be produced in the laboratory by compression of regular ice at 1 GPa and 77 K. At 120 K and atmospheric pressure the HDA phase transforms into the low density amorphous (LDA) phase, which in turn transforms into crystalline cubic ice at 150 K and finally into regular hexagonal ice at 225 K (Mishima 1985). The temperature dependant mm-wave absorption of HDA ice is typical of amorphous solids and is dominated by a broad distribution of two level systems (TLS) at low temperatures. The TLS absorption coefficient has a unique temperature dependent signature in that it becomes weaker with increasing temperature up to about 15 K. At higher temperatures the absorption coefficient again increases due to a phonon assisted tunneling relaxational mechanism. Such changes in the absorption coefficient of high density and low density amorphous ices produces temperature dependent spectral indices (Agladze 1996).

2. Experimental techniques

The spectroscopic samples of the HDA ice are produced by compressing regular ice Ih at liquid nitrogen temperature to 1.66 ± 0.2 GPa. The regular ice is made from HPLC grade water, degassed by triple freezing-thawing procedure and held in indium open-ended cups. These are placed in an 10 mm die set. The entire assembly is then immersed in liquid nitrogen. To prevent the ice from sticking to the anvils both are covered with a $6\mu m$ Teflon film. The thickness of the resulting amorphous ice cylinders used in these experiments varied from 0.4 mm to 15 mm. The samples are removed at atmospheric pressure while still at 77 K, mounted in the sample holder

while still under liquid nitrogen and the assembly is then inserted into a precooled transmission light pipe - detector cryostat.

Temperature dependent transmission spectra in the spectral region $2 - 30 cm^{-1}$ are measured with a lamellar Fourier transform spectrometer together with a germanium bolometer which operates at 0.3 K (Agladze 1996). At the conclusion of these measurements, heating the samples to 145 K and cooling back down to low temperatures prepares the LDA phase. Impurities of methanol (molecular type) in the range 1 to 7 mol%, and of LiCl (ionic type) in the range 0.5 to 5 mol% were used in the present work.

3. Experimental results

The high-density amorphous (HDA) phase has a large mm-wave absorption coefficient with strong temperature dependence, whereas the low-density amorphous (LDA) phase has an absorption coefficient smaller by a factor of 5, and it is practically temperature independent. See Agladze (1998) for more details. The LiCl impurity-induced contribution to the absorption coefficient for the HDA and LDA phases has been measured (Agladze 2001). The low temperature results are shown in Fig. 1(a). At 1.3 K the mm-wave absorption grows in strength with increasing LiCl content in the HDA ice, while for the LDA phase it first decreases and then increases for concentrations higher than 1.5 mol%.

Figure 1(b) presents the results for the molecular methanol doping of the HDA and LDA phases. With increasing methanol concentration the low temperature HDA ice absorption coefficient again increases. For the LDA phase it first decreases and then increases for concentrations higher than 3 mol%. It is proposed that due to phase segregation during freezing, the concentration of impurities is spatially inhomogeneous and that this spatial inhomogeneity is
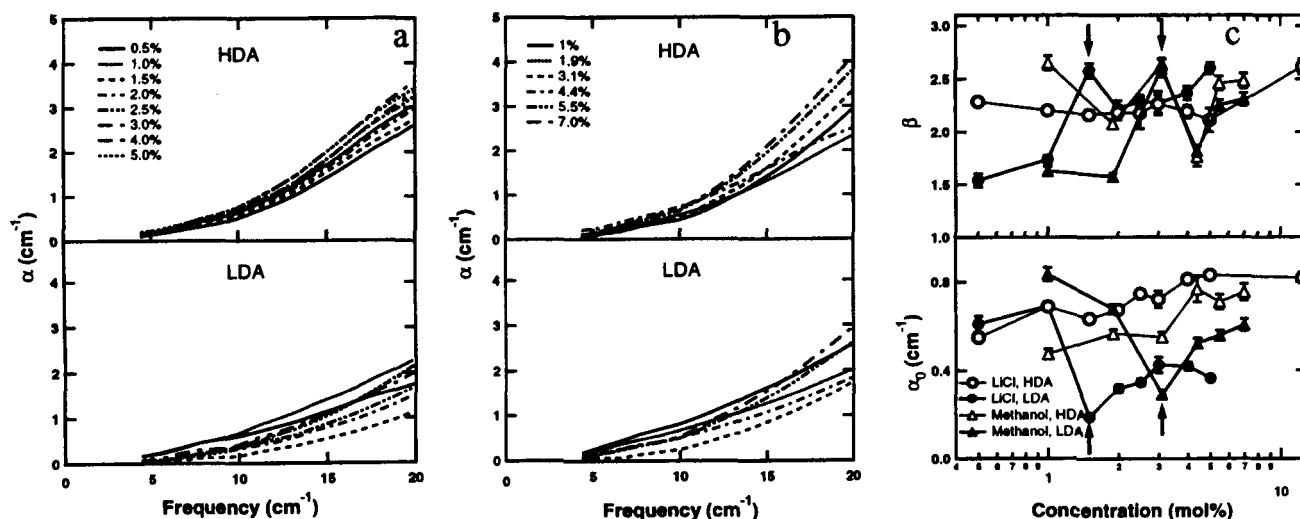
Fig. 1.— Low temperature HDA and LDA ice absorption coefficients versus frequency for different concentration of (a) LiCl, an ionic impurity and of (b) methanol, a molecular impurity. (c) Two parameter power law fits to the low temperature absorption coefficients for HDA and LDA ices as a function of impurity concentration.

These low temperature absorption coefficient data can be characterized by a simple power law with two parameters, namely, $\alpha = \alpha_0(\omega/10cm^{-1})^\beta$, where α_0 is the absorption coefficient at $10cm^{-1}$, is the frequency in wavenumbers $(1/\lambda)$, and β is the spectral index. From the power law fit to the absorption coefficient presented in Fig. 1(c), one observes that the minimum of α_0 coincides with the maximum of the spectral index β, both for methanol and LiCl impurities. The β maximum approaches the pure HDA ice value of 2.9 ± 0.1, suggesting that scattering due to the non-uniformities is minimal for that concentration.

Temperature jump measurements can be used to identify the TLS induced change of the absorption coefficient. In Figure 2(a) the HDA phase is compared for pure amorphous ice and those doped with 5 mol% LiCl and 7 mol% methanol when temperature is varied from 1.3 K to 11 K. There is no dramatic influence by the impurities on the temperature dependent part of the mm-wave absorption although the TLS effect is slightly reduced for methanol.

The temperature jump measurements give very different results for the doped LDA ices. Figure 2(b) shows that for an ionic type dopant (LiCl) the temperature dependent TLS absorption effect is increased several times, while for a molecular dopant (methanol) the size of the change is much more modest. The important find is that both dopants reduce the differences between the temperature dependent properties of the HDA and LDA ices. The change in the size of the TLS effect for all the concentrations are summarized with the temperature jump results presented in 2(c). Here the temperature-induced change in the absorption coefficient is shown at $10cm^{-1}$.
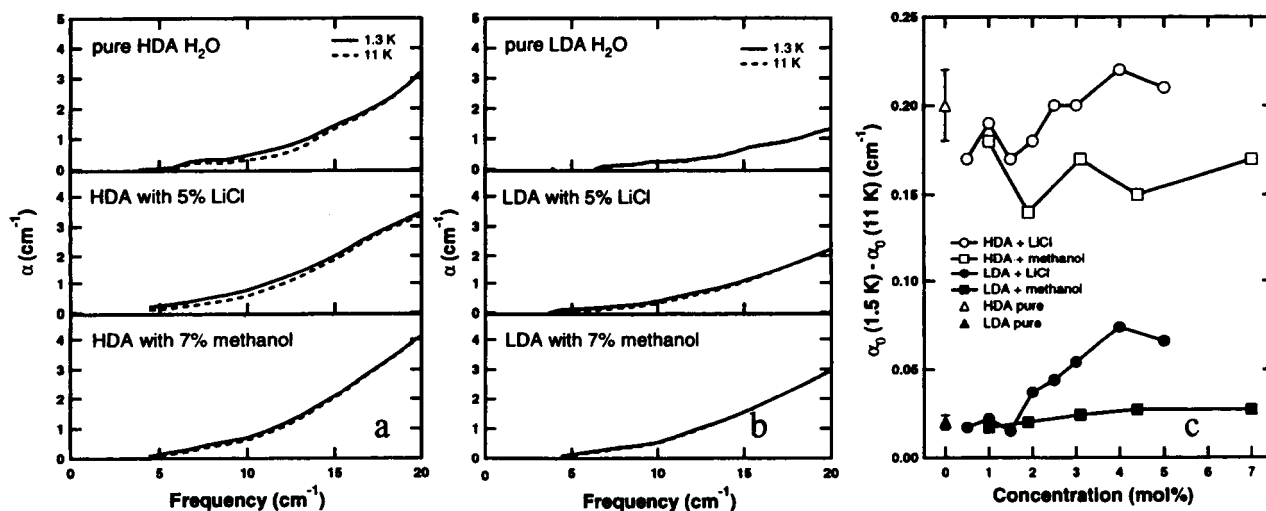
Fig. 2.— Temperature-jump experiments for different (a) HDA and (b) LDA ices to identify the TLS contribution. (c) Temperature induced absorption coefficients at 1 mm-wavelength for both HDA and LDA ices versus impurity concentration.

4. Conclusions

The general finding of our study is that the doping with ionic (LiCl) or molecular (methanol) impurities does not alter the temperature dependence of the absorption coefficient in the HDA phase, but greatly increases its value in the LDA phase. The temperature dependent absorption coefficient increases between 4 and 11 times for methanol and between 4 and 24 times for LiCl for these concentrations in comparison to the pure LDA ice. Since these impurities decrease the difference in the mm-wave absorption coefficient between the HDA and LDA ice phases we conclude that the HDA spectrum can be used to model the mm-wave absorption properties of impure amorphous ice.

REFERENCES

Jenniskens, P., Blake, D. F., Wilson, M. A. & Pohorille, A. 1995, *ApJ*, **455**, 389.

Mishima, O., Calvert, L. D. & Whalley, E. 1984, *Nature*, **310**, 393.

Mishima, O., Calvert, L. D. & Whalley, E. 1985, *Nature*, **314**, 76.

Agladze, N. I., Sievers, A. J., Jones, A. A. Burlitch, J. M. & Beckwith, V. W. 1996, *ApJ*, **462**, 1026.

Agladze, N. I. & Sievers, A. J. 1998, *Phys. Rev. Lett.*, **80**, 4209.

Agladze, N. I. & Sievers, A. J. 1998, *Europhys. Lett.*, **53**, 40.

Unification: UV & IR Observations of Interstellar Dust Along the Same Sightlines

Geoffrey C. Clayton[1], K. D. Gordon[2], M. J. Wolff[3], L. Valencic[1]

[1]*Louisiana State University*

[2]*Steward Observatory*

[3]*Space Science Institute*

1. New Observations

While efforts have been made to study interstellar dust in various Galactic environments at wavelengths from the x-ray to the radio, a single line of sight is rarely subjected to observations over a wide wavelength range. This is particularly true for the UV and IR regimes. The typical interstellar dust sightline used for UV studies has a small column of dust. These sightlines probe the diffuse ISM and avoid all but the very outer edges of dark or molecular clouds. IR studies of dust, on the other hand, concentrate on molecular bands of many different materials from H_2 to polycyclic aromatic hydrocarbons (PAHs). In general, large optical depths of dust in dense clouds are necessary for the formation of these molecules. So to a large extent studies of interstellar dust in the UV and IR have been two "separate worlds." The result has been models of dust grains which are strongly biased toward fitting observations in one wavelength regime or the other. The absence of sightlines for which both UV and IR data are available makes it difficult to reconcile the constraints derived separately from each wavelength regime.

Two features associated with mantles on dust grains are the 3.1 μm water ice and 3.4 μm C-H stretch features. In fact, only two early-type stars, for which UV extinction data exist, have been observed previously. Ultraviolet extinction curves can be obtained only for sightlines toward early-type stars with moderate amounts of dust reddening. Figure 2 clearly shows for HD 29647 (E(B-V)=1.1), and HD 283809 (E(B-V)=1.6) that the 3.1 μm ice feature can be detected for such sightlines. For the first time, we will be able to combine data from the UV and IR to investigate the effects on UV extinction of mantling on interstellar dust grains. Figure 1 shows the unusually weak 2175 Å bumps seen toward HD 29647 and HD 283809.
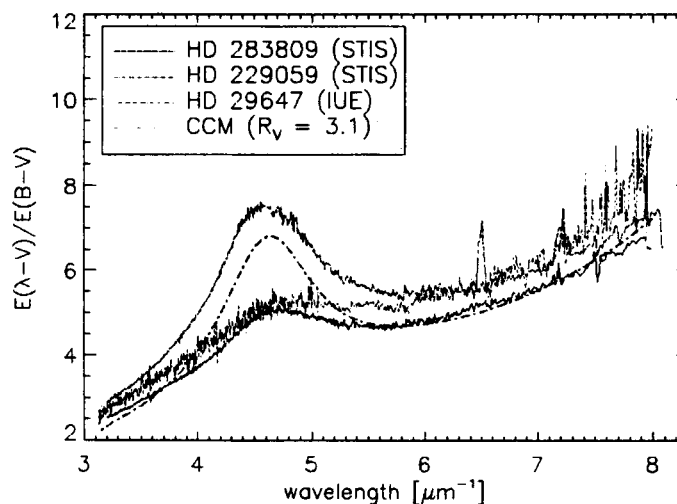
Fig. 1.— Extinction curves using STIS (HD 283809 & HD 229059) and IUE (HD 29647) for heavily reddened (E(B-V) ≥ 1.0) sightlines.
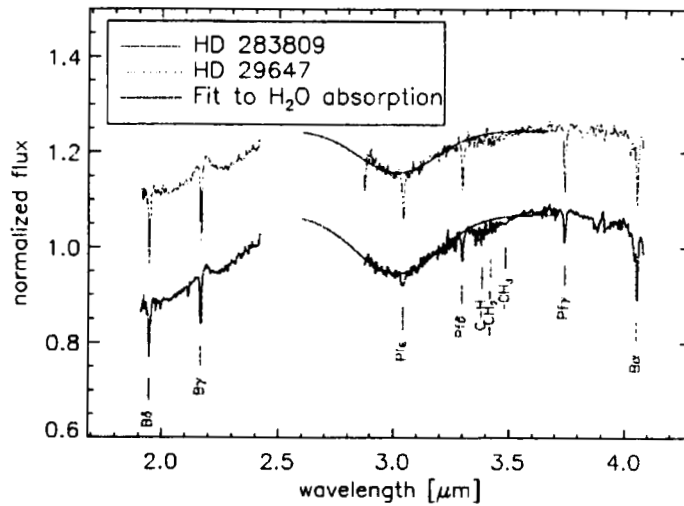
Fig. 2.— SPEX data obtained at IRTF. A blackbody curve has been removed from the spectra. Strong absorption due to water ice is seen in both stars. The 3.4μm feature may be present also.
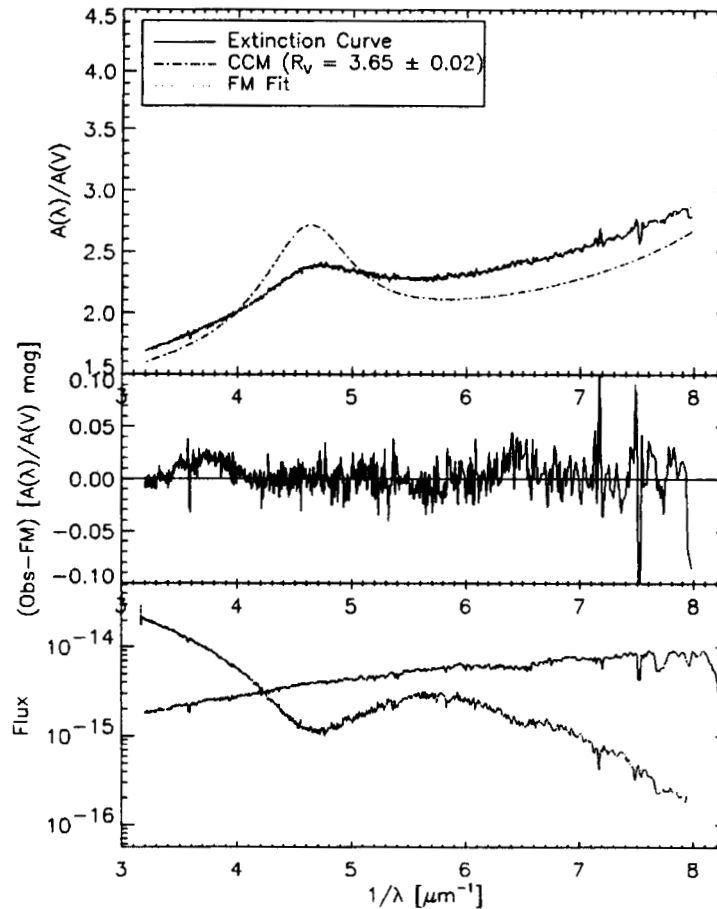
Fig. 3.— Left-hand side: HD 283809/HD 51038 Top panel: The measured extinction curve along with the Fitzpatrick & Massa (FM) fit is shown. The Cardelli, Clayton, & Mathis (1989, (CCM) curve for R_V =3.65 is plotted. Middle panel: The deviations from the FM fit are shown. Positive deviations correspond to absorption features. The apparent feature around 6.5 μm^{-1} is due to stellar mismatch. Bottom panel: The reddened and comparison star spectra are plotted. The comparison star spectrum has been scaled by a constant to fit on the plot with the reddened star spectrum.

2. Grain Models

Until fairly recently, the popular dust grain models were fairly simple, having two or three major grain components. The Mathis model (based largely on UV observations) consisted of power-law size distributions of separate populations of bare spherical silicate and graphite grains (Mathis, Rumpl, & Nordsieck 1977). The Greenberg model (based largely on IR data) consisted of large grains with silicate cores surrounded by organic mantles and small carbonaceous grains, possibly PAHs (e.g., Greenberg 1989). This kind of simple model has been valuable and gives reasonable fits to the observed Milky Way dust extinction, polarization and spectral features, but empirical evidence indicates that "real" interstellar grains are far more complex. This led Mathis & Whiffen (1989) to suggest that the grains are in fact porous composites of many small grains made up of silicates, amorphous carbon, and graphite.

We are using the Maximum Entropy Method (MEM) in conjunction with a range of grain models: starting with simple grain models consisting of separate populations of spherical dust grains and working towards more realistic (i.e., porous and composite) models of dust. The MEM, allowing an unprecedented objectivity, has shown that quantitative details of actual size distributions often seem to bear little resemblance to those of a power-law (cf. Kim, Martin, & Hendry 1994).

REFERENCES

Cardelli, J. A., Clayton, G. C., & Mathis, J. S. 1989, *apj*, **345**, 245.
Greenberg, J.M. 1989, in *IAU Symp. No.* 135, 345.
Kim, S.-H., Martin, P.G., & Hendry, P.D. 1994, *ApJ*, **422**, 164.
Mathis, J., Rumpl, W., & Nordsieck, K. 1977, *ApJ*, **217**, 425.
Mathis, J., & Whiffen, G. 1989, *ApJ*, **341**, 808.

Laboratory Surface Science - The Key to the Gas-Grain Interaction

M. P. Collings, J. W. Dever, H. J. Fraser[1], & M. R. S. McCoustra

School of Chemistry, University of Nottingham, University Park, Nottingham, U.K.

1. Introduction

It is widely recognised by the astronomical community that understanding the chemical process- ing of molecular gas clouds is the key to understanding aspects of the physics of star formation (24, 25), and possibly to understanding the origin of life itself (3). Central to this is the recognition that physical and chemical processes occurring at the surfaces of interstellar grains are crucially impor- tant. Grains provide surfaces upon which a variety of reactions occur, and allow condensation of ices which, when irradiated by photons and cosmic rays, are chemical nanofactories in which more complex molecules are synthesised. The basis of this chemistry is the adsorption and desorption of atoms and molecules from the grains themselves, under both reactive and non-reactive conditions.

As a field of research, surface science has existed for some forty years, since the development of vacuum technology sufficient to achieve ultrahigh vacuum (UHV) conditions. One of the main forces driving the field has been the study of heterogeneous catalysis for industrially important reactions. In such research, a reductionist approach is required - an extremely complex system is simplified to a level where parameters can be controlled and varied individually. The behaviour of the complex system is then understood through a knowledge of the behaviour of the system's many components.

In some respects, interstellar ices are not dissimilar systems to those involved in heterogeneous catalysis. They are complex mixtures with a composition and structure that is variable and not yet fully characterised. The chemistry that occurs within such ices and on its surface, while perhaps not strictly heterogeneous catalysis, can most readily be studied by reducing the ice matrix to a controlled and simplified system. The conditions of low temperature and pressure in the ISM make interstellar ice analogues ideally suited for study in a cryogenic UHV apparatus using existing surface science techniques. Indeed, the value of surface science to the study of these aspects of astrophysics has been recognised. Of forty eight articles in a recent volume the journal *Surface Science*, which was dedicated to a review of the future directions of the field, three dealt with astrophysical applications (9, 14, 26).

It is well known from laboratory studies that water ice can exist in a number of phases under con- ditions of low temperature and pressure (10, 11). Water adsorbed at temperatures prevalent in most molecular clouds ($<$ 30K) will form a high density amorphous phase, I_{hda}, which has a highly porous structure (22, 12). When this phase is heated, a transition to less porous, low density amorphous phase, I_{lda}, occurs gradually over the 32 $\sim$ 80K temperature range (10). Water ice adsorbed in this temperature range will also show a graduated mixture of the two phases. At higher temperatures, the I_{lda} phase crystallises to a cubic structure, I_c, (21) which, under conditions applied in our laboratory, occurs near to 140K.

2. Experimental

Experiments were performed in a UHV chamber that has been described in detail elsewhere (8). Briefly, the apparatus features two analytical techniques - temperature programmed desorption (TPD) and reflection-absorption infrared spectroscopy (RAIRS). This form of infrared spectroscopy has both advantages and disadvantages over the more commonly used transmission infrared spectroscopy. The

---

principle disadvantage is that astronomical spectra are of the transmission form, and therefore experimental RAIR spectra can not be compared directly with them. However, as RAIRS is performed in grazing incidence from a metal substrate, the resulting enhancement of the p-polarised electric field at the surface confers a sensitivity advantage of the order of fifty-fold, and introduces an additional metal surface selection rule that can provide information on the orientation of molecules at the surface. Thus, in a surface analysis experiment, RAIRS can be considered a more powerful technique than transmission infrared spectroscopy. The growth of ice films is calibrated against adsorption on a quartz crystal microbalance (QCM). A value of mass per unit area is obtained, which can be converted to a film thickness using literature values of density and porosity (10, 13). A copper plate covered by a film of polycrystalline gold serves as a sample. This can be cooled to a base temperature of less than 8K by a closed cycle helium cryostat, and heated to well above room temperature while the cryostat is still operating. A base pressure of 10^{-10} mbar is routinely achievable in the chamber, while adsorption of ices is usually performed in the $10^{-7} \sim 10^{-6}$ mbar range. The base pressure of 10^{-10} mbar (corresponding to particle density of $\sim 2 \times 10^6$ cm^{-3}) is several orders of magnitude higher than most dense regions of molecular clouds. However, H_2 is by far the most abundant molecule contributing to the background pressure in our experiment, and so the conditions in the UHV chamber remain a reasonable approximation of the molecular cloud environment. The importance of UHV conditions is demonstrated by considering the rate of adsorption of background gas as a function of pressure. The rate of accumulation of adsorbed material in monolayers per second is

$$rate = SnP/(2\pi m k_B T)^{1/2} \tag{1}$$

where S is sticking probability, n is the surface density of the adsorbate layer (m^{-2}), P is pressure (Pa), m is the mass of the molecule (kg), k_B is the Boltzmann constant, and T is temperature (K). The time required for adsorption of a complete monolayer from the background gas is plotted in fig. 1 as a function of pressure, for molecules of mass 0.018 kg mol^{-1} (i.e. water) at room temperature, assuming a sticking probability of 1 (reasonable for a surface at < 100K) and a surface density of 10^{19} m^{-2}. As is shown, a complete monolayer of adsorbate is accreted in several hours at UHV pressures. At a base pressure typical of high vacuum (HV) experiments (10^{-7} mbar), this occurs in only a few seconds. Over many hours of an experiment, this may represent many thousands of layers of background contaminant. This may dramatically alter the nature of catalytically important surface sites.

3. Results

The results of our temperature programmed desorption experiments for water have been published previously (7). A single desorption peak was observed, with no distinction between multilayer (solid) and monolayer (interfacial) water. This behaviour is the result of hydrogen bonding, which induces a stronger interaction between neighbouring water molecules than exists between water and the gold surface. The desorption of water was modelled using a simple stochastic integration package[2] and a zeroth order desorption process was found to fit the experimental desorption profiles much more accurately than a first order process, as should be expected for the desorption of a solid film. The optimised model produced the kinetic equation:

$$desorption\ rate = \nu[H_2O(s)]^n\ exp\{-E_a/RT\} \tag{2}$$

---

where the pre-exponential factor, ν, is $10^{30\pm2}$ molecules $cm^{-2}\ s^{-1}$, the activation energy for desorption, E_a, is 48.0 ± 0.5 kJ mol^{-1}, and the reaction order, n, is 0, so that the desorption rate is independent of the surface concentration of water molecules, $[H_2O(s)]$. The model was then adjusted to represent the desorption of water in the ISM. The heating rate was reduced to 10^{-9} K s^{-1}, which is typical of heating in some hot core regions (23). The results, plotted in fig. 2, show a sharp desorption of water near to 110K. Temperature programmed desorption studies were also performed for an 'ice mantle' consisting of a layer of I_{hda} with a layer of CO adsorbed over it. Since H_2O and CO are, respectively, the most abundant species in the hydrogenated (polar) and non-hydrogenated (apolar) layers of an ice mantle, this experiment can be considered a simple model of an 'onion layered' mantle structure (1). The desorption characteristics of the water layer were not effected by the presence of the CO, and are not presented. In this experiment ^{13}CO was used to avoid any interference from contaminant N_2. However, experiments with ^{12}CO (not presented) show no difference between the labelled and unlabelled CO. There are four distinct desorption phases in the TPD traces shown in fig. 3. Firstly, a zeroth order desorption occurs for higher CO exposures at about 25K, which from a comparison to TPD results for CO adsorbed alone on a gold surface (not presented), is found to be desorption of CO from a solid (multilayer) environment. A broad desorption in the 30 to 70K range results from desorption of CO from interfacial sites on the H_2O surface. Assuming this desorption to have first order kinetics, an adsorption energy of 10 kJ mol^{-1} is estimated from a Redhead analysis (17), in good agreement with theoretical calculations of the bonding strength of CO to H_2O (2). There is evidence of multiple desorption states in this interfacial peak, however, detailed analysis will be presented in a future publication. A sharp desorption is also apparent at roughly 140K, equivalent to a binding energy far too high to result from CO desorbing from an interfacial site. However, this temperature is co-incidental with that at which the amorphous water phase crystallises, suggesting that this 'molecular volcano' desorption occurs as trapped CO is released during the phase transition. Such behaviour has been previously studied with TPD using a H_2O/CCl_4 system (21), and has also been observed for the H_2O/CO system in other types of experiments (18, 15). However, in all of these cases, the trapped species was adsorbed below the water film, or as an intimate mixture. Here, the CO was absorbed onto the H_2O, implying the CO diffuses into the porous structure of the I_{hda} film, and by some mechanism becomes trapped. A small peak, barely visible on the scale in fig. 3, occurs near to 160K, coincidental with desorption of H_2O. This indicates that not all of the CO that becomes trapped is released in the molecular volcano desorption. The extent of CO entrapment was found to
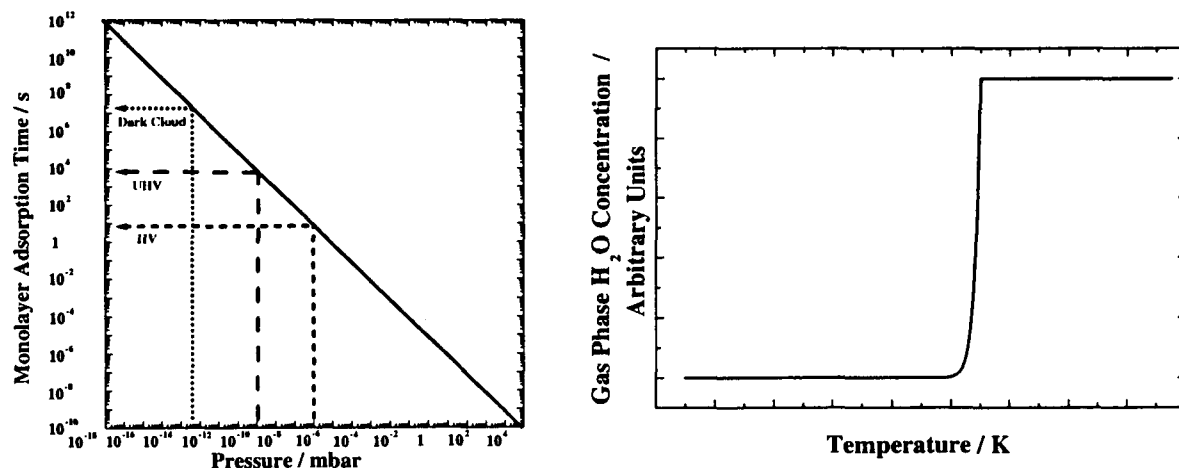
Fig. 1.— (LEFT) The rate of adsorption of room temperature gas phase H_2O on a cold surface (sticking prob = 1) as a function of pressure, assuming a surface density of 10^{19} m^{-2}.

Fig. 2. (RIGHT) Simulation of zeroth order desorption of a ~ 0.06 μm H_2O film, heating rate = 10^{-9} K s^{-1}.

vary with the temperature of water adsorption (5). In a set of experiments where the H_2O and CO exposures where kept constant at 57 and 0.07 μg cm^{-2} respectively, the H_2O film was adsorbed at varied temperature, then the sample cooled to 8K before subsequent CO adsorption. In a I_{hda} film adsorbed at 8K, close to half of the CO becomes trapped at above the temperature for interfacial CO desorption. However, as the temperature of water adsorption was increased over the 30 to 70K range, which should have resulted in a gradual change in the structure to the I_{lda} phase, the extent of trapping was reduced to zero. Therefore, the mechanism that causes CO entrapment must be related to this amorphous phase transition. The H_2O/CO system has also been investigated by RAIRS. The RAIR spectrum of the CO stretch region for a CO overlayer on I_{hda} is shown in fig. 4. Two sharp features at 2143.3 and 2138.6 cm^{-1} are, respectively, the longitudinal and transverse modes of the C-O stretch for solid CO (4). Lydane-Sachs-Teller (LST) splitting of this type can only observed in transmission if the infrared experiment is sensitive to p-polarised radiation only. The film of CO and H_2O ice was then annealed for five minutes at progressively higher temperatures. Between each anneal temperature, the sample was cooled to 8K, and an additional RAIR spectrum recorded. All changes in the spectra are, therefore, irreversible. Annealing to a temperature of 15K, although too low to induce desorption of solid CO, results in the loss of intensity in the solid CO features and the growth of intensity in a new feature at 2153 cm^{-1}, which is associated with CO adsorbed on dangling bond sites on the surface of the water (20, 6, 16, 2). This behaviour is strong evidence for the diffusion of solid CO into the porous structure of the I_{hda} film. Annealing to 20K results in the complete loss of the solid CO features, and the appearance of a two peak profile typical of CO in a water environment (19, 20, 16, 2, 5). The 2153 cm^{-1} feature is diminished and then disappears with annealing through the 30 to 80K temperature range, as the amorphous phase transition occurs. This is unsurprising, as the less porous I_{lda} phase has a vastly reduced internal surface area. The spectra also show a strong CO feature present up to 130K, indicating CO entrapment. The behaviour of the

Fig. 3.— (LEFT) TPD of increasing exposures of CO (up to 0.4 μg cm^{-2}) adsorbed at 8K on to H_2O (17 μg cm^{-2} ~ 0.2 μm) adsorbed at 8K, heating rate = 0.08K s^{-1}.

Fig. 4. (RIGHT) RAIR spectra of the CO stretch region of 0.35 μg cm^{-2} CO adsorbed over 57 μg cm^{-2} H_2O (~ 0.2 μm) at 8K; samples have been annealed for 5 minutes at the temperatures indicated; sharp features in the 45K spectrum are due to gas phase CO transitions, resulting from contamination of the dry air in the purge of the IR optics; increased baseline noise in the 45K, 80K and 130K spectra result from a slight mismatch between the sample spectrum and background spectrum used in data processing.

195

also show a strong CO feature present up to 130K, indicating CO entrapment. The behaviour of the CO/H_2O system under laboratory warm up conditions can be summarised as follows (5). Water ice is adsorbed in the I_{hda} phase at 8K. CO adsorbed onto the water forms a layer of solid CO. As the film is heated, solid CO becomes sufficiently mobile to diffuse into the porous structure of the film, at temperatures as low as 15K. In the 20 to 30K temperature range, this diffusion process competes the diffusion of solid CO into the porous structure of the I_{hda} film. Annealing to 20K results in the complete loss of the solid CO features, and the appearance of a two peak profile typical of CO in a water environment (19, 20, 16, 2, 5). The 2153 cm^{-1} feature is diminished and then disappears with annealing through the 30 to 80K temperature range, as the amorphous phase transition occurs. This is unsurprising, as the less porous I_{lda} phase has a vastly reduced internal surface area. The spectra also show a strong CO feature present up to 130K, indicating CO entrapment. The behaviour of the CO/H_2O system under laboratory warm up conditions can be summarised as follows (5). Water ice is adsorbed in the I_{hda} phase at 8K. CO adsorbed onto the water forms a layer of solid CO. As the film is heated, solid CO becomes sufficiently mobile to diffuse into the porous structure of the film, at temperatures as low as 15K. In the 20 to 30K temperature range, this diffusion process competes with desorption of solid CO. By 30K, CO remains adsorbed only in interfacial sites, both on the external surface of the water film, and the much greater area of the internal surface of pores within the film. Over the 30 to 70K temperature range, desorption of CO from these interfacial sites competes with entrapment caused as the I_{hda} phase is transformed into I_{lda}. Trapped CO is released in an abrupt molecular volcano as the I_{lda} crystallises at 140K, and as the crystalline water desorbs at 160K.

4.   Implications and Conclusions

Our results demonstrate how a carefully designed and rigorous surface science experiment can contribute to the field of astrophysics, by providing accurate data on fundamental processes that occur on and in interstellar ices. The desorption kinetics of water have been evaluated in the laboratory and applied to interstellar conditions. The desorption behaviour of carbon monoxide has been shown to be more complex than can be understood simply from a knowledge of binding energies and desorption kinetics. The retention and release of CO in the ISM at unforeseen temperatures may impact on temperature dependent chemistry in both the gas and solid phases, and influence the star formation process. Some caution must be exercised when applying this model of CO desorption to the interstellar environment, as a variety of factors have yet to be incorporated. Energetic processing may cause structural changes in water ice, and it is not certain whether reactively formed ice will have same structure as condensed ice. Interstellar ices are a complex mixture of compounds, and treating their behaviour as the sum of the behaviour of binary systems may not always be appropriate. Such limitations to the model provide a direction for future research, as the complexity of the model and of our understanding of the system are built up though continued experimentation.

REFERENCES

(1) Allamandola, L. J., Bernstein, M. P., Sandford, S. A., & Walker, R. L. 1999, Space Sci. Rev., 90, 219.
(2) Allouche, A., Verlaque, P., & Pourcin, J. 1998, J. Phys. Chem. B, 102, 89.
(3) Bernstein, M. P., Sandford, S. A., & Allamandola, L. J. 1999, Sci. Am., July, 30.
(4) Chang, H. -C., Richardson, H. H., & Ewing, G. E. 1988, J. Chem. Phys., 89, 7561.
(5) Collings, M. P., Dever, J. W., Fraser, H. J., McCoustra, M. R. S., & Williams, D. A., 2003, ApJ, in print.
(6) Devlin, J. P. 1992, J. Phys. Chem., 96, 6185.
(7) Fraser, H. J., Collings, M. P., McCoustra, M. R. S., & Williams, D. A. 2001, MNRAS, 327, 1165.
(8) Fraser, H. J., Collings, M. P., & McCoustra, M. R. S. 2002, Rev. Sci. Instrum., 73, 2161.
(9) Greenburg, J. M. 2002, Surf. Sci., 500, 793.

(10) Jenniskens, P., & Blake, D. F. 1994, *Science*, **265**, 753.

(11) Jenniskens, P., Blake, D. F., Wilson, M. A., & Pohorille, A. 1995, *ApJ*, **455**, 389.

(12) Kimmel, G. A., Stevenson, K. P., Dohnálek, Z., Smith, R. S., & Kay, B. D. 2001a, *J. Chem. Phys.*, 114, 5284.

(13) Kimmel, G. A., Dohnálek, Z., Stevenson, K. P., Smith, R. S., & Kay B. D. 2001b, *J. Chem. Phys.*, 114, 5295.

(14) Madey, T. E., Johnson, R. M., & Orlando, T. M. 2002, *Surf. Sci.*, **500**, 838 .

(15) Notesco, G., & Bar-Nun, A. 1996, *Icarus*, **122**, 118.

(16) Palumbo, M. E. 1997, *J. Phys. Chem. A*, **101**, 4298.

(17) Rehead, P. A. 1962, *Vacuum*, **12**, 203.

(18) Sandford, S. A., & Allamandola, L. J. 1988, *Icarus*, **76**, 201.

(19) Sandford, S. A., Allamandola, L. J., Tielens, A. G. G. M., & Valero, G. J. 1988, *ApJ*, **329**, 498.

(20) Schmitt, B., Greenburg, J. M., & Grim, R. J. A. 1989, *ApJ*, **340**, 33.

(21) Smith, R. S., Huang, C., Wong, E. K. L., & Kay, B. D. 1997, *Phys. Rev. Lett.*, **79**, 909.

(22) Stevenson, K. P., Kimmel, G. A., Dohnálek, Z., Smith, R. S., & Kay, B. D. 1999, *Science*, **283**, 1505.

(23) Viti, S., & Williams, D. A. 1999, *MNRAS*, **305**, 755.

(24) Williams, D. A. 1993, in *Dust and Chemistry in Astronomy*, ed. T. J. Millar & D. A. Williams, (Bristol, IoP), 143.

(25) Williams, D. A. 1998, *Faraday Discuss., 109*, 1.

(26) Williams, D. A, & Herbst, E. 2002, *Surf. Sci.*, **500**, 823

The Laboratory Production of Complex Organic Molecules in Simulated Interstellar Ices

J. P. Dworkin,[1] S. A. Sandford,[2] M. P. Bernstein,[1] and L. J. Allamandola[2]

1) NASA-Ames Research Center, Moffett Field CA

2) SETI Institute, Mountain View CA

Abstract

Much of the volatiles in interstellar dense clouds exist in ices surrounding dust grains. Their low temperatures preclude most chemical reactions, but ionizing radiation can drive reactions that produce a suite of new species, many of which are complex organics. The Astrochemistry Lab at NASA Ames studies the UV radiation processing of interstellar ice analogs to better identify the resulting products and establish links between interstellar chemistry, the organics in meteorites, and the origin of life on Earth. Once identified, the spectral properties of the products can be quantified to assist with the search for these species in space. Of particular interest are findings that UV irradiation of interstellar ice analogs produces molecules of importance in current living organisms, including quinones, amphiphiles, and amino acids.

1. Quinones (Bernstein *et al.* 2001)

The polycyclic aromatic hydrocarbon (PAH) naphthalene was exposed to ultraviolet radiation in H_2O ice under astrophysical conditions, and the products were analyzed using infrared spectroscopy and high performance liquid chromatography (HPLC). Our HPLC analyses demonstrate that the UV photolysis of H_2O-naphthalene ices results in a mixture of unprocessed naphthalene and oxidized naphthalene compounds. The oxidized photoproducts include both alcohols and ketones. The main products are the two isomers of naphthalene bearing one hydroxy group (naphthols), and an isomer of naphthalene bearing two carbonyls (1,4- napthoquinone). In typical simultaneous deposition/irradiation experiments (equivalent to 30 minutes UV per 0.1 μm ice layer), 1-naphthol and 2-naphthol were observed to be produced with approximately 2.5% and 1.4% yields, respectively, relative to naphthalene. 1,4-Napthoquinone, the next most abundant product, is produced with roughly a 0.4% yield relative to naphthalene. It is interesting that 1,4-napthaquinones, further functionalized, often with a methyl group and a long isoprene chain, play essential roles in biochemistry. While best known as K vitamins and for their role as blood clotting co-factors, napthoquinones, such as the menaquinones, also perform key biochemical functions in organisms all across the tree of life. As one example, the Archaea *Thermoproteus tenax* use menaquinones in the reduction of elemental sulfur to H_2S as their main energy source.

2. Deuterium Enrichments in Meteoritic Aromatics (Sandford *et al.* 2001)

There are a number of processes by which interstellar PAHs can become deuterium enriched, including gas phase ion-molecule reactions, gas-grain reactions, and unimolecular photodissociation. In addition, we have recently shown that, in interstellar ices, PAHs can become

enriched in deuterium by the same ice photolysis processes that make the oxidized aromatics. Each of these various processes is expected to leave a distinctly different signature in the distribution of D enrichment in the PAH population. Ion-molecule reactions would be expected to preferentially deuterate the *larger*, while unimolecular photodissociation should D-enrich only the *smallest* ones. In contrast, in D- enriched interstellar ices, ice photochemistry should produce aromatic deuterium enrichments that are *independent* of PAH molecular size, but which should correlate with specific functional groups, namely the alcohols, ketones, and aliphatic rings produced when PAHs are UV irradiated in H_2O-rich ices. Thus, the regiochemistry of PAH D-enrichment in meteoritic materials, and correlation (or lack thereof) with the presence of specific functionalized aromatic compounds could place constraints on the relative contributions of different interstellar processes that acted on presolar PAHs. In light of the recent work of and the work reported above, searches for a correlation of D-enrichment with PAH size and oxidation state in meteoritic organics would be of particular interest.

3. Vesicles (Dworkin *et al.* 2001)

Laboratory simulations studied to identify the types of molecules which could have been generated in pre-cometary ices were conducted by forming a realistic interstellar mixed-molecular ice ($H_2O:CH_3OH:NH_3:CO = 100:50:1:1$) at ~15 K under high vacuum irradiated with UV from a hydrogen plasma plasma lamp. When the ice was warmed to room temperature there is an oily organic residue which remains. This material was extracted, dried, and analyzed in aqueous media via microscopy. We found that some components of the photochemical product produced water-insoluble fluorescent vesicles under these conditions. The vesicles are roughly 10 - 50 μm in diameter and have apparent internal structures on a 1 μm scale, which are presumably related to phase separations that occur within the organic components of the droplets.

The ready formation of these organic species from simple starting mixtures, the ice chemistry that ensues when these ices are mildly warmed, and the observation that the more complex refractory photoproducts show lipid-like behavior and self-organize into droplets upon exposure to liquid water suggest that extraterrestrial materials could exhibit a far greater range in chemical properties and behavior than previously thought. Given that these materials are readily created under simulated interstellar conditions and that they seem very similar to materials in primitive meteorites, it seems reasonable to seriously consider whether organic material generated in the interstellar medium could indeed have been delivered to the early Earth and contributed to the origin and early evolution of life. Delivery of this material via meteorites, comets, or interplanetary dust particles may have augmented the endogenously generated molecules for the origin or the early evolution of life. For example, since there are only a few known prebiotic synthesis routes for lipids, exogenous material may have been an important source of amphiphilic molecules or, in hydrated environments, vesicle-like structures.

4. Amino Acids (Bernstein *et al.* 2002)

The laboratory ices are comprised primarily of amorphous H_2O ice at 15 K, with 1-10% NH_3, 5-10% CH_3OH, and 1-10% HCN, relative to H_2O. These mixtures are representative of

the composition of interstellar ice mantles in dense clouds and towards protostars. For example, relative to H_2O, NH_3 has been observed at the 10% level in NGC 7538, higher towards GCS3, and CH_3OH has been commonly observed at the 5% level in comets, and higher towards protostellar objects. Thus, H_2O, CH_3OH, and NH_3 are reasonable starting materials because they are among the most abundant molecules frozen onto grains in the dense ISM. In addition, it is reasonable to include HCN since it is abundant in cometary coma and the dense ISM, where the majority of HCN should be frozen onto grains.

The molecules N-formyl glycine, cycloserine (4-amino-3-isoxazolidinone), and glycerol were detected in the organic residue *before* hydrolysis. This is significant as it demonstrates that the amino acids produced are not merely products of hexamethylenetrtramine (HMT) and/or HCN polymer hydrolysis, but exist as free molecules in the residue. After hydrolysis glycine, alanine, serine, glycerol, urea, ethanolamine, and glyceric acid were observed by GC-MS and/or HPLC.

Given that the water on Murchison was probably deuterium depleted, forming deuterium enriched amino acids by parent body aqueous chemistry poses a conundrum. However, low temperature interstellar ices are believed to be deuterium enriched, so deuterium enrichment of meteoritic amino acids would be a logical consequence of photochemistry of already enriched low temperature ices.

Recent detections of slightly non-racemic mixtures of amino acids in meteorites and astronomical observations of circularly polarized radiation (CPR) in OMC-1 have renewed interest in the hypothesis CPR may have led to such enantiomeric excesses. However, only relatively inefficient mechanisms based on selective destruction of a racemic starting population have been demonstrated in the laboratory. The result reported in this paper, of an apparently free racemic chiral molecule from an ice photolysis, now makes it possible to test whether circularly polarized radiation could yield non- racemic mixtures of amino acids by selective *formation* under astrophysically relevant conditions. We are currently exploring this avenue of research.

This demonstration of amino acid formation from an experimental ice simulation suggests that ice photochemistry could have contributed to the amino acids and other compounds (e.g., glycerol, vesicles, and quinones) observed in carbon-rich meteorites. Ice photochemistry potentially provides a single simple explanation for the presence, deuterium enrichment, and enantiomeric excesses of at least some of the amino acids in meteorites. Since our experimental conditions for ice photolysis were designed to simulate the environments of dense interstellar molecular clouds, the birthsites of new stars and planetary systems, the delivery of these materials to the surfaces of newly formed planets may be a universal process. The level of extraterrestrial molecular complexity is just now becoming apparent, and the full implications of this chemical input to the early Earth, and by implication to other habitable planets, are likely to be far reaching.

REFERENCES

Bernstein, Dworkin, Sandford, & Allamandola 2001, *MAPS*, **36**, 351.
Bernstein, Dworkin, Sandford, Cooper, & Allamandola 2002, *Nature*, **416**, 401.
Dworkin, Deamer, Sandford, & Allamandola 2001, *PNAS*, **98**, 815.
Sandford, Bernstein, & Dworkin 2001, *MAPS*, **36**, 1117.

Synchrotron FTIR Examination of Interplanetary Dust Particles: An Effort to Determine the Compounds and Minerals in Interstellar and Circumstellar Dust

G. J. Flynn

Dept. of Physics, SUNY-Plattsburgh, Plattsburgh, NY

L. P. Keller

NASA Johnson Space Center, Houston, TX

Abstract

Some interplanetary dust particles (IDPs), collected by NASA from the Earth's stratosphere, are the most primitive extraterrestrial material available for laboratory analysis. Many exhibit isotopic anomalies in H, N, and O, suggesting they contain preserved interstellar matter. We report the preliminary results of a comparison of the infrared absorption spectra of sub-units of the IDPs with astronomical spectra of interstellar grains.

1. Introduction

Astronomical spectroscopy provides information on the types and abundances of matter present in a variety of astrophysical environments. The infrared region of the spectrum is particularly useful in characterizing the dust. The Infrared Space Observatory (ISO) obtained spectroscopic data over the 2.5 to 200 μm wavelength range. To interpret these spectra it is necessary to have laboratory spectra of minerals in order to match the astronomical spectra to those of identified and well-characterized materials. We have focused our efforts on measuring the infrared spectra of minerals in the interplanetary dust particles (IDPs).

2. Interplanetary Dust Particles

The IDPs, fragments from asteroids and comets, range from about 5 to 50 μm in size. The IDP collection techniques are described in detail by Brownlee (4). Some of the IDPs are particularly interesting because they exhibit isotopic compositions distinctly different from Solar System materials. Messenger (9) reported that "cluster IDPs," which are so weak they break into many fragments on collection, frequently have non-solar D/H and ^{15}N contents. Messenger *et al.* (10) reported about 1% of the silicate grains in the first few cluster IDPs examined showed O isotopic anomalies consistent with them being interstellar. We have begun an infrared survey of the minerals in IDPs and a comparison of the spectra with the features detected by ISO and other infrared observing efforts.

3. Equipment

The infrared spectra were measured using two Fourier Transform InfraRed (FTIR) instruments, a Spectra-Tech IRus and a Nicollet Continuum, installed on the U4-IR and the U10B infrared beamlines at the National Synchrotron Light Source (NSLS). They have about 1,000

times the infrared flux of globar instruments, providing about 100 times better signal to noise. Synchrotron FTIR allows us to compare the absorption features of the silicates, sulfide, and organic matter in the IDPs to infrared features detected in interstellar and/or circumstellar environments.

4. Silicates

The IDPs contain three types of silicates: anhydrous silicates (olivine or pyroxene), hydrated silicates, and glassy (non-crystalline) silicates. Bradley (2) suggested that the glassy silicates found in the IDPs might be the common silicate in the interstellar medium. These silicates, called GEMS (for Glass with Embeded Metal and Sulfide), are typically about 0.5 μm in diameter. We examined GEMS in L2011*B6, one fragment of a cluster IDP. L2011*B6 is dominated by Fe-sulfide, but contains two small lobes of GEMS and some associated carbonaceous material. The infrared spectrum of these GEMS is an excellent match to the broad 9.5 μm feature of the interstellar silicate (3). This is the first time any single, naturally-occuring material has matched the width and shape of the amorphous interstellar silicate feature. This result suggests that either the GEMS in this IDP are interstellar grains or that grain production in our Solar System was sufficiently similar to that in the environment where the interstellar silicates were produced that very similar material was produced in our Solar System. Bradley (2) noted that some GEMS contain small silicate crystals (olivine or pyroxene), and suggested that GEMS were produced by radiation damage and alteration of these anhydrous silicate grains. The infrared spectra of those GEMS that contain anhydrous silicates show the sharp absorption features of olivine or pyroxene superimposed on the broad amorphous silicate feature. The infrared signatures of these GEMS are a good match to the 10 μm features of dust in the comas of Comet Halley and Comet Hale-Bopp, and the dust surrounding the young star HD163296 (see (3)).

5. Sulfide

ISO spectra of some cold, dense molecular clouds show an excess flux from 20 to 26 μm, attributed to FeO based on calculated FeO spectra (1). However, FeO is thermodynamically unstable and rare in meteorites, so it seems an unlikely candidate to explain this feature. Sulfur is known to be depleted in the gas phase in some cold molecular clouds, but the sulfur host was not known. Fe-sulfide, particularly pyrrhotite, is a common mineral in the IDPs and meteorites. Terrestrial pyrrhotite is a good match to the ISO feature (7), while the pyrrhotite in two IDPs exhibits a narrower absorption feature. The difference between IDP and terrestrial pyrrhotite absorption might be due to composition, since the pyrrhotite can span the range from FeS to $Fe_{0.8}S$. This result indicates that pyrrotite is a previously unidentified component of the dust in many cold circumstellar environments. It may have significant implications for astrobiology, since Cody *et al.* (5) suggest sulfide grains may have served as catalysts in the synthesis of organic molecules.

6. Organic Matter

C-H stretching features, near 3.4 μm, have been detected in interstellar grains. Li and Greenberg (8) proposed that the most abundant type of interstellar grain is a glassy silicate

mantled by refractory organic matter. Transmission Electron Microscope (TEM) examination of the IDP L2011*B6 shows carbonaceous material associated with the GEMS. Because the ultramicrotome section is only 70 nm thick, we have not obtained an infrared spectrum of this carbonaceous material. Other IDPs contain carbonaceous units large enough to be examined by infrared spectroscopy. These spectra show the C-H stretching features characteristic of aliphatic hydrocarbons (6).

Simple aliphatic molecules are chains of C-H_2 groups with C-H_3 groups on both ends. Thus the ratio of C-H_3 to C-H_2 absorption measures the length of the chain. The interstellar grains in Pendleton et $al.$ (11) have a higher C-H_3 to C-H_2 ratio than IDPs, suggesting interstellar aliphatic chains are, on average, shorter than those in IDPs. However, we have not yet obtained spectra of the carbonaceous material spatially associated with GEMS in IDPs. That material may be different from the dominant organic matter in IDPs.

7.   Future Work

Amorphous interstellar silicates have two strong features, the 9.5 μm feature matched by GEMS, and a feature near 20 μm. We have, thus far, been unable to measure the 20 μm absorption of the GEMS in L2011*B2. This remains a high priority. A new FTIR facility, that can measure spectra from 2.5 to 200 μm, has been constructed at the NSLS. This should allow us to compare the far-infrared features in IDPs to those measured by ISO.

Acknowledgments

REFERENCES

(1) J. Bouwman et $al.$, $Astron.$ $Astrophys.$, **360**, 213 (2000).

(2) J. P. Bradley, $Science$, **265**, 925 (1994).

(3) J. P. Bradley et $al.$, $Science$, **285**, 1716 (1999).

(4) D. E. Brownlee in $"Cosmic$ $Dust,"$ John Wiley & Sons, **295** (1978).

(5) G. Cody et $al.$ $Science$, **289**, 1337 (2000).

(6) G. J. Flynn et $al.$ in $"A$ New Era in $Bioastronomy,"$ ASP $Conf.$ $Series$, **213**, 191 (2000).

(7) L. P. Keller et $al.$, $Nature$, **417**, 148-150 (2002).

(8) A. Li and J. M. Greenberg, $Astron.$ $Astrophys.$, **323**, 566 (1997).

(9) S. Messenger, $Nature$, **404**, 968 (2000).

(10) S. Messenger et $al.$, $Lunar$ $&$ $Planet.$ $Sci.$ $XXXIII$, **Abs. #1887** (2002).

Nature of the Organic Signature in Dust from the Interstellar Medium: Laboratory Analog Studies

M.M. Freund

NASA Goddard Space Flight Center, Greenbelt, MD

F.T. Freund

Department of Physics, San Jose State University & NASA Ames Research Center

A. Staple and J. Scoville

Stanford University

Abstract

We measured the infrared (IR) ν_{CH} absorption bands around 3.4μm $(2800 - 3000cm^{-1})$ in large laboratory-grown magnesium oxide (MgO) and natural olivine single crystals that crystallized from $CO/CO_2/H_2O$ saturated melts. These bands are very similar to those from many astronomical sources, such as from dust in the diffuse interstellar medium (ISM), from the outflow of evolved stars, etc., and they are characteristic of aliphatic $-CH_2-$ and $-CH_3$ entities. In our laboratory single crystals the ν_{CH} bands arise from C-H entities that were introduced by a solid solution process, and that are imbedded in the mineral matrix in form of polyatomic C_n entities with C atoms bonded to O and to H. Heating breaks the C-H bonds, causing hydrogen to disperse in the mineral matrix. C-H bonds are re- established rapidly during annealing. We propose that dust grains probably contain the same type of internal C_n-H entities in solid matrix rather than an external organic layer covering the grain surfaces. Thermodynamical arguments show that the concentration of organics in solid solution in small grains can be comparable to that found in astronomical environments.

1. Introduction

Many dust models have been proposed to account for the optical extinction (O'Donnell *et al.* 1997), and the $C - H$ stretching bands (ν_{CH}) at 3.4μm seen in absorption in the IR spectra of diffuse sources in the ISM [for a recent review (Pendleton and Allamandola 2002)]. Most models contain either (a) small carbonaceous grains accounting for the "organic" signature, or (b) silicate grains covered by an ice mantle, photolytically processed to a residue of complex organics, or covered by a veneer of hydrogenated amorphous carbon (HAC). Generally, when solids grow from a gas-saturated melt, or grains condense in gas-rich environments, these gaseous components dissolve in the solid matrix. A relevant example is the dissolution of H_2O and CO_2 in MgO, which includes a solid-state redox conversion of the solutes to chemically reduced C and H (Freund *et al.* 2001). Therefore, laboratory-grown MgO and natural olivine crystals display an "organic" IR signature at 3.4μm, similar to that seen in diffuse ISM sources (Pendleton *et al.* 1994). In MgO and olivine the carriers of the organic signature consist of C_n-H-O entities inside the matrix. For single crystals, the total C-H concentration is low ($< 100ppm$), and the 3.4μm absorption bands are fairly narrow, as opposed to the broad astronomical absorption bands. However, using thermodynamical arguments, we show that the amount of dissolved "organics" is a strong function of grain size. This allows us to estimate the total C-H contents in small refractory grains, consistent with astronomical observations of the ν_{SiO}/ν_{CH} band ratios.

2. Results

For H_2O in MgO, we write a proton transfer reaction $H_2O + O^{2-} = 2OH^-$, where two H^+ substitute for one Mg^{2+}. Local charge balance is achieved when two OH^- sit next to the Mg^{2+} vacancy. This local configuration is not stable (King and Freund 1984). It converts by way of an electron transfer from O^{2-} to H^+ to $OH^- + OH^- = O_2^{2-} + H_2$. Similarly, CO_2 is taken up in solid solution, not necessarily as carbonate ($CO_2 + O^{2-} = CO_3^{2-}$), with concomitant electron transfer from O^{2-} onto C: $CO_2 + 2O^{2-} = CO_2^{2-} + O_2^{2-}$. Carbon is reduced to formate with C sitting off-center in the Mg^{2+} vacancy. The formate anion further dissociates: $CO_2^{2-} = CO^- + O^-$, with C entering interstitial sites. C and H_2 are subject to segregation into elastically relaxed portions of the mineral structure. When C-H and C-C bonds form at the expense of C-O bonds, polyatomic C_n-H-O entities, so-called "protomolecules", precipitate inside the matrix (Freund et al. 2001).

Fig. 1 shows ν_{CH} of a laboratory-grown, high purity MgO crystal and of a gem-quality olivine crystal from the upper mantle. The antisymmetric and symmetric ν_{CH} bands are associated with $-CH_2-$ and $-CH_3$ entities, respectively, typical of aliphatic organics with C-C single bonds. The $-CH_2-$ to $-CH_3$ line intensity ratio (taking the background corrected line depth) is quite large: $\sim 8:1$ in MgO and $10:1$ to $12:1$ in olivine. For MgO we also observed a weak ν_{CH} band near $3008 cm^{-1}(3.3\mu m)$, associated with an aromatic CH entity. The strong ν_{CH} bands in MgO are shifted by $4cm^{-1}$ to higher frequencies compared to those in olivine, and are slightly broader. After crushing the crystals, C_n-H-O entities can be solvent-extracted and thereby converted to organic molecules. Crushed MgO yielded predominantly short-chain carboxylic and dicarboxylic acids (Freund et al. 1999). Crushed olivine yielded longer chain-length fatty acids with $6 \leqslant n \geqslant 12$ (Gupta and Freund 1998), consistent with the different $-CH_2-/-CH_3$ line intensity ratios. Upon heating to $550 - 1000K$, the C-H bonds pyrolyze and the ν_{CH} bands disappear. Upon annealing at $300 - 450K$, they reappear within a few days to weeks, their intensities increasing linearly with $\sqrt{t}$, suggesting that the C-H bonds re-establish themselves rapidly during annealing (Freund et al. 2001).

Fig. 2 shows the $3.4\mu m$ band of the Galactic Center source IRS6E (Pendleton et al. 1994). The band positions are identical, but are significantly broader, and their relative intensities different from those of the MgO and olivine crystals. The CH_2/CH_3 ratio of $2-3$ lies in the range of CH_2/CH_3 ratios reported for many sources throughout the galaxy (Sandford et al. 1995), suggesting that the ν_{CH} contributions in the organic matter associated with the dust arises mostly from short-chain aliphatic entities, with $n \approx 4-6$.

The observed C_n-H-O concentrations in our MgO and olivine crystals are much lower ($< 100ppm$) than those inferred from astronomical observations ($\sim 10\%$). However, for very small grains very high C_n-H-O concentrations are possible, as can be shown by thermodynamical arguments. The total solute concentration in a grain becomes a function of not only T, but also of grain size

$$C_{total} \approx \kappa_{eq} \exp[-\frac{H_{sol}}{KT}] + \frac{2r}{d} \frac{\kappa_{eq} \exp[\frac{(H_e - H_{sol})}{kT}]}{1 + \kappa_{eq} \exp[\frac{(H_e - H_{sol})}{kT}]},$$
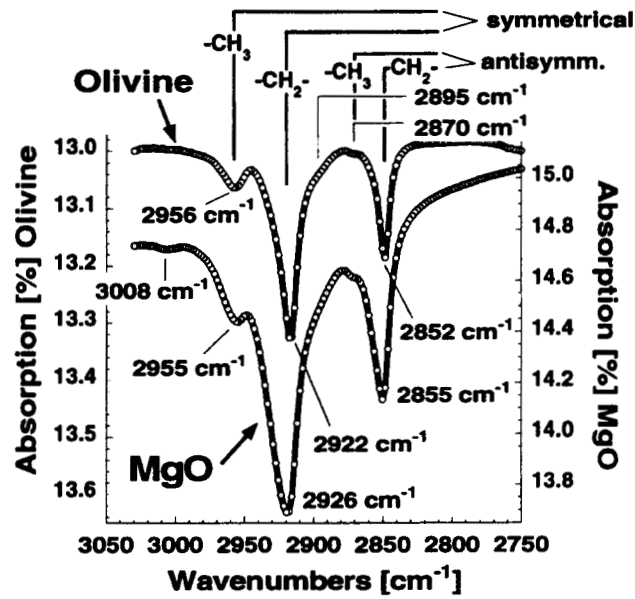
Fig. 1.— The ν_{CH} absorption bands near 3.4μm for olivine (upper), and MgO (lower) (see text).
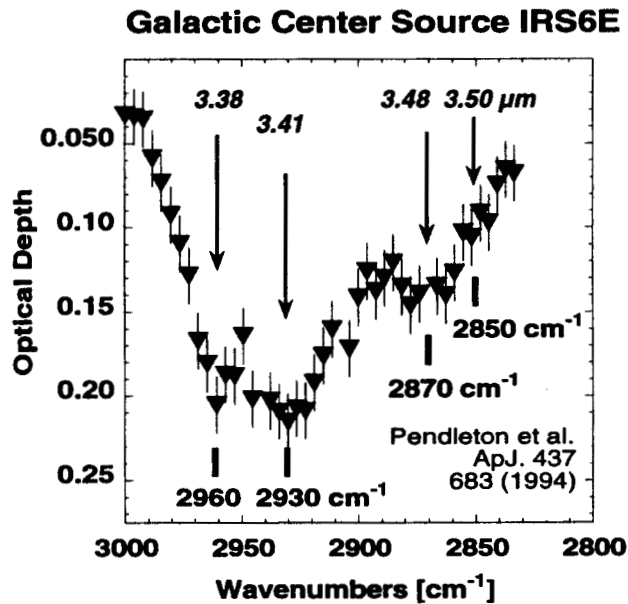
Fig. 2.— The absorption spectra towards the Galactic Center source IRS6E from Pendleton *et al.* (1994).

where H_{sol} is the heat of solution, κ_{eq} is the equilibrium solubility constant, k is the Boltzmann constant, and T is the absolute temperature. The first term is due to the bulk solubility of a solute (C) in a matrix such as MgO. The solubility decreases with decreasing T. In the stiff mineral matrix solute atoms or ions create local stresses, raising the overall energy. The system must respond by lowering the solute concentration. If, however, the solutes can be accommodated where stresses are elastically relaxed, i.e., soft (Freund et al. 2001), higher solute concentrations can be maintained. H_e is the strain energy difference between the stiff interior and the elastically relaxed, soft surface region. If d is the surface area per unit volume, the number of occupied soft sites at saturation is $10/dr^2$, where r= 0.25nm is the width of one atomic layer. Assuming a 5 nm wide "soft" region, with $\kappa_{eq} = 0.06, H_e = 80KJ/mole$ and $H_{sol} = 40KJ/mole$, we get a solute concentration in the bulk of 2% at $T_{cryst} \approx 3000K$ for MgO, but decreases to $\sim 0.01ppm$ at $300K$. The smaller the grains, the larger C_{total}, reaching 0.5%, 5% and 17% in grains of 100 nm, 10 nm, and 3 nm diameter, respectively.

3. Discussion and Summary

If dust in the ISM consists of a solid solution between the mineral component and H_2O/CO_2, formed during condensation from the gas phase, dust grains are expected to contain $C_n - H - O$ entities of aliphatic character in solid matrix. Being imbedded rather than being on the outside, these $C_n - H - O$ are protected from selective sputtering and degradation. The optical depth of the $3.4\mu m$ feature of dust seems to be well correlated with the $9.7\mu m$ Si$-$O stretching band (Sandford et al. 1995)), and $\nu_{CH}/\nu_{SiO} \approx 0.1$ is near-constant along most lines of sight that have been studied. Because small grains in our model have high concentrations of organics, a reasonable size distribution has an almost constant CH concentration, without complicated fine tuning of the size distribution. Thus, these "organics" will continue to contribute to the $3.4\mu m$ band. Likewise, short heat pulses are expected to lead to pyrolysis of the C$-$H bonds, but the ν_{CH} bands of embedded $C_n - H - O$ entities are likely to recover, as they did in laboratory observations of MgO and olivine crystals.

REFERENCES

Freund, F., Gupta, A., and Kumar, D., 1999, *Origins Life Evol. Biosphere*, **29**, 489-509.

Freund, F., Staple, A., and Scoville, J., 2001, *Proc. Natl. Acad. Sci.* , **98**, 2142-2147.

Gupta, A. and Freund, F., 1998, *Lunar and Planetary Institute Conference 29*, Abstr. No. 1107.

King, B.V. and Freund, F., 1984, *Phys. Rev. B*, **29**, 5814-5824.

O'Donnell,J.E. and Mathis, J.S., 1997, *ApJ*, **479**, 806.

Pendleton, Y.J. and Allamandola, L.J., 2002, *ApJS*, **138**, 75-98.

Pendleton, Y.J., {et al., 1994, *ApJ*, **437**, 683-696.

Sandford, S.A., Pendleton, Y.J., and Allamandola, L.J., 1995, *ApJ*, **440**, 697-705.

Synthesis of HCN and HNC in Ion-Irradiated N_2-Rich Ices

M. H. Moore,[1] R. L. Hudson,[2] and R. F. Ferrante[3]

1) NASA Goddard Space Flight Center, Greenbelt, MD

2) Eckerd College, St. Petersburg, FL

3) Department of Chemistry, US Naval Academy, MD

Abstract

Near-IR observations reveal that N_2-rich ice containing small amounts of CH_4, and CO, is abundant on the surfaces of Triton, a moon of Neptune, and Pluto. N_2- rich ices may also exist in interstellar environments. To investigate the radiation chemistry of such ices we performed a systematic IR study of ion-irradiated N_2-rich mixtures containing CH_4 and CO. Irradiation of $N_2 + CH_4$ mixtures at 12 K, showed that HCN, HNC, diazomethane, and NH_3 were produced. We also found that UV photolysis of these ices produced detectable HCN and HNC. Intrinsic band strengths, $A(HCN)$ and $A(HNC)$, were measured and used to calculate yields of HCN and HNC. Similar results were obtained on irradiation of $N_2 + CH_4 + CO$ ices at 12 K, with the main difference being the formation of HNCO. In all cases we observed changes on warming. For example, when the temperature of irradiated $N_2 + CH_4 + CO$ was raised from 12 to 30 K, HCN, HNC, and HNCO reacted with NH_3, and OCN^-, CN^-, N_3^-, and NH_4^+ were produced. These ions, appearing at 30 K, are expected to form and survive on the surfaces of Triton, Pluto, and interstellar grains. Our results have astrobiological implications since some of these radiation products are involved in the syntheses of biomolecules such as amino acids and peptides.

1. Introduction

Near-IR observations reveal that N_2-rich ices containing small amounts of methane (CH_4) and carbon monoxide (CO) are abundant on the surfaces of Pluto and Triton, a moon of Neptune (3, 17). These ices undergo chemical changes due to various ionizing radiations such as solar UV photons, the solar wind plasma, and cosmic rays, with the latter being dominant. For Triton, (5) calculated that 167 - 293 eV $molec^{-1}$ is deposited in the upper ~ 10 m over 4.6 billion years. Pluto's dose is expected to be similar. To date, little has been published on the chemistry of N_2-rich ices (e.g., (9, 18, 2)). Here we report a systematic IR study of proton-irradiated N_2-rich mixtures relevant to Triton and Pluto. Ices were ion-irradiated at 12 K to study the production and stability of new species, and to investigate pathways for product formation. Of special significance in our results are (1) the formation of HCN, HNC, and NH_3 and (2) the reactions of these products on warming to ~ 35 K, producing CN^-, NH_4^+, and other stable ions.

2. Experimental

Details of our experimental set-up have been published (15). Briefly, ices a few micrometers thick are formed by condensation of gas-phase mixtures onto a pre-cooled aluminum mirror at ~ 12 K. Mid-IR spectra of ices were taken before and after energetic processing, usually as 60-scan accumulations (4 cm^{-1} resolution) or 120-scan accumulations (1 cm^{-1} resolution). Ion irradiations were done with a Van de Graaff accelerator (0.8 MeV protons), and UV photolyses with a microwave-discharged hydrogen flow lamp ($E_{avg} \sim 7.41 \pm 0.23$ eV, flux $\sim 3.1 \times 10^{14}$ photons cm^{-2} sec^{-1}). Reagents used were commercially available or prepared and purified with

standard procedures. Band strengths, termed "A" values, of HCN and HNC were needed to determine column densities and product yields in different experiments. A is defined as:

$$A = \frac{\int \tau(\tilde{\nu}) \, d\tilde{\nu}}{N}$$

with the integral being a band's area (cm^{-1}), and N being column density (molec cm^{-2}) calculated from a sample's composition, density, and thickness. Details will be published later, so here we simply state that at 12 K in N_2, $A(\nu_3$ HCN$) = 1.1 \times 10^{-17}$ cm molec^{-1} and $A(\nu_3$ HNC$) = 7.2 \times 10^{-18}$ cm molec^{-1}.

3. Results

Results at $\sim$ 12 K. IR spectra of pure N_2, CH_4, and CO, as well as binary mixtures of these three, were recorded, both for unirradiated and irradiated samples, and details will be reported in a separate publication.

N_2 + CH_4: Mid-IR spectra of N_2 + CH_4 (100:1) before and after ion irradiation are shown in Fig. 1a. Important radiation products in the bottom trace are HNC, HCN, diazomethane (CH_2N_2), and radicals N_3 and CH_3. NH_3 was found as a small band at 971 cm^{-1}. These results demonstrate a condensed-phase pathway for the formation of acids HNC, HCN, and a base (NH_3) in N_2-rich ices containing CH_4. Major products from UV photolysis experiments were CH_2N_2, C_2H_2, and CH_3, the same as reported by (2). The 3286 cm^{-1} feature of HCN was easily detected in irradiated N_2 + CH_4 ice spectra, but it was not easily seen after UV photolysis. Instead, in photolyzed N_2 + CH_4 a weak band of C_2H_2 was observed at 3270 cm^{-1}. To determine if HCN and HNC also were made by UV photolysis, experiments with isotopomers were needed. Figure 1b compares irradiated N_2 + CH_4 and N_2 + CD_4 (100:1). Good evidence that acetylene is not a major contributor in irradiated N_2 + CD_4 (100:1) is the presence of only a very weak C_2D_2 feature at 2435 cm^{-1} in Fig. 1b. This point is important because it implies that HCN is the major source of the 3286 cm^{-1} feature in ion-irradiated N_2 + CH_4. (These conclusions were supported with experiments on $^{15}N_2$ + CH_4 and N_2 + $^{13}CH_4$ ices.) The bottom spectrum of the figure shows that DCN and DNC were indeed made by UV photolysis. In short, these results demonstrate that HCN and HNC are made in both the irradiation and the photolysis experiments. In still other experiments we found that HCN and HNC were detected in irradiated N_2 + CH_4 for three different N_2/CH_4 ratios (100, 50, 4), as were IR features of CH_2N_2. Yields of C_2H_6 and C_3H_8 increased with the initial concentration of CH_4. The C_2H_2 absorption at 3273 cm^{-1} was best seen in the experiment with an N_2/CH_4 ratio of 4, although in more dilute mixtures it was present as a shoulder of the HCN absorption at 3286 cm^{-1}. HCN and HNC did not form when CH_4 was replaced by other simple aliphatic hydrocarbons (C_2H_6, C_2H_4, C_2H_2). To study trends in product formation, we examined N_2 + CD_4 (100:1) ices as a function of radiation dose. This experiment was done with CD_4, instead of CH_4, to circumvent the problem of overlapping bands from HCN and C_2H_2 in the 3290 - 3270 cm^{-1} region. We determined that at 12 K about half of the CD_4 was destroyed after a dose of $\sim$ 3.5 x 10^{19} eV cm^{-2} (2.3 eV molec^{-1} for the calculated column density in this ice (1.5 $\times$ 10^{19} molec cm^{-2})). A similar radiation dose on Triton and Pluto would accumulate in $\sim$ 65 million years of exposure (11).
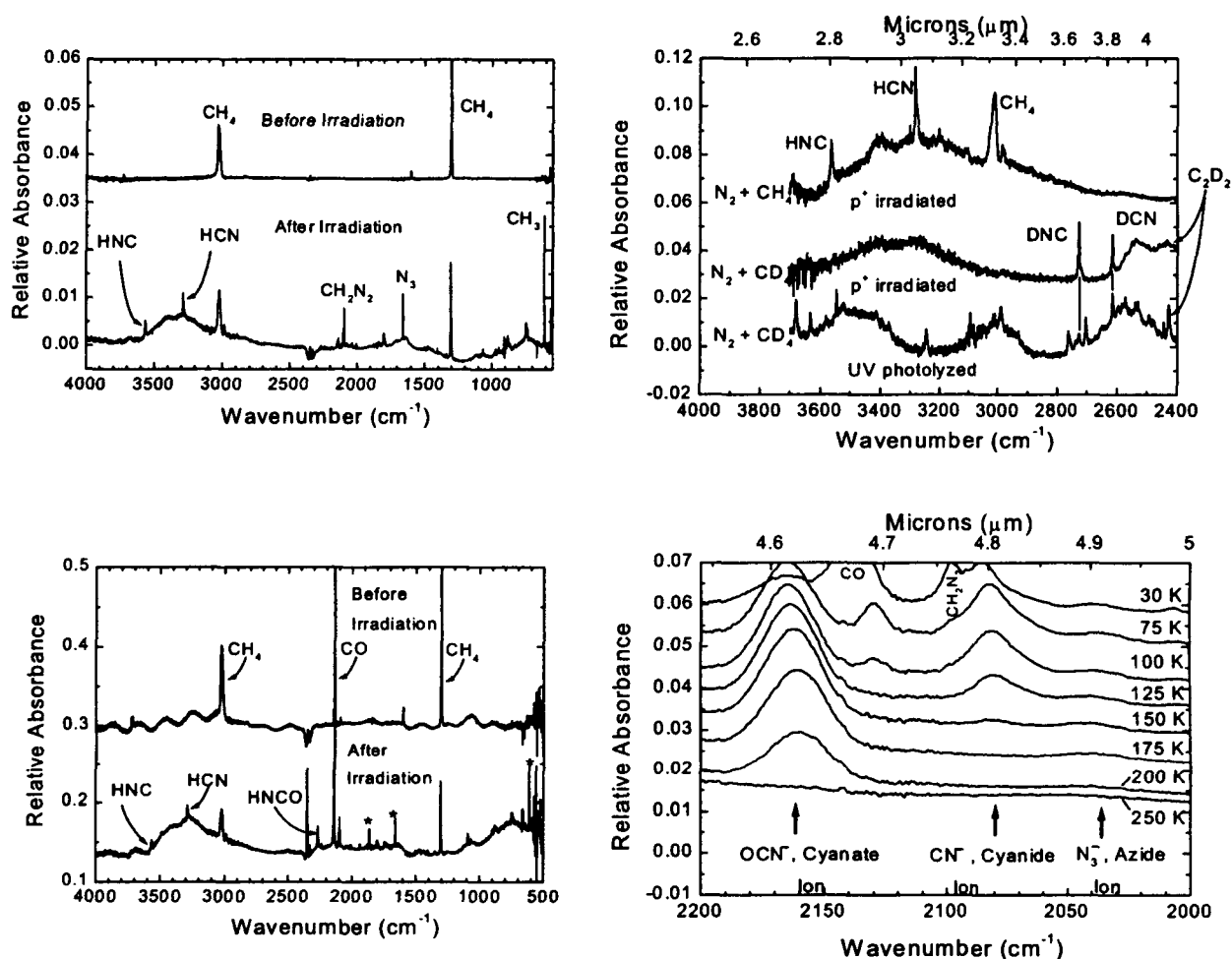
Fig. 1.— Figure 1a (top left), Figure 1b (top right), Figure 1c (bottom left), and Figure 1d (bottom right).

N_2 + CH_4 + CO: HNC and HCN also were detected in irradiated N_2 + CH_4 + CO (100:1:1), demonstrating formation of these products in the presence of CO. Figure 1c shows the relevant spectra. Note that isocyanic acid (HNCO), was seen in this three-component ice. Other products from our UV-photolysis of N_2 + CH_4 + CO (100:1:1) included CH_2N_2, C_2H_6, HCO, and CO_2 (reported in (2)). Ion-irradiated N_2 + CH_4 + CO ices for three $N_2/(CH_4$ + CO) ratios (50, 5, and 0.5) showed HNC and HCN only when the initial ratio was 50. When the ratio was 5 or 0.5, the dominant products included aliphatic hydrocarbons, CO_2, C_3O_2, and a molecule with a C=O bonded feature at 1720 cm^{-1}, probably acetaldehyde.

Results at T ≥ 30 K. The work just described was performed at ~ 12 K. To determine the likely reactions at the higher temperatures of Triton and Pluto, irradiated ices were slowly warmed to 35 - 40 K. As expected, all bands from free radicals (e.g., HCO, N_3, and CH_3) were lost on warming. Moreover, sharp IR features of the base NH_3 and acids HNC, HCN, HNCO, were diminished greatly. Concomitant with these changes was the rise of a broad ammonium, NH_4^+, band around 1460 cm^{-1} and several broad features in the 2200 - 2000 cm^{-1} region. Specifically, warmed irradiated N_2 + CH_4 + CO gave rise to OCN⁻ (2166 cm^{-1}), CN⁻ (2083 cm^{-1}), and N_3^- (2038 cm^{-1}), all identified by extensive experiments with isotopomers,

stability of these anions with temperature. The relative intensities of the ions' IR bands depend on initial concentrations of CH_4 and CO in the ice, the thickness of the ice, and the warming rate. These results demonstrate that reactions triggered by warming occur in our processed ices. Material is lost due to both sublimation and reactions, and residual ions are left behind.

4. Discussion

Reaction Mechanisms. HCN and HNC form in irradiated and in photolyzed $N_2 + CH_4$ and $N_2 + CH_4 + CO$ ices. The most reasonable mechanism for acid formation comes from work by Maier(1996) and involves a rearrangment of diazomethane into nitrilimime (HCNNH), then a loose HN • • • HCN complex forms which can produce both HCN and its isomer, HNC.

Temperature Effects. The changes described above are from acid-base reactions of HCN, HNC, and HNCO with NH_3 to give CN^-, OCN^-, and NH_4^+. In addition, a broad band for N_3^- seen on warming implies that $HN_3 + NH_3 \rightarrow NH_4^+ + N_3^-$ occurs and suggests that HN_3 was formed on ion irradiation.

Relevance to Icy Surfaces. A highlight of our work is the synthesis of nearly equal amounts of HCN and HNC in $N_2 + CH_4$ and $N_2 + CH_4 + CO$ ices. An HNC/HNC ratio near one is appealing as comets typically have a ratio from 0.06 to 0.2 (e.g., (10, 1)), depending on the comet and its distance from the Sun. In addition, cold interstellar molecular clouds have HNC/HCN ratios of 0.2 to 1 (16). Since the molecules we studied, N_2, CH_4, and CO, are all either known or expected in interstellar and cometary environments, we expect our observed solid-phase chemistry to occur outside the laboratory. Ice chemistry may well provide a solution to the "problem" of the high HNC abundances in interstellar space and in comets. A second important finding is the solid-phase acid-base chemistry to produce ions. The icy origin of HCN and HNC, along with acids HNCO and HN_3 (likely) sets the stage for reactions with NH_3 to make NH_4^+, OCN^-, CN^-, and N_3^-. Since these ions are thermally more stable than the volatile reactants N_2, CH_4, and CO, they may accumulate on the surfaces of Triton, Pluto, and comets and be good candidates for future mid-IR observations. It is significant that observations of cold icy grains of embedded protostars already show condensed-phase NH_3 (7, 4), a prominent 2165 cm^{-1} feature due to OCN^- ion (8), and an unidentified 1460 cm^{-1} absorption band, almost certainly due to NH_4^+ (6). Although the actual N_2 and NH_3 budget in molecular clouds is not well determined, the existence of OCN^- supports the idea that low-temperature pathways occur on icy grains. Radiation processing of similar N_2-rich ices on Triton and Pluto could provide an endogenous source of HNC, HCN, HNCO, NH_3, NH_4^+, OCN^-, CN^-, and N_3^- for those worlds. The presence of these species would suggest interesting prebiotic chemistry, as it is well known that many of these are involved in reactions producing biomolecules. For example, the role of HCN and its derivatives in prebiotic evolution is discussed by many authors (e.g., (14)). More recently, the instability of NH_4CN, in the presence of H_2O and NH_3, was examined by (12) who found that adenine, guanine, and amino acids are formed after storage for 25 years at temperatures as low as 77 K. The Pluto-Kuiper Belt Mission will make the first reconnaissance of Pluto as early as 2015, and visit one or more smaller Kuiper Belt Objects. This will be an opportunity to look closely for HCN, HNC, HNCO, OCN^-, CN^-, N_3^-, and NH_4^+. Detecting, and mapping these species could help determine if Pluto and Triton will be

targets for future astrobiology missions. Understanding the radiation chemistry of these remote worlds with N_2-rich surfaces may provide support for the icy origin of HCN and HNC from similarly processed N_2-rich segregated cometary ices. This scenario would strengthen the idea that comets contain interesting biomolecules.

Acknowledgments

REFERENCES

(1) Biver, N. and 11 co-authors 1997, Science, 275, 1915.
(2) Bohn, R. B., Sandford, S. A., Allamandola, L. J., and Cruikshank, D. P. 1994, Icarus, 111, 151.
(3) Cruikshank, D. P., et al., Science, 261, 742.
(4) Datios, E. and d'Hendecourt, L. 2001, A&A, 365, 144.
(5) Delitsky, M. L. and Thompson, W. R. 1987, Icarus, 70, 354.
(6) Demyk, K., et al., 1998, A&A, 339, 553.
(7) Gibb, E. L., Whittet, D. C. G., Chiar, J. E. 2001, ApJ, 558, 702.
(8) Hudson, R. L. Moore, M. H., and Gerakines, P. A. 2002, ApJ, 550, 1140.
(9) Hudson, R. L. and Moore, M. H. 2002, ApJ, 568, 1097.
(10) Irvine, W. M. 1996, Nature, 383, 418.
(11) Johnson, R. E. 1989, JGR-Letters, 16, 1233.
(12) Levy, M., Miller, S. L., Brinton, K., and Bada, J. L. 2000, Icarus, 145, 609.
(13) Maier, G., et al., 1996, Liebigs Ann., 1041.
(14) Matthews, C. N. 1995, Planet. Space Sci., 43, 1365.
(15) Moore, M. H. and Hudson, R. L. 2000, Icarus, 145, 282.
(16) Ohishi, M. and Kaifu, N. 1998, Farad. Disc., 109, 205.
(17) Owen, T. C., et al., 1993, Science, 261, 745.
(18) Satorre, M. A., Palumbo, M. E., Strazzulla, G. 2001, JGR-Planets, 106, 33363.

Condensation Processes in Astrophysical Environments

Joseph A Nuth III

Astrochemistry Branch, NASA Goddard Space Flight Center, Greenbelt, MD

Frans J. M. Rietmeijer

Dept. of Earth and Planetary Sciences, Univ. of New Mexico, Albuquerque, NM

Hugh G. M. Hill

NAS/NRC Resident Research Associate, NASA Goddard Space Flight Center

1. Introduction

Astrophysical systems present an intriguing set of challenges for laboratory chemists. Chemistry occurs in regions considered an excellent vacuum by laboratory standards and at temperatures that would vaporize laboratory equipment. Outflows around Asymptotic Giant Branch (AGB) stars have timescales ranging from seconds to weeks depending on the distance of the region of interest from the star and, on the way significant changes in the state variables are defined. The atmospheres in normal stars may only change significantly on several billion-year timescales. Most laboratory experiments carried out to understand astrophysical processes are not done at conditions that perfectly match the natural suite of state variables or timescales appropriate for natural conditions. Experimenters must make use of simple analog experiments that place limits on the behavior of natural systems, often extrapolating to lower-pressure and/or higher-temperature environments.

Nevertheless, we argue that well-conceived experiments will often provide insights into astrophysical processes that are impossible to obtain through models or observations. This is especially true for complex chemical phenomena such as the formation and metamorphism of refractory grains under a range of astrophysical conditions. Data obtained in our laboratory has been surprising in numerous ways, ranging from the composition of the condensates to the thermal evolution of their spectral properties. None of this information could have been predicted from first principals and would not have been credible even if it had.

2. Dust Condensation Experiments

Our experiments were never intended to replicate the conditions that form grains in circumstellar shells. Such experiments are impractical for numerous reasons. Our apparatus is designed to make large quantities of highly amorphous condensate from a homogeneous vapor-phase. We needed highly amorphous solids, since the synthesis of grains with reproducible degrees of crystallinity is difficult and highly amorphous silicates are a logical starting point for annealing experiments that introduce increasing crystallinity as a function of time and temperature. We found that the infrared spectra of amorphous magnesium silicate grains produced in our laboratory matched those of grains in typical oxygen-rich circumstellar outflows after about 3 hours of vacuum annealing at 1027K. Had our analog grains initially been more crystalline than the natural materials there would have been no easy way to render them amorphous.

Grains are produced at a pressure of $\sim$ 90 torr in an atmosphere dominated by hydrogen at temperatures between $\sim$500K and 1500K. Condensable species are formed via combustion of gasphase precursors such as silane [SiH$_4$], iron pentacarbonyl [Fe(CO)$_5$], or trimethyl aluminum [(CH$_3$)$_3$Al)] and typically constitute less than 10% of the total gas input to the system. Oxygen is introduced separately, just before the furnace. A volatile metal such as magnesium can be placed into the furnace within a graphite crucible. Because the furnace temperature then controls the vapor pressure of this metal, only one metal is placed in the furnace during any given experiment. The total flow velocity through the furnace is $\sim$10 20 cm-s 1. A typical grain forms at the high-temperature flame front near the furnace entrance and spends much less than a second within the furnace. Hot gas and grains are rapidly quenched as they flow into a stainless steel chamber lined with an aluminum substrate that remains at $\sim$300 to 350K.

Condensation and growth are stochastic, kinetically controlled processes. Grains often form fluffy, open aggregates. Typical grains are $\sim$ 2030 nm in radius while aggregates frequently consist of thousands of individual grains; each connected to only two or three neighboring particles. The Dust Generator was designed to produce grains with chemical composition determined stochastically by the composition of the vapor. Though we expected some variation about the average composition we never expected any significant chemical processing during the rapid growth of the condensates. We were wrong. Chemical analyses of individual grains condensed from MgSiO vapors clustered around five distinct compositions: pure SiO$_x$ and MgO grains, low- silica MgO grains and serpentine and smectite dehydroxylate grains at Mg$_3$Si$_2$O$_7$ and Mg$_3$Si$_4$O$_{11}$, respectively (1). In a similar fashion, analyses of FeSiO condensates also produced compositions clustered at the pure oxide end members and at intermediate compositions including the Fe-greenalite (Fe$_3$Si$_2$O$_7$) and Fe-saponite (Fe$_3$Si$_4$O$_{11}$) dehydroxylate compositions, and at a distinct low-Fe ferrosilica composition (2). Figure 1 is a ternary diagram of the composition of individual particles condensed from mixed Fe-MgSiO vapors. The dot is the average composition of the vapor as determined by SEM analysis of the smoke: this represents the average of many thousands of individual, mostly 20 nm-sized grains. Open squares represent individual grains determined by Analytical Election Microscopy. These cluster at the pure end-member compositions (FeO$_y$, MgO and SiO$_x$) and at mixed metastable eutectic grain compositions found in the Mg-SiO and Fe-SiO vapor condensates discussed above. However, what is most notable is that **there were no *mixed* FeMg silicate grains found anywhere** in this sample despite the very rapid nucleation and growth of the particles. There are no eutectic compositions possible in the FeOMgO binary phase diagram and therefore no metastable eutectics along this axis to direct the compositions of growing grains. Absent metastable eutectics along the MgOFeO axis, grain growth is confined to the pure FeOSiO and MgOSiO axes producing pure iron silicate and magnesium silicate grains and the oxides FeO$_y$, MgO and SiO$_x$.

The annealing rate for magnesium silicate smokes is a very steep function of temperature (3,4). Conversely, the time required to reach any given spectral stage is very temperature dependent. More crystalline grains are indicative of longer annealing times and/or higher temperatures. We did not measure the activation energy required to anneal iron silicate smokes, though we noted that temperatures on the order of 1300K were required in order to achieve spectral changes in the iron silicate smokes that evolved on timescales of days to weeks. This
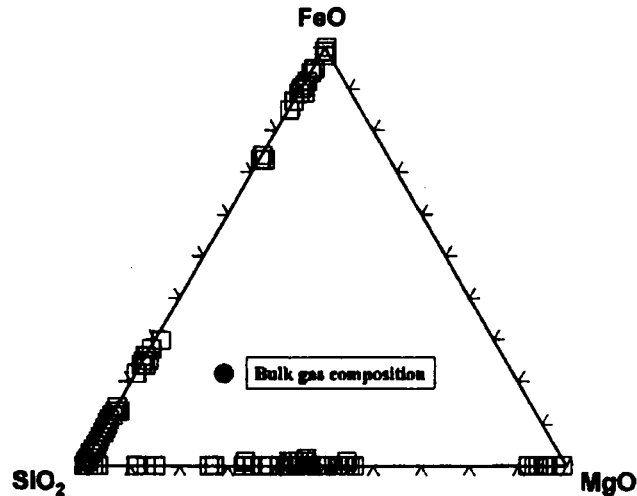
Fig. 1.— Ternary diagram showing the composition of individual 10-20 nm grains condensed from a mixed Fe-Mg-SiO-H_2-O_2 vapor. The large spot in the interior of the diagram represents the approximate composition of the vapor-phase as measured via TEM analysis of the bulk smoke. Modified after Rietmeijer (9).

is 250 to 300K higher than temperatures required for similar evolutionary timescales in magnesium silicates. At such temperatures iron silicates have an appreciable vapor pressure and small grains could easily vaporize before annealing. So for any amorphous grain there are both upper and lower time-temperature bounds to the conditions required to convert it to crystallinity without vaporization.

3. Astrophysical Application

In high mass-loss-rate circumstellar winds, features indicative of pure magnesium olivine and pyroxene were observed. No crystalline silicate minerals containing either aluminum or iron have yet been detected (4,5,6). We believe that the results discussed previously readily explain ISO observations of crystalline magnesium silicates. Our experiments yielded two unexpected conclusions: pure, amorphous, Mg-silicate and Fe-silicate grains condense from a mixed Fe-Mg- SiO vapor; and these Mg-silicate grains anneal at much lower temperatures than do Fe-silicates. Therefore we assume that the initial condensates are amorphous, though pure, iron and magnesium silicates. As the nucleation temperature increases with increasing massloss rate, pure Mg-rich silicates begin annealing just after formation, while iron silicates remain amorphous. The higher the stellar mass outflow rate, the larger the overall fraction of crystalline Mg-silicates. This is in agreement with ISO observations (6) although observational selection effects may obscure the true size of the crystalline mass fraction (8).

REFERENCES

1. Rietmeijer F.J.M., *et al.* (2002b) *Phys. Chem. Chem. Phys.* **4**, 546-551.

2. Rietmeijer F.J.M., Nuth J.A. and Karner J.M. (1999a) *Phys. Chem. Chem. Phys.* **1**, 1511-1516.

3. Hallenbeck S.L., Nuth J.A. and Daukantas P.L (1998) *Icarus* **131**, 198-209.

4. Hallenbeck S.L., Nuth J.A. and Nelson R.N. (2000) *Astrophys. J.* **535**, 247-255.

5. Waters, L.B.F.M., *et al. Astron. Astrophys.* **315**, L361L364.

6. Molster F.J. (2000) Ph.D. thesis, 278p, University of Amsterdam, the Netherlands.

7. Molster F.J., *et al.* (1999) *Nature* **401**, 563-565.

8. Kemper F., *et al.* (2001) *Astron. Astrophys.* **369**, 132-141.

9. Rietmeijer F.J.M. (2002) *Chemie der Erde* **62**, 1-45.

Production of Organic Matter
While Simulating the Interstellar Dust Environment

W.A. Schutte and G.M. Muñoz Caro

Sackler Laboratory for Astrophysics, Leiden Observatory, The Netherlands

U.J. Meierhenrich

Bremen University, Dept. Phys. Chemistry, Leobenerstraße, Bremen, Germany

Abstract

We review the recent detections of amino acids following the recreation of the conditions on interstellar grains in the laboratory.

1. Introduction

Recent results suggest that the photochemistry of interstellar ice analogs is characterized by considerable complexity. While the organic products of such simulations have already been studied for 23 years (Hagen *et al.* 1979), the detection of a broad suite of amino acids (Muñoz Caro *et al.* 2002; Bernstein *et al.* 2002) was not at all anticipated. This detection became possible by the use of a dedicated analysis technique, suggesting that still many more classes of components may await discovery. We review these new results.

2. Experimental

For a thorough description of the experimental set up see Gerakines *et al.* (1995). Central to a vacuum chamber (10^{-7} mbar) is a substrate which is cooled typically to 12 K (although the temperature can be varied). Ice samples are prepared by depositing gas mixtures with simultaneous photolysis by a vacuum UV lamp. Subsequently, the sample is allowed to gradually warm-up to room temperature. Afterwards, a yellow colored material remains on the substrate, which consists of a diversity of organic species; we designate this material Simulated INTerstellar Organic Refractory (SINTOR). IR spectroscopy is used for *in situ* monitoring of the sample during or following the various experimental steps (Deposition, Photolysis, Warmup). Detailed analysis is performed by Gas Chromatrography/Mass Spectroscopy (GC/MS) or by Liquid Chromatography/Mass Spectroscopy (LC/MS). In all reported cases, control experiments were performed with ^{13}C labelled ice samples to exclude contaminants.

3. Results

Recently, our knowledge of the organic photochemistry of interstellar ice analogs was revolutionized by the detection of a large variety of amino acids in the SINTOR. This result was reported in two independent papers (Bernstein *et al.* 2002; Muñoz Caro *et al.* 2002).

Fig. 1 shows the GC trace of the SINTOR from $H_2O/CO_2/CO/CH_3OH/NH_3 = 2/1/1/1/1$ after hydrolysis and derivatization (Muñoz Caro *et al.* 2002). The following amino acids were
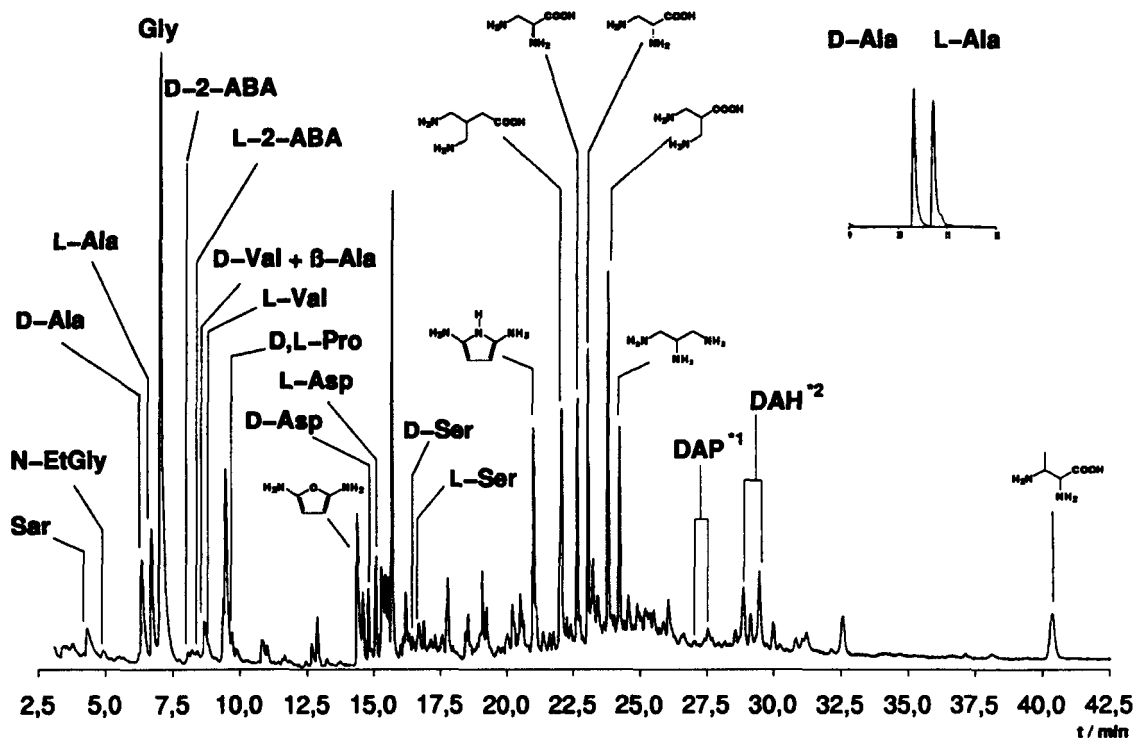
Fig.   1.— Chromatogram of the SINTOR obtained by UV photolysis and warm-up of
$H_2O/CO_2/CO/CH_3OH/NH_3$ = 2/1/1/1/1 (Muñoz Caro *et al.* 2002). The material was treated for amino
acids analysis (for details, see text).

detected: glycine, alanine, sarcosine, 2-aminobutyric acid, n-ethylglycine, valine, proline, ser-
ine, aspartic acid, 2,3-diaminopropanoic acid, 2,3-diaminobutyric acid, 4,4-diaminopentanoic
acid, α-diaminopentanoic acid, β- diaminopentanoic acid, α-diaminohexanoic acid, and β-
diaminohexanoic acid; in addition, 1,2,3- triaminopropane, 2,5-diaminofurane, and 2,5-diamino-
pyrrole were present. Bernstein *et al.* detected glycine, alanine and serine in the SINTOR of
the mixture $H_2O/CH_3OH/NH_3/HCN$=20/2/1/1 by means of LC/MS again after hydrolysis. It
is unclear what causes the large difference in the number of species detected in the Bernstein
et al. and Muñoz Caro *et al.* experiments. Possibilities are the higher dilution of the C and N
containing molecules or the use of HCN in the Bernstein *et al.* experiment. Furthermore, the
# of photons/molecule is very different. By dividing the dose (photons cm^{-2}) by the molecular
column density, we obtain ∼ 5 photons $molec^{-1}$ in the Bernstein *et al.* experiment, as opposed
to 0.15 photons $molec^{-1}$ reported by Muñoz Caro *et al.*

Several chemical routes to amino acids are possible. Woon *et al.*(2002) proposed the production of glycine by formation of the radical CH_3NH_2 from hydrogen addition to HCN, followed by a reaction with COOH (created by CO + OH). More complex amino acids may then be formed after fragmentation of glycine and addition of CH_3, CH_2OH, etc. However, such a mechanism is unlikely, since the ice samples of the Muñoz Caro *et al.* experiments did not include HCN. It has been shown that amino acids can be formed by heating aqueous solutions of H_2CO and NH_3 to 185 C (Fox & Windsor 1970). Once H_2CO has been created by photodissociation of CH_3OH, the localized high excitation conditions created by the absorption of a UV photon in the ice may allow analogous chemistry. This mechanism indeed yields a wide suite of amino acids, similar to the Muñoz Caro *et al.* results. Finally, similar to the astrophysical simulation experiments (Bernstein *et al.* 1995, the main reaction product is hexamethylenetetramine.

4. Astrophysical Implications

Understanding the photochemical formation of organic species from UV processing of analogs of interstellar and solar nebula ice analogs is essential to understand the origin and nature of the variety of organic components seen in comets. The constituents of comets provide a record of the events during the formation of the Solar System. Results as those reviewed in this paper will provide an invaluable background for understanding the nature of the processes that were responsible for converting a large part of the solar nebula ices into organic material. The extend of this conversion as deduced from the high abundance of organics in comets testifies to the dominance of these processes in determining the physical and chemical conditions of the solar nebula prior to the formation of the planetary bodies. Therefore, the nature of the organics in comets may give us a direct window on the the events that led up to the formation of the solar system 4.5 billion years ago.

The formation of species of pre-biological importance, such as amino acids, under simulated space conditions may change our view of how life may originate. Experiment to create amino acids under simulated primitive earth conditions, e.g., energetic processing of a non-reducing gas atmosphere, have been largely unsuccesful. Our experiments suggest that the creation of amino acids in space and their delivery to earth by cometary dust may have been an essential seeding of our planet to allow pre-biological evolution to take place.

REFERENCES

Fox S. W., Windsor C. R. 1970, *Science* **170**, 984.

Hagen, W., Allamandola, L. J., Greenberg, J. M, 1979, *Astrophys. Space Sc.* **65**, 215.

Gerakines, P. A., Schutte, W. A., Greenberg, J. M., van Dishoeck, E. F 1995, *A&A* **296**, 810.

Bernstein, M. P., Sandford, S. A., Allamandola, L. J., *et al.* M. A. 1995, *ApJ* **454**, 327.

Bernstein M.P., Dworkin J.P., Sandford S.A., *et al.* 2002, *Nature* **416**, 401.

Muñoz Caro G. M., Meierhenrich U. J., Schutte W. A., *et al.* 2002, *Nature* **416**, 403.

Fine Particle Production by Spray Pyrolysis Method

H. Suto

Subaru Telescope, Hilo, Hawaii

S. Ohara and T. Fukui

Japan Fine Ceramics Center, Atsuta, Nagoya, Japan

C. Koike

Kyoto Pharmaceutical University, Yamashina, Kyoto, Japan

Abstract

Syntheses of several oxide particles were conducted by the spray pyrolysis method at Japan Fine Ceramics Center aiming to produce spherical particles and to obtain their optical characters free from ambiguity of unknown shape distribution of particles. Our preliminary results are presented for the four oxide particles, SiO_2, Al_2O_3, Mg_2SiO_4, and TiO_2.

1. Introduction

It is vital to get optical characters of cosmic dust analogues under well defined conditions for analysis of observational emission and absorption spectra of cosmic dust. Optical spectra of particles depend on several physical characters such as compositions, crystal phase, amorphous phase, monodispersed or coagulated, size, and shape so that it is important to prepare particles whose physical characters are well defined.

The particle shape effect has been well known to affect the wavelength and numbers of emission features where the real part of dielectric constant is negative (Bohren & Huffman 1983), however the shape effect was often less attentioned in deriving optical characters in the laboratory researches. The object of this research is to prepare submicron size spherical particle of interesting astronomical dust analogues and derive their dielectric constants free from ambiguity coming from particle shape.

In the case of spherical shape and the particle size small compared to the optical wavelength, i.e. Rayleigh limit of particle size, the absorption κ and dielectric constant ϵ are related straightforwardly in simple linear relation,

$$\kappa = 6\pi/\rho\,(n_{med}/\lambda)\ Imag((\epsilon - \epsilon_{med})/(\epsilon - 2\epsilon_{med})) \tag{1}$$

where ρ is the density of particle, and n_{med} is optical constant of medium and ϵ_{med} is dielectric constant of medium. Dielectric constant can be estimated from absorption spectra by fitting the calculation using oscillator model, or by Kramers Kronig method.

We tried spray a pyrolysis method in order to make submicron spherical particles of oxide such as SiO_2, Al_2O_3, Mg_2O_4 and TiO_2.

2. Production Method

Spray pyrolysis is a method that is able to produce sub-micron size spherical particles through pyrolysis or hydrolysis reaction of a droplet containing the precursors (Maric *et al.* 2000; Fukui *et al.* 1997). Solid particles were synthesized from solutions via the following steps:

1) a solution of precursors of the molecules of final composition is prepared;

2) droplets of the solution are made by ultrasonic vibrator (f=1.7MHz) just prior to reactors;

3) the droplets are carried by air or inert gas into the reactors;

4) the droplets pass through 4 reactors during which thermal reactions occur and solvent evaporates;

5) reaction particles are captured with a Teflon film dotted with 5 mm holes.

Fig. 1 is a diagram of our instrument showing the mist/droplet generator on the right side, the four reactors in the center, and the particle trap cavity on the left. The large box at left center is the temperature controller for the reactors.

The spherical boundary of liquid droplets means the composite tends to be produced in spherical shape, especially in the case of the final particles being in amorphous form. The particle size depends on the density of solutions, and the density less than 0.05 mol/L allows particle size to be less than 1 μm. The temperature of the reactor can be raised to 1000C, and the four reactors were set with a gradual temperature increase, (for example, sequentially at 200, 400, 600, 800C), to allow the thermal reaction to proceed moderately, from lower to higher temperature. The typical flow rate of carrier gas is 1L/min So that a droplet resides 10 seconds per reactor. The typical production rate is a few mil gram for a 10-hour run of the flow.

3. Products

With the spray pyrolysis method at JFCC, we have obtained the fine particles of SiO_2, Al_2O_3, TiO_2, and Mg_2SiO_4 which are oxides expected as the major cosmic dust prevailed in circumstellar, interstellar and interplanetary regions.
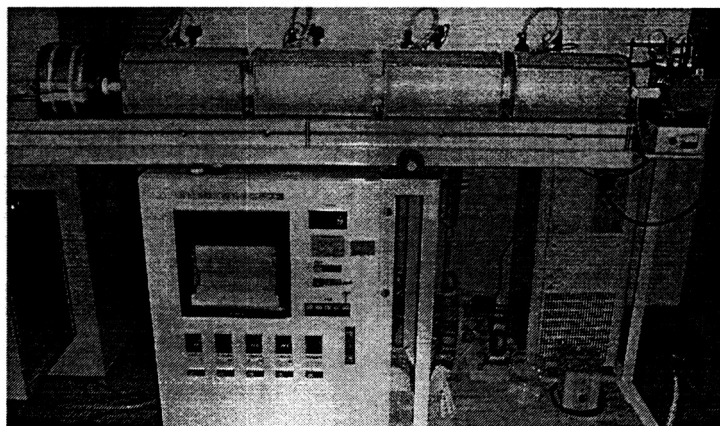
Fig. 1.— Spray pyrolysis instrument

which contains 10 - 20 nm size silica particles. Silica sol was diluted with pure water to make the Si density 0.01 mol / L in the solution, and its mist was flowed into the reactors whose temperatures were 200/400/600/800C. The final particles shape is almost perfect spherical in the SEM images as shown in Fig. 2. In the view of SEM, the particle diameter ranges from 0.1 to 1 μm, while majority have diameters less than 0.3 μm. The X-ray diffraction pattern showed a broad feature of amorphous silica. This is consistent with the differential thermal analysis proving the SiO_2 crystallization occured at 1200C, higher than our reactor temperatures. Very rarely, but tiny holes in the large size particles were seen in the SEM image, so the particle inside may be porous.

Al_2O_3 particles were produced from the colloidal alumina sol (Nissan Chemical Corporation) with the Al density of 0.02 mol / L and the reactor temperatures of 200/400/600/800C. X-ray diffraction pattern indicates that the production is γ-Alumina, but the features are very broad, suggesting amorphous form alumina. Their shape are quit spherical in the SEM image (Fig. 2), and the size range is from 0.1 μm to 1 μm. Very rarely, but broken partilces were seen in SEM image, so the particle may be not well condensed.

Mg_2SiO_4 were obtained from $Mg(NO_3)_2$ $6H_2O$ solution (Nakarai Tesk Corporation) combined with the SiO_2 colloidal sol (Nissan Chemical Corporation) in 2:1 molecular ratio, whose density of Si was 0.01 mol / L. The reactors temperature were 200/400/800/1000C. X-ray diffraction pattern matches Mg_2SiO_4 crystal with showing narrow diffraction features, indicating well crystalline form synthesized. Their shapes are beans-like whose sizes are sub-micron (Fig. 3). The crystallization of the particle should be one of the reason that the shape is off spherical when the particle elongate to a preferred crystal axis such as c-axis.

TiO_2 particles were obtained from TiO_2 colloidal sol (Nissan Chemical Corporation) with the Ti density of 0.01 mol / L and the reactors temperatures 200/400/600/800C. Their shapes were generally spherical (Fig. 3), but the waning and holes were often seen for the particles. They should have porous structures.
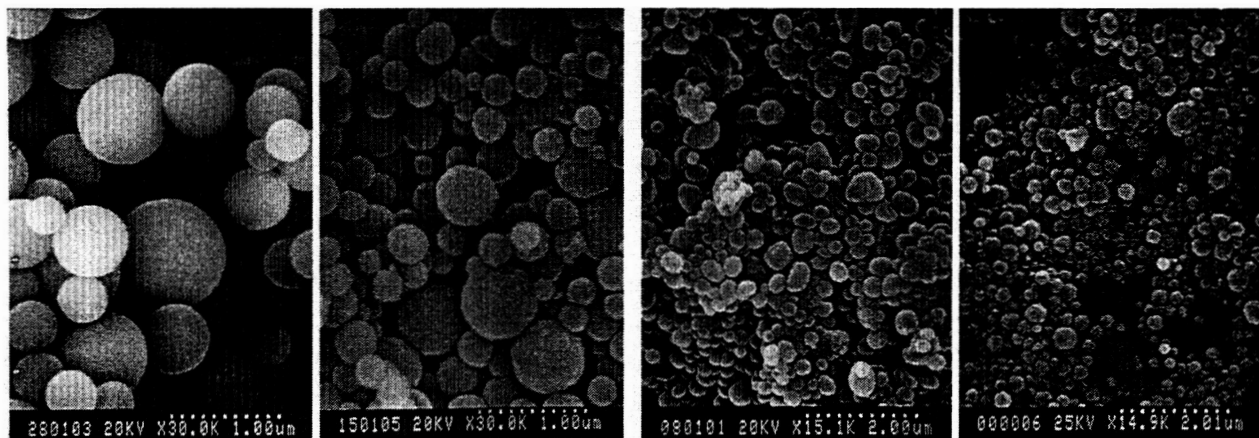
Fig. 2.— SEM images: SiO_2 (left) & Al_2O_3 (right).   Fig 3. — SEM images Mg_2SiO_4 (left) & TiO_2 (right).

4. SiO₂ absorption spectra

The produced SiO₂ particles are highly spheircal so that its shape is well defined. The absorption spectrum of the synthesized amorphous SiO₂ spherical particles were measured at infrared from 2 μm to 100 μm at the room temperature (Fig. 4). Three major features were observed at the wavelengths around 9, 12, and 21 μm where crystal bulk SiO₂ also has the reflection peaks. By fitting the calculation using the oscillator model of dielectric constant

$$\epsilon(\lambda) = \epsilon_\infty + \sum_j S_j \lambda^2 / (\lambda^2 - \lambda_j^2 - i\gamma_j \lambda) \tag{2}$$

to the measured spectrum, the dielectric constant of the amorphous SiO₂ was derived (Fig. 5). In equation (2), ϵ_∞ is the dielectric constant at the short wavelength limit, S_j, λ_j, γ_j are the oscillator strength, transverse optical wavelength, and dumping factor, respectively, and i is the imaginary number unit. The mass absorption coefficient κ is calculated from ϵ as shown in equation (1).
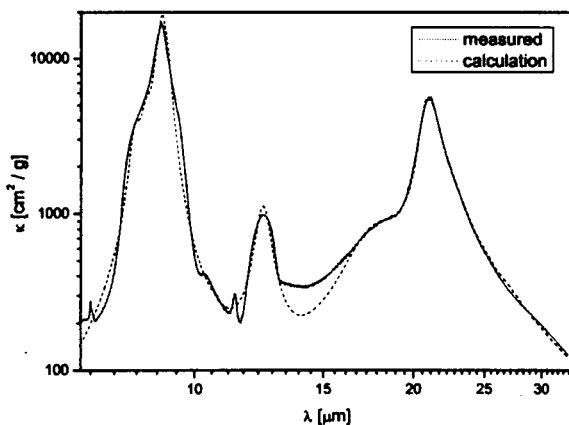
Fig. 4.— SiO₂ absorption spectrum
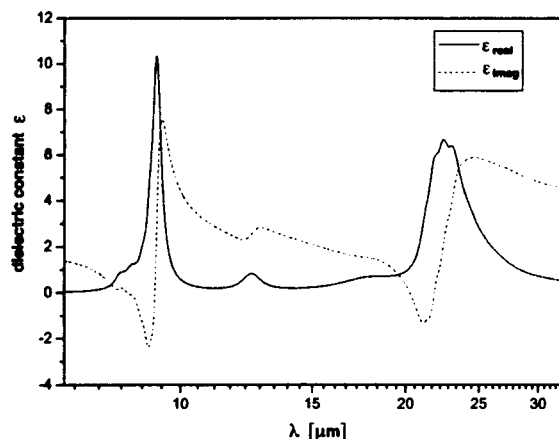
Fig. 5.— SiO₂ dielectric constant.

The fitting was done fairly well, and the result is free from the particle snape effect because of the good spherical shape of our samples, but further considerations of the dielectric model for amorphous materials remain.

REFERENCES

Bohren & Huffman 1983, *Absorption and Scattering of Light by Small Particles*, Wiley & Sons, Inc.

Fukui, T., *et al.*, 1997, *J. Am. Ceram. Soc.*, **80**, 261.

Maric, R., *et al.*, 2000, *J. Materials Science*, **35**, 1397.

Investigations of the Formation of Molecular Hydrogen on Dust Grain Analogues

Gianfranco Vidali and Joseph E. Roser

Syracuse University, Physics Dept., Syracuse, NY

Giulio Manicó, and Valerio Pirronello

Universitá di Catania, DMFCI, Catania, Sicily, Italy

Abstract

In the last four years we have been working to investigate the formation of molecular hydrogen on surfaces of materials of astrophysical interest, such as silicates, carbonaceous particles and ices, and in conditions approximating the ones present in a variety of astrophysical environments. Our experimental studies - the first of their kind and complemented with computer simulations and theoretical analyses - have given not only hydrogen recombination rates under different ISM conditions, but they have also offered new insights into this fundamental astrophysical problem. Here we summarize our experimental methods and most significant results.

1. Introduction

Molecular hydrogen, the lightest and most abundant molecule in the Universe, plays several crucial roles, from aiding the formation of stars to being an active participant, in its neutral or charged state, to most of the reactions occurring in the interstellar medium.

It has long been realized that molecular hydrogen cannot form efficiently in the gas phase, because the release of the energy excess upon formation via radiative decay is not allowed by selection rules, while its formation via the reaction $H + H^- \rightarrow H_2 + e^-$ is not sufficient to explain its abundance except in very specific environments. It has been pointed out that dust grains can act as catalysts in the formation of molecular hydrogen, and simple models (Hollenbach & Salpeter 1971; Hollenbach et al. 1971) showed that, although dust grains are outnumbered by gas atoms 10^{12} to 1, under reasonable hypotheses and values of key parameters, molecular hydrogen can form on grains in numbers to match the observed abundance. However, the dynamics and the rate of formation of H_2 molecules on surfaces of grains have not been clarified yet (for a recent review, see: Pirronello et al. (2000) and references therein).

Smoluchowski (1979, 1981, 1983), in his theoretical work questioned the choice of a crystalline structure for the grain in earlier calculations (Hollenbach & Salpeter 1971; Hollenbach et al. 1971) and considered the formation of H_2 on amorphous surfaces, obtaining a formation efficiency much less than the one required by observations. This stimulated some authors to propose alternative mechanisms of formation of H_2 (Pirronello & Averna 1988; Averna & Pirronello 1991; Watanabe et al. 2000). A few years ago, our group at Syracuse University embarked in a program to conduct carefully designed experiments to study the formation of molecular hydrogen on surfaces in conditions as close to key ISM environments as technically feasible. The work concentrated on measuring the recombination efficiency on different candidates of actual dust grain surfaces and on elucidating the mechanism of H_2 formation (Pirronello et al. 1997a,b; Vidali et al. 1998; Pirronello et al. 1999). Other groups are now taking up the challenge of studying other important aspects of this problem.

2. Experimental

The apparatus used in these investigations was originally designed to study processes occurring on well-characterized surfaces. In state-of-the-art surface science work, probes are used to obtain knowledge of physical and chemical processes at the atomic level. The apparatus, see Fig.1, was modified to address the study of the formation of molecules catalyzed on surfaces of materials of relevance to astrochemistry. It has been described several times in easily accessible publications (Vidali et al. 1998; Pirronello et al. 2000; Manicò et al. 2001). Because of space constraints, here we rather give some overall design considerations that we followed in order to carry out the measurements under conditions as closely as possible to the ones present in key astrophysical environments. First, the apparatus uses ultra-high vacuum (UHV) techniques to keep the background pressure, mostly made up of H_2, in the 10^{-10} torr range (or 10^6 particles/cm^3) to avoid the contamination of the sample. Second, there is the capability of keeping the temperature of the sample in the range of astrophysical interest (10 to 30 K) as well as higher (for cleaning purposes) and lower (for studying processes that, if conducted at higher temperature, would take place too rapidly on the laboratory time scale to be measured). Great care has been given to the design of the sample holder, so the sample is adequately thermally shielded and its temperature is measured reliably (using a calibrated silicon diode in good thermal contact with the sample). Third, the exposure of gases to the sample is obtained using atomic beams. The use of beams allows to control the size of the beam (so it strikes the sample and no other part of the apparatus), its temperature and density. For this application, the use of low energy and low flux beams is essential. Also essential in the study of H_2 formation is the use of beams of two isotopes, H and D, so that the formation of HD can be unequivocally traced to processes on the sample. Therefore, the presence of background H_2 gas or imperfect hydrogen dissociation in the beam source do not influence our measurements. Thus, the innovative aspect of this apparatus is the ability to study astrophysically relevant physical and chemical processes that occur at the surface of grains, whereby in the past lab studies have been carried out to study reactions in the bulk of dust grain analogues.
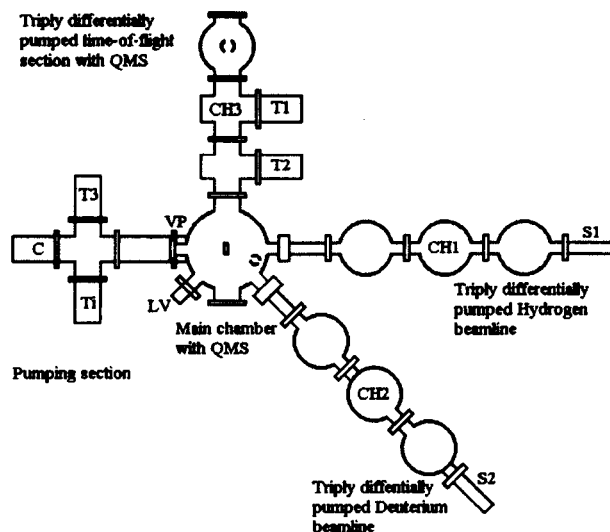
Fig. 1.— Schematic view of the apparatus at Syracuse University used to study physical and chemical processes on dust grain analogues in astrophysically relevant conditions. QMS is the quadrupole mass spectrometer; CH1,CH2 and CH3 are mechanical choppers (beam modulators); VP is the viewport to introduce the laser beam into the UHV chamber for the (2+1)REMPI investigation.

3. Review of Results

In Fig. 2 the recombination efficiency on different analogues of dust grain surfaces is plotted as a function of sample temperature. Here the recombination efficiency is obtained by taking the amount of HD collected in the reaction and dividing it by the measured amount of H and D sent onto the sample. This number is then corrected for the instrumental response and for the probability of forming HD versus H_2 or D_2. The amount of HD collected comes from two sources. The first is the HD that is formed during the time H and D atoms are sent to the surface. This contribution, which physically corresponds to a fast migration of H and D on the surface, is usually small at the lowest temperature. As mentioned elsewhere, the amount reported as the "fast reaction" contribution is typically an overestimate of the true HD formed under these conditions, since there are instrumental effects affecting the measurement that cannot be easily separated from the true contribution. The second source of the collected HD is the one formed during the thermal desorption, when the surface temperature is rapidly ramped providing mobility to atoms. Thus, the thermal desorption experiments can be thought as providing a means to accelerate processes that on grains in actual astrophysical environments would take much longer. Finally, it is worth reminding that in the experiments that we have done so far, the exposure of the surface to H and D was such that the sample is covered with much less than one layer of H or D. Thus, the contribution to HD formation from events in which H hits a D atom (or vice-versa) and forms HD without prior thermalization with the surface (the Eley-Rideal reaction) is expected to be small. The results presented in Fig. 2 were obtained on the following samples: a natural sample of polycrystalline olivine (Pirronello et $al.$ 1997a,b), amorphous carbon samples (Pirronello et $al.$ 1999), and amorphous water ice (Manicò et $al.$ 2001). The size of the symbols gives a measure of the statistical errors, while the scatter of the points for each type of material gives an indication of reproducibility due to preparation methods and instrumental effects.
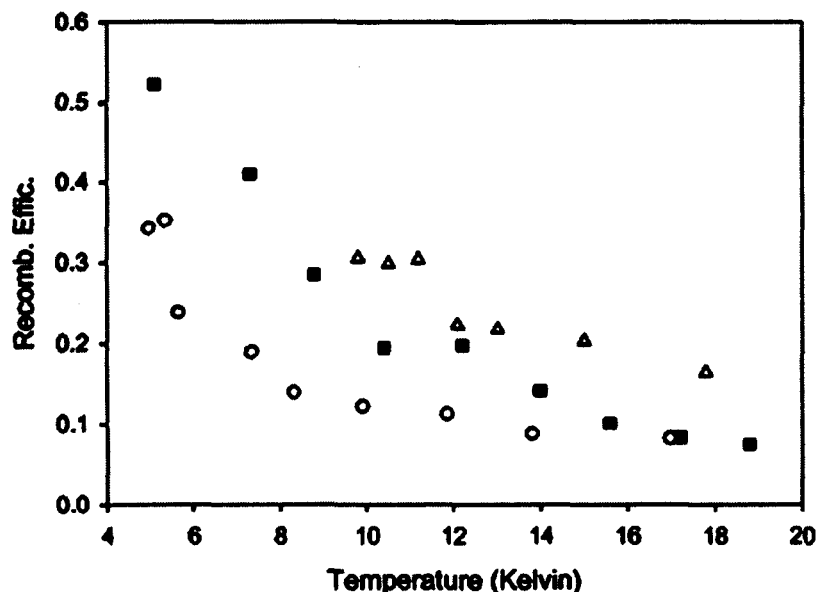
Fig. 2.— Recombination efficiency of molecular hydrogen versus temperature on polycrystalline olivine (circles), amorphous carbon (squares), and high density amorphous ice (triangles). Only the contribution from the thermal desorption experiment is shown, see text. The samples were exposed to roughly comparable amounts of H and D. Data are from Pirronello et $al.$ (1997a); Katz et $al.$ (1999); Manicò et $al.$ (2001).

4. Discussion

It would be desirable to conduct a systematic study of which processes or characteristics of the surface are responsible for a given trend in the recombination efficiency. Given the challenges of conducting these types of experiments, it will take time to amass this needed detailed information. As a first step, we recently began a systematic study of the effect on molecular hydrogen formation of the morphology of different types of amorphous ice and of treatment with UV radiation (Roser et al. 2002). Experiments to provide more specific answers on other aspects influencing the recombination efficiency are currently being designed. In the meantime, one can look at the information provided in Fig.2. It seems to indicate that surfaces that are more disordered, such as amorphous carbon or amorphous water ice, provide a more favorable locus for the formation of molecular hydrogen than polycrystalline olivine. Additional information on the formation of molecular hydrogen on surfaces comes from the study of the kinetics. First, as shown in Pirronello et al. (1997b), there is good experimental evidence that the kinetics of formation of molecular hydrogen on polycrystalline olivine at low temperature and at very low coverage of H is of the second order, signifying that the formation rate depends on the square of the concentration of the reactants. It is customary to obtain an insight into the desorption process by using the following approximation to relate the rate of desorption of particles $(d\mathcal{N}(t)/dt)$ to parameters related to surface processes:

$$-d\mathcal{N}(t)/dt = k_m N(t)^m,\tag{1}$$

where $\mathcal{N}(t)$ is the number of particles desorbing at time t, $N(T)$ is the number of atoms or molecules on the surface at time t (these particles cold be of a different species than the ones desorbing), $k_m = k^{(m)} exp(-E_d/k_B T)$, E_d is the desorption energy, $k^{(m)}$ is a constant, and m is the order of the desorption. For $m = 0$, desorption is independent of coverage, which is the case appropriate for desorption from several layers, since the desorption yield doesn't, in first approximation, depend on the coverage. A typical signature is the presence of a common leading edge for different coverages. $m = 1$ corresponds to first order desorption, and the molecules already formed on the surface leave during the desorption independently from each other; a distinguishing trait is the common trailing edge and the same peak position as a function of coverage. $m = 2$ corresponds to second order desorption, that is the reaction rate depends upon the products of the adatoms' concentrations; in this case, the peak shifts as a function of coverage. The observation that data can be fitted with an $m = 2$ kinetics indicates that the mechanism of formation involves the diffusion of the reactants, thus contradicting the long held assumption that molecular hydrogen would form quickly due to tunneling. Rather, it seems that H (and D) atoms are stuck in deeper wells and can move if given a thermal boost. This led Pirronello et al. (1977b) to propose an expression for the recombination rate that is quadratic in the density of H in ISM clouds:

$$R_{H_2} = \frac{1}{2}(n_H v_H A St_H)^2 n_g \alpha \gamma',\tag{2}$$

where n_H and v_H are the number density and the speed of H atoms in the gas phase, respectively; A is the average cross-sectional area of a grain; t_H is the residence time of adsorbed II atoms on the surface, S is the sticking coefficient, n_g is the number density of dust grains, and α is the hopping rate of a single H adatom. γ' takes into account the possibility that there is an activation energy for recombination. Notice that the quantity that is squared, i.e., $(n_H v_H A St_H)$, is the average number N of H atoms adsorbed on the surface at a given time. Biham et al. (1998) found from an analysis of the rate equations that this is the correct expression of the steady state solution in the case of slow diffusion of reactants on dust grains, while the Hollenbach et al.'s expression, which is linear in the concentration of H in the ISM, holds in the regime of very fast tunneling or large coverage of H on

the grain. The second type of information that can be extracted from the data is about the activation energy of the reaction. Using rate equations, Katz *et al.* (1999) fitted thermal desorption data of H and D on olivine and amorphous carbon to obtain activation energy barriers. No prior assumption on the order of the desorption was made. The results of this theoretical analysis confirmed the picture given above obtained with the use of Eq.(1), and gave a tool to extrapolate the experimental results to conditions in the ISM. The molecular hydrogen formation efficiency on amorphous carbon and water ice (Katz *et al.* 1999; Manicò *et al.* 2001) can explain the abundance of H_2 in diffuse and quiescent dense clouds. An analysis of the formation of HD on different types of amorphous water ice (Roser *et al.* 2002) gives information on the energetic of the reaction $H_{surface} + D_{surface} \rightarrow HD_{desorbing}$ as a function of different ice morphology.

5. Future Investigations

Thirty years ago, when the first model of the formation of molecular hydrogen on dust grains came out, there was no experimental evidence to verify its predictions or to point the way for further refinements. Now there are experimental data on recombination efficiencies and kinetics of recombination which have shed light on this fundamental process. As more experiments are being carried out at Syracuse University and soon elsewhere, detailed information on the influence of the morphology and chemical make-up of surfaces of dust grain analogues will soon be available. Furthermore, at Syracuse University we have set-up a measurement system to determine the kinetic energy of the departing molecules by using time-of-flight mass spectrometry (see Fig.1) as well as their roto-vibrational status - for detecting the internal quantum state of hydrogen molecules we use a (2+1) REMPI (Resonance Enhanced MultiPhoton Ionization) scheme. We are also planning to build an instrument to measure the energy released into the solid by the reaction of molecular hydrogen formation. From the theoretical standpoint, the sophistication of the calculations will have to match that of the experiments; the formation of molecular hydrogen will have to be studied on realistic, disordered surfaces.

Acknowledgments

REFERENCES

Averna, D., & Pirronello, V. 1991, A&A, 245, 239.

Biham, O., Furman, I., Katz, N., Pirronello, V., Vidali, G. 1998 MNRAS, 269, 869.

Hollenbach, D.J., & Salpeter, E.E. 1971, ApJ, 163, 155.

Hollenbach, D.J., Werner, M.W., & Salpeter, E.E. 1971, ApJ, 163, 165.

Katz, N., Furman, I., Biham, O., Pirronello, V., & Vidali, G. 1999, ApJ, 522, 305.

Manicò, G., Raguni, G., Pirronello, V., Roser, J.E., & Vidali, G. 2001, ApJ, 548, L253.

Pirronello, V., & Averna, D. 1988, A&A, 196, 201.

Pirronello. V.. Liu. C.. Shen. L.. & Vidali. G. 1997a. ApJ. 475. L69.

Pirronello, V., *et al.*1997b, ApJ, 483, L131.

Pirronello, V., Liu, C., Roser, J.E., & Vidali, G. 1999, A&A, 344, 681.

Pirronello, V., al., 2000 in Molecular Hydrogen in Space, eds. Combes & Pineau de Forets (Cambridge Univ Press), 71.

Roser, J.E., Manicò, G., Pirronello, V., & Vidali, G. 2002, to be submitted.

Smoluchowski, R. 1979, Astrophys. Space Sci., 65, 29.

Smoluchowski, R. 1981, Astrophys. Space Sci., 75, 353.

Smoluchowski, R. 1983, J. Phys. Chem., 87, 4229.

Vidali, G., Pirronello, V., Liu, C., & Shen, L. 1998, Astrophys. Lett. Commun., 35, 423.

Watanabe, N., Horii, T., &Kouchi, A. 2000, ApJ, 541, 772.

SOLAR SYSTEM

~ ~ *INVITED* ~ ~

A Solar System Perspective on Laboratory Astrophysics

Dale P. Cruikshank

NASA Ames Research Center, Moffett Field, CA

1. Introduction

Planetary science deals with a wide variety of natural materials in a wide variety of environments. These materials include metals, minerals, ices, gases, plasmas, and organic chemicals. In addition, the newly defined discipline of astrobiology introduces biological materials to planetary science. The environments range from the interiors of planets with megapascal pressures to planetary magnetospheres, encompassing planetary mantles, surfaces, atmospheres, and ionospheres. The interplanetary environment includes magnetic and electrical fields, plasma, and dust. In order to understand planetary processes over these vast ranges, the properties of materials must be known, and most of the necessary information comes from the laboratory.

Observations of the bodies and materials in the Solar System are accomplished over the full range of the electromagnetic spectrum by remote sensing from Earth or spacecraft. Comets exemplify this; molecular and atomic identifications are made from the hard ultraviolet to radio wavelengths, while X-rays are emitted as comets interact with the solar wind. Gamma rays from the surfaces of the Moon and asteroids are diagnostic of the mineral and ice content of those bodies; eventually, gamma rays will also be observed by probes to comets.

A number of planetary materials are available in the laboratory for extensive Study: rocks from the Moon, Mars, several asteroids, as well as dust from comets (and perhaps the Kuiper Belt) are closely studied at every level, including atomic (isotopic). Even pre-solar interstellar grains isolated from meteorites are scrutinized for composition and crystalline structure.

Beyond the materials themselves, various agents and processes have altered them over the 4.6-Gy age of the Solar System. Solar radiation, solar wind particles, trapped magnetospheric particles, cosmic rays, and micrometeoroid impacts have produced chemical, physical, and morphological changes in the atmospheres and on the surfaces of all planetary bodies. These processes are not well understood, so studies in a laboratory setting are especially needed.

2. Laboratory Data Needed for Planetary Science

A number of problems in contemporary planetary science have generated specific needs for additional laboratory work, and we review a sampling of those here.

Planetary interiors: For the giant planets, the equations of state for H_2, H_2+He, and H_3 at pressures >3 MPa must be better understood. [1] How do the equations of state change

---

[1]The equations of state describe the relationships of the directly observable quantities that specify the thermodynamic state of a system. For fluids, these are pressure, volume, and temperature (P, V, T); for solids these are the same quantities plus stress and strain components; for ferromagnets these are the same quantities plus the applied field H and magnetization M.

when H_2 is shocked? In the context of the interiors of the Galilean satellites it is important to study saline solutions, while other materials (notably ices) present in the interiors of large planetary satellites and distant bodies in the outermost Solar System (Kuiper Belt objects) require further investigation.

Planetary atmospheres: Various planetary missions already completed or in progress are driving the need for additional laboratory work. In studies of Mars, high accuracy measurements of line strengths of CO_2 and H_2O in the near-infrared are needed. For Jupiter and Saturn, spectral measurements of CO broadening by H_2 and He are relevant. Improved line strengths for PH_3 are needed in the far-infrared (100-500 μm).

In the Cassini investigation of Titan with the CIRS instrument, improved line strengths and line- broadening parameters are needed for several materials, such as nitriles and hydrocarbons throughout the mid- and far-infrared. The nitriles include HCN, HC_3N, and C_2N_2, acetonitrile (CH_3CN), acrylonitrile (CH_2CHCN) and proprionitrile (CH_3CH_2CN) in the 14-50-μm range. Among the hydrocarbons, pure rotation lines of CH_4 near 100 μm will probe the temperature of the lower stratosphere of Titan. Improved line strengths in the 12-30-μm range are needed for methyl acetylene (CH_3CCH) and allene (CH_2CCH_2) are needed. A possible condensate and component of Titan's aerosol smog is diacetylene (C_4H_2) requires further laboratory spectroscopic studies to support the data expected from the CIRS investigation.

There are unsettled questions regarding the colors of the clouds of the outer planets, including the source of the color in Jupiter's Great Red Spot. There may be a "weathering" phenomenon in the clouds, the consequence of which causes the NH_3 clouds of Jupiter and Saturn to lose their NH_3 spectral signatures over time. The coloring agents in the stratospheric clouds of Uranus and Neptune are also not understood.

Planetary surfaces: Surface materials include ices, minerals, and organic solids. There is a large body of reflectance and emittance spectroscopy of minerals, a lesser amount for ices, and very little for organic solids. All areas of laboratory investigation need support, particularly for ices and organic solids. Spectra alone are insufficient for modeling needs, because spectrum matching is an inadequate means for making identifications of materials present on a planetary surface, and is not sufficiently quantitative. Spectrum modeling by scattering theory (e.g., Hapke or Shkuratov) provides a more quantitative evaluation of species present, plus information on particle sizes, and critical details on the mixing of components. Spectrum modeling with scattering theory requires that the complex refractive indices of candidate materials be determined at a suitable spectral resolution and over the necessary range of wavelength. Such data are available for a very limited number of materials, thus restricting the range of modeling parameters that can be explored.

Specifically, there is a need for complex refractive indices from the UV to the mid-IR for minerals, ices, and organic solids of planetary interest. Minerals include igneous silicates, salts, carbonates, sulfides, and oxides. Ices include hydrocarbons and nitriles in amorphous and crystalline phases, and in matricies (N_2, Ar, H_2O). Organic solids include extracts from carbonaceous meteorites, terrestrial kerogens, and synthetic organics (tholins) produced by energy deposition in gases and solids of planetary significance.

Space processing: Planetary materials exposed to the space environment are impacted by solar UV, solar wind particles, galactic cosmic rays, micrometeoroids, and macrometeoritic collisions, all of which serve to alter the chemical, crystal, and microphysical characteristics of surface materials. These processes must be factored into the interpretation of remote sensing observations of planetary bodies, insofar as their effects are understood. There is a wide range of experimental studies that can be conducted in the laboratory to expand our understanding of the processes of sputtering, radiation darkening, organic production, ablation, and others.

3. Facilities

In addition to specific areas of laboratory measurements that are critical for the interpretation of planetary data, this subject has the unique and specialized needs for the study and preservation on Earth of materials from space. Meteorites and interplanetary dust particles collected on the surface, in the ice sheets, and in the high atmosphere, are a priceless treasure of extraterrestrial materials that arrive on our planet free of charge. To extract their secrets, these materials must be studied with the most modern analytical techniques, and they must be preserved for future studies. Additionally, extraterrestrial materials brought to Earth by space expeditions (including Apollo), also require study and preservation. This part of the equation is not free of charge.

Lab Facilities for Returned Samples: Preparations must be made for analysis of the samples returned from the Stardust, Genesis, Muses-C missions, and eventual returns from Mars and a comet nucleus. This can be accomplished through the establishment of a realistic laboratory instrument development program. The development of new analytical technologies is especially urgent, with the greatest need being for development of organic chemistry micro-analysis. As new techniques are established and new analytical equipment becomes available, the program priorities should shift to outfitting and upgrading U.S. labs.

Lab Facilities for the Study of Planetary Materials: Several ambitious NASA planetary missions to planets, comets, and asteroids are in progress or in various stages of advanced planning. Critical to the correct and complete interpretation of the observational data acquired at great expense are laboratory studies that will provide data of the kind mentioned earlier in this report. Such work is often inadequately supported, either in existing laboratory facilities, or through the creation of new laboratories.

Curation: In preparation for the samples to be returned from the Stardust, Genesis, Muses-C, as well as anticipated returns from Mars and a comet nucleus, support for sample curation and handling is urgently needed at a significantly increased level over that which exists today. The proper preservation (and quarantine) of each returned sample for future investigations is of singular importance. The samples returned from each object will impose specific handling and storage demands, which must be addressed by separate, specialized facilities. The funding for these facilities, including long-term operating costs is very unlikely to be included in each mission's budget. In preparation for the return of cold samples from comets, development is needed in the areas of cryocuration, robotic sample handling, and biological quarantine.

Acknowledgments

REFERENCES

Several recent papers on photolysis and radiolysis of outer Solar System ices were published as a special section of *J. Geophys. Res.* 106, pp. 33,273-33,392, 2001.

Two important books on the properties of ices are:
1. Schmitt, B., C. de Bergh, and M. Festou (eds.), *Solar System Ices*, Kluwer Academic Publishers, Dordrecht. 826 pp. 1998.
2. Petrenko, V. F., and R. W. Whitworth. Physics of Ice, Oxford. 373 pp. 1999.

Two books on rocks and minerals of importance in planetary science are:
1. Pieters, C. M., and P. A. J. Englert (eds.) Remote Geochemical Analysis: Elemental and Mineralogical Composition. Cambridge. 594 pp. 1993.
2. Papike, J. J. (ed.) Planetary Materials (Reviews in Mineralogy Vol. 36), Mineralogical Soc. America. 1038 pp. 1999.

The U.S. Geological Survey library of mineral spectra is available:
1. Clark, R. N., G. A. Swayze, A. Gallagher, T. V. V. King, and W. M Calvin, U.S. Geological Survey Digital Spectral Library: Version 1: 0.2 to 3.0 μm. U.S. Geological Survey Open File Report 93-592, http://speclab.cr.usgs.gov, 1340 pp. 1993.

Optical constants for several minerals can be found on the web site:
http://www.astro.uni-jena.de/Users/database/f-dbase.html

Another on-line source of spectra of minerals, rocks, some ices, meteorites, and lunar materials is:
http://speclib.jpl.nasa.gov

Laboratory Studies of the X-ray Emission
Produced by the Interaction of Solar Wind Heavy Ions with Comets

P. Beiersdorfer, H. Chen, M. May, D. Thorn
Lawrence Livermore National Laboratory, Livermore, CA

K. R. Boyce, G. V. Brown, R. L. Kelley, F. S. Porter, C. K. Stahle, A.E. Szymkowiak
NASA Goddard Space Flight Center, Greenbelt, MD

S. M. Kahn
Columbia Astrophysics Laboratory, Columbia University, New York, NY

Abstract

The process of X-ray emission following charge exchange between solar wind heavy ions and cometary gases is studied in the laboratory. The emission is recorded with the spare *ASTRO-E* 6x6 microcalorimeter array. The microcalorimeter affords a resolution of better than 10 eV in the range of X-ray energies of interest and thus individual emission lines can be resolved. Our present measurements focus on the most abundant K-shell heavy ions found in the solar wind. In particular, we measure the K-shell emission of bare C, N, O, and Ne, and their hydrogenlike counter parts interacting with such gases as CO_2, N_2, and CH_4. Several results are noted that had not been considered in the early cometary X-ray models.

1. Introduction

Charge exchange between cometary gases and solar wind heavy ions is likely to be the dominant process of X-ray emission from comets. While charge exchange cross sections have been measured by various facilities, little experimental data has been gathered about the detailed processes that lead to X-ray line formation. To fill this void, we are studying the charge exchange process in the laboratory.

Our studies utilize ions from EBIT-I and EBIT-II, electron beam ion traps at the Lawrence Livermore National Laboratory (Levine *et al.* 1988), the first and second such devices put into operation (in 1986 and 1990, respectively). Ions are produced with the electron beam on in the so-called electron trapping mode, then the beam is turned off and the device is operated in the so-called magnetic trapping mode (Beiersdorfer *et al.* 1996). In this mode, the trap is operated like a Penning trap. Neutral atomic or molecular gases of choice are introduced into the trap, and the ions are allowed to undergo charge exchange reactions.

The charge exchange induced X-ray emission is recorded with the spare *ASTRO-E* microcalorimeter array built at the Goddard Space Flight Center (Porter *et al.* 2000). This calorimeter has unique features that make charge-exchange measurements possible. First, it has a large effective area (≈ 13 mm^2) consisting of 36 individual elements, 32 of which are active. A large area is necessary to observe the rather weak signal from charge exchange, which is about 100 - 1000 times weaker than x-ray emission from electron-impact excitation during

the electron trapping mode. Second, the Goddard calorimeter gives a time-tag to each photon. This is necessary to distiguish between X rays collected during the electron trapping mode and the magnetic trapping mode. Third, the long-term gain stability allows us to collect data for extended periods without compromising the resolving power. Finally, the differential response of our instrumentation is calibrated *in situ*. This is necessary at the low energies of the X rays of interest (< 1000 eV), where the instrumental response is strongly affected by the transmission of the thermal shielding foils.

2. Typical Results

Our present measurements focus on the X-ray emission from K-shell heavy ions. A spectrum of the X-ray emission from hydrogenlike Ne^{9+} following charge exchange between bare Ne^{10+} and neutral neon is shown in Fig. 1. The spectrum shows lines corresponding to transitions from the $2p$, $3p$, $4p$, $5p$, and $6p$ upper levels to the $1s$ ground state. These are labeled Lyα, Lyβ, Lyγ, Lyδ, and Lyϵ, respectively.

The figure also shows the predictions of the cometary X-ray models developed by Häberli *et al.* (1996) and Wegmann *et al.* (1997). Häberli *et al.* included emission from only the $2p$ level. Wegmann *et al.* included emission from all upper levels accessible to population by charge exchange assuming that the amount of emission from each upper level is same for all.

A spectrum of the X-ray emission from heliumlike Ne^{8+} following charge exchange between hydrogenlike Ne^{9+} and neutral neon is shown in Fig. 2. The spectrum is very different from that shown in Fig. 1. First, emission involving high principal quantum numbers is suppressed. Most emission is from lines with an $n = 2$ upper level. Second, the forbidden transition $1s2s\ ^3S_1 \rightarrow 1s^2\ ^1S_0$ produced the strongest X-ray emission. This emission pattern is the direct result of the presence of triplet levels in the heliumlike ion, which strongly determines the radiative properties of the heliumlike ion (Beiersdorfer *et al.* 2001). Triplet levels do not exist in hydrogenlike ions. Predictions from Häberli *et al.* (1996) and Wegmann *et al.* (1997) are again overlayed with the measured spectrum in Fig. 2.

3. Conclusion

Our measurements have produced several suprising results that had not been considered in the early cometary X-ray models. The emission pattern is different for different isoelectronic systems; the forbidden line $1s2s\ ^3S_1 \rightarrow 1s^2\ ^1S_0$ produces the strongest emission in heliumlike ions. The actual emission pattern changes with the collision energy (Beiersdorfer *et al.* 2001). Moreover, the detailed emission depends on the chemical composition of the cometary gases. The complexity of the X-ray emission from cometary (and presumably from planetary) atmospheres implies rich opportunities for using the emission for diagnostic purposes that go beyond merely determining the composition and intensity of the solar wind.

Acknowledgments
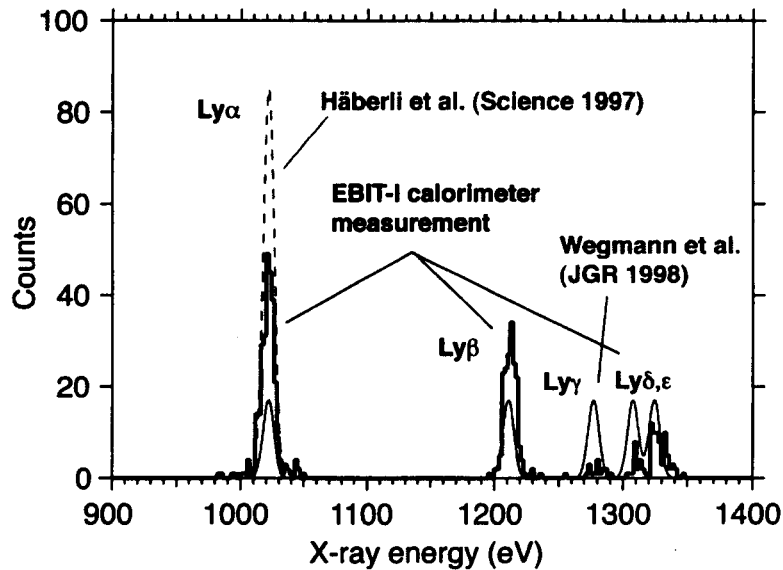
Fig. 1.— Ne IX spectrum measured with the Goddard X-ray microcalorimeter on the Livermore EBIT-II electron beam ion trap. The spectrum was produced by charge exchange recombination of Ne^{10+} with neutral neon.
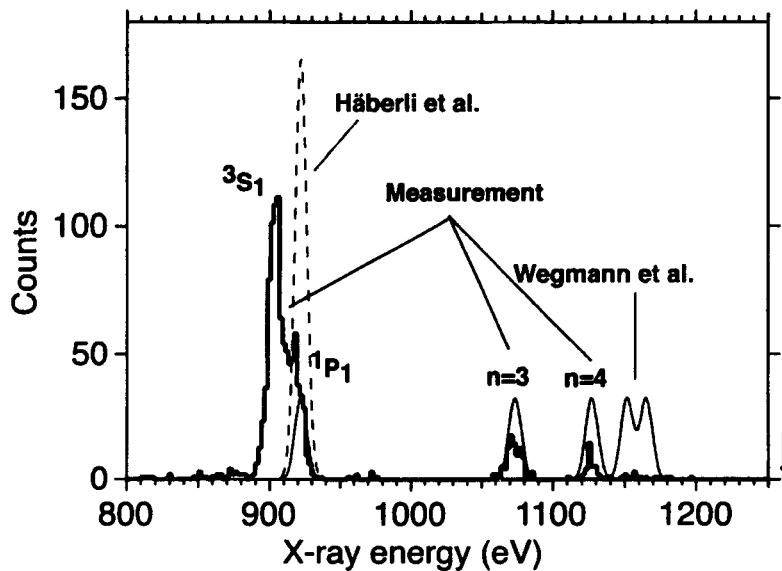
Fig. 2.— Ne VIII spectrum measured with the Goddard X-ray microcalorimeter on the Livermore EBIT-II electron beam ion trap. The spectrum was produced by charge exchange recombination of Ne^{9+} with neutral neon forming excited heliumlike Ne^{8+} ions.

REFERENCES

Beiersdorfer, P., et al., 1996b, Rev. Sci. Instrum. 67, 3818.

Beiersdorfer, P., et al., Ap. J. Letters 549, L147.

Häberli, R. M., et al., Science 276, 939.

Levine, M., et al., 1988, Phys. Scr., T22, 157.

Porter, F. S., et al. 2000, Proc. SPIE, 4140, 407.

Wegmann, R., et al., 1998, Planet. Space Sci. 46, 603.

Temperature Dependence of the Rate Constant for the CH$_3$ Recombination Reaction:
A Loss Process in Outer Planet Atmospheres

R. J. Cody, W. A. Payne, R. P. Thorn, Jr., P. N. Romani, L. J. Stief
NASA/Goddard Space Flight Center

F. L. Nesbitt
Coppin State College

M. A. Iannone
Millersville University

D. C. Tardy
University of Iowa

1. Introduction

The methyl free radical (CH$_3$) has been observed in the atmospheres of Saturn and Neptune by the ISO satellite. There are discrepancies between the column densities for the CH$_3$ radical derived from the ISO observations and the column densities derived from atmospheric photochemical models. For Neptune the model column density is 1.5 times that derived from ISO. For Saturn the model is 6 times that from ISO. The recombination of methyl radicals is the major loss process for methyl in these atmospheres. The serious disagreement between observed and calculated levels of CH$_3$ has led to suggestions that the atmospheric models greatly underestimated the loss of CH$_3$ due to poor knowledge of the rate of the reaction (1) CH$_3$ + CH$_3$ + M $\rightarrow$ C$_2$H$_6$ + M at the low temperatures and pressures of these atmospheric systems. Although the reaction CH$_3$ + CH$_3$ + M $\rightarrow$ C$_2$H$_6$ + M has been extensively studied both theoretically and experimentally, the laboratory conditions have been, with only a few exceptions, higher temperatures (T$\geq$298K), higher pressures (P$\geq$ 10 Torr - 13.3 mbar) or M=Ar rather than H$_2$ or He as the bath gas.

2. Experimental

In an attempt to resolve this problem, we undertook in our laboratory the measurement of the absolute rate constant for the self-reaction of CH$_3$ at T = 155, 202 and 298 K and P = 0.6 - 2.0 Torr nominal pressure with He as the bath gas. The experimental technique is discharge fast flow with mass spectrometric detection and monitoring of the CH$_3$ decay. The methyl radical is generated via the fast reaction F + CH$_4$ $\rightarrow$ CH$_3$ + HF. A microwave discharge generates the fluorine atoms. The CH$_4$ reagent is added through the moveable injector, which allows the CH$_3$ mass spectrometric signals to be measured versus distance and therefore time. Methane was in large excess to ensure rapid and quantitative conversion of F to CH$_3$. The absolute concentration of fluorine atoms used to generate CH$_3$ was determined by measuring the consumption of Cl$_2$ in the fast titration reaction F + Cl$_2$ $\rightarrow$ Cl + FCl. The methyl radicals

were detected at m/z = 15 following low-energy (10 - 11 ev) electron impact ionization. Since large concentrations of methane were required, the low electron energy prevented dissociative ionization of CH_4 to yield CH_3^+. A cooling jacket surrounds the tubular flow tube to vary the temperature of the gas flow. At 202K, the coolant was ethanol circulated from a commercial chiller. At 155K, the coolant was nitrogen gas which had flowed through a copper coil immersed in liquid nitrogen.

Since the recombination reaction of the CH_3 radicals is second order in CH_3, absolute concentrations of the radical are needed for the kinetic data analysis. Integration of the second order rate equation, i.e., $-(d[CH_3]/dt = 2 k_1 [CH_3]^2$, yields the analytical expression for data analysis: Equation 1: $(1/[CH_3]_t) - (1/[CH_3]_0) = 2k_1t$, where $[CH_3]_t$ is the absolute methyl concentration at time = t, $[CH_3]_0$ is the concentration at time = 0 and k_1 is the rate constant for the methyl recombination reaction. The slope of the plot of the inverse of the mass spectrometric signal versus time yields the rate constant via a scaling factor. The $[CH_3]$ equals the measured mass spectrometric signal times a scaling factor (SF). SF can be determined from ratio of the absolute methyl concentration to the corresponding mass spectrometric signal at m/z = 15. However, the absolute $[CH_3]$ comes from the F atom titration and hence gives $[CH_3]$ at t = 0, while the signal is recorded at t = about 3 ms and beyond due to the limitation of finite time for mixing at the tip of the injector and perturbations in flow near the end of the flow tube. For the case of a first order signal decay this is easily handled by a short, linear extrapolation of the signal back to t = 0 in a plot of ln(signal) versus time. In the present experiments which are second order in CH_3, plotting the inverse of the signal versus time yielded the expected linear plots according to Equation 1. However, extrapolation to t = 0 did not yield reasonable and consistent values for the signal at t = 0 and hence the scaling factor. Although the signal decay is mostly second order in CH_3, there are some first order components. Therefore, the scaling factor had to be determined from a calibration decay measurement at low initial methyl concentration.

For the calibration experiments, the methyl concentration was reduced to the lowest possible level where the signal level could still be quantitatively recorded. This was $[CH_3] = (2-4)\times10^{11}$ molecules cm^{-3}. Under these conditions, the signal appeared to exhibit good first order decay, although kinetic modeling showed there is a substantial second order contribution. To verify the correctness of these calibration experiments, a number of them were performed with added molecular chlorine in considerable excess, i.e. $[Cl_2] = (2-3)\times10^{13}$ molecules cm^{-3}. Under these conditions, the CH_3 decays largely by the reaction: $CH_3 + Cl_2 \rightarrow CH_3Cl + Cl$. The methyl decay is strictly first order, and the methyl signal at t= 0 is determined by a short linear extrapolation. Then, the absolute methyl concentration at t = 0 is determined by a titration of the F atoms with Cl_2 as described above for the rate constant decay measurements. Therefore, each experiment required two decay measurements and two F atom titrations.

3. Results

For each temperature and pressure the methyl concentration was varied by at least a factor of two to verify the independence of the rate constant with concentration. The $[CH_3]$ ranged

from (1.2 to 10.8) x 10^{12} molecules cm^{-3}. The rate constants (k_1) are presented below in units of cm^3 $molecule^{-1}$ s^{-1}. The experimental results show that the reaction is in the fall-off region at T = 202 and 298 K. At T = 298K, k_1(0.6 Torr) = 2.15 x 10^{-11} and k_1 (1 Torr) = 2.44 x 10^{-11}. At T = 202K, the rate constant increased from k_1 (0.6 Torr) = 5.04 x 10^{-11} to k_1 (1.0 Torr) = 5.25 x 10^{-11} to k_1 (2.0 Torr) = 6.52 x 10^{-11}. At T = 155 K, the results indicate that the reaction is either at the high pressure limit or so close that we cannot measure a pressure effect upon the rate constant. At T = 155K, k_1 (0.6 Torr) = 6.82 x 10^{-11}, k_1 (1.0 Torr) = 6.98 x 10^{-11} and k_1 (1.5 Torr) = 6.91 x 10^{-11}.

The rate constants for the methyl self-recombination as measured in this study are appropriate for the atmospheric models of Saturn and Neptune in temperature but not in pressure. The lowest pressure we could reach in the flow system is about 0.6 Torr. Therefore, these results will have to be combined with theory to derive the rate constants needed for the atmospheric physical conditions of the outer planets. The experimental rate constants measured in this study and those measured by Slagle et al.(1988) are being used to test the derivation of an analytical expression for the rate constant as a function of both pressure and temperature. The analytical expression will then provide the rate constants at lower pressures for use in the photochemical models of the planetary atmospheres.

Acknowledgments

REFERENCES

Slagle, I. R.; Gutman, D.; Davies, J. W. and Pilling, M. J.; *J. Phys. Chem.* 1988, 92, 2455.

Cryogenic Reflectance Spectroscopy
in Support of Planetary Missions

J. B. Dalton

NASA Ames Research Center, Moffett Field, CA

Abstract

Present understanding of planetary composition is based primarily on remotely-sensed data, and in particular upon ultraviolet, visible, and infrared spectroscopy. Spectra acquired by telescopic and spacecraft instruments are compared to laboratory measurements of pure materials in order to identify surface components based on characteristic absorption features.

Cryogenic spectral measurements are necessary for the study of worlds beyond the Earth's orbit. While some materials exhibit only small spectral changes as a function of temperature (Roush and Dalton 2002), many others are strongly temperature-dependent (Dalton and Clark 1998; Grundy and Schmitt 1998). For example, hydrated salts exhibit different spectral behavior under conditions appropriate to Europa (Dalton 2000) than at terrestrial temperatures (Crowley 1991). The icy satellites of the outer solar system contain significant quantities of volatile ices (Roush 2001) which do not even exist at standard temperature and pressure (STP).

A comprehensive spectral database of ices and minerals covering a wide temperature range will have applications ranging from the study of comets and Kuiper Belt objects to outer planet satellites and the polar regions of Mars. Efforts are presently underway at NASA-Ames to develop capabilities which will contribute to such a database. As spacecraft instruments feature increasing spatial and spectral resolution, appropriate laboratory reference spectra become increasingly critical to accurate interpretation of the spacecraft data.

1. Introduction

Determination of planetary surface composition using remotely-sensed spectoscopic data relies heavily on comparison to reference spectra acquired under controlled conditions in the laboratory. Telescopic and spacecraft observations in the ultraviolet, visible, and infrared portions of the spectrum all require knowledge of the fundamental spectral properties of pure materials in order to identify surface components. However, development of spectral databases for materials relevant to low-temperature surface conditions such as the Martian polar regions, satellites of outer planets, Kuiper belt objects and comets lags significantly behind mission data analysis.

The advent of imaging spectrometers such as the Galileo Near-InfraRed Imaging Spectrometer (NIMS), Mars Global Surveyor Thermal Emission Spectrometer (MGS TES), Mars Odyssey Thermal Emission Imaging Spectrometer (THEMIS), and Cassini Visible and Near-Infrared Imaging Spectrometer (VIMS) heralds a phase of exploration wherein the distributions of surface (and atmospheric) components may be determined with relative ease once the components have been identified. The high spatial resolution achievable with these modern instruments enables scientists to study the composition of individual deposits and other features

of a planet or satellite. Additional imaging spectrometers are under study for the Mars 2005 mission and prospective missions to Europa, Pluto and the Kuiper Belt. Interpretation of these data will require access to reference spectra of surface materials measured under controlled laboratory conditions.

2.   Mars and the Outer Solar System

Most spectral databases for minerals contain measurements performed at standard temperature and pressure (STP), or at room temperature. This is adequate for most terrestrial remote-sensing investigations. However, many minerals exhibit temperature-dependent variations in the strength, position and shape of their absorption features (Roush and Singer 1983; Singer and Roush 1985) which become pronounced at temperatures relevant to Mars, the asteroids, and the outer solar system. At orbits beyond the Earth's, planetary surfaces contain materials which do not even exist at STP. Some, such as carbon dioxide ice, which occurs at the surface of Mars and in its polar caps, are familiar to many scientists; other more esoteric species like ammonia frosts (Dalton *et al.* 2001) or sulfur dioxide ice are rarely encountered even in the laboratory.

The surfaces of the outer planet satellites are characterized by temperatures in the 50 to 150 Kelvin range. Triton, Pluto and Charon (Grundy *et al.* 1993; Satorre *et al.* 2001) reach temperatures as low as 40 K. In this range, terrestrial gases quite literally become minerals. Volatiles such as methane, carbon monoxide, acetylene and nitrogen form ices and compounds which do not exist at STP. Of those that do, the spectra of many exhibit temperature dependencies. Ordinary hexagonal water ice is noted for its strong spectral variations in response to temperature (Grundy and Schmitt 1998). In many other ices, the extent of temperature dependence is not well constrained. Because planetary composition cannot be reliably determined without recourse to reference spectra, there is a strong need for laboratory work to characterize these materials at cryogenic temperatures relevant to solar system objects. Specifically, there is a need for *reflectance* measurements of a host of substances to enable direct comparison with spacecraft and telescopic observations.

3.   Laboratory Measurements

Many materials have been considered likely candidate constituents of icy satellites. These include various compounds and polymorphs of water ice, sulfur, carbon, nitrogen and oxygen, several minerals and hydrated salt compounds, and several organics of varying degrees of complexity (Delitsky and Lane 1997, 1998; Dalton 2000; Roush 2001). Many of these are products of chemistry driven by charged-particle and ultraviolet radiation (Brucato *et al.* 1997; Gerakines *et al.* 2000; Hudson *et al.* 2001; Moore *et al.* 2001; Bernstein *et al.* 2002). A number have been detected from telescopic and spacecraft observations. While most have been studied in the laboratory, few of these measurements are directly applicable to mapping of spatial distributions on icy satellites using spacecraft observations. This is usually because most measurements are not: (1) in *reflectance*; (2) in the same *wavelength* range as the spacecraft instruments; or (3) in the *temperature* range relevant to the planetary body of interest.

Much of the work on ices to date has been concerned primarily with astrophysical ices of the interstellar medium, such as the thorough compendium of Hudgins *et al.* (1993) and other works (Gerakines *et al.* 1996, 1999; Satorre *et al.* 2001; Moore *et al.* 2001). Consequently, the measurements are usually of transmittance (cf. Bernstein *et al.* (1997)) or absorbance (cf. Ehrenfreund *et al.* (1997)); neither can be converted directly to reflectance. While these are useful for identifying frequencies of diagnostic absorption features, reflectance spectra are required to derive any sort of meaningful abundance estimates. Since the shapes, depths, strengths, and positions of diagnostic features differ between transmittance, absorbance and reflectance, published values of reflectance, or of optical constants (Hudgins *et al.* 1993), from which reflectance may be derived, are needed.

A further difficulty of applying transmission or absorption measurements to reflectance spectra of icy satellites is that the laboratory studies are typically done using thin films. This is to prevent saturation in the fundamental absorption bands. However, this also results in extremely weak or nonexistent overtone and combination bands. Reflectance spectra of planetary surfaces, which are optically thick, exhibit strong overtones and combinations, which cannot be interpreted based on the thin-film data.

Published laboratory spectra of pure materials are often acquired with a particular mission (cf. Ehrenfreund *et al.* (1997); Gerakines *et al.* (1999); and others) in mind. Thus the wavelength and temperature ranges tend to be restricted to those of the instruments and bodies of interest for that particular paper. One of the more sensible restrictions is the practice of measuring spectra only in the vicinity of an important absorption feature, as in Bernstein *et al.* (1997). However, on a planetary surface, a given surface component contributes to measured spectral reflectance throughout the spectral range, not just in the immediate vicinity of its strongest absorption frequencies. Contributions to continuum and far-wing effects must be taken into account in interpretations of spacecraft observations. Spacecraft spectrometers typically measure light in the visible to near-infrared wavelengths (.3 to 5 μm; 30,000 to 2000 cm^{-1}) where reflected solar radiance is maximized. Studies of interstellar ices are typically placed in the mid- to far-infrared where fundamental absorptions are concentrated. Since many of the published studies do not cover the wavelength ranges of planetary observations, they are of limited value in interpreting data from planetary missions.

The infrared spectra of many volatile ices (Dalton *et al.* 2001) and minerals (Roush and Singer 1983) display marked temperature dependencies over the range from 4 to 300 Kelvin. An example is the hydrated salts, which are important to studies of the Galilean satellites. These have radically different spectra at 120 Kelvin than at STP (Dalton 2000) and their absorption frequencies vary noticeably over tens of degrees Kelvin. Interstellar ices are typically studied in the range of 4 to 20 Kelvins, which is not appropriate for investigations of solar system objects. Even measurements of volatile ices at 100 Kelvin are not necessarily germane to observations of Pluto, Triton or Kuiper Belt objects at 40-50 Kelvin.

4. Conclusion

A comprehensive spectral database of ices and minerals covering a wide temperature range will have applications ranging from the study of comets and Kuiper Belt objects to outer planet satellites and the polar regions of Mars. Recent efforts at NASA Ames Research Center have led to development of a cryogenic environment chamber capable of spectral reflectance measurements from 325 to 10 Kelvin. This will contribute to the development of a published spectral database which will support investigations of the Martian polar caps, the Galilean satellites, the Saturnian satellites, and objects as far as Pluto / Charon. This will be of great utility to NASA and scientists working with the Mars 2005, Galileo, and Cassini missions, as well as projected missions to Pluto and Europa. As spacecraft instruments achieve increasing spatial and spectral resolution, such laboratory reference spectra become increasingly critical to accurate interpretation of the acquired data.

REFERENCES

Bernstein, M. P., et al. 1997, ApJ, 476, 932-942.

Bernstein, M. P., et al. 2002, Nature 416 409-403.

Brucato, J. R., et al. 1997, Icarus 125, 135-144.

Crowley, J. K. 1991, J. Geophys. Res. 96, 16,231-16,240.

Dalton, J. B. 2000, University of Colorado, Boulder 253pp.

Dalton, J. B., and Clark, R. N. 1998, Eos Trans. Am. Geophys. Union 79, F541.

Dalton, J. B., Curchin, J. M., and Clark, R. N. 2001, Lunar Planet. Sci. 32, 1496.

Delitsky, M. L. and Lane, A. L. 1997, J. Geophys. Res. 102, 16,385-16,390.

Delitsky, M. L. and Lane, A. L. 1998, J. Geophys. Res. 103, 31,391-31,403.

Ehrenfreund, P., et al. 1997, Icarus 130, 1-15.

Gerakines, P. A. and Moore, M. H. 2001, Icarus 154, 372-380.

Gerakines, P. A., 1996, A&A, 312, 289-305.

Gerakines, P. A., 1999, AJ, 522, 357-377.

Gerakines, P. A., Moore, M. H., and Hudson, R. L. 2000, A&A, 257, 793-800.

Grundy, W. M., Schmitt, B., and Quirico, E. 1993, Icarus, 105, 254-258.

Grundy, W. M. and Schmitt, B. 1998, J. Geophys. Res. 103 25,809.

Hudgins, D. M., et al. 1993, ApJS, 86, 713-870.

Hudson, R. L., Moore, M. H. and Gerakines, P. A. 2001, AJ550, 1140-1150.

Moore, M. H., Hudson, R. L., and Gerakines, P. A. 2001, Spectr. Acta A57, 843-858.

Roush, T. L. 2001, J. Geophys. Res. 106, 33,315.

Roush, T. L. and Dalton, J.B. 2002, Lunar Planet. Sci. 33, 1525.

Roush, T. L. and Singer, R. B. 1983, Lunar Planet. Sci. 14, 8458.

Satorre, M. A., Palumbo, M. E. and Strazzulla, G. 2001, J. Geophys. Res. 106 33,363-33,370.

Singer, R. B. and Roush, T. L. 1985, J. Geophys. Res. 90 2434.

C-H Hot Bands in the Near-IR Emission Spectra of Leonids

F.T. Freund

Department of Physics, San Jose State University, SETI Institute

J. Scoville

Stanford University

R. Holm, R. Seelemann

Bayer AG, Leverkusen, Germany

M.M. Freund

NASA Goddard Space Flight Center, Greenbelt, MD

Abstract

The reported infrared (IR) emission spectra from 1999 Leonid fireballs show a 3.4μm C-H emission band and unidentified bands at longer wavelengths. Upon atmospheric entry, the Leonid meteorites were flash-heated to temperatures around 2400K, which would destroy any organics on the surface of the meteorite grains. We propose that the ν_{CH} emission band in the Leonid emission spectra arises from matrix-embedded C_n-H-O entities that are protected from instant pyrolysis. Our model is based on IR absorption ν_{CH} bands, which we observed in laboratory-grown MgO and natural olivine single crystals, where they arise from C_n-H-O units imbedded in the mineral matrix, indicative of aliphatic -CH_2- and -CH_3 organics. Instead of being pyrolyzed, the C_n-H-O entities in the Leonid trails become vibrationally excited to higher levels n = 1, 2, 3 etc. During de- excitation they emit at 3.4μm, due to the (0 => 1) transition, and at longer wavelengths, due to hot bands. As a first step toward verifying this hypothesis we measured the C-H vibrational manifold of hexane (C_6H_{14}). The calculated positions of the (2 => 1), (3 => 2), and possibly (4 => 3) hot bands agree with the Leonid emission bands at 3.5, 3.8 and 4.1μm.

1. Introduction

The 1999 Leonid emission spectra in the C-H stretching region (Russell *et al.* 2000) offer an opportunity to test the hypothesis whether the "organics" in the dust grains in such cometary trail material consist of surface organics, or if they are structurally imbedded within the mineral grains. Furthermore, we can compare these Leonid spectra to "hot" C-H laboratory emission spectra.

Russell *et al.* (2000) recorded the infrared (IR) emission spectrum of persistent 1999 Leonid trains (see Fig. 1), which cooled from $\approx 2400K$ to $\approx 1200K$ in less than 2 minutes. As shown in Fig. 1, there is an emission band around 3.4μm ($2850 - 2900cm^{-1}$), indicative of ν_{CH} emission due to the C-H stretching band of "organic" matter. There are further emission bands at 3.55-3.6μm, 3.8μm, and 4.05-4.1μm, which could not be assigned. Whereas the 3.4μm band is too broad to resolve any splitting into subcomponents at 3.42 and 3.5μm (indicative of symmetrical and antisymmetrical C-H stretching modes, respectively) it is similar to the 3.4μm bands absorption bands from dust in the interstellar medium, ISM (see Pendleton and
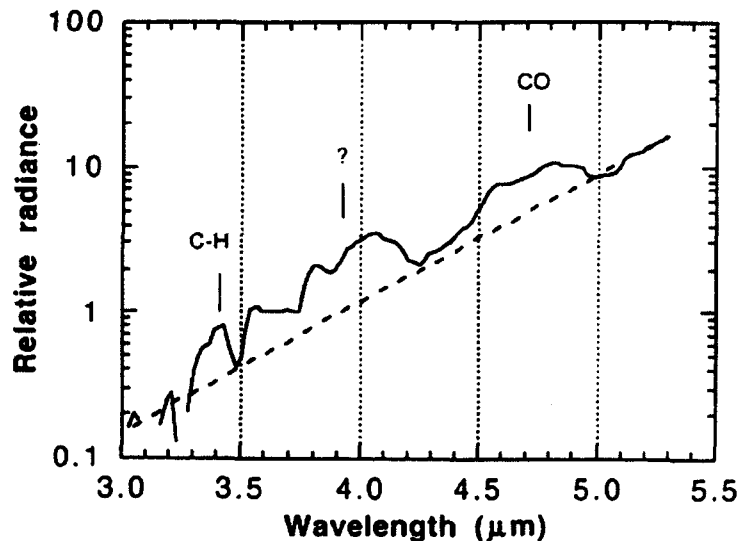
Fig. 1.— Leonid near-IR spectra after Russell *et al.* (2000); note the different emission features.

Allamandola (2002)). These observations support the idea that the dust component in the Leonid parent comet derives from the dust in the pre- solar molecular cloud that formed the solar system. Thus, the "organics" that led to the 3.4μm emission spectrum of the Leonid fireballs should be similar to the "organic" component in the dust in the ISM.

At the estimated temperature of the Leonid train, any surface organics would normally degrade irreversibly through pyrolysis of their C-H bonds during flash heating. When MgO and olivine crystals containing imbedded C_n-H-O entities are heated in the laboratory to temperatures between 550-1000K, the C-H bonds pyrolyze, but recover during annealing (Freund *et al.* 2001). Therefore, even though the C-H bonds break during heating, the H atoms remain close-by in the mineral structure, diffuse back and bond again to the C_n entities. Furthermore, when imbedded C_n-H-O entities are rapidly heated, they will not immediately pyrolyze. They first pass through a series of vibrationally excited states of the C-H oscillator, because these C-H oscillators are confined by the matrix and coupled to the surrounding atoms and ions of the mineral structure. The C_n-H-O are able to transfer a fraction of their vibrational energy to the matrix, which delays C-H bond breakage. Therefore, when the matrix is flash-heated, imbedded C_n-H-O entities will emit hot bands arising from transitions between higher vibrationally excited states of the C-H oscillator.

2. Results

To obtain the vibrational manifold of the C-H oscillator we measured the ν_{CH} absorption spectrum of hexane, C_6H_{14} with a CH_3/CH_2 ratio of 2:4, from the allowed (0 => 1) transition at 3.4μm to the forbidden higher transitions (0 => n) extending well into the VIS region, with n up to 7 as shown in Fig. 2a. From these values we derive the wavelengths of the hot bands as shown in Fig. 2b. From the measured transition energies we obtain $\alpha = 1.29x10^8$, and for -CH_2-: $D_e = 3.62eV$ and CH_3: $D_e = 3.69eV$.
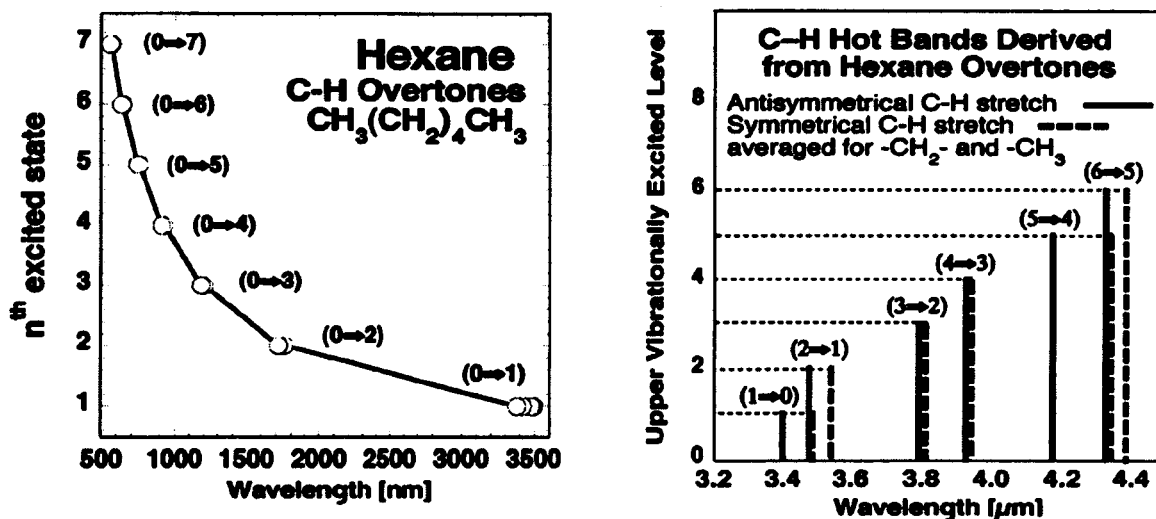
Fig. 2.— (a: left) Series of C-H stretching modes from the fundamental, allowed (0 => 1) transition through the overtones (0 => n) to the 7th excited state. (b: right): Hot bands (n => $n - 1$) calculated from the measured overtone series.

To a good approximation, the C-H vibrational stretching manifold can be described by a Morse potential, wherein D_e is the dissociation energy, α a constant, and r_0 the equilibrium bond distance:

$$V(r) = D_e(1 - \exp{\tfrac{-\alpha(r-r_0)}{r_0}})^2$$

Using this Morse potential, wherein n is the quantum number for the energy Levels, we solve the Schrödinger equation to obtain the eigenvalues:

$$E_n = \tfrac{D_e}{y^2}[2\alpha n + \alpha y - \alpha^2(n^2 + n + \tfrac{1}{4})]$$

The transition energies are $E_{0n} = E_n - E_0$, where E_0 is the ground state energy.

Noting that, $E_0 = \tfrac{D_e\alpha}{y} - \tfrac{D_e\alpha^2}{4y^2}$,   we have $E_n = \tfrac{D_e}{y^2}[2\alpha n - \alpha^2(n^2 + n)] + E_0$

Subtracting the ground state energy E_0 and rearranging the terms gives

$$\tilde{E}_n = (\tfrac{2D_e\alpha}{v} - \tfrac{D_e\alpha^2}{v^2})n - \tfrac{D_e\alpha^2}{v^2}n^2$$

Equating these coefficients to the coefficients of the quadratic fits, we arrive at:

for -CH$_2$: $\dfrac{2\alpha D_e^{3/2}h(2\mu)^{1}/2}{r_0} - \dfrac{2\alpha^2 h^2 D_e^2 \mu}{r_0^2} = 2929.81$ and $\dfrac{2\alpha^2 h^2 D_e^2 \mu}{r_0^2} = 61.81$

for -CH$_3$: $\dfrac{2\alpha D_e^{3/2}h(2\mu)^{1}/2}{r_0} - \dfrac{2\alpha^2 h^2 D_e^2 \mu}{r_0^2} = 3006.8$ and $\dfrac{2\alpha^2 h^2 D_e^2 \mu}{r_0^2} = 63.83.$

We can compare the IR emission spectrum of the 1999 Leonids in Fig. 1 with the expected hot band positions given in Fig. 2b. From this comparison we conclude that the observed Leonid emission bands have a one-to-one correspondence with de-excitation of C-H, with $(3.6\ \mu m, (2 => 1))$, $(3.8\ \mu m, (3 => 2))$, and $(4.0\ \mu m, (4 => 3))$.

3. Discussions and Conclusions

As we have shown, the dust component in the Leonid parent comet probably derives from dust in the pre-solar molecular cloud that formed the solar system, and the $3.4\mu m$ emission spectrum of the Leonid fireballs should be similar to the "organic" component in the dust in the ISM. At the high temperatures during atmospheric entry, any surface "organics" will be destroyed, and they can only survive irreversible pyrolysis if they are well protected. We have shown that imbedded C_n-H-O entities in synthetic MgO and natural olivine will not be irreversibly destroyed. Instead they are able to transfer their thermal energy to the matrix, and they emit in a series of near-IR emission bands. Furthermore, we have seen that there is a one-to-one correspondence between the observed Leonid emission bands and the de-excitation of C-H.

The Leonid spectra as recorded by Russell *et al.* (2000) don't have enough resolution to resolve the different near-IR emission lines. The flash heating of the Leonids could be also simulated in the laboratory using dust grains, which contain structurally imbedded C_n-H-O entities. Furthermore, one should be able to observe the ν_{CH} de-excitation emission hot bands in astrophysical environments, where interstellar dust is subjected to flash- heating, for instance in the front of supernova shockwaves.

REFERENCES

Freund, F., Staple, A., and Scoville, J., 2001, *Proc. Natl. Acad. Sci.*, **98**, 2142-2147.
Pendleton, Y.J. and Allamandola, L.J., 2002, *ApJS*, **138**, 75-98.
Russell, R.W., *et al.*, 2000, *Earth Moon and Planets*, **82**, 439-456.

MALDI TOF MS:
An Exobiology Surface-Science Approach for Europa

Perry A. Gerakines and Thomas J. Wdowiak

*Astro- and Solar-System Physics Program, Department of Physics,
University of Alabama at Birmingham, Birmingham, AL*

Abstract

If Europa is to be of primary exobiological interest, namely as a habitat for extant life, it is obvious that: (i) a hydrosphere must prevail beneath the cryosphere for a long time, (ii) internal energy sources must be present in a sufficient state of activity, and (iii) a reasonable technical means must be available for assessing if indeed life does exist in the hypothesized hydrosphere. This discussion focuses on technological issues, because the the compounding evidence about Europa indicates that the first two are highly likely to be true. We present a consideration of time-of-flight mass spectroscopy (TOF MS) conducted *in-situ* on the cryosphere surface of Europa during a landed robotic mission. We assert that this is a reasonable technical means not only for exploring the composition of the cryosphere itself, but also for locating any biomolecular indicators of extant life brought to the surface through cryosphere activity. We also describe a MALDI (MAtrix Laser Desorption and Ionization) TOF MS system that we are constructing as a proof-of-concept prototype for conducting TOF MS measurements on Europa.

1. Introduction

This paper is the summary of a poster contribution to NASA's Laboratory Astrophysics Workshop (held in 2002 May), which itself was based on a prior publication by Wdowiak *et al.* (2001). The reader is directed to that work for further details.

Observations of Jupiter's satellite Europa continue to compound the evidence that subtantial amounts of liquid water exist beneath its icy surface (as hypothesized by Squyres *et al.* 1983), as well as a possible ice-capped ocean or hydrosphere. Were that hydrosphere to be populated with living organisms, some chemical tracers may be available for detection on the Europan surface. Therefore future missions to the surface of Europa will serve as platforms for *in-situ* investigations relevant to exobiology as well as planetary science. The Jovian magnetosphere inflicts Europa with a proton flux of $1.9 \times 10^9 \, \text{m}^{-2} \text{s}^{-1}$ for $E > 2.5 \, \text{MeV}$ (Vogt *et al.* 1979). Two consequences of this environment are (i) that radiation chemistry will play a significant role in the surface ices, and (ii) that deployed instruments must be radiation hardened. Thus, the challenge is to arrive at an instrument or instrument suite that is robust and yet still capable of high-quality results in the service of both planetary science and exobiology. The development of such devices should be of the highest priority. After consideration of all aspects of the issue, it is our assessment that time-of-flight mass spectroscopy (TOF MS) is the instrumental technique most suitable for deployment on the surface of Europa. It permits a definitive level of identification for small molecular species in the surface ices and any larger biomolecules brought to the surface from the hypothesized hydrosphere through ice-cap activity, were the hydrosphere populated by extant life. Moreover, this technique should be less susceptible to a high-radiation environment than optical devices.

2. Reconciliation of Measurements at Low and High Molecular Weight

Given the potential presence of biomolecules and the technical challenge of actually putting a lander on the surface of Europa, it makes good sense to give the instrument the capability of large biomolecule/biopolymer detection. Recent years have shown the usefulness of mass spectroscopy for such tasks, including the characterization of microorganisms (Fenselau 1994). In life-science laboratories, a method of choice for measurement of large biomolecules is matrix laser desorption and ionization mass spectroscopy (MALDI-MS). The key to MALDI-MS is to place the sample in close proximity to an agent that vaporizes and ionizes under the action of a UV laser pulse, and then transfers its charge to the sample molecules. The most significant benefit of this process is that delicate molecular species such as DNA, which fragment under other ionization techniques (compounding the task of identification), remain intact and are only singly charged.

While strikingly successful for identifying biomolecules, MALDI agents such as 2,5-dihydroxybenzoic acid produce such an intense mass distribution in the low molecular-weight region that they mask the signal of small molecules present in the sample. This is a significant issue for planetary science objectives on Europa. The key, then, to utilizing a TOF MS system on Europa will be to produce an instrument capable of detecting both small and large molecules.

MALDI agents that do not proliferate in the low molecular-weight range are therefore necessary for such an instrument. We propose the use of nanometer-sized metallic particles. By virtue of their size, these particles have very large optical absorption cross-sections, and efficiently vaporize and ionize under the action of a laser. The contribution of this type of MALDI agent to a mass spectrum is merely its atomic weight and can be readily separated from other species in the mass distribution. Cobalt particles 20 nm in diameter have been shown to be useful as MALDI agents (Tanaka *et al.* 1988; Kawabata *et al.* 1998), since their only contribution to the mass spectrum is the Co^+ ion at $m/z = 58.9332$.

Evaporating a metal onto a cryo-ice at 77 K results in, rather than a film, a deposit of small "islands" in the nm-size range (Wdowiak, unpublished result). Methods of dispensing metallic species, such as Co, and other potential MALDI agents mentioned previously onto cryo-ice, by vaporization and other means, are now being explored in our laboratory.

MALDI, as done in biomolecular laboratory measurements, involves mixing the agent and the sample prior to insertion into the instrument. On the other hand, a metal agent couples the laser energy to the material under interrogation through its optical absorption. Although applied to the surface the laser pulse vaporizes both the metal MALDI agent and the sample underneath, and these are mixed in an extremely rapid manner in the vapor phase. This simplifies sample preparation as compared to current laboratory MALDI methods.

The cryogenic conditions on Europa provide a unique opportunity to implement this technique, one that would not be normally used in a room-temperature laboratory. On Europa, the lack of a significant atmosphere and the low ($\sim$ 125 K) temperature make it possible to manufacture nanophase MALDI metal agent deposits directly onto the sample simply by va-
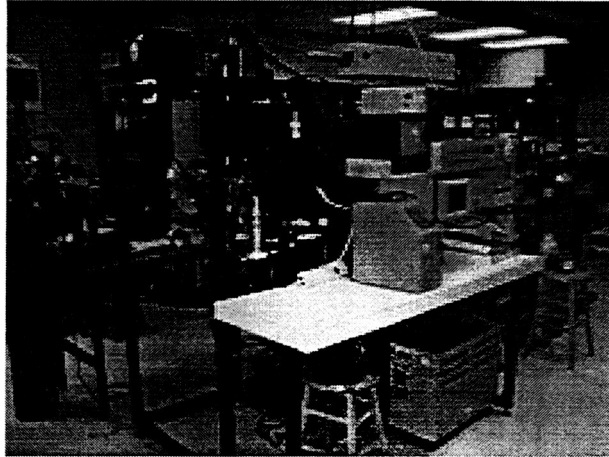
Fig. 1.— Operational system of the test bed. The 266 nm laser is seen horizontal at top, fronted on the left end with the fiber-optic interface/attenuator assembly out of which comes the silica fiber optic cable terminating in the UV optical bench that directs the radiation to a focus in the vacuum chamber. The large box adjacent to the stool under the console table is the 266 nm laser power system. The assemblies at the left end of the test bed are shown in detail in Fig. 2.
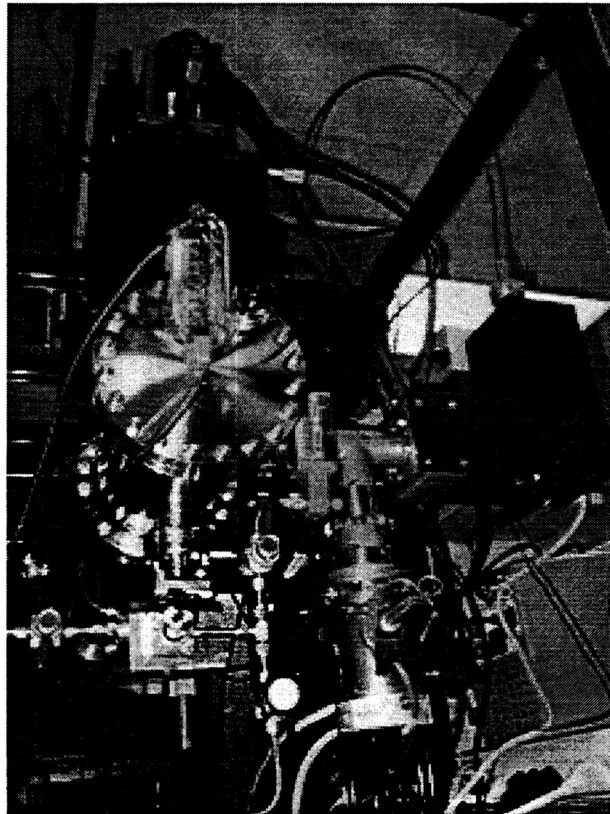
Fig. 2.— The bulkhead plate of the ionization chamber region of the TOF MS (left of center) accomodates the vacuum ionization and thermocouple gauge tubes. Below it is the airlock assembly utilizaed for introducing solid samples during the shakedown stage of the test-bed's development. This will be the position of the cryogenic target assembly. To the right of the chamber, is an airlock LED pressure-status gauge and vacuum tee, below which is a turbomolecular pump and to which the L-shaped UV optics bench is mated. The fibeer-optic UV link from the 266-nm lader can be seen terminating at the top of the UV optical bench. At the upper left, the 1064-nm deosrption laser head can be seen.

porizing the metal onto the cold surface. This permits the use of easily evaporated metals such as aluminum, magnesium, sodium, or potassium as MALDI agents (other metals are of interest as well).

3.   Conclusions and Future Work to be Done

Figures 1 and 2 contain photographs of our current TOF MS system at the University of Alabama at Birmingham. At this time, our work has only included room-temperature samples, but this year a cryo-ice system will be attached to the test bed in order to simulate the low temperatures on Europa (and elsewhere in the outer Solar System). Our instrument will be able to simulate surfaces with temperatures ranging from 6 to 300 K. It will be interfaced at the current position of the room-temperature airlock that is presently being utilized to introduce solid samples. The metal MALDI agent dispenser is also to be added to the system in the coming year.

Acknowledgments

REFERENCES

Fenselau, C., *Mass Spectroscopy for the Characterization of Microorganisms*, Am. Chem. Soc., New York (1994).
Kawabata, S., *et al. Proc. 46th ASMS Conf. on Mass Spectrometry and Allied Topics*, Santa Fe, 1011 (1998).
Squyres, S. W., Reynolds, R. T., and Cassen, P. M., *Nature* **301**, 225-226 (1983).
Tanaka, K., *et al.*, *Rapid Commun. Mass Spectrom.* **1**, 151-153 (1988).
Vogt, R. E., *et al.*, *Science* **204**, 1003-1007 (1979).
Wdowiak, T. J., *et al.*, *Astrobiology* 1(4), 467-476 (2001).

The Atmosphere as Laboratory: Aeronomy by Astronomy

T. G. Slanger, P. C. Cosby, and D. L. Huestis

Molecular Physics Laboratory, SRI International, Menlo Park, CA

Abstract

Astronomical sky spectra, which are byproducts of long-slit observations with echelle spectrographs on large telescopes, provide a unique platform for studying the optical emissions of excited molecules and atoms in the terrestrial atmosphere that can greatly extend present knowledge based on laboratory spectra. This paper summarizes some of the advances that have been made in our understanding of the lower electronic states of O_2 and other species from the sky spectra and from direct observations of the Venus nightglow.

1. Introduction

Astronomical sky spectra are proving to be a rich source of information on emissions in the terrestrial atmosphere, over a broad range of altitudes (85-250 km). The high resolution (0.01 nm) and CCD detection associated with these spectra has led to a variety of new observations, on species as diverse as the electronically-excited states of O_2, many O-atom Rydberg levels, OH, K, N_2^+, He, and Ca^+, over the 330-1000 nm spectral region. From nightglow emission, we have been able to characterize the O_2 states in vibrational levels not previously observed, and have detected $O_2(b)$ state emission from levels v = 0-15, emission to the $O_2(a)$ state in levels v = 1-11, and emission to the ground state in levels v = 0-15. In addition, we are able to see the fully-resolved O_2 UV emissions in the Herzberg I and Chamberlain transitions. There is considerable synergy when we observe the new atmospheric emissions while simultaneously studying the same emitters in the laboratory. [KTC00] In related astronomically-oriented work, we have also made measurements of the Venus nightglow with the Keck and APO telescopes, confirming older results which identified $O_2(c)$ state emission, and establishing for the first time that the oxygen 557.7 nm green line is an important Venus nightglow feature. Examples of the terrestrial spectra are available at http://www-mpl.sri.com/NVAO/download/Osterbrock.html.

2. Discussion

A broad range of emission features are to be found in the sky spectra that we have obtained from the two echelle spectrometers on the Keck telescopes on Mauna Kea, HIRES on Keck I and ESI on Keck II. In general, the HIRES data have been taken at a resolution of 40,000, while the ESI resolution is 8000. For accurate spectroscopy, HIRES is far better, but ESI, having higher sensitivity, collects data more rapidly, and thus is more useful for temporal studies.

Figures 1-5 show examples of what can be obtained from sky spectra. In Figure 1 is shown a spectral region that has in the past been considered devoid of features, so much so that it has been used to measure the background continuum of the nightglow. The $O_2(b\text{-}X)$ 3-2 and 4-3 bands are in fact the strongest of the new $b\text{-}X$ bands, so that choice was unfortunate. Figure 2 shows the range of $b\ {}^1\Sigma_g^+$ state vibrational levels found in the nightglow. The structure of the distribution is not fully understood, but is caused by a combination of the production rates into these individual levels, and the collisional depopulation rates. These are now known

for a number of the levels for O_2 and N_2 colliders, but not yet for the potentially important $O(^3P)$. Table 2 shows the vibrational levels in both the b $^1\Sigma_g^+$ and the a $^1\Delta_g$ states that can be identified in the Keck spectra and from our current laboratory studies.

Table 1. O_2 $(A\,^3\Sigma_u^+ - X\,^3\Sigma_g^-)$
Bands Analyzed From Keck Sky Spectra (51 Bands).

height v' / v''	3	4	5	6	7	8	9	10	11	12	13	14	15	16	17
0					X	X	X	X	X						
1			X	X	X	X									
2	X	X	X	X	X			X	X						
3		X	X	X			X	X			X	X			
4		X	X			X	X			X	X			X	
5					X	X			X	X		X	X		
6				X	X			X	X		X				X
7				X	X		X	X		X	X			X	
8										X			X		

Table 2. Vibrational Levels Accessible in the Laboratory
and in the Keck Sky Spectra for $O_2(a\,^1\Delta_g)$ and $O_2(b\,^1\Sigma_g^+)$.

$a\,^1\Delta_g$ (Keck)	v = 0-11
$a\,^1\Delta_g$ (Lab)	v = 0-2, 16-19
$b\,^1\Sigma_g^+$ (Keck)	v = 0-7, 9-15
$b\,^1\Sigma_g^+$ (Lab)	v = 0-3, 10-15

Figure 3 shows that there are many bands in the blue spectral region, and these originate with the O_2 Herzberg states, A $^3\Sigma_u^+$, A' $^3\Delta_u$, and c $^1\Sigma_u^-$. Shown is the first atmospheric observation of resolved emission from the v = 0 level of the A $^3\Sigma_u^+$ state, which is interesting because of the implications about the development of the vibrational distribution of that state. The spectrum also shows the H_β line, which comes from the geocorona, far higher in the atmosphere than the O_2 features; the next line in the Balmer series, H_γ, is also observed.

Figure 4 shows the presence of a previously unobserved system of O_2, the c-b system. By comparison to the Herzberg I 3-9 band, one sees that it is not a weak transition, as the 3-9 band is one of the three strongest Herzberg I bands longward of 380 nm. The very open structure of the c-b bands is a consequence of the fact that only a Q-branch is observed, and that only alternate rotational levels are populated. Radiative recombination, in which ions and electrons recombine, is a significant ionospheric process. The product is a Rydberg atom, in any of the states up to the O-atom ionization limit. The well-known examples of this process, from ground-based observations, are the 777.4 and 844.6 nm multiplets. However, there are many such multiplets, originating with higher energy levels. Figure 5 shows a particularly clear example, the 5d-3p set of lines in the quintet manifold. The quintets are more prominent in the atmosphere than the triplets, yet laboratory data on the quintets are sparser.
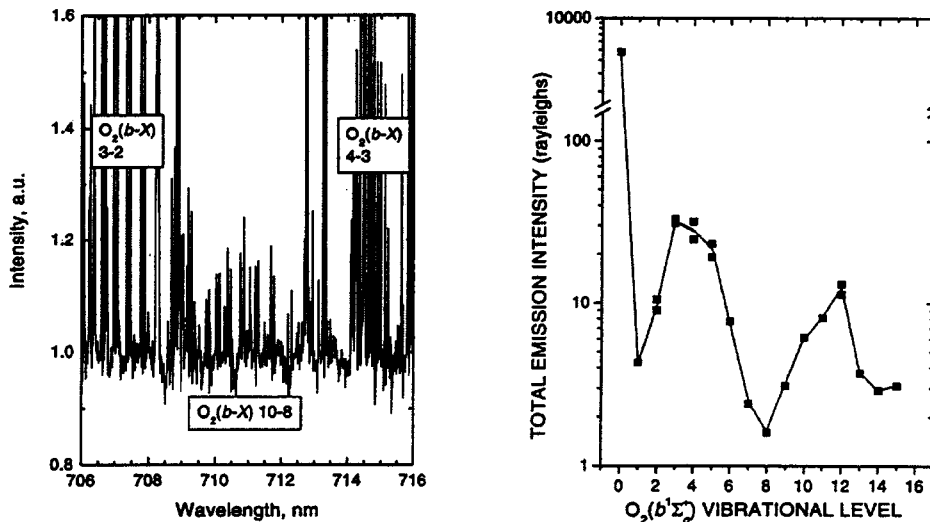
Fig. 1. (LEFT): Until the Keck spectra became available, the only rotationally-resolved atmospheric emission spectrum of the O_2 Atmospheric band system was of the 0-1 band at 865 nm. We now have ~30 resolved bands, of which a sample is shown. Bands are observed up to b $^1\Sigma_g^+$ (v = 15). Summing of files greatly improves the S/N ratio.

Fig. 2. (RIGHT): There are numerous $O_2(b\text{-}X)$ bands seen in the nightglow. By making calibrations against nearby OH bands, we have calculated a vibrational distribution for the b $^1\Sigma_g^+$(v) population. It is tri-modal, the low population near v = 1 presumably related to rapid quenching, and the high population at v = 0 originating from lack of quenching. The minimum at v = 8 is not yet understood, while the increase at higher levels is probably related to cascading from Herzberg states.
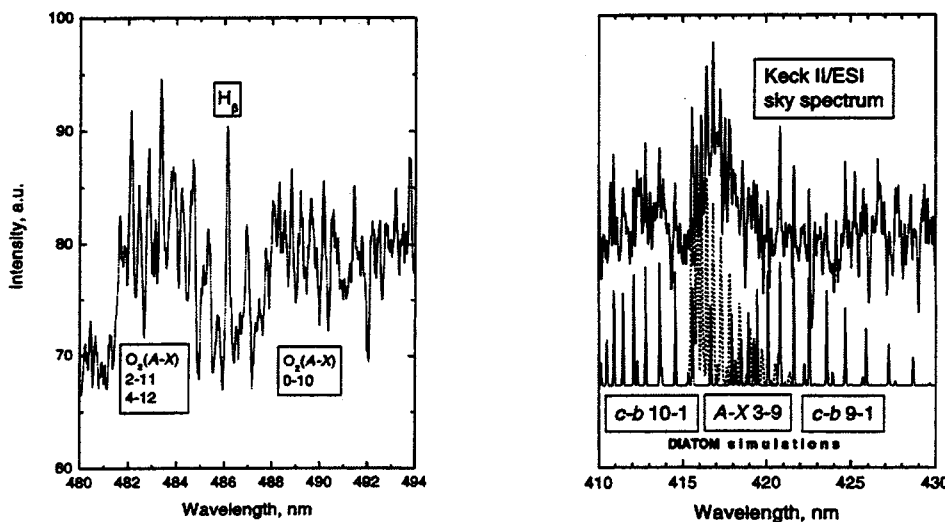
Fig. 3. (LEFT): The O_2 Herzberg I bands are generally considered to be a UV system. The detector sensitivity seen in the Keck spectra permits measurements well into the visible. Shown is the first demonstration of atmospheric emission from the v = 0 level of the A $^3\Sigma_u^+$ state, which is significant because it involves collisional cascading at very low densities, 1 mTorr and less. Table 1 shows the range of emphA-X bands that have been analyzed in the Keck spectra, which are considerably improving our knowledge of O_2 ground state spectroscopy. Similarly, the many Chamberlain $(A'\text{-}a)$ bands that appear supply information on the a $^1\Delta_g$ state.

Fig. 4. (RIGHT): The O_2 $(c$ $^1\Sigma_u^-$ - X $^3\Sigma_g^-)$ Herzberg II system has been considered as the only significant emission from the $O_2(c)$ state, and its emission is very strong in the atmosphere of Venus. Shown in this figure is a new optical transition, the c $^1\Sigma_u^-$ - $b^1\Sigma_g^+$ system. In the terrestrial nightglow, where the $O_2(c\text{-}X)$ emission is weak, it turns out that the c-b bands are much easier to observe, due to the details of the relevant spectroscopy.
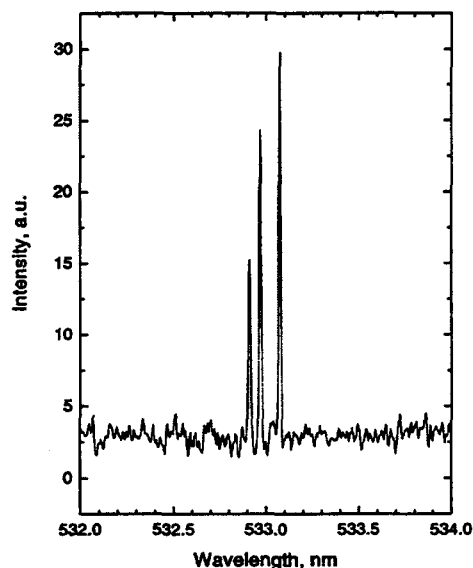
Fig. 5. Ionospheric emission at 777.4 and 844.6 nm is a measure of various processes, but in the nightglow these emissions arise from radiative recombination of O^+. This interaction produces a variety of other transitions not normally seen in the atmosphere, and never previously reported in the nightglow. Shown is the triplet of lines of the $5d$-$3p$ transition of the quintet OI manifold, one multiplet of some thirty that have been identified in the Keck spectra. Observation of these lines is free of the OH contamination existing in other spectral regions.

3. Conclusions

Sky spectra provide a window into the atmosphere that has not previously been exploited. Previous optical aeronomic studies focused on the strongest emitters, regardless of whether the chemistry of other species might be important. We are now able to observe a much larger range of species, which simultaneously gives a stimulus to observing these entities in the laboratory. A good example is the range of vibrationally excited levels in the $O_2(b\ {}^1\Sigma_g^+)$ state, which after their initial detection in the Keck sky spectra were found in laboratory experiments to be generated from collisional relaxation of the Herzberg states. At the same time, the analogous interaction was found for the $O_2(a\ {}^1\Delta_g)$ state. These relaxation pathways were not previously known. The precision of the astronomers' wavelength calibration has enabled us to make spectroscopic advances, particularly for the lowest three O_2 states. Long-standing discrepancies in the ground state levels have been corrected, the $a\ {}^1\Delta_g$ state levels are now known over a much wider range, as is also true for the $b\ {}^1\Sigma_g^+$ state. The discovery of the $O_2(c$-$b)$ bands will lead to improved rotational constants for both states, and also provides a means of monitoring the $c\ {}^1\Sigma_u^-$ state in the terrestrial atmosphere, an ability that was previously marginal at best. The range of ionospheric emissions detectable from the ground has been expanded. Not only can one see a large variety of O^+ transitions, but the rotational distribution in the $O_2(b$-$X)$ 1-1 band, generated by $O({}^1D) + O_2$ energy transfer, provides a method of measuring thermospheric temperatures. Given that sky spectra are being generated world- wide at all major observatories, aeronomers have new opportunities to make advances in the field.

Acknowledgments

REFERENCES

Kalogerakis, K. S., Totth, A., Cosby, P. C., Slanger, T. G., and Copeland, R. A. 2000, *Eos, Trans. Amer. Geophys. Union*, **81**, F944.

Also see the paper in these proceedings by Kalogerakis *et al. Research on Electronically- and Vibrationally-Excited O_2, with Application to Planetary and Terrestrial Atmospheres.*

Low-Temperature Hydrocarbon Photochemistry: CH_3 + CH_3 Recombination in Giant Planet Atmospheres

Gregory P. Smith and David L. Huestis

Molecular Physics Laboratory, SRI International, Menlo Park, CA

Planetary emissions of the methyl radical CH_3 were observed for the first time in 1998 on Saturn and Neptune by the ISO (Infrared Space Observatory) mission satellite. CH_3 is produced by VUV photolysis of CH_4 and is the key photochemical intermediate leading complex organic molecules on the giant planets and moons. The CH_3 emissions from Saturn were unexpectedly weak. A suggested remedy is to increase the rate of the recombination reaction

$$CH_3 + CH_3 + H_2 \rightarrow C_2H_6 + H_2$$
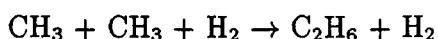
at 140 K to a value at least 10 times that measured at room temperature in rare gases, but within the range of disagreeing theoretical expressions at low temperature.

We are performing laboratory experiments at low temperature and very low pressure. The experiments are supported by RRKM theoretical modeling that is calibrated using the extensive combustion literature. The distinction between "high" and "low" pressure is a significant one. In the so called "low pressure limit" the rate of recombination is limited by the rate of stabilization or energy removal by the third body called "M" (really H_2), and the overall recombination rate coefficient is written as

$$k_{recomb}(M \rightarrow 0) \sim k_0[M]$$

In the "high pressure limit" the buffer gas pressure is sufficiently high to stabilize every collision complex, and the overall recombination rate coefficient becomes pressure independent:

$$k_{recomb}(M \rightarrow \infty) \sim k_\infty$$

RRKM calculations indicate that k_0 rises with decreasing temperature much faster than does k_∞. We used 3 different transition state approaches to calculate temperature dependent values for k_∞, and 3 ways to determine the pressure dependence and k_0, including master equation computations. This effort is designed to provide a good predictive fit to the existing experimental rate data [1,2], and thus furnish a reliable theoretical extrapolation to the lower planetary temperatures and pressures. Previous theory has neglected these conditions. Our recommendations for 65-300K in a hydrogen atmosphere are:

$$k_\infty = 3.59 \times 10^{-10} \ T^{-.262} \ e^{-37/T} \ cm^3 \ mol^{-1} \ s^{-1}$$

$$k_0 = 3.32 \times 10^{-15} \ T^{-2.28} \ e^{131/T} \ cm^6 \ mol^{-2} \ s^{-1}$$

Recommended values for helium and argon bath gases are 50% and 70%, and the falloff is described by a Troe factor F = 0.56 [3].

These results mean that low temperature laboratory experiments need to be performed at quite low pressures, say 0.01 mbar or less in order to extrapolate more reliably to the 0.001 mbar and below characteristic of the relevant regions of the giant planet atmospheres. This is consistent with the recent work in Stief's laboratory [2], in which no pressure dependence was observed at 155 and 202 K for pressures from 0.6 to 2.6 mbar. Our present expression does slightly overpredict their lowest pressure results at 298 K.

We are currently measuring the methyl recombination rate constants using a low pressure Knudsen cell photolysis reactor. The technique photolyzes methyl iodide with quadrupled Nd:YAG laser radiation at 255 nm. Precursor loss and ethane product yields are measured by mass spectrometer at the cell exit aperture. Typical pressure ranges are 0.01 - 0.05 mbar. This method was previously used to measure CF_3 recombination rates [4].

Acknowledgments

REFERENCES

[1] D. Walter, H.-H. Grotheer, J. W. Davies, M. J. Pilling, and A. F. Wagner, *Proc. Combust. Inst.*, 23, 107-114 (1990).
[2] R. J. Cody, W. A. Payne, R. P. Thorn, and L. J. Stief, *Bull. AAS* 32, 1020 (2000) AND R. J. Cody, L. J. Stief, F. L. Nesbitt, and M. A. Iannone, *Bull. AAS*, 33, 1080 (2001).
[3] J. Troe, *J. Chem. Phys.*, 66, 4758-4775 (1977).
[4] N. Selamoglu, M. J. Rossi, and D. M. Golden, *Chem. Phys. Lett.*, 124, 68-62 (1986).

Submillimeter Spectra of Low Temperature Gases and Mixtures

E.H. Wishnow

V-Division, Lawrence Livermore National Laboratory, Livermore, CA

H.P. Gush, M. Halpern, I. Ozier

Physics Dept., Univ. of British Columbia, Vancouver, British Columbia, Canada

Abstract

Submillimeter absorption spectra of nitrogen, nitrogen-argon mixtures, and methane have been measured using temperatures and pressures near to those found in the atmospheres of Titan and Saturn. The experiments show the spectral signature of dimers which will likely appear in far-infrared spectra of Titan that will be obtained by the Composite Infrared Spectrometer (CIRS) onboard the Cassini spacecraft. The recent CIRS spectrum of Jupiter shows far-infrared spectral lines of methane and the corresponding lines are observed in the laboratory. We are extending this work to lower frequencies using a new differential Michelson interferometer that operates over the frequency region 3–30 cm^{-1}.

1. Introduction

We have conducted experiments, and are developing a new spectrometer and absorption cell apparatus, to measure submillimeter spectra of simple gases and gas mixtures. The spectra signatures of dimers is an area of particular interest as these features have been seen in planetary spectra. Dimers are weakly bound pairs of molecules that form stably when the temperature is comparable to the depth of the intermolecular potential. The dimer has a set of vibrational and rotational energy states which depend on the molecules' separation and orientation. Even though the individual molecules that compose the dimer do not possess permanent electric dipole moments, the dimer can possess a dipole moment and transitions between energy states give rise to rotation-vibration spectral lines at low frequencies. The Voyager spectrum of Jupiter shows small H_2-H_2 dimer features located near the S(0) and S(1) transitions of hydrogen at 354 and 587 cm^{-1} respectively (McKellar 1984; Frommhold, Samuelson, & Birnbaum 1984), and the Voyager spectrum of Titan shows features in the same regions which are attributed to the H_2-N_2 dimer (Borysow & Frommhold 1986).

2. Nitrogen and Nitrogen-Argon Spectra

The top panel of Figure 1 shows a comparison of low temperature N_2 and N_2-Ar absorbance spectra ($-\ln(\text{transmission})$). The measurements were conducted using a Fourier transform spectrmeter and multi-reflection absorption cell cooled with liquid argon or liquid nitrogen (Wishnow, Leung, & Gush 1999). The optical path was 52 m and the spectral resolution was 0.24 cm^{-1}. The upper curve is from 538 Torr of N_2 at 78 K (2.54 Amagat) and the lower curve is from a 50/50 mixture of N_2-Ar at 88 K (2.6 Amagat) (Amagat units are a ratio of sample density to Loschmidt's number, the atmospheric number density at STP). The circles are the calculated absorbance for 2.54 Amagat of N_2 at 93 K based on the previous generation of high pressure, low resolution experimental studies Dore & Filabozzi (1987).

The broad continuum is due to the N_2 collision-induced translation-rotation spectrum. The rippled structure superposed on the continuum is due to the presence of dimers and it is enhanced in the N_2-Ar spectrum relative to the pure N_2 spectrum. The dimer structure can only be observed using relatively high spectral resolution and relatively low gas pressures; this structure was not seen in the previous generation of high pressure experiments.

The top panel of Figure 1 shows N_2-Ar spectra with the collision-induced continuum removed. The N2/Ar mixing ratio, total density, and temperature from top to bottom are: 50/50, 5.2 Amagat, 88 K; 24/76, 3.04 Amagat, 88 K; pure N_2, 2.54, 78 K. The detailed structure in the upper two curves is clearly different from the lower, pure N_2 curve. The amplitude of the ripples is obviously enhanced by the presence of argon; notice that the upper curve and lower
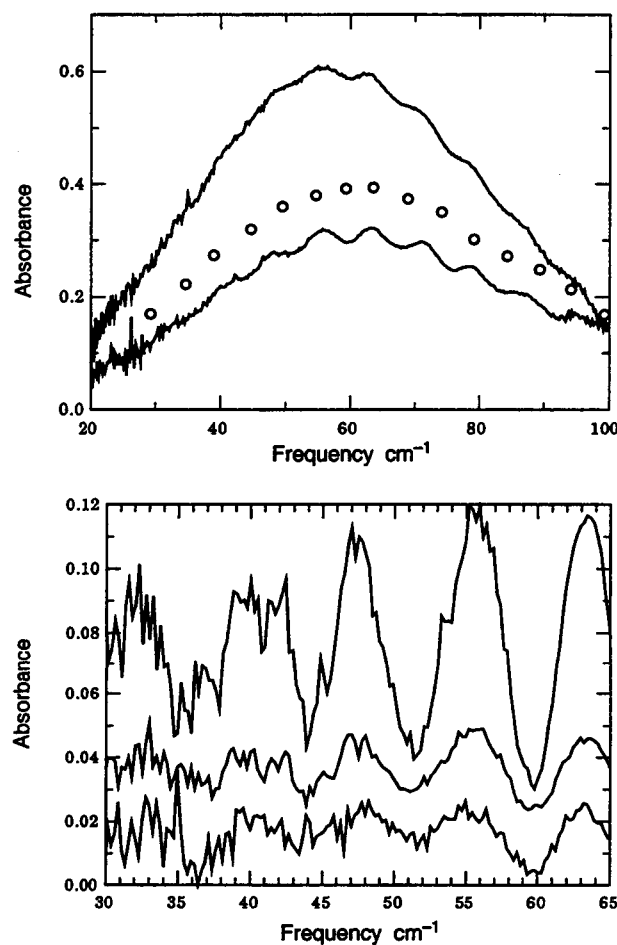
Fig. 1.— Top panel, low temperature N_2 and N_2-Ar spectra. The upper curve is from pure N_2 at 78 K, the circles are pure N_2 at 93 K, the lower curve is for a N_2-Ar mixture at 88 K; all densities are near 2.5 Amagat (see text). Bottom panel, baseline removed N_2 and N_2-Ar spectra. The upper curve is a 50/50 mix of N_2-Ar; the middle curve is a 24/76 mix of N_2-Ar; the lower curve is pure N_2. The curves are offset vertically by an arbitrary amount.

ripples is obviously enhanced by the presence of argon; notice that the upper curve and lower curve have the same amount of N_2 in the gas sample. It is interesting that the minima of the ripples correspond to the rotational transition frequencies of the N_2 molecule. At frequencies between 35 and 50 cm^{-1}, the ripples give way to detailed structure indicating that the N_2 molecule is no longer a free rotator for low N_2 rotational states. This work has been reported previously (Wishnow, Gush, & Ozier 1996), and it is compared to calculated N_2-Ar spectra (Wang, McCourt, & Le Roy 2000).

The rippled structure is likely to be observed in the spectrum of Titan by the CIRS spectrometer on Cassini. The argon abundance determined spectroscopically can be compared to mass spectrometer measurements made by the Huygens descent probe.

3. Methane

Even though the methane molecule is symmetric in the electronic and vibrational ground state, a weak dipole moment arises in a molecule with rotational quantum state $J > 0$ due to centrifugal distortion. Figure 2 shows the first observation of centrifugal distortion spectral lines below 80 cm^{-1}. Early CIRS spectra of Jupiter, courtesy of Don Jennings NASA/GSFC, show methane lines in absorption over the range 60 to 110 cm^{-1}. Analysis of the lab data is underway to support the interpretation of Jupiter spectra and the anticipated data from Saturn.

4. New Spectrometer System

We are developing a new differential Michelson interferometer to study dimer spectra in the frequency region 3-30 cm^{-1}. The system has twin light pipe optical cells 6.11 m long and two ^{3}He cooled bolometers. Each detector measures the interferogram that arises from the difference spectrum of cell 1 and cell 2. In principle, if both cells contain the same quantity of N_2 and argon is added to one cell, the interferogram should be due only to the N_2-Ar dimers.
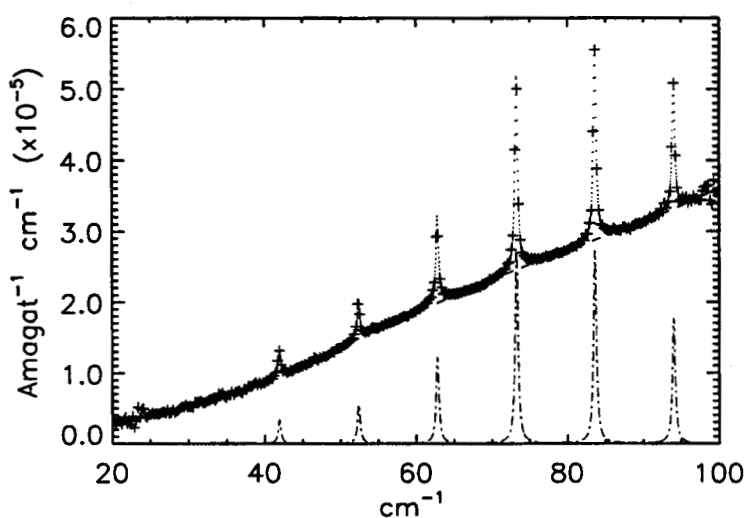
Fig. 2.— The absorption spectrum of methane. '+' are measurements of a 794 Torr methane sample at 113.5 K using a 60 m optical path. The dots are a fit to the data at 10x higher spectral resolution using 6 Lorentzian lines superposed on a quartic continuum; the dot-dash line shows the continuum removed spectrum.

Acknowledgments

REFERENCES

Borysow, A. & Frommhold, L. 1986, *ApJ*, **303**, 495.
Dore, P. & Filabozzi, A. 1987, *Canadian Journal of Physics*, **65**, 90.
Frommhold, L., Samuelson, R., & Birnbaum, G. 1984, *ApJ*, **283**, L79.
McKellar, A. R. W. 1984, *Canadian Journal of Physics*, **62**, 760.
Wang, F., McCourt, F. R. W., & Le Roy, R. J. 2000, *J. Chem. Phys.*, **113**, 98.
Wishnow, E. H., Gush, H. P., & Ozier, I. 1996, *J. Chem. Phys.*, **104**, 3511.
Wishnow, E. H., Leung, A., & Gush, H. P. 1999, *Review of Scientific Instruments*, **70**, 23.

MISSION STATUS REPORT

The *Hubble Space Telescope* and Laboratory Astrophysics

Theodore P. Snow

Center for Astrophysics and Space Astronomy, University of Colorado, Boulder, CO

Abstract

Users of the *Hubble Space Telescope*, particularly the spectrographs, have relied heavily on laboratory measurements in analyzing their data. Conversely, the *HST* has provided data to constrain or derive basic atomic and molecular parameters, thus supporting and supplementing laboratory astrophysics. This paper provides an overview of the interaction between the *HST* and laboratory astrophysics, and summarizes some areas where further lab data are needed in support of *HST* research.

1. Introduction

The interpretation of *HST* observations, particularly spectroscopic data, has depended critically on the availability of basic information on atomic and molecular constants such as oscillator strengths (f-values), excitation cross sections, and ionization thresholds derived from measurements made in the laboratory. The areas where *HST* spectroscopy has depended crucially on lab data are unlimited, but include especially: (1) determinations of stellar composition and abundances based on UV spectra; (2) analyses of interstellar gas absorption lines, atoms, ions, and molecules included; and (3) interpretation of spectral features due to interstellar and interplanetary dust, from the ultraviolet to the infrared.

The interpretation of data from virtually every previous astronomical instrument has depended similarly on data from the lab, but with the advent of the *HST* and other space-based instruments observing in new spectral regions and/or at unprecedented sensitivity levels came new demands for high-precision laboratory measurements. In short, the *HST* (along with other astronomical space-based missions), has put the astronomical measurements far ahead of the lab data needed to interpret them. Hence laboratory astrophysics is scrambling to keep up. This situation will only become more critical as new missions in the current development and launch queue come to fruition. At the same time, data from the *HST* (again, particularly spectra) have provided constraints on basic atomic and molecular quantities such as f-values and chemical branching ratios. For example, while is very difficult to calibrate observations or determine unambiguous abundances well enough to determine *absolute* values of oscillator strengths, collisional rates, or ionization cross sections solely from *HST* data, it is relatively straightforward to measure *relative* values for these parameters, for example within a multiplet or for a given elemental ion where the total abundance can be assumed constant. Thus the interaction between the *HST* and laboratory astrophysics has been very synergistic. In this brief review, we focus on a few areas of this interaction, providing some examples (but by no means claiming to present a comprehensive review). We also provide suggestions for future work in laboratory astrophysics that might strengthen the ties between astronomical observations and laboratory measurements.

2. Selected Examples of *HST*-Lab Astro Interactions

In this section we cite a few selected examples of studies in which *HST* data have been used to derive or refine basic data on such parameters as atomic and molecular oscillator strengths, optical constants for dust, and cross sections for chemical or physical processes. We do not claim to be exhaustive, but instead offer citations of studies that represent the many ways in which *HST* data have been useful for these purposes.

Derivation of Empirical *f*-Values: Many important transitions, particularly in the UV, still lack laboratory measurements of oscillator strengths. This is true both for resonance lines of common elements observed in the interstellar gas and for lines of elements measured in the spectra of stars (particularly problematic are abundance-anomalous stars, where rare elements are found). The underlying idea is that if the abundance or column density of an ion is known, then it should be possible to work backwards to find the oscillator strengths of transitions whose eqivalent width or profile is measured. Several studies using *HST* data have succeeded in doing this, both for transitions observed in the interstellar gas and for elements observed in stars. Because atoms in the interstellar gas are normally in the ground state, in principle it is possible to construct a simple curve of growth based on lines with known *f*-values, and then use the curve to estimate the *f*-values for unknown lines. In practice there are complications, however: the velocity distribution of the gas may not be well known; and many lines are saturated and lie on the flat part of the curve of growth where the relationship between equivalent width and the product $N f \lambda$ is ambiguous.

Despite the difficulties, several studies have been conducted in which empirical *f*-values were derived in this fashion. For example, Howk *et al.* (2000) combined measured line strengths from not only the *HST*, but also *Copernicus* and *FUSE* to derive *f*-values for 11 ground state lines of Fe II. Howk *et al.* combined curve-of-growth, line profile-fitting, and apparent optical depth methods in their analysis in order to find a fully self-consistent set of *f*-values for all the Fe II lines in their sample, including those previously measured and those not previously known. Their results compare favorably with recent theoretical determinations of the oscillator strengths of the same lines (Raassen & Uylings 1998), with a few exceptions for which the empirical values are likely superior to the theoretical ones.

Another recent study has raised issues with regard to atomic oscillator strengths that have been measured in the laboratory, but whose values create discrepancies with the observed line strengths. Jenkins & Tripp (2001) have conducted an exhaustive study of 10 different multiplets of C I lines toward 21 stars, in order to determine the column densities and fine-structure populations (useful as an indicator of cloud pressure). Jenkins & Tripp found that the *f*-values for the weaker C I multiplets appeared to have been systematically underestimated in laboratory studies, and they argue for new laboratory measurements aimed at clearing up the discrepancy. This is therefore not a case where *HST* data were used to determine previously unknown oscillator strenghts, but rather a situation where the empirical data suggest that some of the laboratory measurements may be in error. *HST* data have played the critical role. Many other papers can be cited to show how the *HST* has contributed to the derivation of atomic oscillator strengths (e.g., Federman & Cardelli 1995, who determined *f*-values for a number of S I lines observed in interstellar clouds).

In addition to helping to determine atomic constants, *HST* spectra have also proven useful in determining oscillator strengths for molecular features observed in the diffuse and translucent interstellar gas. This has proven particularly for the widely-observed diatomics CO, which has a number of weak (and therefore unsaturated) intersystem bands (Federman *et al.* 1994; Sheffer *et al.* 2002); and C_2, which has a band (the Mulliken band) in the *HST* UV spectral range that can be compared with the far-red Phillips band in deriving a self-consistent set of f-values (Lambert *et al.* 1995). Thus the combination of *HST* astronomical spectra with laboratory data has helped to constrain the f-values for the UV bands of both molecules.

On the stellar front, the synergism and interdependence of observed and laboratory spectra are, if anything, stronger than for interstellar gas studies. There are many important gaps in our knowledge of both wavelengths and f-values for ultraviolet transitions, even for common elements, and the situation is worse for high ionization states and less common elements. Reviews by Johansson & Leckrone (1996) and by Johansson *et al.* 1998 summarize the problems and the needs. A good example of interaction between *HST* data and laboratory measurements in the analysis of abundances in a particular star is the paper by Nilsson *et al.* (2000), in which new laboratory data on Fe II transitions from excited states were compared with *HST* spectra in order to confirm and test the f-values. Many other papers on stellar composition that are based on UV data have included similar combinations of observed and laboratory spectra.

UV Optical Constants of Dust: While the *HST* has been little- exploited so far in studies of the interstellar dust, that situation is likely to change. First, the reactivation of the NICMOS provides new opportunities to observe and analyze solid-state dust features in the near-IR, something that will be particularly useful in the 1-2 μm spectral region which is not covered by past, present, or planned IR missions but which contains some potentially important features. Second, in 2004 the Cosmic Origins Spectrograph (COS) will be installed aboard the *HST*, and because of its enhanced throughput in the UV, this instrument includes among its science priorities the derivation of UV extinction curves for heavily-reddened stars and the search for and analysis of spectral features in the UV that could be attributed to dust or large molecules such as PAHs. When and if spectral features due to grains or large molecules are detected by the *HST* either in the IR or the UV, their analysis will require laboratory data on the absorption cross sections for the appropriate materials.

3.   Future Interaction between the *HST* and Laboratory Astrophysics

During the preparation of this paper, and in the course of the Laboratory Astrophysics Workshop, a number of important needs were pointed out having to do with the interaction between the *HST* and laboratory astrophysics. Meeting some of these needs will require new laboratory measurements or programs, while others will call for new *HST* observations. Probably the area of most compelling needs is stellar astrophysics, particularly the determination of abundances and other physical properties of stars of all kinds. As noted above, UV line lists are far from complete, and are inadequate even for simply identifying lines, so much work is needed both in the lab and with the telescope. Adding to the frustration of people working in this field is the very uncertain support of groups at NIST and elsewhere who provide and archive atomic data. For example, the NIST group that maintains the Atomic Spectra Database has

lost most or all of its NASA funding in recent years, despite a general world-wide consensus that this center is an essential resource for research in the field.

One *HST* observing project, recently approved as a Treasury Program, will add substantially to the database on stellar UV lines. PI R. C. Peterson and her team will use *HST* spectra of solar-type stars to derive empirical line identifications and atomic parameters, utilizing an iterative procedure to modify the existing UV line lists. The resulting database will be important for many different future *HST* observing programs, including especially stellar abundance measurements in other galaxies. The program has been awarded 110 *HST* orbits over the next three observing cycles, representing a major boost for the use of the *HST* in helping to derive fundamental atomic parameters.

In the area of interstellar atomic and molecular UV absorption lines, there remain a number of specific issues that should be addressed. One interstellar problem that needs additional laboratory support, mentioned above, is the refinement of oscillator strengths for weak multiplets of C I, as described by Jenkins & Tripp (2001). There are a number of other transitions of other species, many of them lying at shorter UV wavelengths than covered by the *HST*, for which the *f*-values are unknown. These transitions are more important for the analysis of *FUSE* data than for the *HST*, however. Also, we reiterate that upcoming *HST* observations using the NICMOS and the COS are likely to produce data on solid-state and large molecular transitions for which laboratory data are currently inadequate. It will be important for the relevant laboratory measurements to be funded and carried out. Finally, we comment that it is very difficult indeed to win observing time with the *HST* in order to carry out any kind of calibration observations, including those aimed at improving atomic or molecular constants. The Space Telescope Science Institute currently offers a special category of proposals for such purposes, but does *not* set aside any reserved time, with the result that these programs invariably lose out in the intense competition. Perhaps the STScI should consider reserving some time for calibrations and atomic and molecular physics.

Acknowledgments

REFERENCES

Federman, S. R. & Cardelli, J. A. 1995, *apj*, **452**, 269.
Federman, S. R., Cardelli, J. A., Sheffer, Y., Lambert, D. L., & Morton, D. C. 1994, *apjl*, **432**, L139.
Howk, J. C., Sembach, K. R., Roth, K. C., & Kruk, J. W. 2000, *apj*, **544**, 867.
Jenkins, E. B. & Tripp, T. M. 2001, *apjs*, **137**, 297.
Johansson, S. & Leckrone, D. S. 1996, in *Model Atmospheres and Spectrum Synthesis*, ASP Conference Series, v. 108, eds. S. Adelman, F. Kupka, & W. Wiese, p. 113.
Johansson, S., Leckrone, D. S., & Davidson, K. 1998 in *The Scientific Impact of the Goddard High Resolution Spectromgraph*, ASP Conference Series, v. 143, eds. J. Brandt, T. Ake, & C. Peterson, p. 155.
Lambert, D. L., Sheffer, Y., & Federman, S. R. 1995, *apj*, **438**, 740.
Nilsson, H., *et al.*, 2000, *aa*, **362**, 410.
Raassen, A. J. J. & Uylings, P. H. M. 1998, *J. Phys. B*, **31**, 3137.
Sheffer, Y., Federman, S. R., & Lambert, D. L. 2002, *apjl*, in press.

APPENDICES

APPENDIX A

AGENDA DAY 1

Wednesday May 1, 2002

09:00   Welcoming Remarks (Farid Salama, SOC/LOC)
09:05   Welcome (Scott Hubbard, Deputy Director of Research, NASA Ames)
09:15   Workshop Goals & Objectives (Hashima Hasan, NASA HQ/OSS)
09:30   Introductory Talk: Martin Harwit, *Current and Future Space Missions. Great Questions of the Next Decade in Connection with Laboratory Astrophysics*

Atomic Astrophysics I
10:00   E. Behar (invited), *High Energy Astrophysics: X-Ray Spectroscopy and Atomic Data*
10:35   E. Takacs, *Spectroscopy of Trapped Ions with a Microcalorimeter on the NIST Electron Beam Ion Trap*
10:55   D.W. Savin, *Ion Storage Ring Measurements of Low Temperature Dielectronic Recombination Rate Coefficients for Modeling X-Ray Photoionized Cosmic Plasmas*
11:15   Coffee Break
11:45   G.J. Ferland, *Laboratory Astrophysics' Needs for Understanding Photoionized Plasmas*
12:05   R.F. Heeter, *Benchmarking Accretion Disk Models Using Photoionized Laboratory Plasmas*

Atomic Astrophysics II
14:00   C. Sneden (invited), *Atomic Data and Stellar Chemical Compositions*
14:35   A. Chutjian, *Measurement of Absolute Excitation Cross Sections in Highly-Charged Ions Using Electron Energy Loss and Merged Beams*
14:55   A. Glassgold, *Microscopic Processes in X-Ray Modulated Star Formation*

Molecular Astrophysics – Small Molecules
15:15   E. Bergin (invited), *Missing Pieces In Our Understanding of Astrochemistry: the Answers are in the Lab*
15:50   Coffee Break
16:15   L. Ziurys, *Sub-mm Spectroscopy of Astrophysically Important Metal-Containing Molecules*
16:35   C.A. Gottlieb, *Precise Laboratory Measurements of Line Frequencies Useful to Studies of Star and Planet Formation*
16:55   J.C. Pearson, *High-Resolution Photoionization and Photoelectron Studies: Laboratory Astrophysics Needs of the Herschel Space Observatory*
17:15   Poster Session & Reception

AGENDA DAY 2

Thursday May 2, 2002

08:30   M. Jura, *SIRTF: Goals and Requirements*
08:50   T. Greene, *The SOFIA Mission and Laboratory Astrophysics Synergies*

Molecular Astrophysics - Large Molecules
09:10   L.B. d'Hendecourt (invited), *The PAH Hypothesis: Dream or Nightmare for Astrophysicists?*
09:45   L.J. Allamandola, *IR Emission from Interstellar PAHs, New Probes of the ISM*
10:05   R.J. Saykally, *Molecular Carbon in the Galaxy: New Laboratory and Observational Studies*

10:25   E. Herbst, *The Submillimeter-Wave Spectra of Interstellar Molecules*
10:45   Coffee Break

Dust & Ices in Astrophysics
11:05   Th. Henning (invited), *Nanoparticles in Space and the Laboratory*
11:40   M.P. Collings, *Laboratory Surface Science: the Key to the Gas-Grain Interaction*
12:00   J.A. Nuth III, *Condensation Processes in Astrophysical Environments: the Composition and Structure of Cometary Grains*
12:20   J.P. Dworkin, *The Laboratory Production of Complex Organic Molecules in Simulated Interstellar Ices*

Solar System
14:00   D. Cruikshank (invited), *A Solar System Perspective on Laboratory Astrophysics*
14:35   T. Roush, *Cryogenic Titan Tholins*
14:55   P. Beiersdorfer, *Laboratory Studies of the X-Ray Emission Generated by the Interaction of Solar Wind Heavy Ions with Comets*
15:15   P.C. Cosby, *Experimental Measurements of Dissociative Recombination Relevant to Planetary Atmospheres*
15:35   Coffee Break
16:00   Report Talk: T. Snow, *HST Science Legacy*
16:20   Report Talk: K. Kirby, *ICAMDATA & APiP*
16:40   Discussion to prepare for Friday Break-out sessions
17:00   Poster Session & Reception

AGENDA DAY 3

Friday May 3, 2002

Community Input - Focus Group Discussions
09:00   Break-out sessions (Co-chaired by SOC members) [1]
        Atomic Astrophysics Sub-Group
        Molecular Astrophysics Sub-Group
        Dust & Ices in Astrophysics Sub-Group
        Solar System Sub-Group

Community Input – Plenary Discussions
13:30   Atomic Astrophysics Summary Presentation
13:45   Molecular Astrophysics Summary Presentation
14:00   Dust & Ices in Astrophysics Summary Presentation
14:15   Solar System Summary Presentation
14:30   Plenary discussion

Community Input – Executive Discussions
15:30   SOC/Executive session
17:30   Adjourn Workshop

---

1 Participants who joined in focus-group discussions are listed in Appendix C.

APPENDIX B

WORKSHOP CHARTER

Purpose of Workshop

The purpose of this Workshop, sponsored by NASA's Office of Space Science (OSS), is to discuss the current state of knowledge in the interdisciplinary field of Laboratory Astrophysics and to assess the needs in regards to current and future NASA's space missions. The Workshop will be organized along the Science Themes defined by NASA's Office of Space Science (OSS), for its strategic planning efforts:
- Origins
- Structure and Evolution of the Universe
- Solar System
- Sun-Earth Connection

In addition to these four themes, the Workshop will also include connections to Astrobiology, the study of life in the Universe.

Agenda

The Workshop will feature invited talks by members of the scientific community representing data users. The invited speakers will provide a broad overview of the needs in the field. The Workshop will also feature shorter talks and posters by data producers (NASA's Space Science programs grantees and others). Break-out groups chaired by the Scientific Organizing Committee members will produce a report on the status of the Laboratory Astrophysics programs supported by NASA and whether these programs meet NASA's needs for the future.

Target audience

- Laboratory Astrophysicists and Astrochemists
- Theoreticians and Modelers
- Observers
- Instrument developers
- Space mission scientists

The Workshop will provide a forum for the scientific community to discuss the latest developments in the field of Laboratory Astrophysics.

Specific Goals

The Workshop will:
- Review the current state-of-the art in laboratory astrophysics
- Review current and future space missions
- Assess how well the current programs are supporting NASA's space missions
- Identify science priorities in support of NASA's space missions
- Provide input to NASA Astronomy and Physics Division for it's strategic planning
- Generate and distribute through the NASA Astrophysics Data System (ADS) science proceedings that will be a reference for the community

APPENDIX C

FOCUS GROUP MEMBERS

ATOMIC ASTROPHYSICS FOCUS GROUP	MOLECULAR ASTROPHYSICS FOCUS GROUP	DUST & ICES IN ASTROPHYSICS FOCUS GROUP	SOLAR SYSTEM FOCUS GROUP
CHAIRPERSONS: James Lawler & Wilton Sanders	CHAIRPERSONS: Farid Salama & Ted Snow	CHAIRPERSONS: John Mathis & Xander Tielens	CHAIRPERSON: Melissa McGrath
Ehud Behar	Lou Allamandola	Mian Abbas	Peter Beiersdorfer
Peter Beiersdorfer	Aldo Apponi	Ted Bergin	Regina Cody
Greg Brown	James Babb	Max Bernstein	Richard Copeland
Ara Chutjian	Ted Bergin	Ludovic Biennier	Dale Cruikshank
Pisin Chen	Duane Carbon	Geoffrey Clayton	Brad Dalton
Gary Ferland	Pin Chen	Mark Collings	Chris Dateo
Thomas Gorczyca	Brian Drouin	David Cornelison	David Huestis
Hashima Hasan	Brian Eichelberger	Louis d'Hendecourt	Winifred Huo
Charles Havener	Richard Freedman	Jason Dworkin	Melissa McGrath
Don Kniffen	Thomas Giesen	M. Samy El-Shall	Ted Roush
Victor Kwong	Carl Gottlieb	George Flynn	Tom Slanger
Martin Laming	Murthy Gudipati	Helen Fraser	Peter Smith
James Lawler	Martin Harwit	Perry Gerakines	Melissa Grady Trainer
Jaan Lepson	Hashima Hasan	Murthy Gudipati	Edward Wishnow
Steven Manson	Thomas Henning	Michael Jura	
Ruth Peterson	Eric Herbst	Andy Mattioda	
Joseph Reader	Donald Kniffen	John Mathis	
Robert Rubin	Stephanie Langhoff	Marla Moore	
Wilton Sanders	Tim Lee	Joseph Nuth III	
Daniel Wolf Savin	Andrew Mattioda	Yvonne Pendleton	
Brian Sharpee	Benjamin McCall	Scott Sandford	
Peter Smith	Cheuk-Yiu Ng	Willem Schutte	
Steven Smith	Kimberlee O'Brien	Alexander Tielens	
Chris Sneden	Jim Pizagno	Gianfranco Vidali	
Endre Takacs	Farid Salama	Jonathan Wrubel	
Anne Thorne	Richard Saykally		
Wolfgang Wiese	Tracey Smith		
	Theodore Snow		
	Anne Thorne		
	Martin Vala		
	Edward Wishnow		
	Lucy Ziurys		

APPENDIX D

PARTICIPANTS' CONTACT INFORMATION

Mian M. Abbas
NASA Marshall Space Flight Center
SD50 - NSSTC
Huntsville AL 35812
tel: 256-961-7680
mian.abbas@msfc.nasa.gov

Sara E. Acevedo
SETI Institute
2035 Landings Drive
Mountain View CA 94043
tel: 650-960-4539
sacevedo @mail.arc.nasa.gov

Joseph Ajello
Jet Propulsion Laboratory MS 183-601
4800 Oak Grove Drive
Pasadena CA 91109
office tel: 818-354-2457
lab tel: 818-354-0120, -3362
jajello@pop.jpl.naa.gov

Lou Allamandola
NASA Ames Research Center MS 245-6
Moffett Field CA 94035-1000
tel: 650-604-6890
lallamandola @mail.arc.nasa.gov

Aldo J. Apponi
The University of Arizona
Departments of Chemisty and Astronomy
933 N. Cherry Ave.
Tucson AZ 85721
tel: 520-621-2553
aapponi@as.arizona.edu

Sushil K. Atreya
The University of Michigan
Space Research Building
2455 Hayward Street
Ann Arbor MI 48109-2143
tel: 734-763-6234
fax: 734-764-5137
atreya@umich.edu

James F. Babb
Harvard-Smithsonian Center for Astrophysics
MS 14
60 Garden St.
Cambridge MA 02138
tel: 617-496-7612
fax: 617-496-7668
jbabb@cfa.harvard.edu

Emma L. Bakes
SETI Institute
MS 245-3
NASA Ames Research Center
Moffett Field CA 94035-1000
tel: 650-604-0787
fax: 650-604-6779
bakes@shivakali.arc.nasa.gov

Raul Baragiola
Laboratory for Space Research
University of Virginia
Charlottesville VA 22904
rb9a@virginia.edu

Charles W. Bauschlicher
NASA Ames Research Center
Mail Stop 230-3
Moffett Field CA 94035-1000
tel: 650-604-6231
fax: 650-604-0350
bauschli@pegasus.arc.nasa.gov

Ehud Behar
Columbia Astrophysics Laboratory
Columbia University, Mail Code 5247
550 West 120th Street
New York NY 10027
tel: 1-212-854-8136
fax: 1-212-854-8121
behar@astro.columbia.edu

Peter Beiersdorfer
Lawrence Livermore National Laboratory
7000 East Avenue, L-260
Livermore CA 94550
tel: 925-423-3985
fax: 925-423-2302
beiersdorfer@llnl.gov

Edwin Bergin
SAO, MS-66
60 Garden Street
Cambridge, MA 02138
tel: 617-496-7740
ebergin@cfa.harvard.edu

Max Bernstein
NASA Ames Research Center
Space Science Division
Mail Stop 245-6
Moffett Field CA 94035-1000
tel: 650-604-0194
fax: 650-604-6779
mbernstein@mail.arc.nasa.gov

Ludovic Biennier
NASA Ames Research Center
Space Science Division
Mail Stop 245-6
Moffett Field CA 94035-1000
tel: 650-604-4217
fax: 650-604-6779
lbiennier@mail.arc.nasa.gov

Bill Borucki
NASA Ames Research Center
Space Science Division
Mail Stop 245-6
Moffett Field CA 94035-1000
tel: 650-604-6492
fax: 650-604-6779
bborucki@mail.arc.nasa.gov

Jesse Bregman
NASA Ames Research Center
Astrophysics Code SSA
MS 245-6
Moffett Field CA 94035-1000
tel: 650 604-6136
fax: 650 604-6779
jbregman@mail.arc.nasa.gov

Greg V. Brown
NASA Goddard Space Flight Center
Laboratory for High Energy Astrophysics
Code 662
Bldg 2, Rm 256
Greenbelt MD 20771
tel: 301-286-2466
fax: 301-286-1684
gvb@milkyway.gsfc.nasa.gov

Linda R. Brown
Jet Propulsion Laboratory
MS 183-601
4800 Oak Grove Dr.
Pasadena CA 91109
tel: 818-354-2940
fax: 818-354-5148
linda@regina.jpl.nasa.gov

Duane Carbon
MS 258-5
NASA Ames Research Center
Moffett Field CA 94035-1000
tel: 650-604-4413
dcarbon@nas.nasa.gov

Pin Chen
Jet Propulsion Laboratory
MS 183-601
4800 Oak Grove Dr.
Pasadena CA 91109
tel: 818-354-
fax: 818-354-5148

Pisin Chen
Stanford Linear Accelerator Center
Stanford University
2575 Sand Hill Rd.
Menlo Park
tel: 650-926-3384
fax: 650-926-5368
chen@slac.stanford.edu

Hyun-Kyung Chung
Lawrence Livermore National Laboratory
7000 East Ave. L-411
Livermore CA 94550
tel: 925-423-3452
fax: 925-423-2463
hchung@llnl.gov

Ara Chutjian
MS 121-114
Jet Propulsion Laboratory
4800 Oak Grove Drive
Pasadena CA 91109
tel: 818-354-7012
fax: 818-393-1899
ara.chutjian@jpl.nasa.gov

Geoffrey C. Clayton
Louisiana State University
Department of Physics & Astronomy
Baton Rouge LA 70803
tel: 225-578-8275
fax: 225-578-5855
gclayton@fenway.phys.lsu.edu

Regina J. Cody
Code 691
NASA Goddard Space Flight Center
Greenbelt MD 20771
tel 301-286-3782
fax 301-286-0212
regina.cody@gsfc.nasa.gov

David H. Cohen
Swarthmore College
Department of Physics and Astronomy
500 College Ave.
Swarthmore PA 19081
tel: 610-328-8587
fax: 610-328-7895
cohen@hven.swarthmore.edu

M.P. Collings
University of Nottingham
Department of Chemistry
Floor A - Physical Chemistry
University Park
Nottingham, NG7 2RD
United Kingdom
tel: 44 115 9513472
fax: 44 115 9513562
pczmpc@unix.ccc.nottingham.ac.uk

Richard A. Copeland
Molecular Physics Laboratory
SRI International
333 Ravenswood Ave.
Menlo Park CA 94025
tel: 650-859-6534
fax: 650-859-6196
richard.copeland@sri.com

David M. Cornelison
Northern Arizona University
Department of Physics and Astronomy
Box 6010
Flagstaff AZ 86011
tel: 928-523-7641
fax: 928-523-1371
David.Cornelison@nau.edu

Philip C. Cosby
Molecular Physics PN-087
SRI International
333 Ravenswood Avenue
Menlo Park CA 94025
tel: 650-859-5128
fax: 650-859-6196
philip.cosby@sri.com

Philippe Crane
NASA Headquarters Code SR
300 E St. SW
Washington, D.C. 20546
tel: 202-358 0377
fax: 202-358 3097
pcrane@hq.nasa.gov

Dale P. Cruikshank
Astrophysics Branch
Mail Stop 245-6
NASA Ames Research Center
Moffett Field CA 94035-1000
tel: 650-604-4244
fax: 650-604-6779
dcruikshank@mail.arc.nasa.gov

James Bradley Dalton
Astrophysics Branch
Mail Stop 245-6
NASA Ames Research Center
Moffett Field CA 94035-1000
tel: 650-604-3148
fax: 650-604-6779
dalton@mail.arc.nasa.gov

Sanford S. Davis
Astrophysics Branch
Mail Stop 245-6
NASA Ames Research Center
Moffett Field CA 94035-1000
tel: 650-604-4197
fax: 650-604-6779
sdavis@mail.arc.nasa.gov

Donald L. DeVincenzi
NASA Ames Research Center
MS 245-6
Moffett Field CA 94035-1000
tel: 650-604-5251
fax: 650-604-6779
ddevincenzi@mail.arc.nasa.gov

Louis B. d'Hendecourt
CNRS
Institut d'Astrophysique Spatiale
"Astrochimie Expérimentale"
Campus d'Orsay - Bat 121
ORSAY - 91405 ORSAY - Cedex
FRANCE
tel: 33 -0-1 69 85 86 40
fax: 33 -0-1 69 85 86 75
ldh@ias.fr

Brian James Drouin
Jet Propulsion Laboratory
4800 Oak Grove Drive
Mail Stop 183-301
Pasadena CA 91109-8099
tel: 818-393-6259
fax: 818-354-8460
bdrouin@mail2.jpl.nasa.gov

Jason P. Dworkin
Mail Stop 245-6
NASA Ames Research Center
Moffett Field CA 94035-1000
tel: 650-604-0789
fax: 650-604-6779
jdworkin@mail.arc.nasa.gov

Brian R. Eichelberger
University of Colorado at Boulder
Department of Chemistry and Biochemistry
Campus Box 215
Boulder CO 80309
tel: 303-492-7396
fax: 303-492-5894
brian.eichelberger@colorado.edu

M. Samy S. El-Shall
Virginia Commonwealth University
Department of Chemistry
1001 W. Main Street
Richmond VA 23284-2006
tel: 804-828-3518
fax: 804-828-8599
selshall@hsc.vcu.edu

Kimberly A. Ennico
Mail Stop 245-6
NASA Ames Research Center
Moffett Field CA 94035-1000
tel: 650-604-6067
fax: 650-604-6779
kennico@mail.arc.nasa.gov

Gary J. Ferland
University of Kentucky
Physics Department, CP 177
Lexington KY 40506
tel: 859-257-8795
fax: 859-323-2846
gary@pa.uky.edu
http://nimbus.pa.uky.edu/cloud

George J. Flynn
Department of Physics
SUNY-Plattsburgh
101 Broad St
Plattsburgh New York 12901
tel: 518 564-3163
fax: 518 564-3152
george.Flynn@plattsburgh.edu

Helen J. Fraser
Raymond and Beverly Sackler
  Laboratory for Astrophysics
University of Leiden
Postbus 9513
2300 RA
Leiden
The Netherlands
tel: 31-71-527-5818
fax: 31-71-527-5819
fraser@strw.leidenUniv.nl

Richard S. Freedman
Space Physics Research Institute
Mail Stop 245-3
NASA Ames Research Center
Moffett Field CA 94035-1000
tel: 650-604-0316
fax: 650-604-6779
freedman@darkstar.arc.nasa.gov

Friedemann T. Freund
MS 239-20
NASA Ames Research Center
Moffett Field CA 94035-1000
tel: 650-604-5183
fax: 650-604-0092
ffreund@mail.arc.nasa.gov

Perry A. Gerakines
310 Campbell Hall
Department of Physics
University of Alabama at Birmingham
1300 University Blvd.
Birmingham AL 35294-1770
tel: 205-934-8064
fax: 205-934-8043
gerakines@uab.edu

Thomas F. Giesen
I. Physikalisches Institut
Universitaet zu Koeln
Zuelpicher Strasse 77
D-50937 Koeln
Germany
tel: 49-221-470-4529
fax: 49-221-470-5162
giesen@ph1.uni-koeln.de

Alfred E. Glassgold
NYU/UCB
601 Campbell Hall
Astronomy Department
University of California
Berkeley CA 94720
tel: 510 642-6708
fax: 510 642-3411
aglassgold@astron.berkeley.edu

David Goorvitch
Mail Stop 245-6
NASA Ames Research Center
Moffett Field CA 94035-1000
tel: 650-604-5502
fax: 650-604-6779
dgoorvitch@mail.arc.nasa.gov

Thomas W. Gorczyca
Department of Physics
Western Michigan University
1903 West Michigan Ave.
Kalamazoo MI 49008-5252
tel: 616-387-4913
fax: 616-387-4939
gorczyca@wmich.edu

Carl A. Gottlieb
Pierce Hall
29 Oxford Street
Cambridge MA 02138
tel: 617-495-9952 (office)
tel: 617-495-9848 (lab)
fax: 617-495-9837
cgottlie@cfa.harvard.edu

James C. Green
University of Colorado
Center for Astrophysics and Space Astronomy
1255 38th Street
Boulder CO 80303
Country:USA
tel: 303-492-7645
fax: 303-492-5941
jgreen@casa.colorado.edu

Tom Greene
Space Science Division
Mail Stop 245-6
NASA Ames Research Center
Moffett Field CA 94035-1000
tel: 650-604-5520
fax: 650-604-6779
tgreene@mail.arc.nasa.gov

Murthy S. Gudipati
Molecular Physics Laboratory
SRI International
333 Ravenswood Avenue
Menlo Park CA 94025
tel: 650-859-2083
fax: 650-859-6196
murthy.gudipati@sri.com

Bob Haberle
Space Science Division
Mail Stop 245-6
NASA Ames Research Center
Moffett Field CA 94035-1000
tel: 650-604-5491
fax: 650-604-6779

Nathan N Haese
455 Moraga Road, Suite C
Moraga CA 94556
tel: 925-285-5144
fax: 925-289-1247
nathanhaese@cal.berkeley.edu

Martin Harwit
Emeritus Professor of Astronomy
Cornell University
511 H. St., SW
Washington DC 20024-2725
tel: 202-479-6877
harwit@verizon.net

Hashima Hasan
NASA Headquarters Code SR
300 E St. SW
Washington DC 20546
tel: 202-358-0692
fax: 202-358-3096
hashima.hasan@hq.nasa.gov

Charles C. Havener
Oak Ridge National Lab
Physics Division, Bld 6003, MS 6372
Oak Ridge TN 37831
tel: 865-574-4704
fax: 865-574-1118
havenercc@ornl.gov

Martin P. Head-Gordon
Department of Chemistry
University of California, Berkeley
Berkeley CA 94720
tel: 510-642-5957
fax: 510-643-1255
mhg@cchem.berkeley.edu

Robert F. Heeter
Lawrence Livermore National Lab
Mailstop L-043
7000 East Avenue
Livermore CA 94550
tel: 925-423-3761
fax: 925-423-5998
heeter@llnl.gov

Thomas Henning
Schillergaesschen 3
Jena 07745
Germany
tel: 49-3641-947530
fax: 49-3641-947532
henning@astro.uni-jena.de

Eric Herbst
Department of Physics
The Ohio State University
174 W. 18th Ave.
Columbus Ohio 43210-1106
tel: 614-292-6951
fax: 614-292-7557
herbst@mps.ohio-state.edu

John Hillman
NASA Headquarters Code SR
300 E St. SW
Washington DC 20546-0001
tel: 202-358-2314
fax: 202-358-3097
jhillman@mail.hq.nasa.gov

284

Douglas M. Hudgins
MS 245-6
NASA Ames Research Center
Moffett Field CA 94035-1000
tel: 650-604-4216
fax: 650-604-6779
dhudgins@mail.arc.nasa.gov

David L. Huestis
SRI International
333 Ravenswood Ave
Menlo Park CA 94025
tel: 650.859.3464
fax: 650.859.6196
david.huestis@sri.com

William E. Johnston
Information and Computing Sciences,
Lawrence Berkeley National Laboratory
MS B50B-2239
Berkeley CA 94720
http://www-itg.lbl.gov/~johnston

Michael Jura
UCLA
Department of Physics and Astronomy
Los Angeles California 90095-1562
tel: 310-825-4302
fax: 310-206-2096
jura@astro.ucla.edu

Konstantinos Kalogerakis
Molecular Physics Laboratory
PN021
SRI International
333 Ravenswood Ave.
Menlo Park CA 94025
tel: 650-859-3398
fax: 650-859-6196
ksk@sri.com

Louis Kaluzienski
NASA Headquarters Code SR
300 E St. SW
Washington DC 20546-0001
tel: 202-358-0365
fax: 202-358-3096
lkaluzie@mail.hq.nasa.gov

Kate P. Kirby
Harvard-Smithsonian Center for Astrophysics
Mail Stop 14
60 Garden Street
Cambridge MA 02138
tel: 617-495-7237
fax: 617-495-5970
kkirby@cfa.harvard.edu

Donald Kniffen
NASA Headquarters Code SR
300 E St. SW
Washington DC 20546-0001
tel: 202-358-0351
fax: 202-358-3097
dkniffen@mail.hq.nasa.gov

David Koch
Mail Stop 245-6
NASA Ames Research Center
Moffett Field CA 94035-1000
tel: 650-604-6548
fax: 650-604-6779
dkoch@mail.arc.nasa.gov

Robert L. Kurucz
Harvard-Smithsonian Center for Astrophysics
60 Garden Street
Cambridge MA 02138
tel: 617-495-7429
fax: 617-495-7049
rkurucz@cfa.harvard.edu

Victor H.S. Kwong
UNLV
Department of Physics
4505 Maryland Parkway
Las Vegas Nevada 89154-4002
tel: 702-895-1700
fax: 702-895-0804
vhs@physics.unlv.edu

Martin Laming
US Naval Research Laboratory
4555 Overlook Ave, SW
Washington DC 20375
tel: 202-767-4415
fax: 202-404-7997
jlaming@ssd5.nrl.navy.mil

Stephanie Langhoff
Mail Stop 200-1
NASA Ames Research Center
Moffett Field CA 94035-1000
tel: 650-604-
fax: 650-604-
slanghoff@mail.arc.nasa.gov

James E. Lawler
Department of Physics
University of Wisconsin
1150 University Ave.
Madison WI 53706
tel: 608-262-2918
fax: 608-265-2334
jelawler@facstaff.wisc.edu

David Leckrone
Code 440 (Bldg. 7, Rm. 281)
NASA Goddard Space Flight Center
Greenbelt MD 20771
tel: 301-286-5975
fax: 301-286-1670
dleckrone@hst.nasa.gov

Jaan K. Lepson
UC Berkeley - SSL
Space Sciences Lab 7450
University of California
Berkeley CA 94720
tel: 925-455-9817
fax: same -warn me first-
lepson@ssl.berkeley.edu

Steven T. Manson
Department of Physics and Astronomy
Georgia State University
Atlanta Georgia 30303
tel: 404-651-3082
fax: 404-651-1427
smanson@gsu.edu

John S. Mathis
University of Wisconsin
Department of Astronomy
475 N. Charter St.
Madison WI 53706-1582
tel: 608-262-5994
fax: 608-263-6386
mathis@astro.wisc.edu

Andrew L. Mattioda
MS 245-6
NASA Ames Research Center
Moffett Field CA 94035-1000
tel: 650-604-1075
fax: 650-604-6779
amattioda@mail.arc.nasa.gov

Benjamin J. McCall
University of California at Berkeley
601 Campbell Hall
Berkeley CA 94720
tel: 510-643-1499
fax: 510-642-8566
bjmccall@astro.berkeley.edu

Melissa McGrath
Space Telescope Science Institute
STScI
3700 San Martin Dr.
Baltimore MD 21218
tel: 410-338-4545
fax: 410-338-4767
mcgrath@stsci.edu

Hugh Miller
Department of Physics & Astronomy
Science Annex Bldg; 4th Floor
Georgia State University
29 Peachtree Center Ave.
Atlanta GA 30303
tel: 404-651-1368
fax: 404-651-1389
miller@chara.gsu.edu

Marla H. Moore
NASA Goddard Space Flight Center
Code 691
Greenbelt MD 20771
tel: 301-286-9031
fax: 301-286-0440
ummhm@lepvax.gsfc.nasa.gov

David Morrison
NASA Ames Research Center
MS 245-6
Moffett Field CA 94035-1000
tel: 650-604-
fax: 650-604-6779
dmorrison@mail.arc.nasa.gov

Cheuk-Yiu Ng
Department of Chemistry
University of California at Davis
One Shields Avenue
Davis CA 95616
tel: 530-754-9645
fax: 530-752-8995
cyng@chem.ucdavis.edu

Joseph Nuth
Astrochemistry Branch
Code 691
NASA Goddard Space Flight Center
Greenbelt MD 20771
fax 301-286-0212
Joseph.Nuth@gsfc.nasa.gov

Kimberlee M. O'Brien
UCSD/Mesa College
P.O. Box 128504
San Diego CA 92112
tel: 858 272 9677
kmaxine@nethere.net

John C. Pearson
Mail Stop 301-429
Jet Propulsion Laboratory
California Institute of Technology
4800 Oak Grove Dr
Pasadena CA 91109
tel: 818-354-6822
fax: 818-393-2430
John.C.Pearson@jpl.nasa.gov

Yvonne Pendleton
Astrophysics Branch
Mail Stop 245-6
NASA Ames Research Center
Moffett Field CA 94035-1000
tel: 650-604-4391
fax: 650-604-6779
ypendleton@mail.arc.nasa.gov

Ruth C. Peterson
Astrophysical Advances and UCO/Lick
peterson@ucolick.org

Thomas Phillips
Caltech
Department of Physics
MS 320-47
1200 East California Blvd.
Pasadena CA 91125
tel: 626-395-4278
fax: 626-796-8806
phillips@submm.caltech.edu

Jim L. Pizagno
Department of Astronomy
The Ohio State University
140 W. 18th Avenue
Columbus OH 43210-1173
tel: 614-292-9994
fax: 614-292-2928
jpizagno@astronomy.ohio-state.edu

Joseph Reader
National Institute of Standards and Technology
Stop 8421
100 Bureau Drive
Gaithersburg MD 20855
tel: 301-975-3222
fax: 301-975-5485
joseph.reader@nist.gov

Thomas L. Roellig
MS 245-6
NASA Ames Research Center
Moffett Field CA 94035-1000
tel: 650-604-6426
fax: 650-604-6779
troellig@mail.arc.nasa.gov

Ted L. Roush
Planetary Systems Branch
MS 245-3
NASA Ames Research Center
Moffett Field CA 94035-1000
tel: 650 604 3526
fax: 650-604-6779
troush@mail.arc.nasa.gov

Robert H. Rubin
Orion Enterprises
MS 245-3
NASA Ames Research Center
Moffett Field CA 94035-1000
tel: 650-604-6450
fax: 650-604-6779
rubin@cygnus.arc.nasa.gov

Farid Salama
Space Science Division
MS 245-6
NASA Ames Research Center
Moffett Field CA 94035-1000
tel: 650-604-3384
fax: 650-604-6779
fsalama@mail.arc.nasa.gov

Wilton T. Sanders
University of Wisconsin
Department of Physics
1150 University Ave.
Madison WI 53706
tel: 608-262-5916
fax: 608-263-0361
sanders@physics.wisc.edu

Scott A. Sandford
Astrophysics Branch
Mail Stop 245-6
NASA-Ames Research Center
Moffett Field CA 94035-1000
tel: 650-604-6849
fax: 650-604-6779
ssandford@mail.arc.nasa.gov

Daniel Wolf Savin
Columbia Astrophysics Laboratory
Mail Code 5247
550 West 120th Street
New York NY 10027
tel: 212-854-4124
fax: 212-854-8121
savin@astro.columbia.edu

Richard J. Saykally
Department of Chemistry
University of California, Berkeley
D31 Hildebrand Hall
Berkeley CA 94720-1460
tel: 510-642-8269
fax: 510-642-8566
saykally@uclink4.berkeley.edu

Jeff Scargle
Mail Stop 245-3
NASA-Ames Research Center
Moffett Field CA 94035-1000
tel: 650-604-6849
fax: 650-604-6779
jscargle@mail.arc.nasa.gov

Willem A. Schutte
Sackler Laboratory for Astrophysics
Leiden Observatory
P.O. Box 9513
Leiden
2300 RA
The Netherlands
tel: 31-71-5275801
fax: 31-71-5275819
schutte@strw.leidenuniv.nl

Brian D. Sharpee
316 B Physics and Astronomy Building
Michigan State University
Department of Physics and Astronomy
East Lansing Michigan 48824
tel: 517-432-0386
fax: 517-353-4500
sharpee@pa.msu.edu

Thomas G. Slanger
Molecular Physics Laboratory
PN021
SRI International
333 Ravenswood Ave.
Menlo Park CA 94025
tel: 650-859-3398
fax: 650-859-6196
slanger@mplvax.sri.com

Bruce Smith
Space Science Division
MS 245-3
NASA Ames Research Center
Moffett Field CA 94035-1000
tel: 650-604-5515
fax: 650-604-6779
bsmith@mail.arc.nasa.gov

Gregory P. Smith
PS067
SRI International
333 Ravenswood Ave.
Menlo Park CA 94025
tel: 650-859-3496
fax: 650-859-6196
smith@mplvax.sri.com

Peter Smith
Harvard-Smithsonian, CfA
MS 50
60 Garden St.
Cambridge MA 02138
tel: 617-495-4984
fax: 617-495-7455
plsmith@cfa.harvard.edu

Steven J. Smith
Mail Stop 121/104
Jet Propulsion Laboratory
4800 Oak Grove Drive
Pasadena CA 91109
tel: 818-354-8177
steven.j.smith@jpl.nasa.gov

Tracey L. Smith
Louisiana State University
550 Lee Drive #62
Baton Rouge LA 70808
tel: 225 768 7140
fax: 225 578 5855
tsmith@dirty.phys.lsu.edu

Chris Sneden
Department of Astronomy
University of Texas
Austin TX 78712
tel: 512 471 3302
fax: 512 471 6016
chris@verdi.as.utexas.edu

Theodore P. Snow
CASA - University of Colorado
389 UCB
Boulder CO 80309-0389
tel: 303-492-7669
fax: 303-492-7178
tsnow@casa.colorado.edu

Phillip C. Stancil
The University of Georgia
Department of Physics and Astronomy
Athens GA 30602-2451
tel: 706-542-2885
fax: 706-542-2492
stancil@physast.uga.edu

Guy Stringfellow
CASA - University of Colorado
389 UCB
Boulder CO 80309-0389
tel: 303-492-6056
fax: 303-492-4052
Guy.Stringfellow@Colorado.edu

Hiroshi Suto
Subaru Telescope
650 North Aohoku Place
Hilo HI 96720
tel: 808 934 5960
fax: 808 934 5984
suto@naoj.org

Endre Takacs
MIT
NIST, Bldg 221, Rm. B228
Gaithersburg MD 20899-8421
tel: 301-975-8244
fax: 301-975-3038
etakacs@nist.govetakacs@nist.gov

Anne P. Thorne
QOLS
Blackett Laboratory
Imperial College
Prince Consort Rd.
London SW7 2BZ
Great Britain
tel: 44-207-594-7589
fax: 44-207-594-7777
a.thorne@ic.ac.uk

Alexander Tielens
Kapteyn Astronomical Institute
Postbus 800
Groningen
9700 AV
The Netherlands
tel: 31-50-3634092
fax: 31-50-3636100
tielens@astro.rug.nl

Melissa Grady Trainer
CIRES 318
Campus Box 216
University of Colorado at Boulder
Boulder CO 80309-0216
tel: 303-492-1433
fax: 303-492-1149
melissa.trainer@colorado.edu

Martin Vala
University of Florida
Gainesville, FL 32611
tel: 353-392-0529
fax: 352-392-0872
mvala@chem.ufl.edu

Gianfranco Vidali
Syracuse University
201 Physics Bldg.
Syracuse NY 13244-1130
tel: 315-443-9115 (voice)
tel: 315-443-1801 (lab)
fax: 315-443-9103
gvidali@mailbox.syr.edu

Michael Way
M.S. 245-6
NASA Ames Research Center
Moffett Field CA 94035-1000
tel: 650-604-5115
fax: 650-604-6779
mway@mail.arc.nasa.gov

Wolfgang L. Wiese
National Institute of Standards and Technology
Mail Stop 8420
100 Bureau Drive
Gaithersburg MD 20899-8420
tel: 301-975-3201
fax: 301-990-1350
wolfgang.wiese@nist.gov

Edward H. Wishnow
L-043
Lawrence Livermore National Laboratory
7000 East Av.
Livermore CA 94551
tel: 925 422-7208
wishnow@llnl.gov

Jonathan P. Wrubel
LASSP
C-19 Clark Hall
Cornell University
Ithaca NY 14853
tel: 607-255-3941
fax: 607-255-6428
jpw22@cornell.edu

Lucy M. Ziurys
The University of Arizona
Departments of Chemisty and Astronomy
933 N. Cherry Ave.
Tucson AZ 85721
tel: 520-621-6525
fax: 520-621-1530
lziurys@as.arizona.edu

APPENDIX E

SCIENCE ORGANIZING COMMITTEE CONTACT INFORMATION

David Leckrone
NASA Goddard Space Flight Center
Code 440 (Bldg. 7, Rm. 281)
Greenbelt MD 20771
tel: (301) 286-5975
fax: (301) 286-1670
dleckrone@hst.nasa.gov

John S. Mathis
Univ. of Wisconsin
Dept. of Astronomy
475 N. Charter St.
Madison WI 53706-1582
tel: (608) 262-5994
fax: (608) 263-6386
mathis@astro.wisc.edu

Melissa McGrath
Space Telescope Science Inst.
3700 San Martin Dr.
Baltimore MD 21218
tel: 410-338-4545
fax: 410-338-4767
mcgrath@stsci.edu

Hugh Miller
Georgia State Univ.
Dept. of Physics & Astronomy
Science Annex Bldg; 4th Floor
29 Peachtree Center Ave.
Atlanta GA 30303
tel: 404-651-1368
fax: 404-651-1389
miller@chara.gsu.edu

Thomas Phillips
Caltech
Dept. of Physics, MS 320-47
1200 East California Blvd.
Pasadena CA 91125
tel: 626-395-4278
fax: 626-796-8806
phillips@submm.caltech.edu

Farid Salama (Chairperson)
NASA Ames Research Center
Space Science Division
MS 245-6
Moffett Field CA 94035
tel: (650) 604-3384
fax: (650) 604-6779
fsalama@mail.arc.nasa.gov

Wilton Sanders
Univ. of Wisconsin
Dept. of Physics
1150 University Ave.
Madison WI 53706
tel: (608) 262-5916
fax: (608) 263-6738
sanders@wisp.physics.wisc.edu

Peter Smith
Harvard-Smithsonian, CfA
60 Garden St., MS 50
Cambridge MA 02138
tel: 617-495-4984
fax: 617-495-7455
plsmith@cfa.harvard.edu

Theodore P. Snow
CASA - University of Colorado
389 UCB
Boulder CO 80309-0389
tel: 303-492-7669
fax: 303-492-7178
tsnow@casa.colorado.edu

Alexander Tielens
Kapteyn Astronomical Institute
Postbus 800
Groningen
9700 AV
The Netherlands
tel: 31-50-3634092
fax: 31-50-3636100
tielens@astro.rug.nl

Ex-officio SOC Members:

Philippe Crane
Discipline Scientist
NASA Headquarters Code SR
300 E St. SW
Washington D.C. 20546
tel: 202-358-0377
fax: 202-358-3097
pcrane@hq.nasa.gov

Eric P. Smith
Discipline Scientist
NASA Headquarters Code SR
300 E St. SW
Washington DC 20546
tel: 202-358-2439
fax: 202-358 3097
esmith1@mail.hq.nasa.gov

Hashima Hasan
Discipline Scientist
NASA Headquarters Code SR
300 E St. SW
Washington DC 20546
tel: 202-358-0692
fax: 202-358-3096
hashima.hasan@hq.nasa.gov

Jay A. Frogel
Discipline Scientist
NASA Headquarters Code SR
300 E St. SW
Washington DC 20546-0001
tel: 202-358-1319
fax: 202-358-3097
jfrogel@ mail.hq.nasa.gov

John Hillman
Discipline Scientist
NASA Headquarters Code SR
300 E St. SW
Washington DC 20546-0001
tel: 202-358-2314
fax: 202-358-3097
jhillman@mail.hq.nasa.gov

James E. Lawler
NASA APWG
Department of Physics
University of Wisconsin
1150 University Ave.
Madison WI 53706
tel: 608-262-2918
fax: 608-265-2334
jelawler@facstaff.wisc.edu

Louis Kaluzienski
Discipline Scientist
NASA Headquarters Code SR
300 E St. SW
Washington DC 20546-0001
tel: 202-358-0365
fax: 202-358-3096
lkaluzie@mail.hq.nasa.gov

Guy Stringfellow
CASA - University of Colorado
389 UCB
Boulder CO 80309-0389
tel: 303-492-6056
fax: 303-492-4052
Guy.Stringfellow@Colorado.edu

Donald Kniffen
Discipline Scientist
NASA Headquarters Code SR
300 E St. SW
Washington DC 20546-0001
tel: 202-358-0351
fax: 202-358-3097
dkniffen@mail.hq.nasa.gov

APPENDIX F

AUTHOR INDEX

REPORT DOCUMENTATION PAGE		Form Approved OMB No. 0704-0188

The public reporting burden for this collection of information is estimated to average 1 hour per response, including the time for reviewing instructions, searching existing data sources, gathering and maintaining the data needed, and completing and reviewing the collection of information. Send comments regarding this burden estimate or any other aspect of this collection of information, including suggestions for reducing this burden, to Department of Defense, Washington Headquarters Services, Directorate for Information Operations and Reports (0704-0188), 1215 Jefferson Davis Highway, Suite 1204, Arlington, VA 22202-4302. Respondents should be aware that notwithstanding any other provision of law, no person shall be subject to any penalty for failing to comply with a collection of information if it does not display a currently valid OMB control number.
PLEASE DO NOT RETURN YOUR FORM TO THE ABOVE ADDRESS.

1. REPORT DATE (DD-MM-YYYY) 30/11/02	2. REPORT TYPE Conference Proceedings	3. DATES COVERED (From - To)

4. TITLE AND SUBTITLE *Proceedings of the NASA Laboratory Astrophysics Workshop*	5a. CONTRACT NUMBER
	5b. GRANT NUMBER
	5c. PROGRAM ELEMENT NUMBER
6. AUTHOR(S) F. Salama, ed.	5d. PROJECT NUMBER
	5e. TASK NUMBER
	5f. WORK UNIT NUMBER 344-89-02-23

7. PERFORMING ORGANIZATION NAME(S) AND ADDRESS(ES) Ames Research Center Moffett Field CA 94035-1000	8. PERFORMING ORGANIZATION REPORT NUMBER A – 0309205

9. SPONSORING/MONITORING AGENCY NAME(S) AND ADDRESS(ES) National Aeronautics and Space Administration Washington, D.C. 20546-0001	10. SPONSORING/MONITOR'S ACRONYM(S)
	11. SPONSORING/MONITORING REPORT NUMBER NASA/CP–2002–211863

12. DISTRIBUTION/AVAILABILITY STATEMENT
Unclassified-Unlimited   Distribution: Standard
Subject Category 88   Availability: NASA CASI (301) 621-0390

13. SUPPLEMENTARY NOTES
  POC: Farid Salama

14. ABSTRACT
This document is the proceedings of the NASA Laboratory Astrophysics Workshop, convened May 1–3, 2002 at NASA's Ames Research Center. Sponsored by the NASA Office of Space Science (OSS), this programmatic workshop is held periodically by NASA to discuss the current state of knowledge in the interdisciplinary field of laboratory astrophysics and to identify the science priorities ('needs') in support of NASA's space missions. An important goal of the Workshop is to provide input to OSS in the form of a white paper for incorporation in it's strategic planning. This report comprises a record of the complete proceedings of the Workshop and the Laboratory Astrophysics White Paper drafted at the Workshop.

15. SUBJECT TERMS

  Laboratory Astrophysics; White Paper

16. SECURITY CLASSIFICATION OF:			17. LIMITATION OF ABSTRACT	18. NUMBER OF PAGES	19b. NAME OF RESPONSIBLE PERSON Farid Salama
a. REPORT	b. ABSTRACT	c. THIS PAGE			
Uncl.	Uncl.	Uncl.	Uncl.	320	19b. TELEPHONE NUMBER (Include area code) 650-604-3384

Standard Form 298 (Rev. 8-98)
Prescribed by ANSI Std. Z39-18